UNIVERSIDADE FEDERAL DE SANTA CATARINA
CENTRO TECNOLÓGICO
PROGRAMA DE PÓS-GRADUAÇÃO EM ENGENHARIA QUÍMICA

Ígor Henrique de Mello Rodrigues Ciolin

CROSSLINKED GELATIN NANOCARRIERS FOR HYDROPHILIC DRUGS

Florianópolis
2023

Ígor Henrique de Mello Rodrigues Ciolin

CROSSLINKED GELATIN NANOCARRIERS FOR HYDROPHILIC DRUGS

Dissertação submetida ao Programa de Pós-Graduação em Engenharia Química da Universidade Federal de Santa Catarina para obtenção do título de Mestre em Engenharia Química.

Orientadora: Profa. Dra. Claudia Sayer
Coorientadores: Prof. Dr. Pedro Henrique Hermes de Araújo
Dr. Thiago Ouriques Machado

Florianópolis
2023

Ciolin, Ígor Henrique de Mello Rodrigues
Crosslinked gelatin nanocarriers for hydrophilic drug/Henrique de Mello Rodrigues Ciolin ; orientadora, Claudia Sayer, coorientador, Pedro Henrique Hermes de Araújo, coorientador, Thiago Ouriques Machado, 2024.
182 p.

Dissertação (mestrado) - Universidade Federal de Santa Catarina, Centro Tecnológico, Programa de Pós-Graduação em Engenharia Química, Florianópolis, 2024.

Inclui referências.

1. Engenharia Química. 2. Nanoencapsulation. 3. Biopolymers. 4. Nanogels. 5. Inverse miniemulsion. I. Sayer, Claudia. II. de Araújo, Pedro Henrique Hermes. III. Machado, Thiago Ouriques IV. Universidade Federal de Santa Catarina. Programa de Pós-Graduação em Engenharia Química. V. Título.

Ígor Henrique de Mello Rodrigues Ciolin

CROSSLINKED GELATIN NANOCARRIERS FOR HYDROPHILIC DRUGS

O presente trabalho em nível de mestrado foi avaliado e aprovado por banca examinadora composta pelos seguintes membros:

Profa. Cristiane da Costa, Dra.
Universidade Federal de Santa Catarina
Membro interno

Prof. Marcelo Lanza, Dr.
Universidade Federal de Santa Catarina
Membro externo

Profa. Claudia Sayer, Dra.
Universidade Federal de Santa Catarina
Orientadora

Certificamos que esta é a versão original e final do trabalho de conclusão que foi julgado adequado para obtenção do título de mestre em Engenharia Química.

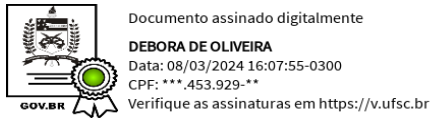

Débora de Oliveira
Coordenação do Programa de Pós-Graduação

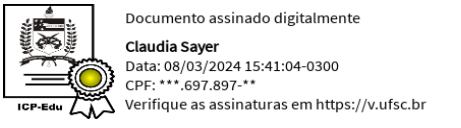

Profa. Claudia Sayer, Dra.
Orientadora

Florianópolis, 2023.

Aos pesquisadores que fazem Ciência no Brasil;

Às vítimas da covid-19;

Aos meus avós, Aparecida, Antônio e Ítala;

Ao meu tio, André Luiz e,

À minha querida irmã Jacqueline,

Por todos os laços inquebrantáveis que nos unem (...)

Dedico.

ACKOWLEDGMENTS

À causa primária de todas as coisas, à inteligência suprema, pela oportunidade a mim concedida de evoluir nesta existência.

Aos meus mentores espirituais, por todo amparo durante esta árdua e brilhante caminhada, nós conseguimos!

Aos meus pais, irmão e familiares, obrigado por tudo.

Aos meus queridos amigos pelos momentos felizes compartilhados.

À Dra. Silvia Cristina Martin por todos os ensinamentos, você é especial! E, aos amigos do GED. Rolando Perri Cefali, por todo apoio recebido.

À família Rufino, especialmente, Josymarie, Marilene e Nora.

Ao amigo, Prof. Dr. Luiz da Silveira Neto, sou muito grato a você!

Aos meus colegas de laboratório, MSc. Jaqueline Guessi, MSc. Juliana Zanatta, MSc. Vanessa Meneghini, MSc. Isabela Tolentino, MSc. Rafael Amaral e MSc. Yuri Barreiros, por todas as experiências enriquecedoras, desejo muito sucesso a todos vocês.

À orientadora, Profa. Dra. Claudia Sayer, por me aceitar neste grupo de pesquisa, por todas as orientações, reuniões e sugestões essenciais para o desenvolvimento deste trabalho. Agradeço por sua paciência, compreensão e sabedoria ao me orientar. Obrigado por acreditar no meu potencial e por todo conhecimento a mim transmitido, o meu mais sincero agradecimento e reconhecimento.

Aos coorientadores, Prof. Dr. Pedro Henrique Hermes de Araújo e ao Dr. Thiago Ouriques Machado, por todas as ideias valiosas e colaboração, financeira e intelectual. Grato pela disponibilidade, ideação, correções e por toda atenção dispensada.

Ao acadêmico de iniciação científica, Matheus Fagundes da Silveira, agradeço por todo auxílio durante os experimentos.

Aos Professores da banca avaliadora por todos os apontamentos, contribuição e disponibilidade em corrigir e melhorar este trabalho.

Ao Prof. Dr. Ricardo Antônio Machado pelas trocas de ideias no laboratório, e às Profas. Dras. Jaciane Lutz Ienckzak e Cristiane da Costa pelos conhecimentos transmitidos em aulas, agradeço.

Aos Profs. Drs. Daiane Lenhard, Eliane Colla, Daniel Walker, Carolina Garcia, Elisa Ponsano, Gláucia Moreira, César Lenzi, por todas as orientações, inspiração e conhecimento técnico que me proporcionaram durante minha caminhada acadêmica, parte disto tem vocês.

Ao Sr. Milvo Zancanaro e à empresa Gelnex pela doação da gelatina e disposição em colaborar.

À Universidade Federal de Santa Catarina (UFSC) pela estrutura cedida, ao Programa de Pós-graduação em Engenharia Química (PósEnq) e à Capes/CNPQ pelos recursos financeiros disponibilizados, principalmente, aos Departamentos de Engenharia Química e de Alimentos (EQA), Química (CFM) e Biologia (CCB), aos Laboratórios de Controle e Processos de Polimerização (LCP), Central de Microscopia Eletrônica (LCME), de Termodinâmica e Tecnologia Supercrítica (LATESC), de Engenharia Biológica (LiEB), Interdisciplinar do Desenvolvimento de Nanoestruturas (LINDEN), de Propriedades Físicas de Alimentos (PROFI), Multiusuário de Estudos em Biologia (LAMEB), às Centrais de Análises (EQA/CFM) e a todos os profissionais envolvidos.

Especialmente, ao MSc. Luiz Paulo (CFM), Fernanda e Leandro (Central de Análises), MSc. Adenilson (LATESC), Maísa e Flávia (Lameb) e Victor Ribeiro (IQ-UFRGS).

Por fim, a todos que, com boa intenção e verdadeira consideração, contribuíram de forma positiva para realização deste trabalho e conclusão desta etapa da minha vida.

"A gratidão é a assinatura de Deus colocada na Sua obra, a vida sem gratidão, é estéril e vazia de significado existencial" (Joanna de Ângelis).

Sou profundamente grato,

Ígor Henrique Ciolin

“Os laboratórios são templos em que a inteligência é concitada
ao serviço de *Deus*, e, ainda mesmo quando a cerebração se perverte,
transitoriamente subornada pela hegemonia política, geradora
de guerras, o progresso da Ciência, como conquista divina,
permanece na exaltação do bem, rumo a glorioso porvir”.
(EMMANUEL, 1954).

RESUMO EXPANDIDO

Introdução

A gelatina é um biopolímero natural, hidrofílico e anfótero, obtido a partir da hidrólise ácida, alcalina ou enzimática do colágeno e possui uma cadeia rica de 18 aminoácidos, incluindo as sequências RGD (arginina – glicina – ácido aspártico) responsáveis por facilitar a adesão celular. Devido as suas diversas características valiosas e desejáveis como, biocompatibilidade, biodegradabilidade e baixa toxicidade, tem sido uma escolha promissora na síntese de materiais híbridos para aplicações biomédicas, principalmente, no desenvolvimento de hidrogéis e nanogéis. Entretanto, a baixa estabilidade térmica e mecânica limita sua utilização direta sendo necessário modificações para torná-la utilizável nestes dispositivos. Por outro lado, os poli(β-amino ésteres) são uma classe de polímeros conhecida por suas propriedades inerentes às aminas terciárias e ésteres, como responsividade ao pH e biodegradabilidade, sendo amplamente escolhidos como plataformas eficazes para a encapsulação e entrega controlada de medicamentos, em terapia gênica, bem como, no preparo de hidro- e nanogéis. A síntese destes polímeros, se dá por meio da reação de adição de aza-Michael entre aminas e ésteres insaturados e a característica catiônica destes compostos os tornam candidatos especiais para estes tipos de aplicações devido, principalmente, à propriedade pH responsiva. Além disso, a reação de aza-Michael é uma abordagem viável para síntese de poli(β-amino ésteres) por ser considerada uma reação rápida e de alta quimioseletividade, permitir o uso de condições reacionais mais brandas e sem a necessidade da utilização de catalisadores e/ou metais pesados, solventes de fácil remoção e a não geração de produtos reacionais secundários indesejáveis. Já, os ésteres acrílicos, derivados do ácido acrílico, que é sintetizado a partir do petróleo, mas que também pode ser sintetizado a partir de biomassa, também são compostos interessantes por suas propriedades superabsorventes e biodegradáveis, sendo os diacrilatos, usualmente empregados como agentes reticulantes na criação de diversos tipos de materiais e nas mais variadas aplicações. Na área biomédica, têm sido utilizados na síntese de hidrogéis, *scaffolds*, nanopartículas e fibras. Por possuir pontos reativos como as duplas ligações, permite a junção a polímeros mais biodegradáveis e biocompatíveis a fim de modificá-los, inclusive, térmica e mecanicamente, por meio da formação de novas ligações covalentes e redes tridimensionais. Neste sentido, os biomateriais acrilados oferecem a vantagem de possuírem grupos acrílicos, que são altamente reativos, pendentes ao longo da cadeia polimérica, sendo propícios a pós-modificações como a fotopolimerização e/ou fotoreticulação, permitindo a síntese de materiais com propriedades melhoradas e ajustáveis. Uma outra abordagem, diz respeito à síntese e à utilização de partículas biopoliméricas, como as nanopartículas (NPs), para entrega controlada de medicamentos, as quais, oferecem a vantagem de possuírem uma grande área superficial susceptível a diversas modificações, contribuindo para melhorar a biodisponibilidade, a solubilidade e a estabilidade dos fármacos. Além disso, podem direcionar a liberação a locais específicos, reduzindo os efeitos colaterais, promovendo uma liberação sustentada e melhorando a eficácia terapêutica. Entre os diversos fármacos hidrofílicos existentes, a doxorrubicina (DOX) é um fármaco hidrofílico antraciclinico amplamente utilizada como agente quimioterápico no tratamento de diversos tipos de cânceres. Geralmente, os fármacos hidrofílicos não são compatíveis com os sistemas de encapsulação hidrofóbicos e seu encapsulamento em NPs também hidrofílicas, é um desafio a ser superado, de forma a criar dispositivos de entrega que garantam uma liberação sustentada sem se desintegrarem rapidamente frente aos estímulos externos, como pH e temperatura. Para isso, diversas técnicas têm sido comumente reportadas na literatura para a modificação destas matrizes poliméricas, como a reticulação e a

copolimerização, entre outras. Com base no exposto, a síntese de biomateriais à base de gelatina modificada para fins biomédicos, como os poli(β-amino ésteres), emerge como valiosas alternativas biocompatíveis e biodegradáveis para o preparo de hidrogéis e nanogéis com propriedades tunáveis para o carreamento de fármacos hidrofílicos, entre outras aplicações, auxiliando no desenvolvimento de tratamentos e dispositivos terapêuticos mais seguros e eficazes.

Objetivo

Este trabalho objetivou a síntese de poli(β-amino ésteres) em forma de hidrogéis e nanogéis à base de gelatina "acrilada" e/ou reticulada com 1,4-butanodiol diacrilato (1,4-BDDA) via reação de adição de aza-Michael em solução e via polimerização interfacial em miniemulsão inversa, respectivamente, e suas posteriores caracterizações para servirem como potenciais plataformas biocompatíveis para a entrega controlada de fármacos hidrofílicos. Além disso, objetivou-se aumentar a densidade de reticulação das nanopartículas de gelatina (GNPs) a partir da fotopolimerização via radicais livres.

Métodos

A gelatina pura foi caracterizada em relação ao peso molecular (cromatografia de permeação em gel, GPC, e por difração de luz), propriedades físicas e químicas e quanto ao seu teor de aminas primárias livres (TNBS). Os hidrogéis foram sintetizados utilizando-se três formulações distintas na proporção molar de 1:0,5, 1:1 e 1:1,5 mmol ε-NH_2: mmol reticulante via adição de aza-Michael em solução, catalisada por DBU durante 24 h sob agitação magnética sendo, posteriormente, purificados e liofilizados. Os hidrogéis acrilados e/ou reticulados foram caracterizados quanto à densidade real (picnometria a Hélio), estrutura química (FTIR), amorfismo/cristalinidade (DRX), propriedades térmicas (TGA e DSC), razão de intumescimento (SR), fração insolúvel e grau de modificação (DM) pelo ensaio com TNBS. Além disso, as equações de Flory-Rehner foram utilizadas para descrever a reticulação dos hidrogéis a partir dos dados de intumescimento. Para a síntese de GNPs, foram preparadas quatro formulações com três concentrações distintas de reticulante na proporção molar de 1:1,2, 1:4 e 1:8 mmol ε-NH_2: mmol reticulante. As GNPs acriladas e/ou reticuladas foram sintetizadas em miniemulsão inversa via reação interfacial. Posteriormente, as formulações submetidas à foto-cura foram preparadas na presença do fotoiniciador 2,2-Dimethoxy-2-phenylacetophenone (DMPA) na proporção de 2% (massa fotoiniciador:massa de gelatina) sob irradiação de luz ultravioleta (UV) por 15 min e intensidade de 4,13 mV em câmara UV pré-aquecida por 20 min. As GNPs foram caracterizadas quanto ao DM pelo ensaio com TNBS, diâmetro médio das partículas (D_p) e índice de polidispersão (PDI) via espalhamento dinâmico da luz (DLS), estabilidade coloidal (potencial zeta), morfologia e tamanho de partícula por microscopia eletrônica de transmissão (MET), fluorescência por microscopias óptica e confocal de varredura a laser (CLSM) e eficiência de encapsulação (EE) via espectrofotometria no UV-Vis.

Resultados e discussão

A gelatina pura apresentou densidade (ρ = 1,34 g·cm^{-3}) e volume específico ($\bar{v}$ = 0,748 cm^3·g^{-1}) com valores muito próximos aos relatados pela literatura. Os valores das densidades dos hidrogéis (ρ = 1,29 a 1,39 g·cm^{-3}) também se encontram na faixa reportada. O teor total de aminas primárias livres (ε-NH_2) na gelatina pura foi de 0,305 ± 0,0065 mmol de lisina·$g_{gelatina}^{-1}$. O grau de modificação (DM) e a extensão da modificação (X_m) dos hidrogéis aumentaram com o aumento da concentração de reticulante e variaram entre 26 e 62% e 0,078 ± 0.001 e 0,20 ± 0.014 mmol de

lisina·$g_{gelatina}^{-1}$, respectivamente. As propriedades como razão de intumescimento (SR) e tamanho da malha da rede tiveram seus valores aumentados com o aumento do DM. Adicionalmente, a partir dos valores de densidade de reticulação (q) calculados pela teoria de Flory-Rehner verificou-se que o hidrogel mais reticulado foi aquele sintetizado com a menor concentração de reticulante, que também apresentou menores SR e peso molecular entre os pontos de reticulação ($\overline{M_C}$) e maior módulo de cisalhamento (G). A estabilidade térmica apresentou ligeira redução nas formulações que apresentaram maiores DM, sendo este efeito, atribuído ao efeito plastificante do reticulante utilizado. Além disso, nanopartículas de gelatina (GNPs) estáveis e com distribuição de tamanho de partículas uniforme foram obtidas. Os diâmetros das GNPs em meio orgânico variaram entre 185 e 202 nm com PDI < 0,2 em todas as formulações avaliadas. Para as nanopartículas redispersas verificou-se uma larga distribuição de tamanhos de partículas e altos índices de polidispersão em todas as formulações. Ainda, o diâmetro de algumas amostras contendo DOX não foram possíveis de serem medidos pela característica colorida e fluorescente das amostras e limitações instrumentais. A responsividade ao pH foi avaliada através do potencial zeta (ζ), em que, valores negativos foram obtidos para todas as formulações, sendo maiores em módulo (74 mV) para as GNPs redispersas em água destilada em pH 6,5 e preparadas com máxima concentração de reticulante (0,1 g). Entretanto, estudos preliminares conduzidos em solução de PBS em pH 3,0 revelaram um comportamento catiônico (+ 7,6 ± 3,2 mV) e aumento do diâmetro das GNPs, indicando o efeito significativo da variação do pH no intumescimento e no diâmetro médio das GNPs. Os potenciais negativos encontrados foram associados ao próprio alto ponto isoelétrico (PI) da gelatina tipo A, ao efeito *shielding* de Debye-Hückel, ao excesso de surfactante proveniente do próprio processo de redispersão, ao pK_a básico (6,5) do reticulante utilizado, e, ao possível deslocamento no ponto isoelétrico original da gelatina pelo consumo dos grupos lisina envolvidos na reação e à presença dos resíduos livres de arginina, que possuem pK_a mais elevado (12,5). Pelas análises microscópicas foi possível identificar a morfologia quase perfeitamente esférica das GNPs redispersas com leves achatamentos e distribuição larga de tamanhos com valor médio de D_p = 499,3 ± 178,5 nm medidos por MET utilizando-se o software ImageJ. Contudo, partículas de tamanhos menores também foram identificadas e impossíveis de serem contadas devido a limitação de magnificação do microscópio. Além disso, a partir da microscopia óptica verificou-se o sucesso na encapsulação do fármaco dentro das GNPs por meio da fluorescência emitida pela DOX em 585 nm. No entanto, a partir da microscopia confocal, não foi possível afirmar com certeza se a fluorescência observada é proveniente da DOX livre ou encapsulada, sendo recomendados estudos de internalização celular para uma melhor avaliação. Entretanto, a eficiência de encapsulação da DOX medida por UV-vis variou entre 94,5 e 96,2% e entre 27,2 e 34,5% com máximo carregamento de 31,3 ± 2,16 e 11,2 ± 0,74 $\mu_{gDOX}\cdot g_{polímero}^{-1}$ quando redispersas em meio orgânico e aquoso, respectivamente.

Conclusão

A reação de adição de aza-Michael é uma ferramenta viável para síntese de hidrogéis de gelatina em solução. Além disso, a variação da concentração de reticulante propiciou a síntese de hidrogéis e nanogéis com propriedades ajustáveis. As GNPs apresentam-se como potenciais carreadoras deste fármaco, com uma encapsulação moderada de DOX. Os biomateriais sintetizados emergem como alternativas biocompatíveis e biodegradáveis com características desejáveis para utilização em fins biomédicos.

Palavras-chave: Reticulação. Biomateriais. Entrega de fármacos.

RESUMO

A gelatina é um biopolímero natural hidrofílico obtida a partir da hidrólise do colágeno e amplamente utilizada como parte na síntese de dispositivos biomédicos, principalmente, por sua biodegradabilidade, biocompatibilidade e baixa toxicidade. Entretanto, devido a sua pobre resistência mecânica e baixa estabilidade térmica tem sido usualmente modificada para fins biomédicos específicos. A rica cadeia de aminoácidos e a presença de grupos funcionais diversos permite a síntese de biomateriais com características desejáveis e propriedades aprimoradas. Neste sentido, os poli(β-aminoésteres), PBAEs, tem emergido como um valioso nanocarreador (NC) de fármacos por aumentar a permeabilidade a membranas e devido as características inerentes às aminas terciárias e aos ésteres, como capacidade pH-responsiva e biodegradabilidade. Portanto, neste estudo, objetivou-se a síntese de nanopartículas (NPs) hidrofílicas, biocompatíveis e biodegradáveis, "acriladas" e/ou reticuladas para servirem como NCs de fármacos também hidrofílicos em aplicações biomédicas. Para tanto, nanogéis e hidrogéis de PBAEs à base de gelatina modificada foram sintetizados e caracterizados. A reação de adição de aza-Michael foi empregada para desenvolver os hidrogéis utilizando 1,4-butanodiol diacrilato como reticulante em solução. As GNPs "acriladas" e/ou reticuladas foram preparadas via polimerização interfacial com o mesmo reticulante em miniemulsão inversa e/ou seguida de fotopolimerização por radicais livres, utilizando-se um fotoiniciador. A gelatina pura foi caracterizada quanto ao peso molecular (GPC e SLS), propriedades físicas, térmicas e grupos amino primários livres (ensaio com TNBS). Os hidrogéis sintetizados foram caracterizados por FTIR, DRX, TGA, DSC, grau de modificação (DM), razão de intumescimento e pela teoria de Flory-Rehner, já para as GNPs, avaliou-se o tamanho de partícula e índice de polidispersão, potencial zeta, DM, eficiência de encapsulação e morfologia. A gelatina possui peso molecular em torno de M_w = 539.127 g·mol^{-1} e ε = 0,305 mmol de lisina·$g_{gelatina}^{-1}$. Hidrogéis com DM entre 26,4 e 62,9% foram obtidos e a incorporação do reticulante foi verificada pelos espectros de FTIR e DRX. Em relação à gelatina pura, a estabilidade térmica dos hidrogéis apresentou ligeira redução para as formulações com maiores DM, sendo este comportamento, atribuído ao efeito plastificante do reticulante utilizado. Foi observado um aumento na razão de intumescimento e no tamanho da malha da rede com o aumento do DM. Adicionalmente, para as GNPs foram obtidos DM entre 45,6 e 70,4% e partículas com diâmetros médios entre 185 e 202 nm e distribuição de tamanhos estreita (PDI < 0,2). Para as GNPs redispersas em diferentes pH e a 37 ºC, os potenciais zeta negativos foram associados à contribuição de diversos efeitos observados. A máxima eficiência de encapsulação nas GNPs redispersas foi de 34,5% com 11,2 $\mu g_{DOX} \cdot g_{polímero}^{-1}$ encapsulada. Estruturas aproximadamente esféricas com diâmetro médio de 499,3 ± 178,5 nm foram observadas pela microscopia eletrônica de transmissão. O estudo de fluorescência por microscopia óptica confirmou o encapsulamento da DOX, no entanto, não foi possível obter informações conclusivas a respeito do encapsulamento e liberação do fármaco a partir da microscopia confocal. Contudo, hidrogéis e nanogéis com propriedades ajustáveis foram desenvolvidos como potenciais plataformas biocompatíveis e biodegradáveis para o encapsulamento e entrega de fármacos hidrofílicos para fins biomédicos.

Palavras-chave: Biopolímeros; Química click; Reticulação.

ABSTRACT

Gelatin is a hydrophilic natural biopolymer obtained from the hydrolysis of collagen and widely used as part of the synthesis of biomedical devices, mainly due to its biodegradability, biocompatibility, and low toxicity. However, due to its poor mechanical resistance and low thermal stability, it has usually been modified for specific biomedical purposes. The rich amino acid chain and the presence of diverse functional groups allows the synthesis of biomaterials with desirable characteristics and improved properties. In this sense, the poly(β-amino esters), PBAEs, has emerged as a valuable nanocarrier (NC) for drugs by facilitating the membranes permeability and by having inherent characteristics of tertiary amines and esters, such as pH-responsiveness and biodegradability. Therefore, the goal of this study was the synthesis of hydrophilic, biocompatible, and biodegradable NPs, "acrylated" and/or crosslinked to serve as NCs for hydrophilic drugs in biomedical applications. For that, nanogels and hydrogels of PBAEs based on modified gelatin were synthesized and characterized. The aza-Michael addition reaction was employed to develop the hydrogels using 1,4-butanediol diacrylate as a crosslinker in solution. The "acrylated" and/or crosslinked GNPs were prepared via interfacial polymerization with the same crosslinker in inverse miniemulsion and/or followed by free radical photopolymerization using a photoinitiator. Neat gelatin was characterized in relation to its molecular weight (GPC and SLS), physical and thermal properties and free primary amino groups (TNBS test). The hydrogels synthesized were characterized by FTIR, XRD, TGA, DSC, modification degree (DM), swelling ratio and by Flory-Rehner theory, while for GNPs, the particle size and polydispersity index, zeta potential, DM, encapsulation efficiency and morphology. Gelatin has a molecular weight of around M_w = 539.127 g·mol^{-1} and ε = 0.305 mmol of lysine·$g_{gelatin}^{-1}$. Hydrogels with DM between 26.4 and 62.9% were obtained and crosslinker incorporation was verified by FTIR and XRD spectra. In relation to neat gelatin, the thermal stability of the hydrogels showed a slight reduction for formulations with higher DM, this behavior being attributed to the plasticizing effect of the crosslinker used. An increase in the swelling ratio and mesh size of the network was observed with DM increases. Additionally, for GNPs, DM between 45.6 and 70.4% and particles with average diameters between 185 and 202 nm were obtained with a narrow particle size distribution (PDI < 0.2). For redispersed GNPs at different pH and at 37 ºC, the negative zeta potentials were associated with the contribution of several observed effects. The maximum encapsulation efficiency in the redispersed GNPs was 34.5% with 11.2 $\mu g_{DOX} \cdot g_{polymer}^{-1}$ encapsulated. Furthermore, approximately spherical structures with an average diameter of 499.3 ± 178.5 nm were observed by transmission electron microscopy. The fluorescence study by optical microscopy confirmed DOX encapsulation, however, it was not possible to obtain conclusive information regarding encapsulation and release of DOX from confocal microscopy. However, hydrogels and nanogels with tunable properties have been developed as potential biocompatible and biodegradable platforms for the encapsulation and delivery of hydrophilic drugs for biomedical purposes.

Keywords: Biopolymers; Click chemistry; Crosslinking.

LIST OF FIGURES

LIST OF TABLES

LIST OF ABBREVIATIONS AND ACRONYMS

^{1}H-NMR Hydrogen Proton Nuclear Magnetic Resonance
1,4-BDDA 1,4-Butanediol diacrylate
2,4,6-TNBS 2,4,6 – Trinitrobenzenesulfonic acid
3D Three Dimensional
ATR Attenuated Transmission Reflectance
COP Conference of the Parties of the United Nations for Climate Change Conference
DBU 1,8-Diazobicyclo [5.4.0]undec-7-ene
DHCPs Disposable Health Care Products
DLS Dynamic Light Scattering
DOX Doxorubicin
DMPA 2,2-Dimethoxy-2-phenylacetophenone
DNA Deoxyribonucleic acid
DSC Differential Scanning Calorimetry
ECM Extracellular Matrix
EE Encapsulation Efficiency (%)
EGDMA Ethyleneglycol dimethacrylate
EPR – Enhanced Permeability and Retention Effect
FDA Food and Drug Administration
FTIR Fourier Transform Infrared Spectroscopy
GRAS Generally Recognized as Safe
GPC Gel Permeation Chromatography
GNPs Gelatin Nanoparticles
GTA Glutaraldehyde
HCl Hydrochloric acid
HEMA Hydroxyethyl methacrylate
IG2959 Irgacure 2959 (2-hydroxy-4'-(2-hydroxyethoxy)-2-methylpropiophenone)
IP Isoelectric Point
$NaHCO_3$ Sodium carbonate
$NaNO_3$ Sodium nitrate
NC Nanocarrier
NH_2 Primary amine
NH Secondary amine
NHS n-Hydroxysuccinimide
NPs Nanoparticles
ONU United Nations Organization
PCL Polycaprolactone
PDI Polydispersity index
PGPR Polyglycerol polyricinoleate
pH Hydrogenionic potential
PI Photoinitiator
PLA Polylactic acid

RGD Arginine-Glycine-Aspartic acid
R.I. Refractive Index
RNA Ribonucleic acid
SDS Sodium Dodecyl Sulfate
SLS Static Light Scattering
SR Swelling Ratio
TGA Thermogravimetric Analysis
TEM Transmission Electron Microscopy
UNFCCC United Nations for Climate Change Conference
UV Ultraviolet
XRD X-ray diffraction
ZnSe Zinc Selenide

LIST OF SYMBOLS

Å Angstrom
b Path length (cm)
cm Centimeters
cm³ Cubic centimeters
ε Epsilon (free amino groups)
DM Degree of modification
D_p Particle diameter
G Shear modulus
g Grams
kPa Kilopascal
L Liter
$\overline{M_C}$ Average molecular weight between crosslinks ($g \cdot mol^{-1}$)
M_n Number Average Molecular Weight ($g \cdot mol^{-1}$)
M_w Weight Average Molecular Weight ($g \cdot mol^{-1}$ or kDa)
MHz Megahertz
mL Milliliter
mmols Milimols
mV milivolts
nm Nanometers
ρ Rho (density)
q Crosslinking density ($mol \cdot g^{-1}$)
Q_v Equilibrium volumetric swelling ratio
ξ Xi (mesh size)
T Temperature
% Percentage
ºC Degree Celsius
µg Micrograms
µL Microliter
$\upsilon_{2,s}$ Volume fraction
X_m modification extent
χ Chi (Flory-Huggins's parameter)
w/w Weight/Weight
w/v Weight/Volume
ζ Zeta (zeta potential)

TABLE OF CONTENTS

1 INTRODUCTION

The growing concern for safer materials and more sustainable ecological solutions has become an attractive research field in polymer chemistry (CHIONG et al., 2021). In this context, the global plastic consumption scenario received great attention in the last decades (MASSUGA et al., 2022). Annually, the worldwide plastic disposal accounts more than 150 million ton of solid waste (RAHIMI & GARCÍA, 2017). Meanwhile, the effects of micro and nano-plastics accumulation originated from modern lifestyle has raised an alert regarding global climate issues and the harmful effects on animal and human health (LAI; LIU; QU, 2022). However, some efforts to minimize the side effects of large-scale production and consequently incorrect disposal are proposed in literature and by the United Nations (ONU) as in the 27^{th} Global Climate Change Conference (COP 27) (UNCC, 2022; NAGALAKSHMAIAH et al., 2019).

The use of synthetic plastics and petroleum derivatives date back to early 20^{th} century when discovered by Leo Baekland in 1907 (CHALMIN, 2019; BAEKELAND, 1909). During the first half of the 20^{th} century, plastics were seen as the "wonder material" for being lightweight and resilient and strong at the same time. After a couple of decades, many problems associated with their production and disposal have come to light, especially the environmental impacts (CHIONG et al., 2021). In addition, despite the benefits, the responsible and ethical use of plastics in biomedical field is essential to ensure patient safety and environmental sustainability, and issues such as degradation over time, the release of potentially toxic chemicals, and the need for proper recycling to minimize environmental impacts must be considered (MASSUGA et al., 2022).

Nevertheless, the search for cleaner and more efficient solutions to replace them has driven the development of more sustainable and recyclable polymers. In recent years, studies on biocompatibility and biodegradability of polymers have gained space in the scientific community (SAMIR et al., 2022). The biodegradable and biocompatible polymers play a crucial role in the promotion of human health, environmental preservation and in technological and economic advancement (CHIONG et al., 2021; THANAVEL & SEONG SOO, 2013). These interesting and eco-friendly organic molecules found uses in several industrial segments as biomedical, pharmaceutical, agricultural, electronical, water treatments process and for food packaging (CAO & UHRICH, 2019; CHIONG et al., 2021; RAHIMI & GARCÍA, 2017). Their properties of

great value offer the advantage of degrading under milder environmental and/or physiological conditions without producing side toxic compounds (WEI et al., 2020). In the biomedical field, they have been chosen due to their high performance, being commonly employed in tissue engineering, regenerative medicine, wound healing treatments or in controlled drug delivery systems as biocompatible and biodegradable devices in diverse architecture forms, such as beads, scaffolds, fibers, hydrogels, implants, protheses or nanocarriers (GOBI et al., 2021; MUIR & BURDICK, 2020; PARK et al., 2017).

To quote, the most hydrophilic, biocompatible and biodegradable polymers reported include the proteins and polyssacharides, such as chitosan (Aranaz et al. 2021; Kou, Peters & Mucalo, 2022), pectin (Li et al. 2021a; Roman-Benn et al. 2023), starch (Apriyanto, Compart & Fettke, 2022), alginate (Bi et al. 2022; Jadach, Świetlik & Froelich, 2022 and Mollah et al. 2021), and the synthetic polyvinyl alcohol (PVA) (Halima, 2016; Williams, Yo & Atala, 2019). On the other hand, the hydrophobics biocompatible and biodegradable include, the bio-based and semicrystalline, polylactic acid (PLA) (Deshmukh et al. 2017; Freeland et al. 2022; Mochizuki, 2009) and the synthetic and semicrystalline, polycaprolactone (PCL) (Arakawa & Deforest, 2017; Shadi, Karimi & Entezami, 2015 and Vandewalle et al. 2018), among others (Li et al. 2018[b] and Zang & Naebe, 2021).

In addition to the previously cited polymers, gelatin notoriety improved for presenting suitable characteristics such as amphoterism, high hydrophilicity, a rich amino acid composition that allows several chemical modifications and the RGD sequence which helps to promote cellular adhesion (BARANWAL et al., 2022; YOON et al., 2016). However, the use of native gelatin for biomedical applications presents some challenges main due to its poor mechanical strength, temperature, and water sensitivity, potential allergenicity, enzymatic degradation by proteolytic enzymes, and the needed of sterilization without affect their properties as well as the limited control over crosslinking (ALIPAL et al., 2021; FADDA et al., 2003; SKOPINSKA-WISNIEWSKA; TUSZYNSKA; OLEWNIK-KRUSZKOWSKA, 2021). From that, the use of modified gelatins is required and prominent and has been employed in biomedical devices as hydrogels for wound healing treatments, scaffolds in tissue engineering or as nanocarriers in controlled release of several molecules as drugs (Yasmin et al. 2017), peptides (Witting et al. 2015) and genes (Móran et al. 2015; Truong-Le et al. 1999) due to its affinity with

the plasmatic membrane which facilitates the endocytosis process by their usually cationic character (TSENG et al., 2013).

Furthermore, when used as nanocarriers (NCs) or drug markers, gelatin nanoparticles (GNPs) also have attracted great interest by its biocompatibility and biodegradability and have been prepared by several techniques, such as coacervation, nanoprecipitation (Baseer et al. 2019 and Khan, 2014), desolvation and mini-emulsification (Ethirajan et al. 2008). At the same time, the nanometric size helps to promote advantageous properties by providing a higher surface area available for modifications and by increasing and improving the bioavailability, solubility, and retention time, as well as the therapeutic value of bioactive molecules and water-soluble compounds (HUEPPE, WURM; LANDFESTER, 2002; GÜLSU; KILLI; ALPER, 2022).

An alternative approach to improve the poor characteristics of gelatin is the synthesis of poly(β-amino esters) or (PBAEs) synthesized via amine-acrylate addition reaction and that possess suitable characteristics such as the biocompatibility, biodegradability and responsiveness for biomedical applications (LIU et al., 2019; IQBAL & ZHAO, 2021; SHOOSHTARI & VAN DE MARK, 2001). According to Billiet et al. (2013) and Karimi et al. (2020), the aza-Michael addition reaction is a reliable approach for this purpose since it usually does not produce any undesirable side product (< 1 – 2%) while reacting primary and secondary amines with diacrylates. In addition, it has been considered a green route for PBAE synthesis by attending some click-chemistry requirements and by allowing achieving polymers with special properties such as pH-responsiveness and biodegradability that are inherent to tertiary amines and hydrolysable esters, respectively (LIU et al., 2019; MANZANARES-GUEVARA et al., 2018). The modified-gelatin hydrogels matrixes have found a wide range of applications due to its interesting features, such as charge reversal properties, the ability of mimic ECM (extracellular matrix) facilitating the nutrients and gases diffusion, the encapsulation and releasing of drugs and molecules or as constructions for cells-laden (NICHOL et al., 2010; BILLIET et al., 2013).

Based on these considerations, we intend to synthesize surface crosslinked gelatin nanoparticles (GNPs) that will serve as carrier platforms for hydrophilic drugs via an inverse miniemulsion approach by two distinct crosslinking strategies at the liquid-liquid interface: (1) aza-Michael addition reaction and (2) aza-Michael addition reaction followed by free radical photopolymerization. To the best of our knowledge, to date, only one study carried out by Ethirajan et al. (2008) has reported crosslinked GNPs synthesis

by inverse miniemulsion technique. However, some of the crosslinkers generally used for gelatin crosslinking, such as glutaraldehyde (GTA) and polyethylene glycol (PEG), have proven to be cytotoxic under some conditions and can render impracticable the intended biomedical applications (EDWARDS; DI; DYE, 2007; KHAN, 2014).

In this work, the aza-Michael addition was employed to prepare crosslinked poly(β-amino ester) gelatin-based hydrogels in solution and characterize to further nanoscale evaluate. In addition, we propose two routes for GNPs crosslinking using a diacrylate as a crosslinker agent (1,4-butanediol diacrylate) that allows to synthesize crosslinked nano-poly(β-amino esters) gelatin-based and the former followed by photopolymerization and/or photo-crosslinking reaction using DMPA (2,2-dimethoxy-2-phenylacetophenone) as photoinitiator. Finally, as a model drug, doxorubicin was encapsulated due to its high hydrophilicity and several biomedical applications as in cancer treatments and encapsulation efficiency studies were performed.

1.1 OBJECTIVES

1.1.1 General Objective

Synthesize crosslinked gelatin-based poly(β-amino esters) nanogels to serve as carriers of hydrophilic drugs.

1.1.2 Specific objectives

1. Synthesize covalently crosslinked gelatin hydrogels via aza-Michael addition reaction in solution through solution polymerization and characterize its thermal properties, swelling behavior physical and chemical composition;
2. Synthesize covalently crosslinked gelatin nanoparticles via interfacial aza-Michael addition reaction in inverse miniemulsion and characterize their morphology, particle size, PDI and colloidal stability;
3. Synthesize covalently crosslinked gelatin nanoparticles via dual curing photopolymerization technique in inverse miniemulsion and characterize their morphology, particle size, PDI and colloidal stability;
4. Evaluate the encapsulation efficiency of the hydrophilic model drug doxorubicin (DOX) in the GNPs redispersed in water.

2 LITERATURE REVIEW

2.1 BIO-BASED HYDROPHILIC POLYMERS IN THE BIOMEDICAL FIELD

In the last few years, researchers have made some efforts to synthesize environmentally friendly, biocompatible, and biodegradable polymers for the use in biomedical applications (FLARIS; SINGH, 2009; GEORGE et al., 2020). The natural biopolymers have raised as an interesting alternative for creation of biomedical devices mainly by being made up of repeating units that plays essential roles in a wide range of biological processes (KUMAR; KARISHMA, 2022; MUIR & BURIDCK, 2020; UDAYAKUMAR et al., 2021; WEI et al., 2020; YAASHIKAA).

The biopolymers are a class of polymers that can be obtained from vegetal or animal sources or produced by living organisms via fermentative processes and may be found in nature as structural components of cells, tissues, and organisms (LELKES et al., 2022). Generally, they possess special and valuable properties and characteristics extremely desirable to several uses, such as biocompatibility, biodegradability, stimuli-responsiveness, and cell-adhesion (CHOI; PARK; LEE, 2022; MUIR & BURDICK, 2020).

In this context, a novel and diverse class of materials has being developed from the inherent characteristics of these biopolymers including several biomedical devices, such as in tissue engineering (Park et al. 2017 and Okamoto & John, 2013), wound healing treatments (Singh; Shitiz; Singh, 2017 and Vijayakumar et al. 2019), scaffolds (Tian et al. 2020 and Park et al. 2017) beads (Ma et al., 2013; Rawat & Maiti, 2021; Vikulina & Campbell, 2021), fibers (Temesgen et al. 2021; Strassburg, Mayer & Scheibel, 2022), hydrogels (Dhand, Galarraga & Burdick, 2021; Muir & Burdick, 2020) and nanoparticles (Gobi et al. 2021; Jacob et al. 2018 and Singh, 2011) among others applications, e.g. food packing, food emulsions, edible films and etc. as reported in the review of Udayakumar et al. (2021).

As mentioned by Dickinson (2017), by having their own variety of structures, they are frequently used as stabilizing agents assisting in the formation of gel-like structures. Nonetheless, the process of obtaining and purifying is high cost, making the use of these materials more difficult, reinforcing the need to conduct studies in this regard

to overcome these challenges (AWE et al., 2017; EFTHIMIADOU et al., 2018; UDAYAKUMAR et al., 2021).

Among them, the polysaccharides, polypeptides, and polyesters are the most employed, such as pectin, dextran, lignin, cellulose, chitosan, and gelatin (YAASHIKAA; KUMAR; KARISHMA, 2022). Moreover, due to reduced thermal and mechanical properties are commonly modified from an infinite of reactional routes by possessing desirable chemical groups which are susceptible to modifications to improve and enhance its properties according to their specific objective and functionality (LÓPEZ et al., 2020). In addition, biopolymer modifications also help to offers responsiveness to several stimuli such as pH, UV radiation, enzymatic and radical degradation which may affect their entirely application by susceptibility in interact with the biological substrates (UDAYAKUMAR et al., 2021).

Nevertheless, in some cases, chemical modification of more hydrophobic biopolymers is carried out with the aim of making them more hydrophilic by adding chemical groups of more water-affinity (SHEEHAN et al., 2022). On the other hand, proteins highlighted among the most hydrophilic biopolymers due to the large amounts of functional amino groups, carboxylic acids, amides, and hydroxyls present in the polymer chain, which allow greater interaction with water and biological fluids (MUIR & BURDICK, 2020).

In this sense, gelatin notoriety has gained space in scientific community and has been widely used for presenting such characteristics that are essential for biomedical applications and in the construction of several biomaterials and medical devices currently employed for these purposes, e.g., bone regeneration (Dong et al. 2019 and Echave et al. 2017), cell administration (Li et al. 2018 and Xu et al. 2013), implants (Langley et al. 1999 and Wong et al. 2010) among others (Sharma; Kaith; Arora, 2022).

2.1.1 Gelatin

Several sources (e.g., bovine, porcine and marine) and animal parts (e.g., skin, tissues, cartilage, ligaments, and bones) from which collagen and gelatin can be extracted are reported in the literature (NITSUWAT et al., 2021; SUHAIMA et al., 2022). Collagen is the main protein that constitutes the extracellular matrix (ECM) in animals and has a three-dimensional structure in triple helix form (BRODSKY; RAMSHAW, 1997). On the other hand, gelatin (Figure 1) is a biomacromolecule, composed of a heterogeneous

mixture of water-soluble proteins of high molecular masses, that are extracted from partially hydrolyzed collagen and isolated after denaturation (BOZEC; ODLYHA, 2011; OFOKANSI et al., 2010). In addition, denaturation provides gelatin the advantage of relatively low antigenicity and gelling point compared to collagen (YOON et al., 2016). Furthermore, different types of gelatins can be obtained from different hydrolysis conditions, type A gelatin is obtained from acid hydrolysis and type B gelatin from alkaline hydrolysis (ALIPAL et al., 2021). Then, the molecular configuration and distribution of functional groups are some of the main differences between gelatins of different types.

Figure 1 – Chemical structure of gelatin.

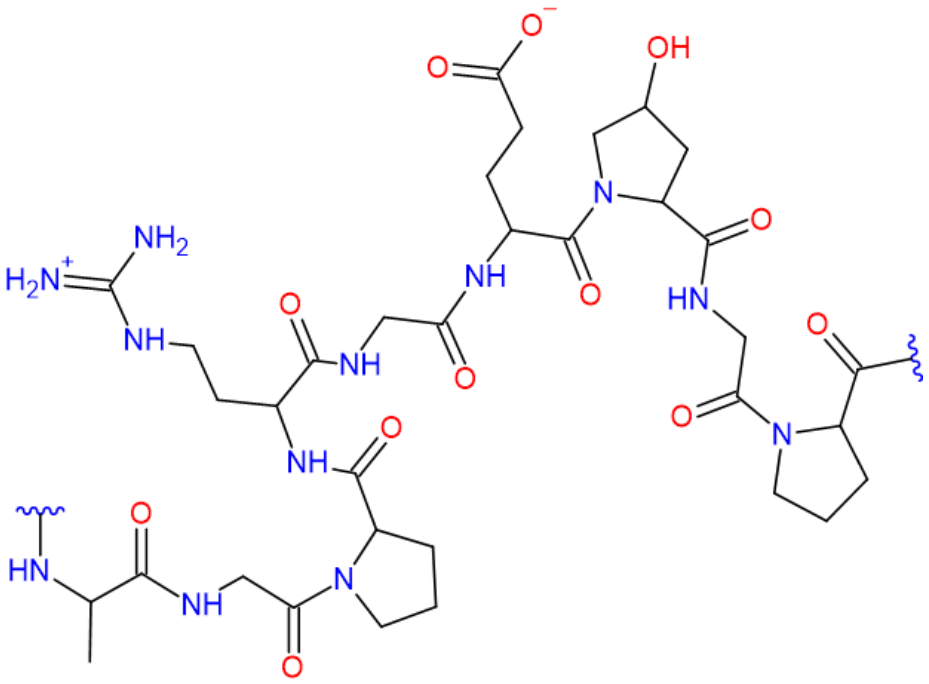

Drawn in ChemSketch (2022).
Source: Author (2022) adapted from Noor et al. (2021).

Nonetheless, the study conducted by Johlin (1930) has proved the relation of IP with the minimum physical properties of pure gelatin such as conductivity, osmotic pressure, viscosity among others. In gelatin, the IP varies according to the type and source from which it is extracted due to differences in moieties of carboxyl, amino and guanidino groups on the side chains (SU & WANG, 2015). For instance, the presence of amino groups is greater in type A gelatins and of carboxylic groups in type B gelatins. Therewith, type A gelatins also have a higher IP (6 – 9) since the acid treatment is not able to cleave

the amide bonds of the glutamine and asparagine portions present in collagen. However, in type B gelatins, cleavage occurs, leading to a lower IP (4.7 – 5.4) due to a higher production of acidic amino acids and, consequently, a higher proportion of carboxylic groups, making them negatively charged when at pH neutral (BASEER et al. 2019). Another type of gelatin is mentioned in the study carried out by Ji et al. (2022) were they mentioned the "type E" gelatin, in which gelatin was obtained after enzymatic hydrolysis with IP varying from 7.0 to 9.0.

For instance, the study conducted by Aramwit et al. (2015) has proved that the efficiency of drug delivery from gelatin nanoparticles differs for each type of gelatin, being higher in type B because it was more crosslinked than type A. In addition, type B gelatin is also more biocompatible compared to type A. Another study carried out by Lee et al. (2016), the authors reported that type A gelatin is more suitable for bioink applications by produce printed constructions with better resolutions than type B at the same extrusion pressure, however, when using type B gelatin, they found a slightly degree of methacryloylation than using type A. Additionally, as shown by Baydin et al. (2022), type A gelatin is more stable on long-term storage than type B gelatin by being more resistant to hydrolysis.

Gelatin is considered a versatile biopolymer due to its amino acid-rich composition and, among natural polymers, it is preferred and known for its relatively low cost and for presenting excellent and desirable characteristics for the design and development of new functional materials, such as biodegradability, hydrophilicity, low toxicity, biocompatibility, as it is anti-carcinogenic and has non-immunogenic properties (KHRAMTSOV et al., 2021; SULTANA; ALI; AHAMAD, 2018; YOON et al., 2016). It is soluble in water, glycerol, and acetic acid and insoluble in practically all organic solvents such as alcohol, chloroform, ether, acetone, and others (GHORANI et al., 2020; LARSON & GREENBERG, 1933; SANWLANI; KUMAR; BOHIDAR, 2011).

However, a study conducted by Mehta et al. (2017) has shown the potential ability to achieve high solubility (> 87%) of gelatin capsule waste via extraction with protic ionic liquids (alkyl ammonium nitrates and their binary mixture system with 1-butyl-3-methyl imidazolium chloride). In addition to these characteristics, it has an amphoteric behavior and the property of gel formation at mild temperatures (≈ 35 ºC). The phase behavior in solution is influenced by water activity, temperature and pH, factors that justify its use in drug delivery systems (MASULLO et al., 2020; MIYAWAKI; OMOTE; MATSUHIRA, 2015).

It is mainly composed of 18 amino acids, which provide a high biological value and protein content, distinguishing it from other polymers by the presence of a sequence of amino acid chains that, for example, facilitates cell adhesion and spreading, such as Arg-Gly-Asp (RGD) which are also the cell attachment sites recognized by many integrins (MUIR & BURDICK, 2020; YOON et al., 2016; XING et al., 2014). As mentioned by Wang et al. (2012), these amino acids play a key role in the final biological performance of gelatin compared to synthetic polymers that lack these cellular recognition sites. Nonetheless, their physicochemical characteristics may vary according to the source and extraction method (e.g., molecular mass, proximate composition, isoelectric point (IP), bloom (gel strength), mesh (granulometry) etc.) (HUE et al., 2017; MULYANI et al., 2017; TU et al., 2015). In this context, the isoelectric point (IP) is related to the structural and colloidal stability of proteins and can lead them to aggregation caused by changes in physiological factors such as temperature, ion concentration and pH (LAUTENBACH; HOSSEINPOUR; PEUKERT, 2021).

According to Osorio and co-workers (2007), the force (weight) necessary to depress a given sample area of gel by a distance of 4 mm is defined by bloom and as the bloom number increases the stronger the gel is. Another important parameter is the molecular weight distribution that is highly heterogeneous and consists of water-soluble protein fractions (α (~$90 \cdot 10^3$ g·mol^{-1}), β (~$180 \cdot 10^3$ g·mol^{-1}) and γ (~$300 \cdot 10^3$ g·mol^{-1}) peptide chains) of different molecular weights (JI et al., 2022; TU et al., 2015; ALIPAL et al., 2021; MARIOD & FADUL, 2013). According to the manufacturer data, the average molecular mass is proportional to bloom number, and it may vary in the range of 20 – 25 kDa for low bloom gelatins (50 – 125), 40 – 50 kDa for medium bloom gelatins (175 – 225) and 50 – 100 kDa for high bloom gelatins (225 – 325) (SIGMA ALDRICH, 2023).

However, higher values for gelatin molecular weight can be found in the literature since it is partly formed by aggregates of high molecular weight, then, the common techniques (e.g., polyacrylamide gel electrophoresis and SEC/GPC) used for the determination have some limitations and don't allow to quantify molar masses higher than $7.5 \cdot 10^7$ g·mol^{-1}. From this, new approaches have been developed to this end, like in the study carried out by Duthen and co-workers (2018), the authors applied a chemometric approach based on UV absorbance and the Asymmetrical Flow Field Flow Fractionation coupled to an Ultraviolet and Multi Angle Light Scattering (AsFIFFF-UV/MALS) to evaluate the molecular mass of 49 different types of type A industrial

gelatins and they found molar masses higher than $1 \cdot 10^7$ g·mol^{-1} with good correlation (R^2 ≥ 79%) between the approaches used.

As presented in Table 1, among the main amino acids present in its molecular chain, glycine, proline and 4-hydroxyproline stand out in greater amounts (≈ 57%), while glutamic acid, alanine, arginine, and aspartic acid amino acids families are present in the lower concentrations (≈ 43%) (SULTANA; ALI; AHAMAD, 2018; ALIPAL et al., 2021).

Table 1 – Gelatin amino acid composition from different quantification techniques.

Amino acid (aa)	g aa/100 g of gelatin	g aa/100 g of raw protein	Reference
Alanine	10.7	8.6	
Arginine	4.5	7.3	
Aspartic acid	4.8	5.8	
Glutamic acid	7.7	10.2	
Glycine	32.6	22.2	
Histidine	0.6	1.0	
Hydroxyproline	10.0	11.9	
Isoleucine	1.1	1.4	Gelita (2019)[a];
Leucine	2.3	2.7	Billiet et al. (2013)[b];
Methionine	0.7	0.9	Farris, Song and
Phenylalanine	1.4	2.1	Huang (2010)[c].
Proline	12.1	12.7	
Serine	3.4	3.2	
Threonine	1.7	1.8	
Lysine	2.6	3.6	
Hydroxylysine	1.1	1.6	
Tyrosine	0.4	0.8	
Valine	2.3	2.4	

[a]Determined by HPLC via fluorescence detection (results expressed in wt.%);
[b]Determined by HPLC via fluorometrically detection (results expressed in weight);
[c]Determined by colorimetric essay via fluorescence titration (results expressed in mol%);
Source: Author (2023).

Especially, because of its interesting characteristics, numerous functional groups and unique peptide sequences, gelatin is generally recognized as safe (GRAS) for human consumption by the United States Food and Drug Administration (FDA) and a promising platform for several applications, including biomedical ones (e.g., controlled drug delivery systems of peptides, genes, DNA, RNA, and other molecules) (FDA, 2022).

For these reasons, it is quite suitable for chemical/physical hydrogels synthesis in various forms such as sheets, films, fibers, membranes, micro and nanoparticles by reacting it with small molecules containing highly reactive functional groups (e.g., aldehydes (El-Meligy et al. 2022 and Lin et al. 2019), esters (Wang et al. 2018 and Zhuang, Tao and Cui, 2015), acrylates (Nath et al. 2020 and Golubevas et al. 2020), methacrylates (Bupphathong et al. 2022 and Xiao et al. 2019) and others (Yang et al. 2016 and Yung et al. 2007).

2.1.2 Quantification of free primary amine groups in gelatin

The determination of the total amount of free primary amines in gelatin is necessary, as it allows the synthesis of biomaterials with adjustable formulations by modifying reaction stoichiometry as a function of crosslinker concentration, in addition to providing additional information about composition of the material itself. With this purpose, several colorimetric and instrumental approaches have been reported in literature for free primary amines quantification in biomaterials, including gelatin (e.g., TNBS acid essay (Baseer et al. 2019 and Kuijpers et al. 2000), ninhydrin essay (Zatorski et al. 2020), fluorescence titration (Farris, Song and Huang, 2010) and HPLC (Billiet et al. 2013). However, there is no consensus on which is the most suitable method to be applied, and combined methods are often used.

The ninhydrin (2,2-dihydroxyindane-1,3-dione) quantification method consists of a chemical reaction between the ammonia, free primary or secondary amino groups (DAS & BANIK, 2021; RUHEMANN, 1910). The ninhydrin reaction with gelatin occurs in a stoichiometric ratio of (1:2) in the presence of a solvent (e.g., water, ethanol, butanol, or acetone), at temperatures between 70 and 100 °C, according to the reaction shown in Figure 2. After reaction time of 30 min, the solution acquires a purple color, indicating the presence of the formed compound (Ruhemann's purple) which is read at 570 nm and, frequently, amino acids (lysine, leucine, and others) calibration curves are used as reference (ZATORSKI et al., 2020).

The ninhydrin quantification method is more sensitive than TNBS because it can react with ammonia in addition to α-amino groups. Nevertheless, although being a simple method, offers some disadvantages such as more complex analytical procedure, fast reversible reaction time with water, leading to sample color changing, which difficults the measurement standardization (CLEGG; LEE; MCGILLIGAN, 1982). Moreover, it is

not effective to detect proteins with high molecular weight by the steric hindrance which limits the reaction between ninhydrin and α-amino groups (PERRETT; NAYUNI, 2014; SAPKOTA & ARYAL, 2022; TIWARI, 2015). Nonetheless, in the case of gelatin, polymer precipitation with ethanol can also occur and optimal range of temperature, solvent, ninhydrin, and polymer concentration are needed to allow a correct estimation as verified by Zatorski et al. (2020).

Figure 2 – Summarized reaction mechanism with ninhydrin.

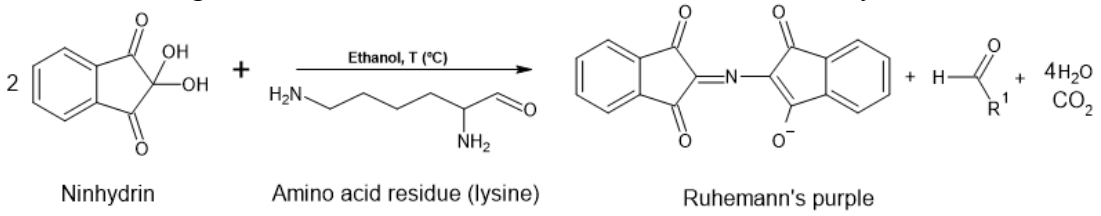

Draw in ChemSketch (2022).
Source: Author (2022) based on C. Lennard, in Encyclopedia of Analytical Science, 2005.

Another commonly used colorimetric method reported for ε-amino groups determination in gelatin is the 2,4,6-tribenzenesulfonic acid (TNBS) essay. According to Fields (1972), in this method is used milder reaction conditions compared to ninhydrin test and accordingly to Shinoda & Satake (1961) study, in the higher molecular weight peptides, the TNBS approach is more sensitive than ninhydrin test.

However, differently from the ninhydrin test, by using this technique, the reaction between amino groups takes place with sulfonic groups present in TNBS, producing an orange-yellow colored compound as shown in the global reaction (Figure 3). The hydrolyzed final product is diluted in water, and, in sequence, ethyl ether or ethyl acetate are added to remove the excess TNBS not reacted and then the hydrolysate is separated from the aqueous phase. After this, an aliquot is withdrawn and diluted again in distilled water, heated to remove the remaining ether and, subsequently, the absorbance is measured at 340 to 420 nm and values are generally quantified in mols of lysine·$g_{gelatin}^{-1}$ (CAYOT & TAINTURIER, 1997; KALE; BAJAJ, 2010; KONGTON et al., 2016; LEE et al., 2015; YOON et al., 2016).

Figure 3 – Global reaction between 2,4,6-TNBS acid with amino acid moiety.

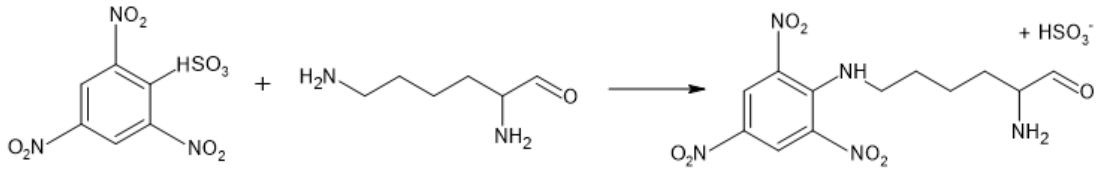

2,4,6-TNBS Amino acid residue (lysine) Orange-yellow colored product

Draw in ChemSketch (2023).
Source: Author (2023) based on Cayot & Tainturier (1997).

An instrumental and efficient approach to determine the remaining free amine content (lysine and hydroxylysine are the most referenced used amino acids) in gelatin is the ^{1}H-NMR technique. This method is based on the degree of modification (DM) of these amino acids and has been utilized as proposed by authors Claaßen et al. (2018) and Billiet et al. (2013) during the synthesis of modified gelatins. It basically consists of an integrating determined peaks in gelatin derivative polymers and its later comparison with the original peaks from non-modified polymer, then, spectra are associated to specific amino acids peaks by utilizing the own amino acid inert hydrogens as reference (e.g., phenylalanine, leucine, or isoleucine moieties) or any standard solvent (e.g., thetramethylpropylsilane (TMPS)).

In Zatorski and co-workers (2020) study, the ninhydrin essay and ^{1}H-NMR spectroscopic technique were used to quantify the degree of functionalization in chemically modified gelatin and the concentration of free primary amines in freeze-dried pure gelatin, respectively. In addition to amino groups quantification, in another study, Van Hoorick et al. (2017) applied the ^{1}H-NMR technique, which also proved to be efficient in the quantification of carboxylic groups in photocrosslinkable gelatins, synthesized from functionalization of these functional groups with 2-aminoethyl methacrylate hydrochloride (AEMA·HCl).

Finally, as gelatin is a complex heterogeneous material, the concentration of free primary amines and carboxylic groups present in the final polymer may vary according to the source, method and treatments by which it is extracted as well as to specific characteristics of material as aforementioned. Then, the approximate values of 0.315 mmol (Kuijpers et al. 2000), 0.30 mmol (Zatorski et al. 2020), 0.292 mmol (Sisso, Boit and Deforest, 2020), 0.35 mmol (Claaßen et al. 2018) of ε-amino groups/g gelatin for type A gelatin and 0.33 mmol (Ofner & Bubnis, 1996), 0.385 mmol (Van Hoorick et al. 2017) and 0.23 mmol (Grover et al. 2012) of ε-amino groups/g gelatin for type B gelatins are reported. In addition, for carboxylic (COOH) groups, approximately values of 0.846

mmol (Sisso, Boit and Deforest, 2020) and 0.77 mmol (Kuijpers et al. 2000) carboxylic groups/g gel for type A gelatins and 1.26 mmol (Ofner & Bubnis, 1996), 1.09 mmol (Van Hoorick et al. 2017) 1.18 mmol (Kuijpers et al. 2000) carboxylic groups/g gel for type B gelatin are reported.

2.1.3 Gelatin crosslinking

As previously mentioned, due to its poor mechanical and thermal resistance and high hydrophilicity, in its raw natural form, gelatin applications are generally limited to its modified form, which directly contributes to the development of new methodologies (EHRMANN, 2021). However, as it is an extensive and complex molecule, rich in functional groups, it has characteristics and structure favorable to modifications via chemical derivatization, such as functionalization (Van Hoorick et al. 2017; Claaßen et al. 2018), copolymerization (Dang, Li & Yang, 2019 and Kuznetsova et al. 2020) and crosslinking (Ethirajan et al. 2008 and Liu et al. 2020). Therefore, such approaches are used to obtain new molecules with moldable characteristics for specific purposes (DANIELSEN et al., 2021). In addition, a variety of reactive molecules have been used in gelatin modification via amino, carboxyl and hydroxyl groups (FARRIS; SONG; HUANG, 2010; LIN et al., 2019).

Recently, among the different approaches, crosslinking has been widely used to improve thermal, mechanical and water sensitivity properties in devices for long-term use (DANIELSEN et al., 2021). Therewith, the low thermal and mechanical strength of gelatin hydrogels can be overcome through crosslinking, from the formation of interpenetrating networks (IPNs) or through crystallization, which induces the formation of crystallites that drastically reinforce the polymeric structure for example (FAROOQ; TEUWEN; DRANSFELD, 2020; MYUNG et al., 2008).

Hydrogels are hydrophilic three-dimensional polymeric networks that can be physically or chemically synthesized from synthetic or natural polymers (HABANJAR et al., 2021; MAITRA & SHUKLA, 2014). They also can mimic the natural extracellular matrix (ECM) being used three-dimensional cell culture and therapy or in wound healing treatments as dressings due to their high fluid absorption capacity, as well as in drug delivery and tissue engineering by promote high cell adhesion and proliferation (YOON et al., 2016; VANDERHOOFT et al., 2009). Furthermore, hydrogels also exhibit appreciable characteristics such as thermo-responsiveness, elasticity and swelling (ability

to absorb/swell in the presence of water and/or biological fluids without dissolving) and such properties might be attributed to crosslinking in the polymeric chain (DANIELSEN et al., 2021; SPONCHIONI; PALMIERO; MOSCATELLI, 2019). In the case of gelatin, crosslinking has been utilized to prepare hydrogels that are stable under physiological temperature (37 ºC) and with better resistance towards degradation by proteolytic enzymes such as collagenases and gelatinases (NICHOL et al., 2010).

In summary, crosslinking (Figure 4) consists in the formation of reversible physical bonds (e.g., hydrogen, ionic and van der Waal's bonds) or irreversible covalent chemical bonds in the polymeric structure (PARHI, 2017).

Figure 4 – General hydrogel synthesis via chemical crosslinking reaction.

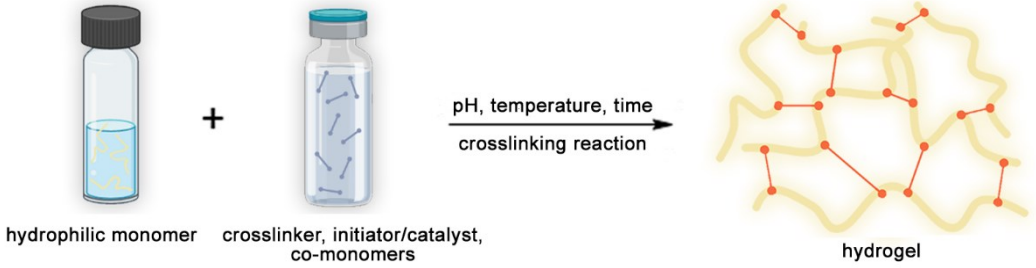

Drawn in Biorender and Photoshop CS6 (2023);
Source: Author (2023).

In summary, chemical, or physical crosslinking is commonly employed to keep the spatial structure (shape) of hydrogel and improve drug circulation time in vivo. Gelatin hydrogels have also been synthesized and crosslinked by enzymatic reactions, with tyrosinase and transglutaminase (LIU et al., 2020). In terms of stimuli-responsiveness, in physically crosslinked hydrogels they are often reversible, while in chemically crosslinked hydrogels they are not (PARHI, 2017).

In addition, the crosslinking degree (ϵ) is another extremely important parameter since the physical state of hydrogels is altered by changes in the crosslinking degree. Some examples can be found in the works carried out by Dou et al. (2023) and Zhai et al. (2017). Furthermore, in applications such as controlled release or culture of adjustable 3D cells, the precise control of crosslinking density (q) is necessary, as it is related to extrudability, rigidity and shear-thinning properties of synthesized materials which directly impact their use (GHAVAMINEJAD et al., 2020). The properties of gelatin-based materials are strongly affected by the crosslinking degree, as observed in the work of Lin & Gu (2015). The crosslinker concentration also helps to tune the inherent properties of hydrogels, especially the swelling ratio (KHAN & RANJHA, 2014).

However, not only the crosslinker concentration can affect the final characteristics of these biomaterials, but also pH and temperature in which the crosslinking reaction takes place, among others (e.g., reactants concentration). It is known that these factors can directly affect the stability of proteins leading to their complexation and precipitation (LI et al., 2023; SALMINEN et al., 2022). In the case of gelatin, pH can influence density and charge distribution, as it determines the protonation degree of amino groups and the presence of negative charges on the carboxylic groups (GHANI, 2016).

Thereupon, crosslinked polymers are classified into polymers with low or high crosslinking density according to the average amount of crosslinking per unit volume (YE et al., 2015). This parameter can be measured and obtained from several sources, such as colorimetric or extraction methods and by means of the Flory-Rehner theory.

From that, several techniques and chemical compounds have been used to crosslinking gelatin (Table 1). The crosslinking agents are additives used in organic synthesis to promote the formation of covalent bonds between polymers chains, creating a three-dimensional structure main through of the abstraction of hydrogen atoms, formation of free radicals, or other chemical reactions depending on the type of polymer and crosslinking agent employed. It can occur through various methods, and the choice of technique depends on the specific requirements of the final product (GENG et al., 2021; GHAZINEZHAD; BOZORGIAN; GHOLAMI DASTNAEI, 2022).

For instance, there is a consensus in literature, as observed in the works of Ethirajan et al. (2008), Farris, Song and Huang (2010) and Zhan et al. (2016), that the gelatin crosslinking with glutaraldehyde occurs through nucleophilic addition between the aldehyde functional groups with the ε-amino groups of deprotonated lysine and hydroxylysine, however, these materials have proven cytotoxicity, requiring the search for alternative compounds that improve its biocompatibility and biodegradability.

2.2 SUPERABSORBENT POLYMERS (SAPs)

Since its development in the early of 1940’s, the superabsorbent polymers (SAPs) class have been widely used (about 95% of total market share) in disposable health care products (DHCPs) such as baby diapers, female sanitary, incontinence,

hygienics and bio-related products as well as applications in constructions and agriculture in the last 80 years (GOOCH, 2010).

To date, the most widely used class of superabsorbent polymers are the crosslinked acrylated polymers derived from poly(acrylic acids), such as the poly(acrylamides), poly(acrylonitriles) and their salts, due to their unique properties such as the presence of hydrophilic groups and the properly crosslinked structure (CHEN et al., 2022). From this point, among others interesting features, they are preferred due to their notably superior water absorbent properties and highly hydrophilic network that can imbibe and retain great amounts of liquids even under pressure (VENKATACHALAM & KALIAPPA, 2023). Moreover, their absorption mechanism is based on osmotic pressure and when compared to usual hydrogels, they also have the advantage of taking up a thousand times their own weight unlike most hydrogels that can take up no more than ten times (BEHERA & MAHANWAR, 2020).

For now, the market share is expected to increase up to 12.9 billion USD until 2024 due to population growth and the average age of people (CHEN et al., 2022). However, the currently used SAPs used in DHCPs are predominantly crosslinked polyacrylic acid based and even though they have superior water absorption characteristics, high molecular weight, long carbon-carbon chain (C-C) and crosslinked structure also have a poor biodegradability (AJEKWENE, 2020; CHOI; PARK; LEE, 2022). The raw materials used to its synthesis are usually petroleum-based and after use are quite contaminated, possessing a high liquid content and being difficult to recycle or unsuitable for energy generation (VENKATACHALAM & KALIAPPA, 2023).

Due to the growing environmental concern regarding microplastic pollution, according to Chen et al. (2022), the development of biodegradable alternatives can be the ultimate eco-friendly solution to overcome this problem. Until now, some alternatives have been proposed such as the synthesis of superabsorbent polymers based on biopolymers, the polysaccharides (cellulose, starch, chitosan, pectin and guar gum) and proteins (gelatin and amino acids) are the most used by having a significant number of hydrophilic groups in their structure (CHOI; PARK; LEE, 2022; ZOHOURIAN & KABIRI, 2008). Furthermore, these materials have been synthesized from the modification (e.g., grafting or crosslinking) of these natural polymers with acrylated polymers to make them more biodegradable and biocompatible (ARSLAN, 2020; AJEKWENE, 2020). For example, it is known that the grafting of acrylic acid moieties

can provides a high-water absorption capacity to these polymers-type (VENKATACHALAM & KALIAPPA, 2023).

In view of the problem exposed, the acrylic (AEs) or diacrylic esters (DAEs) have been widely studied as acrylic compounds for polymer modifications and PABEs synthesis by their known desirable properties. The diols-AEs or -DAEs stand out as superabsorbent polymers derived from acrylic acid commonly used as multifunctional crosslinker agents.

The 1,4-butanediol diacrylate (Figure 5) or 1,4-BDDA (*CAS* number: 1070-70-8) and its chemical derivative family is one of the most crosslinkers reported. The IUPAC name is 4-prop-2-enoyloxybutyl prop-2-enoate or synonyms names butane-1,4-diyl diacrylate, tetramethylene glycol diacrylate, butylene diacrylate, among others (PUBCHEM, 2023). It is considered as colorless and sweet-tasting liquid with molecular weight of 198.22 $g \cdot mol^{-1}$, molecular formula: $C_{10}H_{14}O_4$, containing ~75% ppm hydroquinone as inhibitor, density = 1.051 $g \cdot mL^{-1}$ at 25 ºC, refractive index = 1.456, boiling temperature = 340.95 ºC at 760 mmHg, fulgor point > 113 ºC, water solubility = 3.1 $g \cdot L^{-1}$ and extensively used in applied in drying technology of coatings, inks and adhesives (SIGMA ALDRICH, 2023a, 2023b; CHEMSPIDER, 2023).

Figure 5 – Chemical structure of 1,4-butanediol diacrylate.

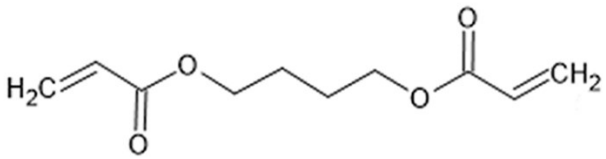

Drawn in ChemSketch (2023);
Source: Author (2023).

In addition to 1,4-butanediol diacryate, the 1,6-hexanediol diacrylate (1,6-HDDA), trimethylolpropane triacrylate (TMPTA), ethylene glycol dimethacrylate (EGDMA), triethylene glycol dimethacrylate (TEGDMA) and bisphenol A glycerolate (1 glycerol/phenol) diacrylate (BGDA) are also employed as crosslinkers agents (GONZÁLEZ et al., 2015).

Due to the presence of hydrolytically degradable ester bonds, they improve the biodegradability of modified compounds being able to reduce the cytotoxicity caused by necrosis and apoptosis (ELTOUKHY, et al., 2012; LIU et al., 2019). Based on the manufacturer's safety data sheet (SDS), toxicity tests indicated irritation to the skin, eyes,

mucous membranes and upper respiratory tract in rats and rabbits. It did not show mutagenicity in germ cells by Ames, micronucleus, and gene mutation tests in mammalian cells in vitro. However, biodegradability tests after 22 days of aerobic exposure resulted in 90 – 100% biodegradability. Further, information on carcinogenicity is still scarce (SIGMA ALDRICH, 2023b).

As mentioned by Shooshtari & Van de Mark (2001a) the acrylic esters also modify physical and chemical properties as well as the long-term performance of the polymeric system mainly due to the inherent SAPs and esters characteristics and due to the chemical structure susceptible and favorable (two double bonds (CH_2=CH_2)) to several type of modifications, such as nucleophilic addition. In addition, according to Bukhari et al. (2015), it is well-known the polyanionic nature of the poly(acrylic acids) and their derivatives, being frequently used in the design of pH-responsiveness macromolecular devices manly for drug delivery applications. The dissociation constant (pK_a) of poly(acrylic acid) is estimated to be between 4.5 and 5.0 which favors a high swelling at physiological conditions (pH 7.4) due to the ionization of anionic carboxylic acid groups. For AE or DAEs, the polyanionic nature is related to acrylate groups on their structure which can donate electrons and form anions (acrylate ion, CH2=CHCOO$^-$) when the COO- bond is broken and an electron from this group is donated to another. From that, as informed by the Human Metabolome Database (HMDB, 2023), the dissociation constant (pK_a) of the methacrylic or acrylic esters are usually strongest basic, and equal to (6.5) for 1,4-butanediol diacrylate (1,4-BDDA) and (9.5) for ethylene glycol dimethacrylate (EGDMA) at 25 ºC, determined by ChemAxon software. In addition, as mentioned by Briede et al. (2022) and as can be found in the technical bulletin of the Braskem (2023), the acrylic esters and polyesters stand out among the most used plasticizing compounds.

Furthermore, the use of aza-Michael addition reaction with acrylic compounds makes it possible to obtain PBAEs which are proven biodegradable polymers with some special characteristics according to mentioned by Liu et al. (2019). The presence of protonable amino groups, as tertiary ones, makes them cationic (protonated) when pH close to neutrality or acid, also presenting the pH-responsiveness behavior. Moreover, crosslinking usually gives to polymer a more hydrophobic characteristic (but not necessarily) due to insertion of hydrophobic crosslinker moieties in the original polymer backbone, giving it a greater resistance to degradation, as previously mentioned, and such

characteristics are suitable for biomedical applications in terms of controlled release and delivery of drugs, tissue regeneration and wound healing treatments.

2.3 GELATIN CROSSLINKING VIA AZA-MICHAEL ADDITION REACTION

The aza-Michael addition reactions were discovered and proposed by Arthur Michael in 1887 during addition of sodium diethylmalonate and sodium ethylacetatoacetate to synthesize ethyl cinnamate (MICHAEL, 1887). From that, Michael's 1,2- and 1,4- addition reactions are one of the largest and most diverse classes of reactions and have received relevant attention in recent decades being basically composed of nucleophilic additions to unsaturated carbonyl groups allowing construction of β-amino carbonyl derivatives such as poly(β-amino esters) (CORNILLE et al., 2017; DALPOZZO; BARTOLI; BENCIVENNI, 2011; PEYRTON & AVÉROUS, 2021).

In addition, aza-Michael addition reaction find many uses that vary from synthesis of amphoteric surfactants to in situ polymer modifications in biological systems or to hyperbranched polymers (dendrimers) and meets some click chemistry requirements such as orthogonality, high efficiency and speed, use of mild conditions (e.g. absence of metallic catalysts, non-use of solvents or solvents of easy separation, low temperatures, in addition to allowing high yields without generating by-products), presenting themselves as valuable tools in polymer synthesis (BERNE et al., 2022; CHEN & MA, 2014).

Therefore, the occurrence of the 1,2- or 1,4- additions (Figure 6 – a) and b), respectively) depends on many factors and it is often determined by polarity of the medium and nature of nucleophile since during nucleophile addition there is a competition between 1,2- and 1,4- addition products (MALKAR; JADHAV; YADAV, 2020). On the one hand, when using strong bases as nucleophiles, additions to carbonyl are faster, and the predominance of 1,2- addition products is expected, in these cases, both types of reactions are irreversible and are under kinetic control. Inversely, using weak bases as nucleophiles (e.g., amines and alcohols) the 1,2- additions are generally reversible and are under thermodynamic control, and, in this case, 1,4- additions products are predominant due to the retention of carbonyl stable group (BERGMANN; GINSBURG; PAPPO, 1959; MATHER et al., 2006).

Finally, the α,β-unsaturated enones or carbonyls refers to conjugation of a double bond to a carbonyl group which, in turn, pass on the electrophilic character of carbonyl carbon to beta carbon of the double bond. In this context, 1,4- additions, also known as conjugated addition refers to conjugated addition of a nucleophile (Michael donors) to unsaturated molecules with electron-withdrawing substituents (Michael acceptors), such as α,β-unsaturated carbonyl compounds (esters, aldehydes, ketones, carboxylic acid derivatives, nitriles, beta carbons and others) which may or not catalyzed by base, acid or metal (BERNE et al., 2022; VINOGRADOV; TUROVA; ZLOTIN, 2019).

Figure 6 – General (a) 1,2- and (b) 1,4- aza-Michael addition reaction products.

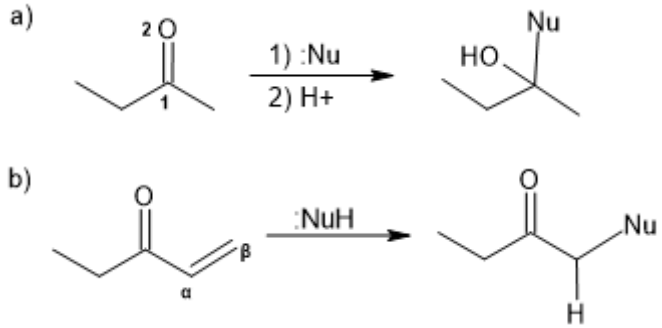

Drawn in ChemSketch (2022);
Source: Author (2022) based on Machado (2019).

The main nucleophiles used are water (H_2O), alcohols (R-OH), thiols (R-SH), primary and secondary amines (R-NH_2 and R-NH), hydrogen bromides (HBr), cyanides (KCN) and/or any carbanion stabilized (PEYRTON & AVÉROUS, 2021; WORCH et al., 2021). Frequently, thiols are more nucleophilic than amines and bases (catalysts) are commonly added to deprotonate them, e.g., DBU (1,8-Diazabicyclo[5.4.0]undec-7-ene) (ARSLAN, 2020; XIANG et al., 2020). On the other hand, when using an amine, the catalysts additions may not be necessary, since they can function as both in this type of reaction (GENEST, et al., 2017; VINOGRADOV; TUROVA; ZLOTIN, 2019). In the case of amines, the reaction involves a primary or secondary amino group as the nucleophile and an electron-deficient alkene group as the acceptor, and the reactions can be carried out under various conditions and stoichiometric ratios (CORNILLE et al., 2017). The reactivity of Michael donors generally increases with donor nucleophilicity of the donor but also depends on steric hindrance (GENEST et al., 2017). Furthermore, the reaction rate is highly affected by steric hindrance which depends on the type of nucleophile and acceptor used (MATHER et al., 2006).

According to literature, the order of reactivity for amine addition to unsaturated esters typically decreases in following order: acrylates > maleates > fumarates > methacrylates (SHOOSHTARI, 2000). This information can be confirmed in the work carried out by Imanzadeh et al. (2010) during PBAE synthesis via aza-Michael addition of 1,2,3,6-Tetrahydrophthalimide to symmetrical fumaric esters and acrylic esters under solvent-free conditions, they observed when using methyl acrylate and ethyl crotonate as Michael acceptor were unsuitable for this type of reaction. Furthermore, according to acrylic reactivity order, most methacrylates have much lower reactivity than acrylates and this is due to the steric hindrance caused by methyl groups in the polymer chain and less often used as Michael acceptors as reported by Genest et al. (2017) and Mallik & Das (1960).

Figure 7 presents, the 1,4-aza-Michael addition reaction mechanism that can be described by a generic three-step model. The first step (a) consists of nucleophilic attack by nucleophile on the beta carbonyl carbon. In the second step (b) proton transfer takes place, in which the nucleophile bonds to carbon at position (1) and hydrogen bonds to oxygen at position (4). The third step (c) consists of tautomerization mechanism (process which protons are transported from one site to another by several steps using a solvent as an intermediate) whereby the final product is obtained (BERNE et al., 2022).

Figure 7 – General 1,4- aza-Michael addition reaction mechanism.

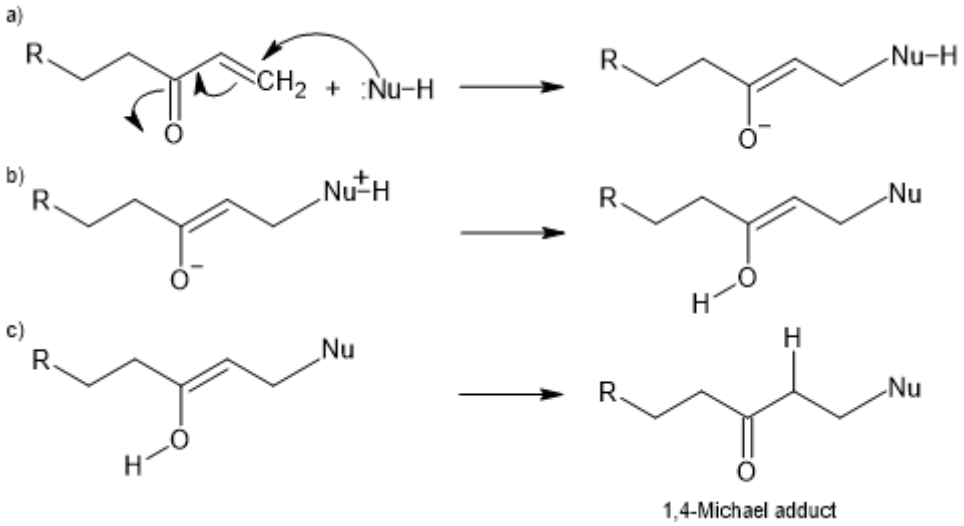

Drawn in ChemSketch, (2022);
Source: Author (2022) based on Machado (2019).

In addition to its use in polymer synthesis, aza-Michael additions also have been used in crosslinking reactions of several polymers with high functional monomers, as an

example in the work of González et al. (2015), thermosetting resins were prepared by aza-Michael addition reaction of poly(ethyleimine) (PEI) and diethylenetriamine (DETA) with some diacrylates. Moreover, after aza-Michael crosslinking reactions, polymers were submitted to a photopolymerization (dual cure) mediated by UV light to fully crosslink oligomers from acrylate moieties excess still present in the system that were not crosslinked by Michael addition, authors achieved an acrylate conversion (> 70%) and proved the efficiency of this approach.

Another point to note is during crosslinking via aza-Michael reactions, pH control is a crucial factor in reaction medium, because at high pH values, few amino groups are protonated, and more amino groups are free and available to react. On the contrary, at low pH values, amino groups are highly protonated which can significantly reduce crosslinking possibility. In some cases, tertiary amines can act as both nucleophile and catalyst in these reactions (GONZÁLEZ et al., 2015). Although aza-Michael additions have several proved advantages, as the low side reactions, the high chemoselectivity limits their usefulness in organic synthesis and the biggest challenge when using amines as nucleophiles is the competition with aminolysis reactions (BASSAM et al., 2013; BILLIET et al., 2013; RIVERA-RAMÍREZ et al., 2015; XU et al., 2015).

The versatility of using this reaction for different purposes can be found in the work carried out by Machado et al. (2020) when authors used the click aza-Michael addition to synthesize fungicides-loaded lignin-methacrylate nanocarriers which were crosslinked with bio-based amines as nucleophiles (spermine and spermidine) to serve as carriers in drug delivery for plants.

Currently, this approach has also been used for the construction of biomedical devices such as hydrogels, fibers and nanoparticles from natural biopolymers (e.g., chitosan and gelatin) allowing the construction of poly(β-amino esters) that have proven biodegradability and pH responsiveness, as proposed in the present study.

2.3.1 Poly(β-amino esters) (PBAEs)

The poly(β-amino esters) or (PBAEs) are a class of synthetic polymers synthesized from the addition reaction (or aza-Michael addition) between primary or secondary amines with acrylated or diacrylated esters (DEVALAPALLY et al. 2007; HAMMARLING et al. 2018; LIU et al. 2019). The PBAEs are composed of repeating

units containing both amino and ester groups and can be engineered to be biodegradable and biocompatible, water-soluble, or insoluble, and in relation to other interesting properties such as cationic charge density, crystallinity and degradation kinetics being considered suitable and safety for several biomedical applications (DEVALAPALLY et al. 2007; LYNN & LANGER, 2000; SHENOY et al., 2005a). Other commonly applications concern to wastewater treatments and the improvement of papermaking processes.

According to Mather et al. (2006), the poly(β-amino esters) synthesized from diacrylates are potentially biodegradable due to the hydrolytic instability of ester linkages. Additionally, the structure and degradability of these compounds can be adjusted using a wide range of diamines and diacrylates. As pointed out by Lynn & Langer (2000), in the early 2000s, the poly(β-amino esters) synthesized via aza-Michael addition between bifunctional amines and diacrylates received little attention. However, as stated by Mather et al. (2006) and Slaughter et al. (2009) the aza-Michael addition reaction is rapid, highly specific, and not require an initiation step being commonly applied to hydrogels synthesis by mixing an acrylated macromer with aminated or thiolated macromers obtaining polymers such as segmented elastomers to high T_g engineering thermoplastics.

In the biomedical field, the main uses are related to drug delivery devices at acidic microenvironments and at the endolysosomal compartments of cells or as gene transfection agents due to their ability of condense and protect anionic DNA molecules and oligonucleotides for intracellular delivery as can be found in Mather et al. (2006); Devalapally et al. (2007) and Potineni et al. (2003). As mentioned by Liu et al. (2019), the polycationic characteristic of the PBAEs is due to the presence of secondary and tertiary amines moieties in the polymeric chain. In addition, their unique structure allows the controlled release of molecules over time and have been explored for their potential to enhance the effectiveness of treatments and by have lower toxicity than many other polycations such as polyethyleneimine and poly(L-lysine) (SHENOY et al. 2005b). For in vivo use, the PBAEs must be synthesized with hydrolysable portions in order to degrade under physiological conditions via ester hydrolysis and quickly break down into smaller non-toxic components such as bis(β-amino acids) and low molecular weight diols, reducing the side effects and the risk of body-long-term accumulation (LIU et al. 2019; SHOOSHTARI & VAN DE MARK, 2001).

Based on the exposed, in the early 1960s, Mallik & Das (1960) proposed two 1,4-additions step-by-step mechanisms to react secondary amines with acrylic esters

mentioning that reaction can lead to an intermediate zwitterionic compound formation in which is neutralized by protons from the hydrogen donors from acceptor or solvent (e.g., water and methanol) as shown in Figure 8, a) and b).

Figure 8 – 1,4-additions mechanisms for secondary amines to acrylic esters.

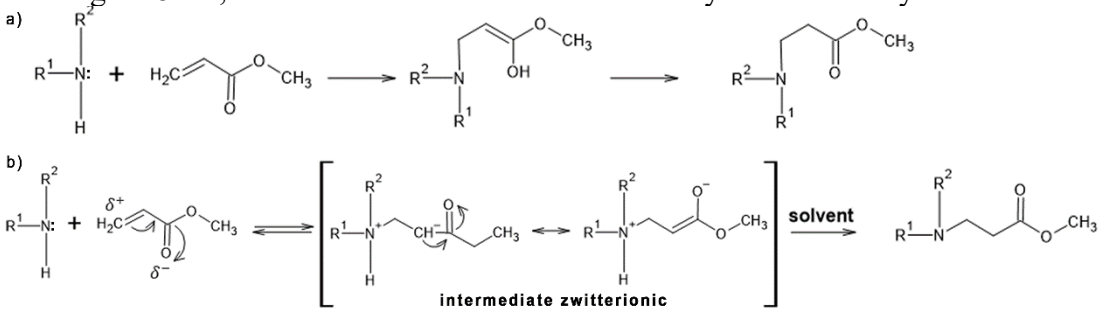

Drawn in ChemSketch and Photoshop CS6 (2023);
Source: Author (2023) adapted and reproduced from Mallik & Das (1960).

Decades later, Bernasconi (1989) proposed the ionic mechanism of these reactions involving several steps. The Shooshtari & Van de Mark's research group worked on PBAE synthesis via aza-Michael addition reaction in the past recent decades. In 2001, the authors studied the kinetic reaction parameters of several amines-co-acrylic esters and proposed a concerted mechanism involving a cyclic intermolecular proton transfer from the amine nucleophile to the oxygen of the ester moiety followed by enol-keto tautomerization to PBAE synthesis, according to adapted scheme of Figure 9.

Nonetheless, they mentioned that according to this mechanism, the rate of addition is higher in protic solvents or in the presence of excess amine and Y might be any hydrogen bond donor-acceptor group. Furthermore, the rate and product distribution of the reactions as a function of solvent, acceptors and amines structures, temperature, catalysts, as well as the effect of molar ratio of the reactants were also studied.

Figure 9 – aza-Michael addition mechanism from secondary amine to unsaturated ester.

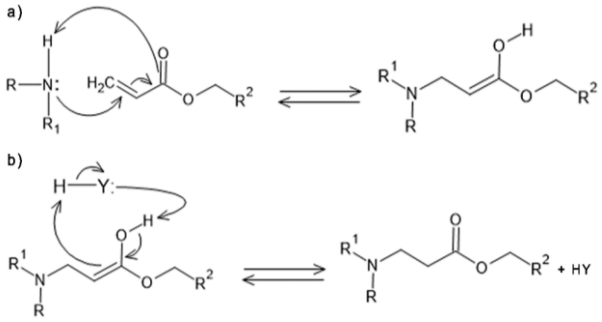

Drawn in ChemSketch and Photoshop CS6 (2023);
Source: Author (2023) adapted from Shooshtari & Van de Mark (2001).

However, it is difficult to state what mechanism really occurs, since the zwitterionic compound was not isolated (Figure 8, b) and in the second case (Figure 9, a, and b), the reaction mechanism was not evaluated by kinetic studies (GENEST et al., 2017).

In another work published in (2001[b]) the dimerization and macrocycle formation through primary amines (n-propyl amine, benzylamine, ethanolamine and pentanolamine) with several diacrylated esters (mono, di, tri, tetra ethyleneglycol diacrylate and neopentylglycol diacrylate) as an attempt to determine the systems propensity to oligomerization or macrocyclic formation was also investigated, Figure 10.

Figure 10 – Michael addition of primary amines to neopentyl glycol diacrylate.

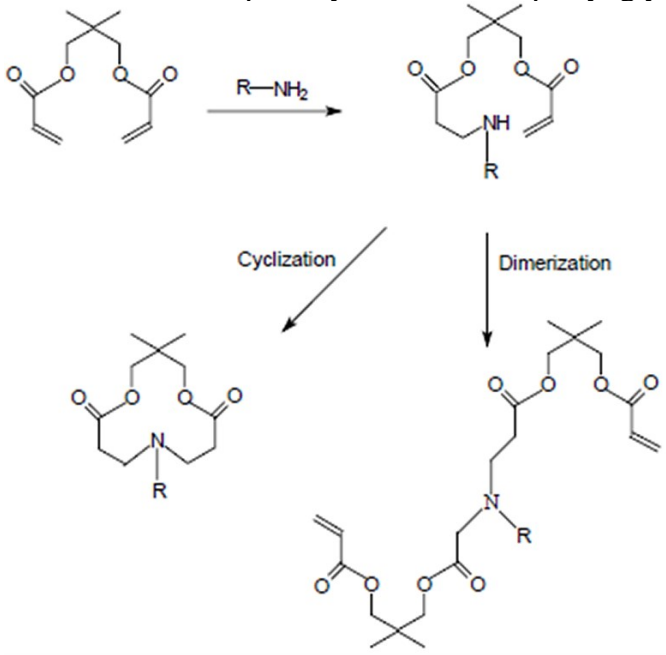

Source: Reproduced from Shooshtari & Van de Mark (2001).

The authors mentioned that a secondary amine is obtaining when a primary amine adds to a vinyl ester of a diacrylate. In addition, a linear poly(β-amino ester) is obtained from the dimmer adduct if amine adds intermolecularly while a macrocycle is formed when the second addition is intramolecular. From that, a reaction mechanism between amines and diacrylated esters was proposed with yields higher than 86%. Nevertheless, moderate yields when using butanediol diacrylate (29%) and hexanediol diacrylate (25%) with benzylamine to form macrocycle were also obtained suggesting these diacrylates are better candidates to polymerization reactions.

2.3.2 Amines characteristic groups

In Chemistry, the nitrogen atom is extremely useful and important as it has great industrial relevance in the polymer synthesis, dyes, pharmaceutical devices, and explosives (OUELLETTE & RAWN, 2015, pgs. 465–494). It is considered the fourth most abundant chemical element, being found mainly in amino acids and proteins, as well as in nucleic acids and other cellular molecules (LAWRENCE, 2004). It has five valence electrons and can form three covalent bonds with carbon or hydrogen atoms in neutral compounds and single, double, or triple bonds when in a functional group (Figure 11) (BRUICE, 2017).

Figure 11 – Amines chemical structure.

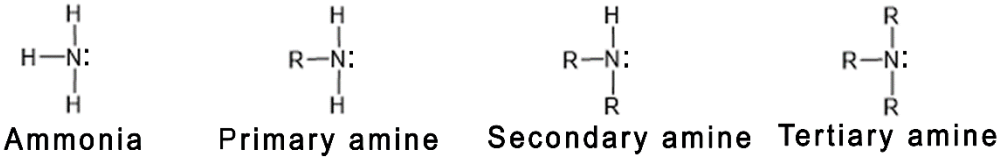

Drawn in ChemSketch and Photoshop CS6 (2023);
Source: Author (2023).

The amines are ammonia-derivatives, and the primary and secondary amines have higher boiling points than hydrocarbons and tertiary amines of similar molecular weight due to the possibility of functioning as hydrogen donors or acceptors and forming intramolecular hydrogen bonds even with water (BAKHTIAR & HARDY, 1997, pgs. 195–216; MEISLICH et al., 2013). On the other hand, tertiary amines do not have hydrogen atoms bonded and cannot form hydrogen bonds, however, they also react with water because the nonbonding pair of electrons from nitrogen atom accept hydrogen atom from water (FROIDEVAUX et al., 2016; OMPRAKASH RATHI & SUBRAY SHANKARLING, 2020). Generally, amines with until five carbon atoms are water-soluble and has its solubility decreases with increasing molecular weight because the hydrophilic part of the functional group is less significant than the rest of the polymeric chain (LAWRENCE, 2004; OUELLETTE & RAWN, 2015, pgs. 465–494).

The amides possess an amino group, or a substituted amino group bonded to a carbonyl carbon atom. Furthermore, the classification of amides is based on the number of carbon groups bonded to the nitrogen atom (Figure 12) and the other two bonds may be to hydrogen atoms, aryl, or alkyl groups (BAKHTIAR & HARDY, 1997, pgs. 261–269; BRUICE, 2017).

Figure 12 – Amides chemical structure.

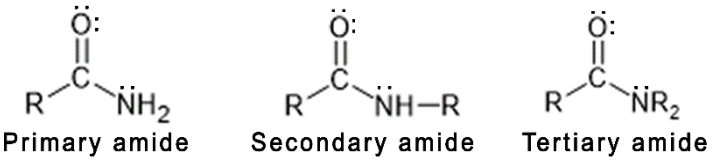

Drawn in ChemSketch and Photoshop CS6 (2023);
Source: Author (2023).

The primary and secondary amides can form strong intermolecular hydrogen bond from the carbonyl oxygen atom reaction with amide hydrogen atom (C=O···H—N) (BAKHTIAR & HARDY, 1997 pgs. 261–269; BRUICE, 2017). Therefore, tertiary amides cannot form intermolecular hydrogen bonds, however, even low molecular weight tertiary amides are water-soluble because the carbonyl oxygen atom can also form hydrogen bonds with the hydrogen atoms of water (MEISLICH et al., 2013; OUELLETTE & RAWN, 2015, pgs. 465–494). In addition, amides have high boiling points and are generally solid at room temperature (except formamide) but substituted amides have lower melting points (LAWRENCE, 2004).

2.4 FLORY-REHNER THEORY OF POLYMER NETWORK SWELLING

In the early 1940s, Paul Flory and John Rehner (1943) were the first researchers to investigate swelling thermodynamics in polymeric (rubber) lattice structures and proposed a model to describe the isotropic swelling behavior of these structures in their study named as "*Thermodynamics of High Polymer Solutions"*. Later, this model was modified by Sthepen Bruck (1961) which included anisotropic polymer system.

Eventually, under certain conditions, 3D polymeric networks, such as hydrogels, can absorb large amounts of liquids (e.g., water and body fluids) and swell, leading to an elastic shrinkage force. Although, the new molecular configuration is more unlikely, which implies a decrease in the system entropy due to the stretching of the chains caused by the increase in the volume of the network. Then, an equilibrium is occasionally reached when the two forces are equal (CANAL & PEPPAS, 1989; SLAUGHTER et al., 2009).

In the proposed model, the authors assume that the elastic and mixing contributions, with the energy of swelling of dry polymeric networks, are separable and

additive. Thereat, the change in the total Gibbs's energy (ΔG) that is involved in the mixing process of a lattice and a pure solvent is calculated by the difference between the change in the energy of mixing (ΔG_{mix}) and the change in the elastic energy (ΔG_{el}), Equation (1).

$$\Delta G = \Delta G_{mix} - \Delta G_{el} \quad (1)$$

The Flory-Huggins lattice theory differentiated in terms of moles of solvent molecules at constant temperature and pressure is presented in Equation 2. From that, at equilibrium conditions, the net chemical potential between the solvent within the gel and the surrounding solution can be defined as zero and the elastic and mixing potentials are equating, Equation 3.

In addition, the variation of the energy of mixing ΔG_{mix} is a quantitative description of the compatibility between the polymer and solvent is commonly called as polymer-solvent interaction parameter (χ) as mentioned by Flory & Rehner, (1943), Flory & Krigbaum (1951), Tompa, (1956) and Slaughter et al. (2009).

$$\frac{\Delta G_{mix}}{kT} \approx N_p \ln \varphi_p + N_s \ln \varphi_s + \chi N_s \varphi_p \quad (2)$$

$$\frac{\Delta G_{mix}}{kT} \approx N_s \ln \varphi_s + \chi N_s \varphi_p \quad (3)$$

In which, k is the Boltzmann constant, $J \cdot K^{-1}$; T is the temperature, K; N_s is the number of solvent molecules; N_p is the number of polymer molecules; φ_s and φ_p are the volumetric fractions of solvent and polymer, dimensionless, respectively and χ is the polymer-solvent interaction parameter, dimensionless.

According to the rubber elasticity and equilibrium swelling theories, it is possible to estimate several important parameters of crosslinked polymeric networks such as the average molecular weight between crosslinks ($\overline{M_C}$), the volumetric fraction of swollen polymer ($\upsilon_{2,s}$) and the network mesh size (ξ) (SLAUGHTER et al., 2009).

The volumetric fraction of the polymer ($\upsilon_{2,s}$) in the swollen state and the equilibrium volumetric swelling (Q_v) are calculated using Equations (4) and (5) as

proposed by Gilchrist et al. (2019) and Vigata et al. (2021). The $\upsilon_{2,s}$ parameter indicates the diffusion capacity of solvent in the crosslinked polymeric network.

$$\upsilon_{2,s} = \frac{1}{Q_v} \tag{4}$$

$$Q_v = 1 + \left(\frac{\rho_p}{\rho_s}\right)(SR - 1) \tag{5}$$

In which, $\upsilon_{2,s}$ is the volume fraction of hydrogel in the swollen state, dimensionless; SR is the swelling ratio, dimensionless and ρ_p and ρ_s is the density of polymer and solvent, in g·cm^{-3}, respectively.

The average molecular weight between crosslinks ($\overline{M_C}$) has its value increased with the increase of the swelling ratio and it represents the degree of crosslinking of the hydrogel networks. According to Lin & Metters (2006), $\overline{M_C}$ in a neutral divinyl crosslinked network can be estimated by the Flory-Rehner theory, Equation (6).

$$\frac{1}{\overline{M_C}} = \frac{2}{\overline{M_n}} - \frac{\frac{\bar{v}}{\bar{V}_1}\left[ln\left(1 - \upsilon_{2,s}\right) + \upsilon_{2,s} + \chi \cdot {\upsilon_{2,s}}^2\right]}{\left[\left(\upsilon_{2,s}\right)^{\frac{1}{3}} - \frac{1}{2}\left(\upsilon_{2,s}\right)\right]} \tag{6}$$

Several authors have made modifications in the original Flory-Rehner's Equation, with the inclusion of some terms. Thus, the Peppas & Merril's Equation (1977), Equation (7), is commonly applied to determine the molecular weight between crosslinks ($\overline{M_C}$) as proposed by Vigata et al. (2021) and Lin & Metters (2006) for polymers crosslinked in solvents.

However, as mentioned by Cavallo et al. (2017), this approach is only valid and suitable for loosely crosslinked networks, in which the number of repeating units between two crosslinks is large enough for the chains to be represented by a Gaussian distribution.

$$\frac{1}{\overline{M_C}} = \frac{2}{\overline{M_n}} - \frac{\frac{\bar{v}}{\bar{V}_1} \times \left[ln\left(1 - \upsilon_{2,s}\right) + \upsilon_{2,s} + \chi \cdot {\upsilon_{2,s}}^2\right]}{\upsilon_{2,r}\left[\left(\frac{\upsilon_{2,s}}{\upsilon_{2,r}}\right)^{\frac{1}{3}} - \frac{1}{2}\left(\frac{\upsilon_{2,s}}{\upsilon_{2,r}}\right)\right]} \tag{7}$$

In which, $\bar{v}$ is the specific volume of polymer, in $cm^3 \cdot g^{-1}$; $v_{2,r}$ is the volume fraction of hydrogel in the relaxed state (immediately after crosslinking but before full swelling), dimensionless.

The Flory-Huggins parameter or polymer-solvent interaction coefficient or chi parameter (χ) can be obtained as proposed by Xue, Champ and Huglin (2001) and Venkatachalam & Kaliappa (2023), from the expression valid at swelling equilibrium, Equation (8).

$$\ln(1 - v_{2,s}) + v_{2,s} + \chi {v_{2,s}}^2 + v_e \bar{V} \left({v_{2,s}}^{1/3} - 2 v_{2,s} f^{-1} \right) = 0 \quad (8)$$

According to the authors, the three first terms of Equation (8) are related to the mixing contribution and the remaining terms to the elastic contribution. This latter has only a slight effect on the χ and, thus, Equation 8 can be reduced to Equation 9.

$$\ln(1 - v_{2,s}) + v_{2,s} + \chi {v_{2,s}}^2 \sim 0 \quad (9)$$

Finally, after expansion of logarithmic series followed by truncation of terms in $({v_{2,s}}^4, {v_{2,s}}^5, {v_{2,s}}^6 \ldots)$ the χ value can be experimentally calculated according to Equation 10.

$$\chi = 0.5 + \frac{v_{2,s}}{3} \quad (10)$$

It is reported in the literature that the χ value equal to 0.50 is closer to an ideal solution, positive χ values (*polymer-solvent interaction or Flory-Huggins or Chi's parameter*) denotes that the polymer–solvent contacts are less favored compared with the polymer–polymer and solvent–solvent contacts while negative χ values polymer–solvent contacts are preferred, promoting solvation of the polymer by mixing of polymer with the solvent (TERAOKA, 2002; pgs. 73 & 74).

As mentioned by Venkatachalam & Kaliappa (2023), crosslinking density (q) is another parameter that can explain swelling and deswelling of polymers and can be

expressed as the crosslinking network chain per gram. The crosslinking density may be calculated by using the modified Flory swelling equation as proposed by Xing et al. (2014), according to Equation (11).

$$q = \frac{-\left[\ln\left(1 - \upsilon_{2,s}\right) + \upsilon_{2,s} + \chi \cdot {\upsilon_{2,s}}^2\right]}{\bar{V}_1 \cdot \rho_{polymer}\left[\left({\upsilon_{2,s}}^{1/3} + {\upsilon_{2,s}}/2\right)\right]} \quad (11)$$

In which, q is the crosslinking density, in mol·g^{-1}; $\bar{V}_1$ is the molar volume of the solvent, in cm^{-3}·mol; $\rho_{polymer}$ is the density of the polymer, in g·cm^{-3}; χ is the polymer-solvent interact parameter, dimensionless and $\upsilon_{2,s}$ is the volume fraction in swollen state, dimensionless.

Some authors have proposed the obtaining of crosslinking density (q) per volume unit (mol·cm^{-3}) through Equation 12, as can be found in Billiet et al. (2013), Lee, Bouhadir & Mooney (2004) and Cao et al. (2020).

$$q = \left(\frac{1}{\bar{\upsilon}_p \cdot \overline{M_C}}\right) \quad (12)$$

In which, q is the crosslinking density, in mol·cm^{-3}; $\bar{\upsilon}_p$ is the specific volume of polymer, in cm^3·g^{-1}; $\overline{M_C}$ is the molecular weight between crosslinks, in g·mol^{-1};

The shear modulus (G) is defined as a critical parameter of the mechanical properties of a biomaterial as it influences the structural stability, force transmission as well as biomechanical compatibility. It can be calculated from the Gaussian statistics model as proposed by Billiet et al. (2013) and Lee, Bouhadir & Mooney (2004) according to Equation 13.

$$G = \left(\frac{cRT}{\overline{M_C}}\right) \cdot \left(1 - \frac{2\overline{M_C}}{\overline{M_n}}\right) \cdot {Q_v}^{-1/3} \quad (13)$$

In which, G is the shear modulus in kPa; c is the polymer concentration in solution, in g·L^{-1}; R (0.082) is the universal gas constant, in atm·L·mol^{-1}·K^{-1}; T is temperature, in K;

Q_v is the equilibrium volumetric swelling, dimensionless; $\overline{M_C}$ is the molecular weight between crosslinks and M_n is the average number molecular weight, both in g·mol^{-1}.

The porosity can be described by the mesh size (ξ) and is used to quantify the average linear distance between crosslinks and to determine the maximum size of solutes that can diffuse in a gel (SLAUGHTER et al., 2009). Additionally, by knowing the unperturbed polymer chain distance $(r_0{}^2)^{1/2}$, (Equation 14), and the extension ratio or elongation factor (α), (Equation 15), the mesh size (ξ) of network can be estimated by Equation 16 (CANAL & PEPPAS, 1989; CAVALLO et al., 2017).

$$(r_0{}^2)^{1/2} = l \times \left(2\frac{\overline{M_C}}{M_r}\right)^{1/2} \times C_n{}^{1/2} \tag{14}$$

In which l is the bond length of the polymer backbone, in Å; M_r is the molecular weight of the repeating unit, in g·mol^{-1} and C_n is the Flory's characteristic ratio, dimensionless.

$$\alpha = \left(\upsilon_{2,s}\right)^{-\frac{1}{3}} \tag{15}$$

$$\xi = \alpha \times (r_0{}^2)^{1/2} \tag{16}$$

In which α is the elongation factor or extension ratio and $\upsilon_{2,s}$ is the volume fraction in the swollen state, both dimensionless.

Although, the C_n value is commonly tabulated, for large polymer chains as in polypeptides (e.g., gelatin) its value tends to infinite and the Flory's characteristic ratio (C_∞) can be estimated by Equation (17) as proposed by Ma et al. (2013).

$$l_p = (C_\infty + 1) \cdot \frac{l_s}{2} \tag{17}$$

In which, l_p is the persistence length and l_s is the bond length of the polymer backbone, both in Å and C_∞ is the Flory's characteristic ratio, dimensionless.

Finally, the mesh size (ξ) is obtained by Equations (18) and (19).

$$\xi = l \times \left(\frac{2C_\infty \overline{M_C}}{M_r}\right)^{1/2} \times \left(\upsilon_{2,s}\right)^{-\frac{1}{3}} \quad (18)$$

However, as mentioned by Ma et al. (2013) the factor (2) is generally used for vinyl polymers which has one double bond available to react and must be replaced by (3) when the repetitive unit consists of two available double bonds (e.g., divinyl polymers) or to a correct value when has more than (2).

$$\xi = l \times \left(\frac{3C_\infty \overline{M_C}}{M_r}\right)^{1/2} \times \left(\upsilon_{2,s}\right)^{-\frac{1}{3}} \quad (19)$$

In which, ξ is the network mesh size, in Å; l is the bond length of the polymer backbone, in Å; C_∞ is the Flory's characteristic ratio, dimensionless, $\overline{M_C}$ is the molecular weight between crosslinks and M_r is the molecular weight of the repeating unit, both in g·mol^{-1}.

From the exposed, the calculated Flory-Rehner parameters are presented in the Scheme of Figure 13.

Figure 13 – Scheme of Flory-Rehner parameters of hydrogels.

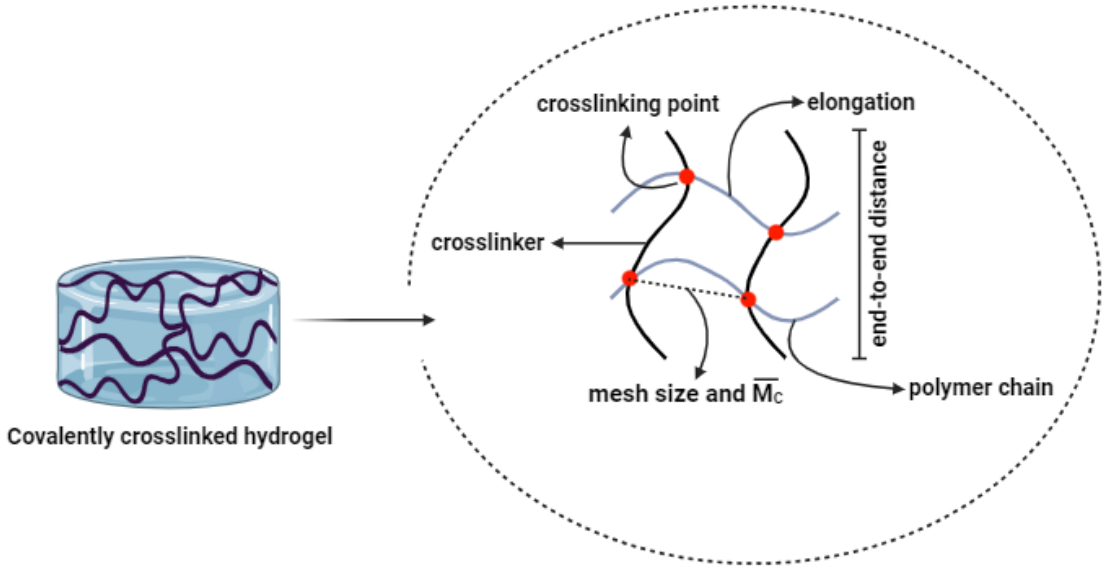

Drawn in biorender.com and Photoshop CS6 (2023);
Source: Author (2023).

2.5 GELATIN NANOPARTICLES (GNPs) AS CARRIERS FOR HYDROPHILIC DRUGS

The development of new approaches for effective delivery of macromolecules is a very promising field of research (HUEPPE; WURM; LANDFESTER, 2022). However, the challenge in the controlled delivery of these compounds is associated with their non-specific biodistribution and the short half-life at the desired sites of action, mainly due to rapid metabolization before reaching specific sites of action and phagocytic metabolism (CROSSEN & GOSWAMI, 2022). Such challenges are related to the structural instability of these molecules, additionally, to the low permeability to biological membranes (CHAWLA; RANI; MISHRA, 2021).

Moreover, the burst effect or burst release is the phenomenon associated with rapid diffusion and the high amount of drug released that occurs during the initial periods of release before the drug reaches a stable release profile (HUANG & BRAZEL, 2001). In some cases, this effect is desirable and has been used as a strategy in the drug administration, for example, in wound healing systems, as it promotes immediate relief to the patient followed by a prolonged release, helping in the healing process (SETTERSTROM; TICE; MYERS, 1984). However, it remains a challenge to be overcome due to the unpredictability and lack of control of the payload to be released both in vitro and in vivo. In addition, it hampers the development of controlled release devices by reducing the effective useful life of these devices that aim to reduce the amount of drug administered to patients while maintaining the same therapeutic effect (BHATTACHARJEE, 2021; CAM et al., 2020; WANG et al., 2017).

From that, nanoparticulated delivery systems, such as nanoparticles (NPs), has attracted a lot of attention in recent years and have been developed to circumvent these obstacles in macromolecules delivery (e.g., drugs, peptides, and nucleic acids) as they are considered efficient in carrying of several substances (HUEPPE; WURM; LANDFESTER, 2022). Furthermore, in terms of therapeutic effects, controlled and targeted drug delivery, NPs have advantages over conventional methods used by facilitating intracellular uptake and bioavailability at the target site (increasing the solubility of low-solubility molecules), by having characteristics of enhanced permeability and retention effect (EPR) (decreasing the side effects of chemotherapeutic drugs and increasing drug permeation across the cell membrane) and by enhance the

pharmacokinetics and pharmacodynamic control compared to free drugs (increasing their therapeutic efficacy and potential) (GÜLSU; KILLI; ALPER, 2022; JOSEPH et al., 2023; SHARMA; KUMAR; MISHRA, 2016). For this reason, the use of nanocarriers (NCs) offers a new approach for complete delivery of active molecules to specific targets and desirable characteristics when compared to particles with larger dimensions (CHAWLA; RANI; MISHRA, 2021; CROSSEN & GOSWAMI, 2022).

The preparation methods and the use of hydrophobic nanoparticles it is well established in literature (REZAEI; FATHI; JAFARI, 2019; RISTROPH & PRUD'HOMME, 2019; WEISSMUELLER et al., 2016), however, these systems may present limitations in terms of practical applications (e.g., the low encapsulation potential of hydrophilic compounds, like proteins) and according to Joseph et al. (2023), for choosing the appropriate material, some selection criteria must be considered, such as:

(a) the desired size of the NPs;

(b) the physicochemical properties of the drug, e.g., aqueous solubility and stability;

(c) desired drug release profile;

(d) surface charge;

(e) immunogenicity and toxicity of the final product and,

(f) biodegradability and biocompatibility of the nanomaterials.

Consequently, the choice of the polymer to affects the properties of NPs and their subsequent application as nanocarriers (GÜLSU; KILLI; ALPER, 2022; HUEPPE; WURM; LANDFESTER, 2022). Moreover, recent studies pointed to advantages in using nanoparticulate systems from protein biomaterials due to specific characteristics (WEISSMUELLER et al., 2016). Some biomaterials, such as polysaccharides (Plucinski, Lyu & Schmidt, 2021; Venkatesan, Kim and Anil, 2022) and proteins (Defrates et al. 2018; Ristroph & Prud'Homme, 2019) have also been studied as potential constituents in these systems and applied as pharmaceutical and nutraceutical delivery vehicles. In the last decade, researchers have made efforts to synthesize NPs from natural polymers (JADOUN & ANNA DILFI, 2021). Generally, these polymers have a low mechanical strength, nonetheless, have been widely used in biomedical applications due to their unique characteristics (e.g., biocompatible, non-toxic, do not cause inflammatory responses in the host, among others) (DE; MAHATA; KIM, 2022; IDREES et al., 2020).

Among natural polymers, gelatin is one of the most used biopolymers and noteworthy for having properties of high biological value, as aforementioned. The literature is rich in works that report the use of gelatin nanoparticles (GNPs) as carriers of a wide variety of therapeutic compounds, including gene materials (Madkhali, Mekhail and Wettig, 2019), peptide (Aramwit et al. 2015) and non-peptide (Ofokansi et al. 2010 and Aramwit et al. 2015) sources. In the last decade, some studies showed that GNPs are promising candidates for drug delivery in immunotherapy treatments (BU et al., 2021; KLIER et al., 2012; SARFRAZ et al., 2016). Furthermore, another very interesting feature is its cationic character, since GNPs may interact electrostatically with anionic terminal portions of proteins, glycans or phospholipids present in the plasma membrane and induce cellular uptake by promoting its association in cells by various endocytic cellular mechanisms (BANNUNAH et al., 2014; ARAMWIT et al., 2015). Despite of these advances, non-crosslinked GNPs have been shown to be unstable in aqueous media, tending to dissolve over time by having low thermal and mechanical resistances (YASMIN et al., 2017).

Different techniques have been reported for the preparation of GNPs, as summarized in Table 2.

Table 2 – Preparation technique, crosslinker and particle size of GNPs.

Technique	Crosslinker[a]	Particle size (nm)	Reference
Coacervation	-	~ 50	Mohanty et al. (2005)
Emulsion Solvent evaporation	GTA	397 - 501	Aramwit et al. (2015)
Nanoprecipitation	DIC	~ 200 – 300	Baseer et al. (2019)
	NaCas	~ 190	Lemes et al. (2017)
Desolvatation	GTA	~ 280	Coester et al. (2000)
	GTA	~ 272 – 479	Ofokansi et al. (2010)
	GTA	~130 – 190	Khramtsov et al. (2021)
Two-step desolvatation	GTA	130 – 260	Zwiorek et al. (2007)
		10.3	Gülsu, Killi and Alper (2022)
Inverse miniemulsion	GTA	~ 180 – 230	Ethirajan et al. (2008)

[a]Crosslinker: DIC – diisopropylcarbodiimide; FTIC-D – fluorescein isothiocyanate dextran; GTA – glutaraldehyde; NaCas – sodium caseinate;
Source: Author (2023).

As platforms in drug delivery, stimulus-responsive polymers have been widely used due to the advantage of being biologically active, providing stable delivery and controlled release rates (ELTOUKHY et al., 2012).

In summary, responsiveness concerns the variations caused in the external environment that act as stimuli that induce specific responses in the polymer itself. Such variations may be related to temperature, pH, presence or absence of oxygen, light, enzymes or specific ligands, ionic strength, magnetic or electric fields, among others.

A study conducted by Qin et al. (2019), the authors synthesized thermo, oxidation, pH, and CO_2-responsive polymers from aza and Thiol Michael reactions in one pot by reacting amines and thiols. Other techniques are used to produce stimuli-responsive biopolymers and one of the approaches used is the cationization in which through the introduction of amino groups portions (e.g., ethylenediamine-co-gelatin) in the polymer chain, cationic polymers are obtained, as carried out by Fukunaka et al. (2002) and Hori et al. (2007).

In this context, a simple and quite viable tool for obtaining responsive stimulus-GNPs is the use the nucleophilic aza-Michael addition reaction. This reaction is an interesting approach in the synthesis of cationic polymers (pH-responsiveness) among other several advantages (LIU et al., 2019; QIN et al., 2019).

For gelatin, free primary and secondary amino groups react with other compounds (e.g., aldehydes, α, β-unsaturated esters, ketones, etc.) forming strong covalent bonds (ETHIRAJAN et al., 2008; ELTOUKHY et al., 2012). Allied to this, it has been proven that gelatin hydrogels, such as GNPs, also have a cationic character at neutral pH environments due to amines charge transition showing pH-responsiveness and charge reversible properties (GÜLSU; KILLI; ALPER, 2022; MADKHALI; MEKHAIL; WETTIG et al., 2019).

From this, new possible configurations may emerge through the formation of tertiary amines during the aza-Michael reaction, which can become protonated with pH variations and be destabilized at acidic environment (LYNN & LANGER, 2000). In addition, these amino groups are capable of electrostatically interacting with the negative charges of drugs (Potineni et al. 2003) or genes (Eltoukhy et al. 2012) producing a nanocomposite (LIU et al., 2019). As mentioned by Lynn, Amiji & Langer (2001), these polymers rapidly solubilized at pH below 6.5 even though the unprotonated polymer is insoluble in aqueous media at physiological pH.

Furthermore, such stimuli are essential conditions in the use of these platforms, in view of changes in physiological pH, making them excellent candidates for specific biomedical applications such as a vehicle to achieve delivery in intracellular conditions (IYER et al., 2013; LYNN; AMIJI & LANGER, 2001). As proven in the Potineni et al. (2003) study, the poly(ethylene oxide)-modified poly(β-amino ester) nanoparticles were rapidly internalized by non-specific endocytosis releasing their content (paclitaxel) due to the low intracellular pH.

2.5.1 Inverse miniemulsion polymerization

In view of the aforementioned techniques for NPs preparation, obtaining polymeric particles in the submicrometric range can be achieved through direct or inverse miniemulsion polymerization that have been widely studied in recent decades and possess numerous advantages (WANG et al., 2015). From that, the first reported miniemulsion polymerization mechanism was proposed by Ugelstad, El-Aasser and Vanderhoff (1973) during the styrene polymerization.

In this context, miniemulsion polymerization refers to the reaction that takes place in a dispersed system with a very complex particle formation mechanism (EL-AASSER & SUDOL, 2004). It consists of a process, in which the application of extreme shear forces in an emulsion, containing a monomer or monomers mixture, surfactant and an osmotic pressure agent (e.g., salt/water) are dispersed in a continuous phase, with the use of high energy with the aid of high shear equipment (e.g., ultrasound, turrax) (GHARIEH; KHOEE; MAHDAVIAN, 2019).

The miniemulsion involves the dispersion of many monomer droplets, from the miniemulsification of dispersed phase, thus, this process allows the formation of droplets (Figure 14) and NPs with narrow and stable size distribution for long periods of time (CAPEK, 2010; GUO et al., 2012). However, the literature does not present a consensus on the range of sizes that comprise the nanometric scale and the values can vary between 50 and 500 nm (HUEPPE; WURM; LANDFESTER, 2022).

Figure 14 – Scheme of droplet formation in miniemulsion polymerization process.

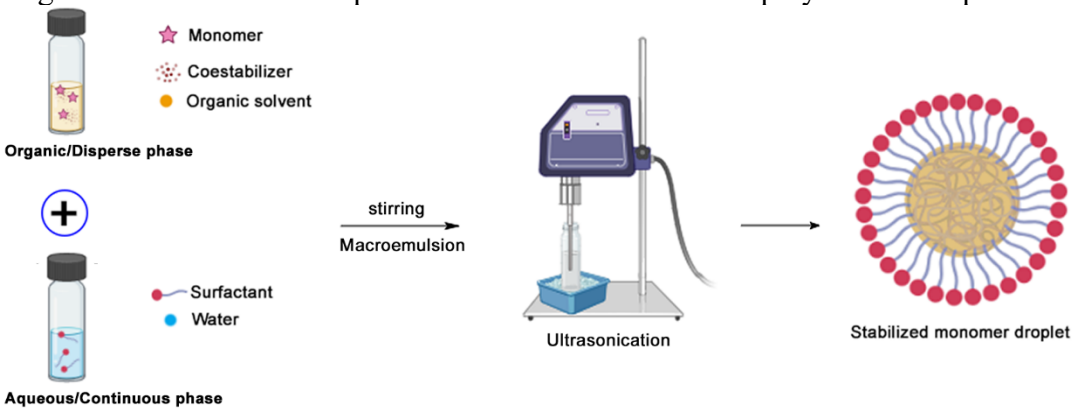

Drawn in biorender.com and Photoshop CS6 (2022);
Source: Author (2022).

Some advantages are achieved over conventional bulk and suspension polymerization methods by the occurrence of the radicals compartmentalization mechanism in submicrometric particles, such as: high reaction rates and high molecular weights, wide molecular mass distribution, few problems related to heat transfer or mixing during polymerization (due to the low viscosity of continuous phase) and problems with residual monomers can be minimized by the high conversion of monomer to polymer, are widely used commercially, however, the process is not without its disadvantages (ASUA, 2002; EL-AASER & SUDOL, 2004).

The distinction between the two systems, direct and inverse, is that in the inverse miniemulsion, the aqueous soluble monomer is dispersed in a continuous oil phase and usually the low HLB non-ionic surfactant is less homogeneously adsorbed on the particle surface (LANDFESTER, 2006). The first reported mechanism for any inverse emulsion polymerization was proposed in 1987 by Hunkeler, Hamielec & Baade for the acrylamide polymerization ("inverse-micro-suspension") and more deeply studied into a developed kinetic model from 1989s (HERNÁNDEZ-BARAJAS & HUNKELER, 1997; HUNKELER & HAMIELEC, 1991; HUNKELER; HAMIELEC; BAAD, 1989).

In inverse miniemulsion systems, stability is a problem before and during the polymerization of the monomer, since the dispersions are thermodynamically unstable and water separation can occur and, consequently, the shelf life is reduced. In this sense, stability in inverse miniemulsions can be achieved from the ideal combination between an effective surfactant and an osmotic pressure agent (practically insoluble in the continuous phase). To obtain a condensed interface, blends of non-ionic surfactants are commonly used to promote steric stabilization in these systems, in addition to reducing the aggregation and diffusion of the monomer from the smaller to the larger droplets and

preventing the process of diffusional degradation (Ostwald ripening). The addition of a lipophobe in the monomeric phase induces the formation of nanodroplets with osmotic stability and, therefore, these miniemulsions have long-term stability against collisional and diffusional degradation (EL-AASER & SUDOL, 2004).

A generic inverse miniemulsion polymerization scheme is shown in Figure 15 and this procedure is based on the works carried out by Peres et al. (2018) and Steinmacher (2014) during hydrophilic nanoparticles synthesis. Initially, the aqueous/dispersed and organic/continuous phases (1) are mixed by magnetic stirring leading to a macroemulsion formation. Subsequently, the macroemulsion is ultrasonicated at a predetermined time interval and stabilized monomer droplets appears after phases breakdown due to high energy imputed, (Figure – 15, a). In sequence (b), the continuous/organic phase (2) is dropwise to the previously ultrasonicated droplet dispersion and subjected to another ultrasonication step. From that, the polymerization reaction proceeds and, at the end of the process, a latex with polymerized and stable NPs is obtained.

Figure 15 – General scheme of inverse miniemulsion polymerization process.

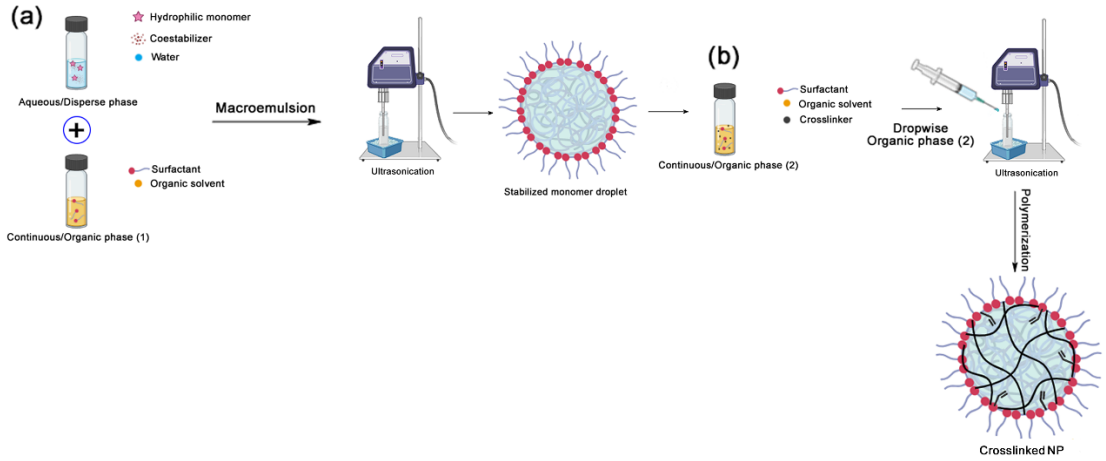

Drawn in biorender.com and Photoshop CS6 (2022);
Source: Author (2022).

2.5.2 Interfacial polymerization

Interfacial polymerization is known by its oldest applications such as nylon and polyester synthesis (CHENG et al., 2017; RAAIJMAKERS & BENES, 2016). In addition, new approaches and applications have been developed from its use, as for instance in nanoparticulate devices for drug delivery (BASEER et al., 2019).

Though, this type of polymerization requires that two co-reactants are immiscible and one of the phases can also be dispersed in another. Subsequently, each phase containing the reactive monomers are solubilized or in the oil phase or in the water phase and reaction takes place at the interface (FALCA et al., 2021; RADMANESH et al., 2023). Frequently, the oil phase is emulsified in water phase (direct emulsion), but inverse systems (water-oil) have also been reported, as proposed in the present work (RAAIJMAKERS & BENES, 2016; SONG; FAN & WANG, 2017; ZHANG; FAN & WANG, 2020).

In addition, interfacial polymerization is suitable for a wide range of monomers and a diversity of polymers can be obtained from this approach, such as polyesters (Cheng et al. 2017), polyurethanes (Bossion et al. 2017 and Wang et al. 2020), polycarbonates (Garrison et al. 2021 and Kyriacos, 2017), polyamides (Gohil & Ray, 2017 and Seah et al. 2020), polyimides (Kim, Lee & Kim, 2000 and Yang, Zhen & Su, 2017), including thin-film composites (Seman, Khayet & Hilal, 2010), nanofiltration membranes (Arribas et al. 2020 and Zhang et al. 2013) and functional materials as micro and nanocapsules with active ingredients among others (Wang et al. 2021).

Additionally, the interfacial polymerization presents several advantages over the classical step-growth polymerization such as, mild reaction conditions with high final molecular weights and high reaction rates, respectively. It is one of the well-established methods for nanoparticulate systems synthesis and as mentioned by Landfester (2006) several polymerization mechanisms have been applied for NPs and polymer synthesis through reactions at interface such as anionic polymerization (Hui et al. 2018; Limouzin et al. 2003) free radical polymerization (Shenoy & Bowman, 2013; Wu et al. 2006) polycondensation (Cho, Kwon and Cho, 2002; Su, Wang and Ren, 2007; photopolymerization (Liu et al. 2013; Raaijmakers & Benes, 2016) among others techniques (SHEN, 2023).

In this context, the crosslinking via interfacial polymerization have also been used to hydrophilic nanoparticles synthesis by the addition of adequate quantities of crosslinkers, monomers and co-monomers allowing reactions to take place at droplet interface and, consequently, the polymeric nanoparticles formed can be resuspended in water, buffers and/or biological fluid (HUEPPE; WURM; LANDFESTER, 2022; SHEN, 2023). As mentioned by Baseer et al. (2019) due to crosslinker hydrophobicity, only the surface functional groups are accessible to crosslinking. Furthermore, the crosslinker does

not diffuse into the interior of the hydrophilic NPs and once all available functional groups are crosslinked, no further crosslinking is expected to occur.

A general scheme of crosslinking through interfacial polymerization in nanoparticulate system is shown in Figure 16. As illustrated, polymerization reaction occurs at the liquid-liquid interface, resulting in crosslinked polymeric NPs at the end of reaction. However, as stated in literature, it can also be performed in liquid-gas and liquid-solid systems (RADMANESH et al., 2023; SHEN, 2023).

Figure 16 – Scheme of interfacial crosslinking reaction.

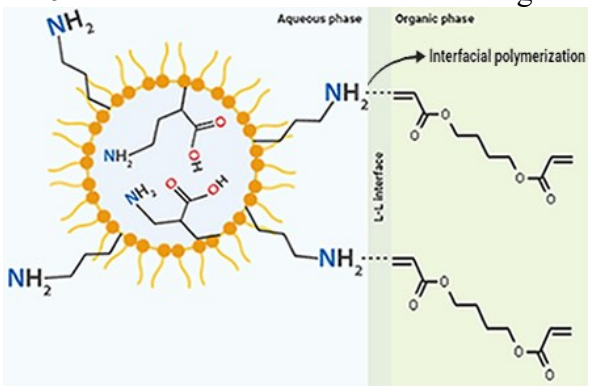

Source: Author (2023).
Drawn in biorender.com and Photoshop CS6 (2023).

In the work conducted by Baseer et al. (2019), authors synthesized gelatin nanoparticles (GNPs) by coacervation and performed the crosslinking via interfacial polymerization using diisopropylcarbodiimide (DIC) as crosslinker. The study carried out by Liu et al. (2013), authors used an interfacial thiol-ene polymerization to synthesize hybrid microcapsules to encapsulate hydrophobic and hydrophilic dyes. In addition, different drugs such as ivermectin (Valarini Junior et al. 2021) and paclitaxel (Li et al. 2009), also are encapsulated in hydrophilic and hydrophobic nanoparticles prepared through interfacial polymerizations improving its properties by the surface-modification.

For instance, in the Sayer's and Hermes de Araújo's research group, authors have published some reports using interfacial polymerizations during NPs prepare for encapsulation of hydrophilic molecules as can be seen in the works carried out by Peres et al. (2018) when encapsulated doxorubicin as drug model within crosslinked glutamic acid-based nanogels and Steinmacher et al. (2017) with sulforhodamine 101 (SR 101) dye within crosslinked starch nanocapsules.

2.5.3 Free-radical photopolymerization and photo-crosslinking

Another widely applied approach in polymer synthesis or modification is the UV-curing or photopolymerization reaction in which a liquid monomer can be transformed into a solid polymer using light. It has been utilized in several applications such as inkjet printing (Check, Chartoff and Chang, 2015; Wagner, Mühlberger and Paulik, 2019), adhesives (Besse et al. 2016; Gziut et al. 2023; Ye et al. 2007), and has gained attention by its use in patterned structures synthesis (Hwang & Park, 2021; Lim et al. 2023) and in crosslinking of polymeric systems (Ovsianikov & Chichkov, 2012; Zhu et al. 2020) due to inherent advantages over traditional polymerization methods such as low process time, quickly curing at room temperature, reduced energy consumption and can be carried out in solvent-free conditions and in cases when substrates are temperature sensitive (BAROLI, 2006; FISHER et al., 2001). This reaction is initiated by monomer exposure to a specific light wavelength that triggers a chain reaction and lead to a crosslinked polymer chain formation. In the biomedical field, photopolymerization have been used to prepare 3D hydrogels and bioprinting, encapsulation of cells, drug delivery systems among others (TOMAL & ORTYL, 2020).

Nonetheless, some applications needed a photoinitiator (PI) to start the photopolymerization reaction mediated by UV light exposure (PAPPAS & ASMUS, 1982; SCHWALM, 2001). However, it is also reported that some photopolymerization reactions can be carried out without photoinitiator, and in these cases, the own monomer or co-reactants can photopolymerize by itself upon UV light (BAUER et al., 2014; WAGNER; MÜHLBERGER; PAULIK, 2019). An example of this molecules is the acrylates and methacrylates due to their versatility and high reactivity (BAUER et al., 2014; LLORENTE et al., 2021; PAPPAS & ASMUS, 1982). Methacrylates possess lower toxicity, faster curing, and the lower reactivity than acrylates (LANG et al., 2022).

In this context, the most used photoinitiators are based on alkyl-phenones, phospin oxides or aromatic ketones such as DMPA (hydrophobic initiator) and Irgacure 2959 (hydrophilic initiator) (BARCELOS et al., 2020; EREN et al., 2021; MUCCI & VALLO, 2012; NOWAK et al., 2017). However, is reported that the use of photoinitiators may modify the final polymer characteristics by promoting yellowing or migration (DESSAUER, 2006; GREEN, 2010; SCHROEDER; ARENAS; VALLO, 2007). Thereupon, in protein-based systems, photoinitiators have been chosen carefully once they also can damage protein structure (TOMAL & ORTYL, 2020).

It is important to mention that in the presence of photoinitiator, the absence of oxygen is necessary to avoid the inhibition that may be caused by peroxy-radicals formed when oxygen readily bind with free-radicals generated from photoinitiator photolysis (TOMAL & ORTYL, 2020). To overcome these challenges several approaches are commonly used such as, amine additions, inert conditions by adding nitrogen (N_2) gas purge, red light irradiation with dye sensitizer or by using wax barrier coatings (WAGNER; MÜHLBERGER; PAULIK, 2019).

Among the widely used photoinitiators, DMPA has gained prominence in applications such as dental resins, because it is colorless, improves aesthetic properties and has been shown to be efficient in the photopolymerization of acrylates and methacrylates with fast polymerization times (40 to 60 s). In the Schroeder, Arenas and Vallo (2007) and Lizymol & Krishnan (2008) works, UV-curing photopolymerization was carried out to crosslinking methacrylates during dental composite resins synthesis.

In the study conducted by Mucci & Vallo (2012), the authors evaluated photopolymerization of dental resins from methacrylate monomers and mentioned that in vitrifying systems the reactants diffusion is highly suppressed and changes in the photofragmentation and secondary photoreactions are expected to occur. Nonetheless, they proved the polymerizing resin was transformed from a viscous liquid to a rigid glass during photolysis of DMPA in methacrylate monomer.

The free-radical polymerization is a very efficient and complex mechanism that can be associated at least three mainly phases, initiation, propagation, and termination (TOMAL & ORTYL, 2020). The initiation mechanism may be excited by visible, thermal, ultraviolet, or redox initiator form free radicals. On the other hand, the propagation step refers to reaction between radicals and monomers that became highly reactive and will react with further monomers. By the end, the termination step can be by two different mechanisms through chain transfer or radical combination developing polymeric matrices (LANG et al., 2022; MATYJASZEWSKI & DAVIS, 2002; SALDIVAR-GUERRA; VIVALDO-LIMA, 2013).

Some works employs the ultraviolet light for a photopolymerization at the interface (CHECK; CHARTOFF; CHANG, 2015; LIU et al., 2013; RAAIJMAKERS & BENES, 2016). In nanoparticulated systems it has been used to promote crosslinking density throughout several interfacial polymerization techniques as reported in the work carried out by Liu et al. (2013).

In principle, the free radical polymerization technology is usually used to polymerize mixtures of vinyl monomers such as acrylates and methacrylates being one of the most widely produced classes of polymers (LANG et al., 2022) In addition, hydrogels can also be obtained by free radical polymerization of water-soluble polymers derivatized with vinyl polymerizable groups (ARSLAN, 2020; BUKHARI et al., 2015).

On the other hand, photo-crosslinking is a versatile tool to create controlled chemical connections between molecules and consist of the introduction of photo-reactive groups into molecules of interest that will be chemically linked through light (LIM et al., 2020; XIE; YANG; WANG, 2019). This approach has been extensively applied for the synthesis/modification of polymers, in the study of biomolecular interactions such as protein-protein and protein-DNA, and for drug delivery systems in which drugs are encapsulated within a crosslinked matrix (ZHANG et al., 2022).

From the exposed, it can be found several approaches that have been used to photopolymerize or photo-crosslink polymers through use of UV light. Furthermore, among the most reported reaction routes, click reactions such as thiol-ene, aza-Michael and thiol-Michael stand out as the most promising techniques.

To exemplify, the general schemes (without step by step) of aza-Michael photo-crosslinking reaction between free amino groups from a generic primary amine with a generic diacrylate and diacrylate homopolymerization (without step by step) via free radical photopolymerization were presented in the schemes of Figures 17 and 18.

Figure 17 – Scheme of aza-Michael photo-crosslinking reaction.

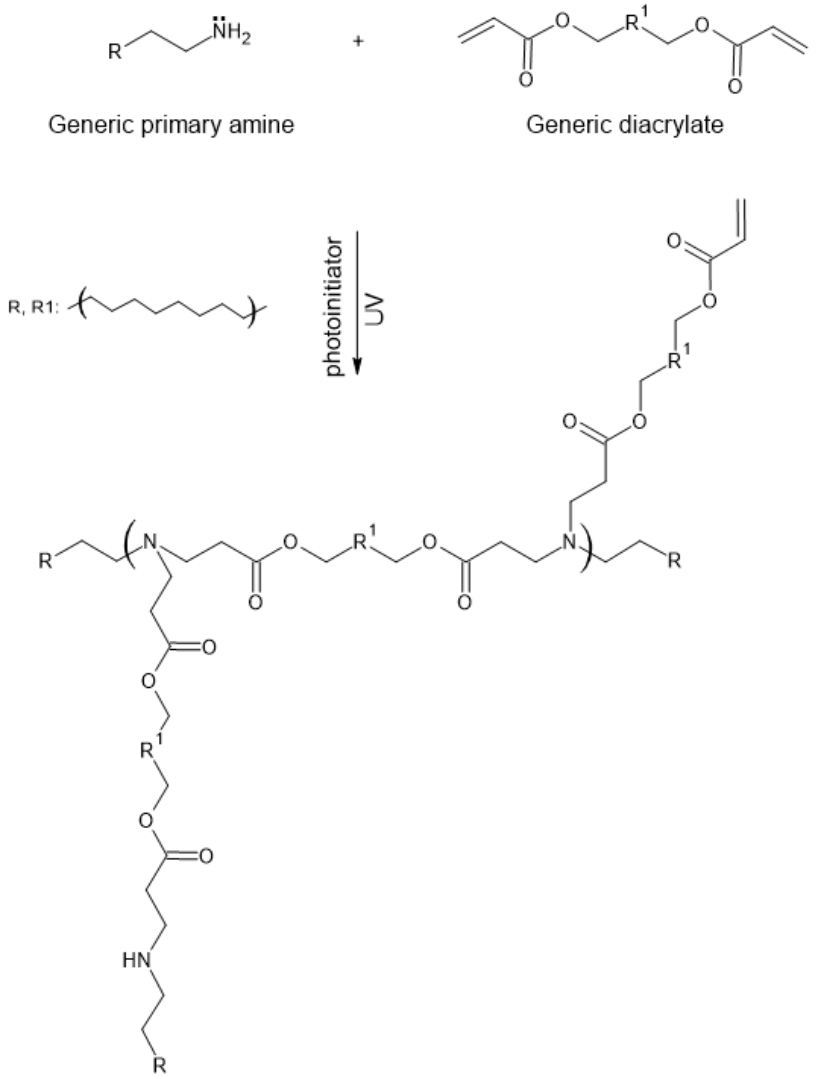

Drawn in Chemsketch and Photoshop CS6 (2023);
Source: Author (2023).

The free radical polymerization reaction starts with the initiator decomposition producing radicals. These radicals bind to vinylic groups of the acrylate leading to the initiation radical and starting the propagation which is followed by termination. In addition, by undergoing a polymerization reaction upon heating or light, acrylic and methacrylic molecules can form a highly stable crosslinked polymer network as demonstrated in Figure 18.

Figure 18 – Scheme of diacrylate monomer homopolymerization crosslinking reaction.

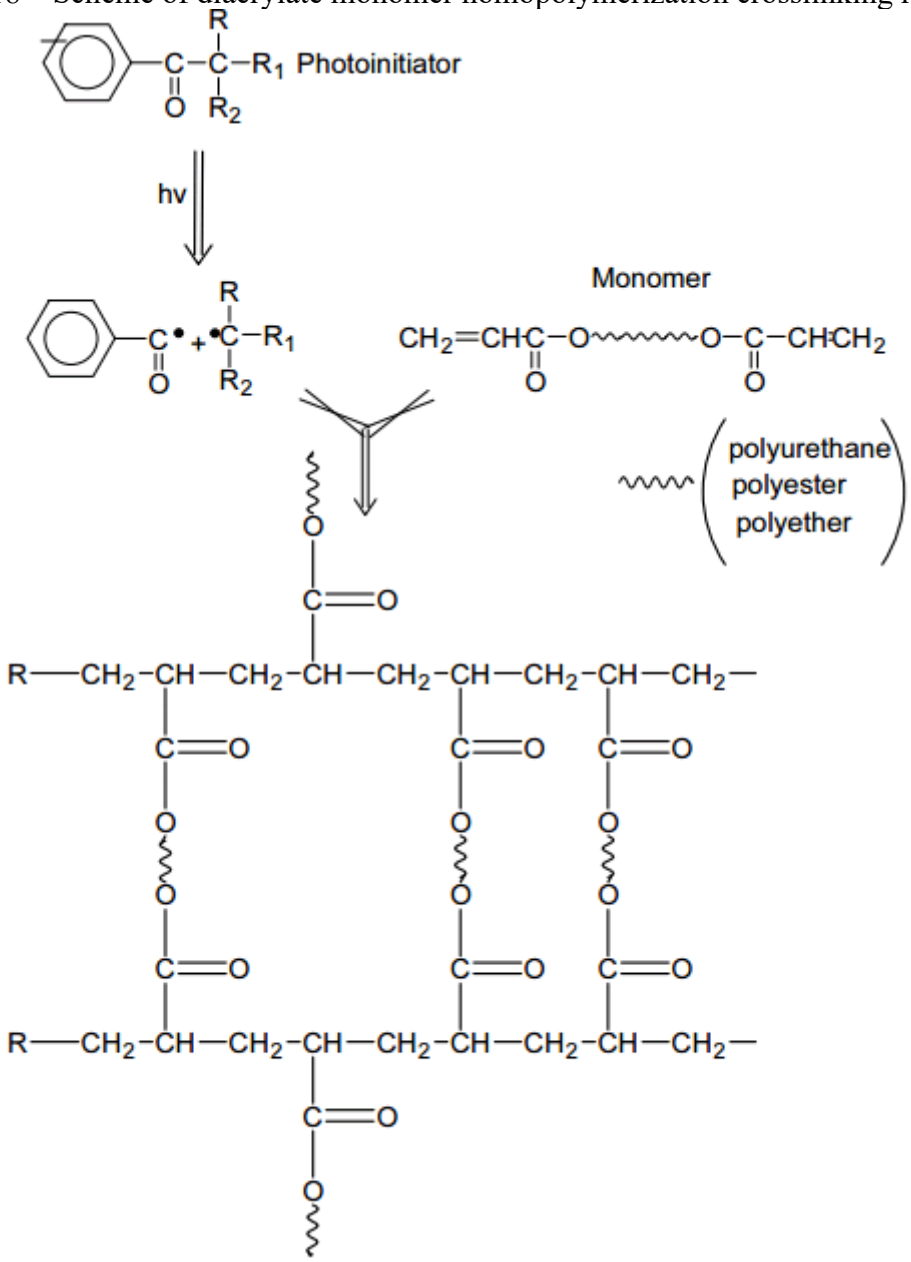

Source: Reproduced from Grigale-Sorocina et al. (2016).

2.6 DOXORUBICIN (DOX)

Doxorubicin (hydroxyldaunorubicin, $C_{27}H_{29}NO_{11}$), Figure 19, is a chemotherapeutic drug that belongs to the anthracycline group and has been used in various cancer treatments by its potent antitumor activity (PERES et al., 2018). It is derived from the bacterium *Streptomyces peucetius* and considered as an antibiotic that has high solubility and stability. Some studies report its use as a chemotherapeutic agent

since the 1960s to treat sarcomas (e.g., tissues and bones), cancers (e.g., lung, ovary, bladder, breast, and thyroid) and various types of leukemia (HUANG et al., 2020).

Figure 19 – DOX chemical structure and red fluorescence by optical microscopy.

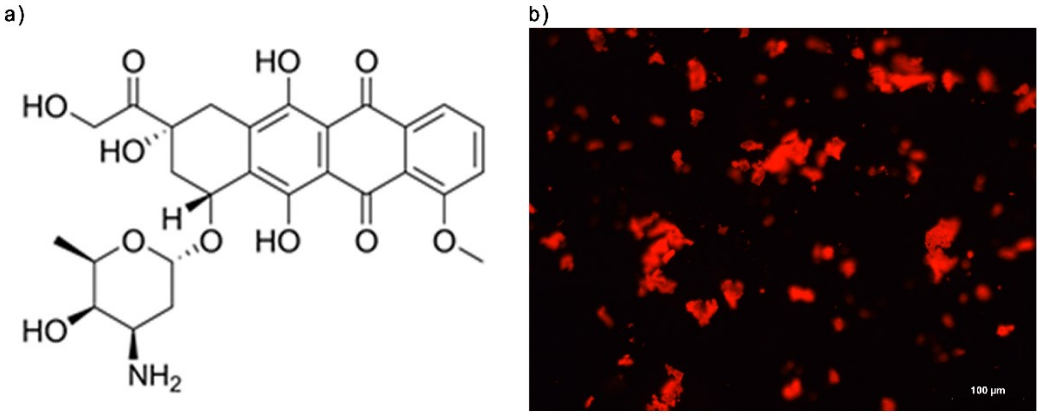

a) DOX chemical structure and b) DOX fluorescence at 585 nm.
Drawn in ChemSketch (2023);
Source: Author (2023).

According to National Library of Medicine (NIH), DOX can be administered by different ways, generally, is provided intravenously but the clinical applications are limited because of its side effects, specifically cardiotoxicity and development of chemoresistance, being often used in combination with other chemotherapy drugs to increase its effectiveness (GRECO et al., 2023; OBIREDDY et al., 2020). It has been reported that the DOX also induces cardiotoxicity by the increasing of reactive oxygen species (ROS) and through the upregulation of death receptor-mediated apoptosis in cardiomyocytes. Additionally, is proved that the DOX release is accelerated in an acidic condition (CARVALHO et al., 2009; HUANG et al., 2020; ZHAO & ZHANG, 2017). As related by Huang et al. (2020) and Zhao & Zhang, (2017) another side effects, including weakness vomiting, nausea, diarrhea, and tiredness during the drug administration may experienced by patients and the balance between its therapeutic benefits and potential side effects needs to be carefully managed during its use.

Moreover, DOX works by interfering with the DNA in cancer cells, preventing them from growing and dividing, its widely use can be associated to the inhibition of DNA and RNA synthesis and DNA strand breakage by being the main mechanism of drug action, which can intercalate within DNA base pairs and prevent further macromolecular biosynthesis (JAISWAL et al., 2021). However, when bonded with iron also limits DNA synthesis due to oxidative damage caused by free radicals. In addition,

by inhibiting the topoisomerase II enzyme, it induces apoptosis and, consequently, DNA damage (JOHNSON-ARBOR & DUBEY, 2022). As mentioned by Gewirtz (1999), the antiproliferation and cytotoxicity effects are not only related to these cited mechanisms but also to the increase of free radical formation and lipid peroxidation.

From the exposed, in the study conducted by Peres and co-workers (2018), the N-acryloyl-L-glutamic acid and poly(L-glutamic acid-co-BIS) nanogels were used to encapsulate doxorubicin showing high encapsulation efficiency (≈ 85%) when redispersed in the aqueous media. According to authors, by being highly hydrophilic, its encapsulation in hydrophilic polymers is favored due to possible drug-polymer interactions through strong hydrogen bonds and commonly used in controlled release systems.

In another study carried out by Fan et al. (2018), DOX-loaded glycyrrhetinic acid modified gelatin (GA-GEL) micelles were synthesized via emulsion-solvent evaporation method to serve as carriers for drug delivery in hepatocellular carcinoma (HCC) therapy. The mean diameters of micelles varied between 195 – 235 nm and encapsulation efficiency from 63.6 up to 96.2% with drug loading of 8.3 up to 12.5%. In the Huang et al. (2020) work, magnetic nanoparticles of (DOX–gelatin) core and (Fe_3O_4–alginate) shell layer were developed to function as targeted anticancer drug delivery vehicles with encapsulation rate of 64.6 ± 11.8%. The results show that NPs have the potential for use in targeted drug delivery in cancer therapy and as mentioned by authors, the embedding of DOX in the gelatin inner core prevents the risk of cardiotoxicity while the alginate outer layer provides a controlled drug release rate and stabilizes the NPs structures. Furthermore, doxorubicin is a chromophore and has been investigated as a potential photosensitizer in photochemotherapy (PCT) by being capable of absorbing visible light. Studies are being conducted to increase the anticancer activity of DOX using photochemotherapy. In the study by Greco et al. (2023) it was reported that depending on its concentration, DOX can generate peroxides and singlet oxygen after irradiation with white light LED (24 $mW \cdot cm^{-2}$) for 30 min.

2.7 THE STATE-OF-THE-ART

The nanotechnology applied to encapsulation and release of drugs has advanced considerably in the recent decades and has shown to be a promising field of research. Several reports related an infinity of approaches and start materials to synthesize nanoparticles for these purposes. One the one hand, the biodegradability and biocompatibility are some of crucial criteria to the development of a reliable and efficient drug delivery systems. On the other hand, even though great advances had been reached until now, still there some challenges to be overcome in this area.

One of the main lacks and challenges refers to the encapsulation of hydrophilic molecules or drugs into matrixes with also hydrophilic cores in way to promote their controlled and sustained release at specific conditions and desired sites of action, helping to reduce the burst release effect and by the chosen of biocompatible and biodegradable materials that will not generate undesirable and toxic compounds that are harmful to health.

In this context, and as reported in the literature, due to its intrinsic and interesting characteristics such as biocompatibility, biodegradability, capacity of gel-network formation and charge reversal properties, gelatin had been widely used as part for the synthesis of hybrid biomedical materials. Commonly, it has also been modified to provide specific properties as the ability of encapsulate hydrophilic drugs and the controlled drug release in response to pH changes. In addition, for the nanoparticulated system, the use of inverse miniemulsion technique is an interesting approach to nanoparticle synthesis and drug encapsulation, as it allows the obtaining of stable particles, with narrow distribution and reduced size.

Based on that, this work highlighted the synthesis of hydrogels and nanogels made up from functionalized and/or crosslinked gelatin to serve as biomedical devices in these types of applications. Additionally, we investigated the encapsulation of a hydrophilic drug into a hydrophilic core using the inverse miniemulsion technique for synthesis and crosslinking through the environmentally friendly click-reaction of aza-Michael addition with different polymerization systems and approaches. Further, these materials were also characterized in terms of their specific characteristics.

From all previously mentioned, the innovative potential of this work concerns to:

- The use of a biocompatible and biodegradable natural polymer (gelatin) coupled (“acrylated” or crosslinked) with another proved biodegradable crosslinker (1,4-butanediol diacrylate) in order to increase its biodegradability and biocompatibility, to reduce the side effects and potential cytotoxicity as well as an alternative to other synthetic and non-compatible materials used for biomedical purposes;
- The engineering of properties of great interest from the biomedical point of view;
- The creation of macroscopic hydrogels susceptible to post-polymerization modifications such as photo-crosslinking due to their pendant vinyl portions present;
- The synthesis of modified (“acrylated” or crosslinked) gelatin nanoparticles (GNPs) by means of inverse miniemulsion technique that will be serve as nanocarriers of hydrophilic drugs (doxorubicin) envisaging a controlled and sustained release with the aim of minimizing the potential side-effects and the increasing of drug therapeutic efficacy at acidic cell environments for cancer treatments;
- The use of a post free radical photopolymerization or free radical photo-crosslinking to improve their degree of modification or crosslinking.

In summary, the state-of-the-art of this work fits into a field of research in advanced nanotechnology contributing to the development of more effective and innovative approaches and formulations that can result in more efficient treatments, with lower side effects and better therapeutic drug targeting which would benefit patients and health.

3 MATERIALS AND METHODS

3.1 EXPERIMENTAL PROCEDURE

3.1.1 Materials

Gelatin from porcine skin, type A, bloom strength 280, 8 mesh, was kindly gifted by Gelnex (Itá, Santa Catarina) and was used as the starting material for all reactions. Additional information about gelatin composition is available in Table 21, Appendix A. 1,4-Butanediol diacrylate (1,4-BDDA, $C_{10}H_{14}O_4$, 198.22 g·mol^{-1}), 1,8-diazobicyclo [5.4.0]undec-7-ene (DBU, $C_9H_{16}N_2$, 152.24 g·mol^{-1}), 2,4,6-trinitrobenzenesulfonic acid solution 5% w/v in water (TNBS, $C_6H_3N_3O_9S$, 293.17 g·mol^{-1}), deuterium oxide (D_2O, 20.03 g·mol^{-1}), ethylene glycol dimethacrylate (EGDMA, $C_{10}H_{14}O_4$, 198.22 g·mol^{-1}), 2-hydroxyethyl methacrylate (HEMA, $C_6H_{10}O_3$, 130.14 g·mol^{-1}), acrylic acid ($C_3H_4O_2$, 72.06 g·mol^{-1}) and butyl acrylate ($C_7H_{12}O_2$, 128.17 g·mol^{-1}) were purchased from Sigma Aldrich and were used without further purification. Further chemicals and solvents include cyclohexane (C_6H_{12}, 84.16 g·mol^{-1}, Dinâmica), polyglycerol polyricinoleate (PGPR, $C_{21}H_{42}O_6$, 390.6 g·mol^{-1}, Dhaymers), diethyl ether ($(C_2H_5)_2O$, 74.12 g·mol^{-1}, Dinâmica), hydrochloric acid (HCl, 36.5 g·mol^{-1}, Dinâmica), sodium bicarbonate ($NaHCO_3$, 105.98 g·mol^{-1}, Neon), doxorubicin hydrochloride (DOX, $C_{27}H_{29}NO_{11}$·HCl, 579.98 g·mol^{-1}), 2-hydroxy-4'-(2-hydroxyethoxy)-2-methylpropiophenone (Irgacure 2959, 224.25 g·mol^{-1}), 2,2-Dimethoxy-2-phenylacetophenone (DMPA, $C_{16}H_{16}O_3$, 256.301 g·mol^{-1}), potassium persulfate (KPS, $K_2S_2O_8$, 270.322 g·mol^{-1}) and distilled water (H_2O, 18 g·mol^{-1}).

3.1.2 Methods

3.1.3 Characterization of the Molecular Weight (M_w) of the Gelatin

The gelatin molecular weight was accessed by two different approaches. The first approach was the gel permeation chromatography (GPC) in aqueous solution of $NaNO_3$ (0.1 M) as proposed by Peres et al. (2018) and the analyses were carried out at the Laboratory of Size Exclusion Chromatography (LASEC – UFRGS/RS) using a size exclusion chromatographer (Viscotek, GPCmax VE-2001, Malvern Instruments GmbH, Markham, Canada).

For that, freeze-dried neat gelatin was solubilized in hot distilled water at the concentration of 5 mg·mL^{-1} at 50 ºC for 2 h. This solution was filtered through a 0.22 µm syringe filter (Millex-GP Filter) and the volume of 100 µL was injected into a column equipped with refraction index detector (model 2410) at 35 ºC with a flow rate of 0.50 mL·min^{-1}. The results were compared against polyethylene oxide standard and number-average and weight-average molecular weights and dispersity were calculated with OmniSEC software. Afterwards, the data were treated with the software Origin 9.0.

In the second approach, the M_w was obtained from the Rayleigh Equation, (Equation 20), according to the methodology proposed by Fredheim, Braaten and Christensen, (2002); Harding & Jumel, (1998); Karimi et al. (2020); Puskás et al. (2013) and the manufacturer's instructions (ANTON PAAR, 2023; MALVERN INSTRUMENTS, 2015[a]; 2017[b]). In sequence, an aqueous solution of pure dried gelatin at 2 mg·mL^{-1} was diluted in the range of 0.1 to 2.0 mg·mL^{-1} in distilled water at 50 ºC and stirred for 1 h until complete dissolution. Then, the solutions were analyzed by static light scattering (SLS) with a glass cuvette at 50 ºC using a Nanosizer (Malvern Instruments GmbH, U.K) and the following parameters: scattering angle of (173º - NIBS default); the refractive index (R.I.) of gelatin was considered equal to 1.450, as used for proteins determination; absorption coefficient value of a = 0.0010; coil model with R_g = 1.56 R_h; refractive index increment of $dn{\cdot}dC^{-1}$ = 0.100. Analyses were carried out in triplicate; the means and the standard deviations were also calculated.

$$\frac{KC}{R_\theta} = \frac{1}{M_w} + 2A_2C \tag{20}$$

In which R_θ is the Rayleigh ratio; K is the Debye's/optical constant; C is the polymer concentration in mg·mL^{-1}; M_w is the average molecular weight in kDa; A_2 is the second virial coefficient in mL·mol·g^{-2} and $KC \cdot {R_\theta}^{-1}$ is given in mol·kg^{-1}.

3.1.4 ε-Amino groups quantification by 2,4,6-Trinitobenzenic sulfonic acid (TNBS) essay

TNBS test is a colorimetric approach commonly used to determine free amine content in heterogeneous biomaterials, in which TNBS reacts with primary amino groups forming a yellow-colored hydrolyzed product, according to the reaction presented in Figure 3. Herein, this approach was employed in the freeze-dried pure gelatin and in the freeze-dried crosslinked gelatin hydrogels, respectively, and also in the oven dried crosslinked gelatin nanoparticles.

For all experiments, analyses were carried out in 20 mL glass sealed and covered test tubes, where 11 mg of freeze-dried gelatin, crosslinked gelatin hydrogels or dried crosslinked GNPs were dissolved in 1 mL of 4% sodium bicarbonate ($NaHCO_3$) solution and 1 mL of TNBS (0.5% w/v) solution in water bath at 40 °C for 4 h. In sequence, 3 mL of HCl (6 N) was added to each sample and followed by autoclaving at 121 ºC and 1.03 bar for 1 h. The hydrolyzed mass was diluted in 5 mL of distilled water followed by the addition of 5 mL of diethyl ether to remove the TNBS excess (not reacted) and samples were submitted to a vortex mixer (KASVI, K45-2810, São José dos Pinhais, Brazil) for 1 min. Then, 5 mL of aqueous phase (yellow/orange phase) was removed and heated open in a hot water bath at 50 ºC for 15 min to evaporate residual diethyl ether in the sample. In sequence, samples were again diluted with 15 mL of distilled water, cooled down to room temperature and their absorbance was measured at 349 nm using a 96-well microplate reader (Biotek® – EPOCHH-SN, Agilent Technologies, Santa Clara, USA). At the same conditions mentioned above, blanks were prepared in duplicate, but in this case, HCl (6 N) volumes were added before TNBS to avoid the reaction between primary amines with sulfonic groups of TNBS.

Finally, the ε-amino groups could be determined according to Equation (21) as proposed by Campiglio et al. (2020) and Ofner & Bubnis (1996). However, it is reported that due to the uncertainty in the molecular weight (M_w) of gelatin, in the most of cases, Equation (21) may be modified to Equation (22) with results presented as mols of lysine·$g_{gelatin}^{-1}$ as proposed in the works of Baseer et al. (2019) and Kale & Bajaj (2010).

$$\frac{mols\ of\ lysine}{mols\ of\ protein} = \frac{2(ABS)(0.020)(M_w)}{1.46 \times 10^4 (b)(x)} \tag{21}$$

In which, *ABS* represents sample absorbance, dimensionless; *0.020* is the sample volume in L; M_w is the protein molecular weight in g·mol^{-1}; the constant *1.46×10^4* is the molar absorptivity of TNP-lys in L·mol^{-1}·cm^{-1}; *b* is the cell path length in cm and *x* is the sample weight in g.

$$\frac{mols\ of\ lysine}{g\ of\ gelatin} = \frac{2(ABS)(0.020)}{1.46 \times 10^4(b)(x)} \quad (22)$$

In which, *ABS* represents sample absorbance, dimensionless; *0.020* is the sample volume in L; the constant *1.46×10^4* is the molar absorptivity of TNP-lys in L·mol^{-1}·cm^{-1}; *b* is the cell path length in cm and *x* is the sample weight in g.

Due to asymmetrical consumption of the acrylates in 1,4-BDDA, some aza-Michael adducts bear an acrylate group from incomplete crosslinking. In this case, we refer to that as an "acrylation" because even though aza-Michael addition has taken place, free acrylate groups have been inserted in the gelatin. Then, the consumption of free amino groups was named as modification degree (DM).

The DM was estimated as proposed by Campiglio et al. (2020) and Zatorski et al. (2020) according to Equation 23.

$$DM\ (\%) = \left(1 - \frac{ABS_F}{ABS_I}\right) \times 100 \quad (23)$$

In which ABS_F is the absorbance of synthesized hydrogel and ABS_I being the absorbance of pure polymer, both dimensionless.

The modification extent (X_m) is defined as the number of amino groups lost after reaction and was calculated as reported by Ofner & Bubnis (1996) according to Equation 24.

$$Modification\ extent\ (X_m) = \left(\varepsilon_0 - \varepsilon_f\right) \quad (24)$$

In which ε_0 is the total free amine content in the pure polymer and ε_f is the total remained free amine content after functionalization, both in mmol of lysine·$g_{hydrogel}^{-1}$.

3.1.5 Synthesis of chemically crosslinked gelatin hydrogels

In the present work, three different formulations of gelatin hydrogels with different crosslinker concentrations were prepared in solution according to a methodology adapted from Peres et al. (2018) and Yoon et al. (2016) as shown in Table 3. Initially, dried pure gelatin was solubilized in distilled water, 20% w/w to solvent, at 50 ºC under magnetic stirring at 200 rpm for 1 h until a clear gelatin solution was formed. Afterwards, DBU (equal concentration of mmol DBU to mmol of 1,4-BBDA) was added to elevate the medium pH and to facilitate the nucleophilic attack in diacrylate double bonds by deprotonated amines as proposed by Arslan (2020). Subsequently, the crosslinker 1,4-butanediol diacrylate (1,4-BDDA) was added dropwise in the following molar ratios of ε-amino groups-to-crosslinker: 1:0.5, 1:1 and 1:1.5, then the reactions were carried out for 24 h to form crosslinked poly(β-amino ester) gelatin-based hydrogels. The ratios were based on our TNBS results, 0.305 mmol of ε-amino groups·$g_{gelatin}^{-1}$. The solution pH was measured with a benchtop pHmeter (KASVI, K39-1410A, Brazil) with automatic temperature compensation (ATC) and all formulations were presented in Table 3.

Table 3 – Formulations for the synthesis of gelatin hydrogels in solution.

Sample	$Weight_{theorithical}$	$n_{theorithical}$	$Weight_{real}$	n_{real}
G_0.15 (pH = 10.9)				
Gelatin	10.0	0.0030	10.0047 ± 0.0049	$0.0030 \pm 1.46 \cdot 10^{-6}$
DBU	0.228	0.0015	0.2320 ± 0.0029	$0.0015 \pm 1.9 \cdot 10^{-5}$
1,4-BDDA	0.297	0.0015	0.3044 ± 0.0065	$0.0015 \pm 3.28 \cdot 10^{-5}$
Water	50.0	2.7777	50.0142 ± 0.0113	$2.7786 \pm 6.29 \cdot 10^{-4}$
G_0.30 (pH = 12.8)				
Gelatin	10.0	0.0030	10.0242 ± 0.0226	$0.0030 \pm 6.79 \cdot 10^{-6}$
DBU	0.456	0.0030	0.4538 ± 0.0032	$0.0030 \pm 2.09 \cdot 10^{-5}$
1,4-BDDA	0.594	0.0030	0.5952 ± 0.0006	$0.0030 \pm 2.85 \cdot 10^{-6}$
Water	50.0	2.7777	50.1225 ± 0.1696	$2.7846 \pm 9.42 \cdot 10^{-3}$
G_0.45 (pH = 14.0)				
Gelatin	10.0	0.0030	10.0026 ± 0.0021	$0.0030 \pm 6.36 \cdot 10^{-7}$
DBU	0.685	0.0045	0.6880 ± 0.0052	$0.0045 \pm 3.44 \cdot 10^{-5}$
1,4-BDDA	0.891	0.0045	0.8980 ± 0.0085	$0.0045 \pm 4.28 \cdot 10^{-5}$
Water	50.0	2.7777	50.0080 ± 0.0012	$2.7782 \pm 6.68 \cdot 10^{-5}$

Results are shown as mean (n = 2) followed by ± standard deviation (SD);
Parameters: $Weight_{theoretical}$ and $Weight_{real}$ (g); $n_{theoretical}$ and n_{real} (mol);
Source: Author (2023).

After the reaction time, a purification step was carried out by adding 500 mL of hot distilled water at 50 ºC to the reactor to solubilize unreacted gelatin and to remove DBU and crosslinker excesses. This solution was filtered through a stainless-steel sieve (d = 80 mm) and hydrogels were transferred again to the reaction flask. This step was repeated once again by adding 500 mL of hot distilled water at 50 ºC under magnetic stirring at 200 rpm and followed by sieve filtration. Finally, the purified hydrogels were frozen at -80 ºC and submitted to freeze-drying (L101, Liotop, Brazil) for 48 h. Then, the final product was stored in a desiccator until further use.

The flowchart containing the synthesis (step-by-step) of the chemically crosslinked gelatin hydrogels is shown in Figure 20.

Figure 20 – Flowchart of chemically crosslinked gelatin hydrogels synthesis.

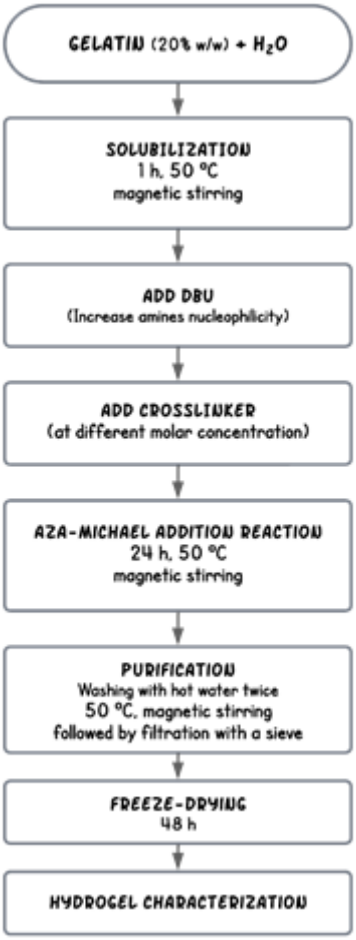

Drawn in lucidachart.app
Source: Author (2023).

3.1.6 Swelling Ratio (SR)

The equilibrium water content of the hydrogels was defined as the weight ratio of water content to dried hydrogels. To evaluate the SR of gelatin hydrogels, approximately 30 mg of dried hydrogels were soaked into distilled water for 72 h at 37 °C. After that, hydrogels were removed from distilled water, placed between two pieces of dried filter paper to remove water excess, and then weighed (w_s). The swelling ratio of hydrogels were determined according to Equation (25).

$$Swelling\ Ratio\ (\%) = \left(\frac{w_s - w_d}{w_d}\right) \times 100 \quad (25)$$

In which w_s is the in g and w_d is the dry weight of hydrogel in g;

3.1.7 Insoluble fraction evaluation

The insoluble fraction of the hydrogels was estimated according to the methodology proposed by Bukhari et al. (2015) & Suhail et al. (2021) with some modifications. Since crosslinked polymers must not be soluble in any solvent, the purification process after crosslinking removes non-reacted and non-crosslinked (soluble fraction, Equation 26) components from hydrogels.

Then, after purification and swelling experiments, the swelled hydrogels were weighed and submitted to drying in a vacuum oven at 37 ºC for 72 h (same time of swelling experiments) and a constant weight (w_i) was reached (when the total water content was removed). Subsequently, samples were weighed once again. Analyses were carried out in sextuplicate, and mean values and standard deviations were also calculated. Finally, the hydrogel's insoluble fraction was determined by Equation (27).

$$Sol\ fraction\ (\%) = \left(\frac{w_0 - w_i}{w_0}\right) \times 100 \quad (26)$$

$$Insoluble\ fraction\ (\%) = 100 - Sol\ fraction \quad (27)$$

In which w_0 and w_1 is the initial hydrogel weight before and after extraction process, respectively, in g.

3.1.8 Polymer density by helium picnometry

Gas pycnometry is a non-destructive and inert method to determine sample volume, specific volume, and real specific mass (true density) of materials. This method is based on Arquimedes principle of fluid flow. For that, these parameters of freeze-dried neat gelatin and freeze-dried hydrogels were determined in one cycle consisted of 10 measurements to obtain an average density and volume by He-picnometry as proposed by Andrade (2015) and Billiet et al. (2013) using a pycnometer (Accu Pyc II 1340, Micromeritics Instrument Corporation, Norcross, USA). The parameters were obtained from the equipment by adding a known sample mass (1 g) into equipment cylinder and helium was injected at constant temperature (25 ºC) until equipment pressure equilibrate. Results were presented in the Table 23, Appendix A.

3.1.9 Analysis of the network structure by Flory-Rehner theory

The Flory-Rehner theory was also used to evaluate the network crosslinking based on swelling experiments (after 72 h, at 37 ºC) and parameters such as equilibrium polymer swollen (Q_v), polymer volume fraction ($v_{2,s}$), Flory-Huggins interact parameter or Chi parameter (χ), molecular weight between crosslinks ($\overline{M_C}$), crosslinking density (q), shear modulus (G), Flory's characteristic ratio (C_n or C_∞), unperturbed end-to-end chain distance $(r_0^2)^{1/2}$, elongation factor (α) and the network mesh size (ξ) were obtained from the calculated parameters of Flory-Rehner Equations (Equations 4 to 19) presented in the previously topics.

For the estimation, it was required a set of information about the system that was obtained either from previous analyses or the literature, the polymer density ($\rho_{gelatin}$ = 1.34 g·cm^{-3}) by pycnometer data, solvent density ($\rho_{solvent}$ = 1.0 g·cm^{-3}) as suggest by USGS (2018), swelling ratio (SR) values at 72 h, average molecular weight of gelatin before crosslinking (M_n = 471,278 g·mol^{-1}) by GPC, molar volume of water ($\bar{V}_1$ = 18.01 mL·mol^{-1}) as proposed by Vigata et al. (2021) and the specific volume of gelatin ($\bar{v}$ = 0.7486 mL·g^{-1}) by pycnometer data. The molecular weight of the repeat unit (M_r) was considered as the average molecular weight of the amino acid composition and it was used as equal to 91.91 g·mol^{-1} for porcine type A gelatin (bloom ~300) as reported by Vigata et al. (2021) and Gilchrist et al. (2019).

The Flory's characteristic ratio (C_n or C_∞) was calculated according to Equation (17) as proposed by Ma et al. (2013) and was estimated to be equal to 7.8193.

For the root-mean-square end-to-end distance of the polymer chains between two adjacent crosslinks $(r_0{}^2)^{1/2}$, the factor used is equal to 3 because the repetitive unit already consists of 2 bonds (1,4-BDDA) instead of 1 like for vinyl polymers as proposed by Ma et al. (2013).

The calculated amino acid bond length (l = 1.44 Å) was determined by Equation (28) as reported by Osetrov, Uspenskaya and Sitnikova (2021) and Ma et al. (2013). The segment length (l_s) is equal to 4.32 Å obtained by Equation (29) according to Mark, (1999) and Berg & Tymoczko (2018). The persistence length (l_p) estimated to be equal to 20 as proposed by Mark, (1999) and Berg & Tymoczko (2018).

$$l = \frac{1.53\ \text{Å} + 1.47\ \text{Å} + 1.32\ \text{Å}}{3} \tag{28}$$

$$l_s = 1.53\ \text{Å} + 1.47\ \text{Å} + 1.32\ \text{Å} \tag{29}$$

3.1.10 Fourier transform infrared (FTIR) spectroscopy

The neat gelatin and gelatin hydrogels samples were analyzed by FTIR spectroscopy using the ATR (attenuated total reflection) mode with a ZnSe crystal as proposed by Kumar et al. (2020). Freeze-dried neat gelatin was chosen as polymer reference and all spectra were recorded in a range of 4000 – 650 cm^{-1} with 32 scans using the spectrophotometer Cary 660 FTIR, Agilent Technologies, USA. Finally, the obtained data were normalized in relation to amide I with peak located at around 1635 cm^{-1} as proposed by Zachariášová et al. (2019), using Origin 9.0 software and the vibration bands were associated with the principal chemical groups.

3.1.11 X-ray diffraction (XRD)

To evaluate the influence of crosslinking on the solid-state structure, XRD was carried out in the freeze-dried neat gelatin and in the freeze-dried hydrogels, as proposed by Kulkarni et al. (2021), Al Islam et al. (2016) and Swaroop et al. (2019). Then, freeze-dried samples in the form of milled powders were subjected to XRD analysis at room

temperature with a step size of 0.05, velocity = 5º·min^{-1} and 2θ = 5 – 45º using the diffractometer MiniFlex600 XRD, Rigaku, Auburn Hills, Texas, USA. The obtained data were treated with smoothing and plotted using Origin 9.0 software.

3.1.12 Thermal analyses (TGA & DSC)

Thermal analyses of pure gelatin and synthesized hydrogels were performed by thermogravimetric analysis (TGA) and differential scanning calorimetry (DSC) in a STA 449-F3 Jupiter equipment and samples (freeze-dried neat gelatin and crosslinked hydrogels) with approximately 10 mg each were heated from 25 up to 700 °C with a heating rate of 10 °C·min^{-1} under N_2 purge of 20 mL·min^{-1} using a hermetic aluminum pan as proposed by González et al. (2015) and Al Islam et al. (2016). For the DSC curves obtained from this approach, the thermal history of samples was not erased. Additionally, DSC analysis was also carried out in a calorimeter (Jade-DSC, Perkin Elmer 600, USA) using a hermetic aluminum pan, approximately 5 mg of freeze-dried gelatin and crosslinked hydrogels were heated with a first heating ramp from -30 to 100 ºC at 10 ºC·min^{-1} and cooling ramp at -5 ºC·min^{-1}. Subsequently, the second heating ramp from -30 to 220 °C at 5 °C·min^{-1} and cooling ramp at -5 ºC·min^{-1} under N_2 atmosphere of with a 20 mL·min^{-1} flow was carried out as proposed by Kumar et al. (2020). The thermal history of samples was erased in the first cycle.

3.1.13 Synthesis of crosslinked gelatin nanoparticles

Chemically crosslinked GNPs were synthesized via interfacial aza-Michael addition reaction in inverse miniemulsion with three distinct crosslinker concentrations in relation to the free primary amino groups of gelatin (1:1.2, 1:4 and 1:8 mmol of NH_2:mmol of crosslinker), according to the scheme presented in Figure 22. The dispersed aqueous phase was prepared by dissolving gelatin (0.2025 g) and DBU (0.0407 g) in a 0.15 M NaCl aqueous solution (1.0262 g). In sequence, the continuous organic phase (1) consisting of PGPR (0.1267 g), and cyclohexane (7.5 g) was added to the aqueous phase and was stirred magnetically at 100 rpm for 1 h. The pre-emulsion (macroemulsion) was homogenized by sonication using a sonicator (Sonic Dismembrator model 500, Fisher Scientific) for 3 min at 40 % amplitude intensity with pulse cycles of 20 s sonication and 10 s pauses in a 25 mL beaker under ice cooling bath. Afterwards, a second continuous

organic phase (organic phase 2) containing the crosslinker, 1,4-BDDA (0.01, 0.05 or 0.1 g), cyclohexane (2.5 g) and PGPR (0.015 g) was dripped in the miniemulsion, mixed for 15 s under magnetic stirring without temperature, and followed by another sonication step at the same previously conditions (time: 3 min, amplitude: 40 % and pulses: 20 s ON and 10 s OFF in a 25 mL beaker under ice cooling bath) and reaction proceeded for 24 h at 50 ºC. Subsequently, 6 mL of cyclohexane was added to the latex followed by evaporation at 25 ºC for approximately 24 h, this process was carried out twice (total evaporation time ≈ 48 h). This solvent evaporation step was followed either by GNPs redispersion in SDS (0.3 wt.%) aqueous solution or by dual curing photopolymerization. When used, doxorubicin (1.5 wt.% to monomer) was added in the dispersed aqueous phase.

The general methodology for the preparation of pure GNPs and DOX-loaded are represented in the schemes of Figures 21 and 22. The formulations for the pure GNPs (G_0.01; G_0.05 and G_0.1) and DOX-loaded GNPs (DOXG_0.01; DOXG_0.05 and DOXG_0.1) synthesis with different crosslinker concentrations are presented in Tables 4 and 5, respectively. All reactants were added in weight (g) and results are shown as mean (n = 2) followed by ± standard deviation (SD).

Figure 21 – Scheme of pure GNPs prepare via inverse miniemulsion.

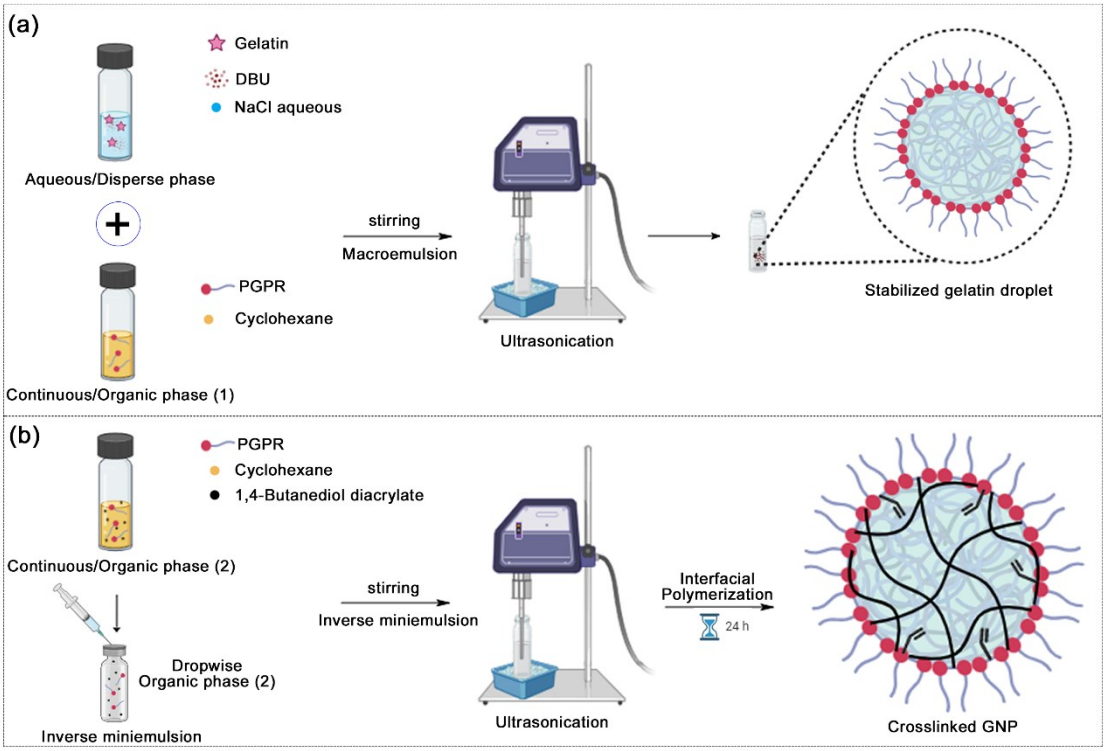

Drawn in biorender.com and Photoshop CS6 (2023).
Source: Author (2023).

Table 4 – Formulations of inverse miniemulsion for pure GNPs.

	$Weight_{theoretical}$	$Weight_{real}$		
		0.01 g 1,4-BDDA	**0.05 g 1,4-BDDA**	**0.1 g 1,4-BDDA**
Organic phase 1				
Cyclohexane	7.5	7.5058 ± 0.0008	7.5085 ± 0.0049	7.5072 ± 0.0069
PGPR	0.1267	0.1266 ± 0.0001	0.1267 ± 0.0001	0.1267 ± 0.0002
Organic phase 2				
Cyclohexane	2.5	2.5079 ± 0.0081	2.5056 ± 0.0014	2.5210 ± 0.0019
1,4-BDDA	0.01 or 0.05 or 0.1	0.0109 ± 0.0001	0.0525 ± 0.0007	0.1011 ± 0.0002
PGPR	0.015	0.0152 ± 0.0002	0.0153 ± 0.0002	0.0154 ± 0.0002
Aqueous phase				
Gelatin	0.2025	0.2026 ± 0.0002	0.2026 ± 0.0000	0.2026 ± 0.0002
DBU	0.0407	0.0406 ± 0.0003	0.0409 ± 0.0001	0.0407 ± 0.0001
NaCl(aq) 0.15 M	1.0262	1.0262 ± 0.0002	1.0264 ± 0.0001	1.0262 ± 0.0001

Formulations: Doxorubicin Gelatin_Crosslinker concentration, (G_0.01; G_0.05; G_0.1);
Source: Author (2023).

Figure 22 – Scheme of GNPs-DOX loaded prepare via inverse miniemulsion.

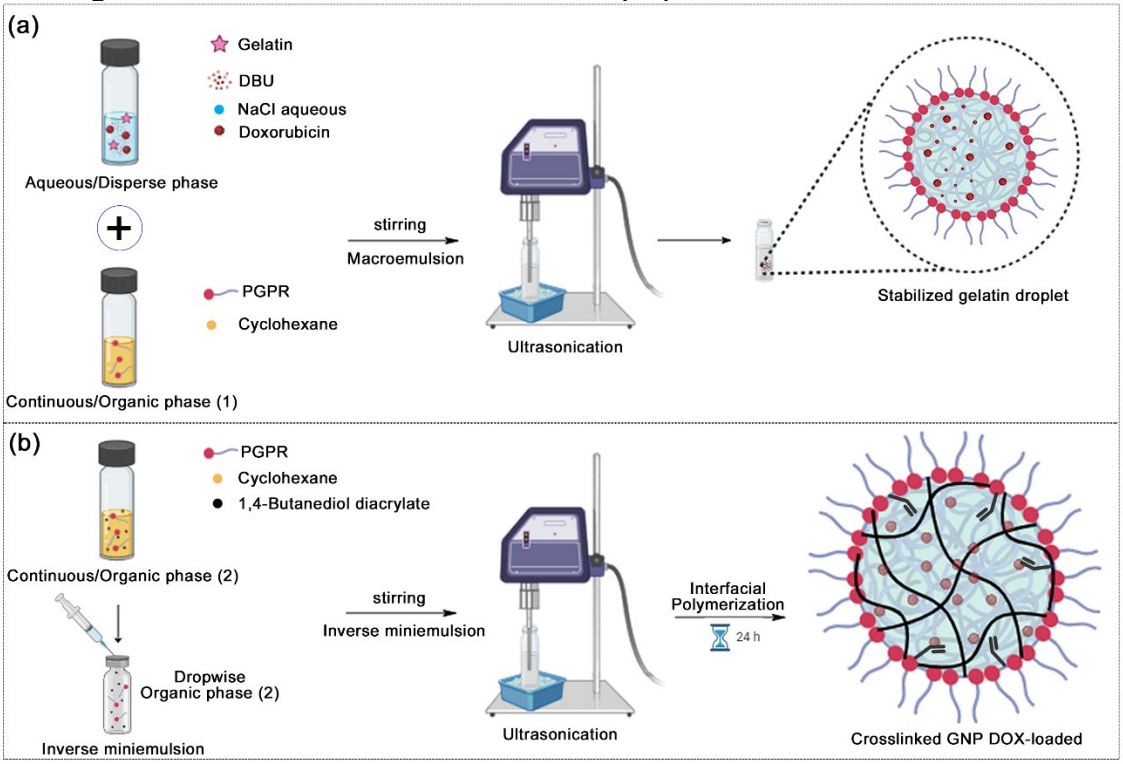

Drawn in biorender.com and Photoshop CS6 (2023).
Source: Author (2023).

Table 5 – Formulations of inverse miniemulsion for crosslinked DOX-loaded GNPs.

	$Weight_{theoretical}$	$Weight_{real}$		
		0.01 g 1,4-BDDA	**0.05 g 1,4-BDDA**	**0.1 g 1,4-BDDA**
Organic phase 1				
Cyclohexane	7.5	7.5062 ± 0.0071	7.5131 ± 0.0071	7.5209 ± 0.0161
PGPR	0.1267	0.1267 ± 0.0002	0.1268 ± 0.0071	0.1268 ± 0.0002
Organic phase 2				
Cyclohexane	2.5	2.5076 ± 0.0038	2.5063 ± 0.0072	2.5036 ± 0.0021
1,4-BDDA	0.01 or 0.05 or 0.1	0.0105 ± 0.0008	0.0530 ± 0.0014	0.1013 ± 0.0001
PGPR	0.015	0.0152 ± 0.0001	0.0152 ± 0.0001	0.0151 ± 0.0002
Aqueous phase				
Gelatin	0.2025	0.2023 ± 0.0002	0.2026 ± 0.0003	0.2026 ± 0.0005
DBU	0.0407	0.0409 ± 0.0001	0.0407 ± 0.0001	0.0409 ± 0.0006
DOX (1.5%)	0.0030	0.0032 ± 0.0001	0.0033 ± 0.0002	0.0031 ± 0.0001
$NaCl_{(aq)}$ 0.15 M	1.0262	1.0263 ± 0.0002	1.0262 ± 0.0001	1.0264 ± 0.0004

Formulations: Doxorubicin Gelatin_Crosslinker weight (DOXG_0.01; DOXG_0.05; DOXG_0.1);
Source: Author (2023).

3.1.14 GNPs prepared via free radical photopolymerization and photo-crosslinking reactions

As supported by Baseer et al. (2019), some of free ε-amino groups may be not free at GNPs surface but rather spatially oriented to within nanoparticle, which can reduce their availability to crosslinking at interface. To circumvent that, a dual curing photopolymerization and/or photo-crosslinking approach was applied to improve crosslinking density of the GNPs. In addition, as mentioned by Llorente et al. (2021) and Lang et al. (2022), the photopolymerization reactions are a suitable approach in crosslinking reactions with acrylates groups because they are highly reactive and the reaction occurs rapidly and, they can homopolymerize producing high molecular weight polymers and promoting the improvement of crosslinking density (q).

To prepare photo-crosslinked GNPs, the procedure used to prepare inverse miniemulsion was kept the same. The general methodology for the preparation of photopolymerized GNPs and photopolymerized GNPs DOX-loaded via interfacial crosslinking in inverse miniemulsion is represented in the scheme of Figure 23.

Figure 23 – Scheme of photo-cured GNPs-DOX loaded prepare.

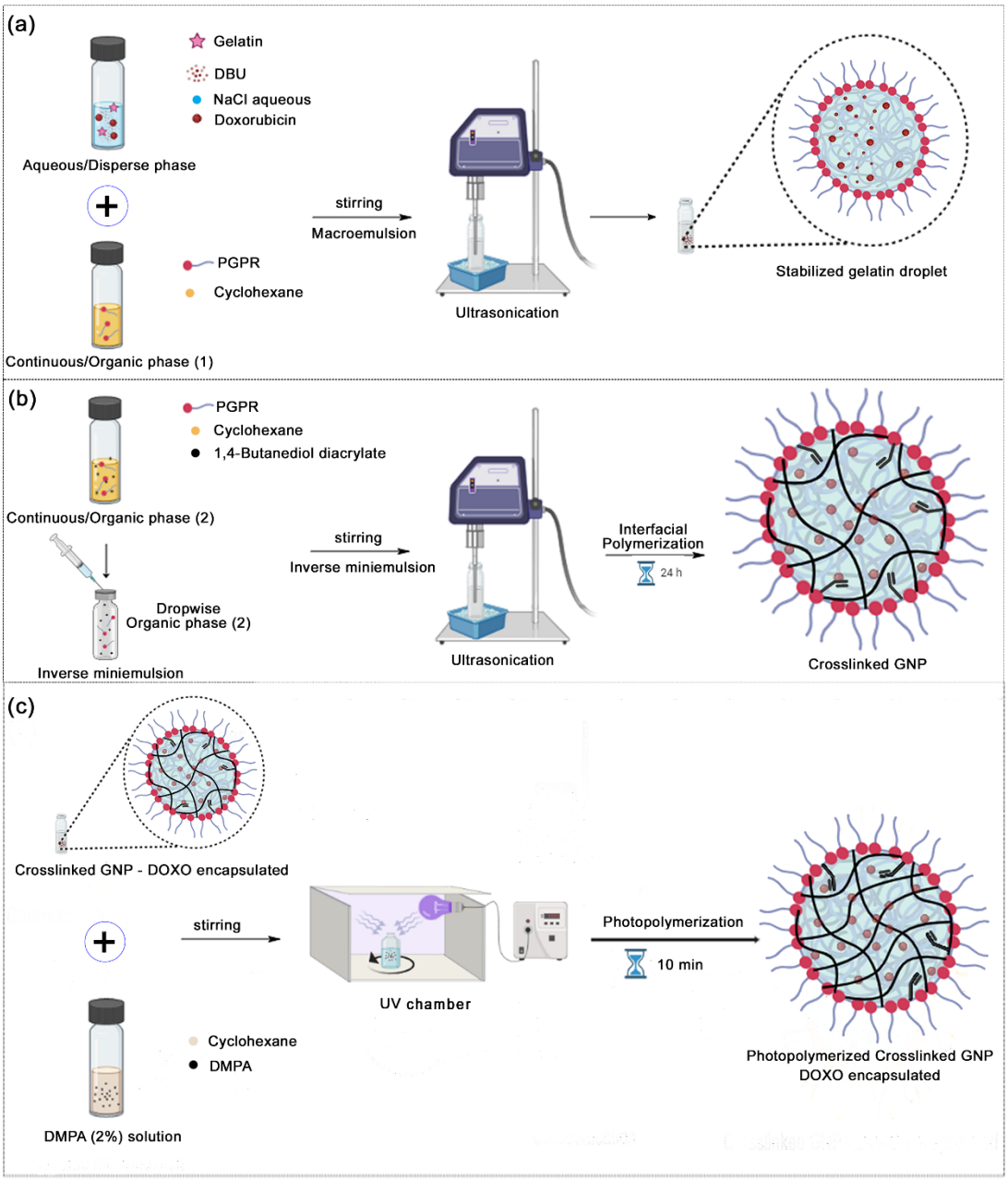

Drawn in biorender.com and Photoshop CS6 (2023).
Source: Author (2023).

After GNPs crosslinking by interfacial aza-Michael addition reaction, the latexes were submitted to a photo-curing according to a methodology adapted from Liu et al. (2013). For that, a DMPA solution was added dropwise into the latex, in a concentration of 2 wt.% in relation to gelatin, to react with the residual acrylate groups of the crosslinking agent that did not undergo aza-Michael addition previously used to crosslink the GNPs. The photoinitiator (DMPA) solution was prepared by dissolving 4.05 mg of DMPA in 0.5 mL of cyclohexane in a N_2 purged glass vial in the dark and this solution was stirred for 5 min. The free radical photo-curing reactions were carried out in a pre-

heated UV chamber (~ 40 ºC) with power output of 4.13 mW·cm^{-2} for 15 min in an open glass vial, under magnetic stirring at 200 rpm. Additionally, to evaluate the photo-curing efficiency in the free amine's consumption, the modification degree (DM) of the photo-cured GNPs was estimated by TNBS essay after latex purification and drying. When used, DOX (1.5 wt.% to monomer) was added in aqueous phase.

The formulations of the inverse miniemulsions for photo-cured GNPs (PHG_0.01; PHG_0.05 and PHG_0.1) and photo-cured DOX-loaded GNPs (PHDOXG_0.01; PHDOXG_0.05 and PHDOXG_0.1) synthesis with different crosslinker concentrations are presented in Tables 6 and 7, respectively. All reactants were added in weight (g) and results are shown as mean (n = 2) followed by ± standard deviation (SD).

Table 6 – Formulations for crosslinked photo-cured GNPs.

	Weight$_{theoretical}$	**Weight$_{real}$**		
		0.01 g 1,4-BDDA	**0.05 g 1,4-BDDA**	**0.1 g 1,4-BDDA**
Organic phase 1				
Cyclohexane	7.5	7.5053 ± 0.0001	7.5054 ± 0.0002	7.5041 ± 0.0026
PGPR	0.1267	0.1267 ± 0.0001	0.1266 ± 0.0001	0.1267 ± 0.0001
Organic phase 2				
Cyclohexane	2.5	2.5185 ± 0.0192	2.5084 ± 0.0040	2.5171 ± 0.0212
1,4-BDDA	0.01 or 0.05 or 0.1	0.0120 ± 0.0006	0.0520 ± 0.0014	0.1011 ± 0.0011
PGPR	0.015	0.0152 ± 0.0001	0.0151 ± 0.0001	0.0152 ± 0.0001
Aqueous phase				
Gelatin	0.2025	0.2026 ± 0.0001	0.2026 ± 0.0001	0.2026 ± 0.0001
DBU	0.0407	0.0408 ± 0.0001	0.0408 ± 0.0001	0.0407 ± 0.0001
$NaCl_{(aq)}$ 0.15 M	1.0262	1.0263 ± 0.0002	1.0263 ± 0.0001	1.0263 ± 0.0001
2PP *(two photon polymerization)*				
DMPA (2%)	0.0020	0.0024 ± 0.0005	0.0022 ± 0.0001	0.0022 ± 0.0003

Formulations: Photo-cured Gelatin_Crosslinker weight (PHG_0.01; PHG_0.05; PHG_0.1);
Source: Author (2023).

Table 7 – Formulations for crosslinked photo-cured GNPs DOX-loaded.

	$Weight_{theoretical}$	$Weight_{real}$		
		0.01 g 1,4-BDDA	**0.05 g 1,4-BDDA**	**0.1 g 1,4-BDDA**
Organic phase 1				
Cyclohexane	7.5	7.5037 ± 0.0021	7.5042 ± 0.0018	7.5107 ± 0.0080
PGPR	0.1267	0.1267 ± 0.0001	0.1268 ± 0.0001	0.1267 ± 0.0001
Organic phase 2				
Cyclohexane	2.5	2.5121 ± 0.0163	2.5031 ± 0.0029	2.5123 ± 0.0123
	0.01			
1,4-BDDA	0.05	0.0115 ± 0.0007	0.0515 ± 0.0007	0.1015 ± 0.0007
	0.1			
PGPR	0.015	0.0152 ± 0.0001	0.0151 ± 0.0001	0.0152 ± 0.0001
Aqueous phase				
Gelatin	0.2025	0.2026 ± 0.0001	0.2026 ± 0.0001	0.2026 ± 0.0001
DBU	0.0407	0.0407 ± 0.0001	0.0407 ± 0.0001	0.0407 ± 0.0001
$NaCl_{(aq)}$ 0.15 M	1.0262	1.0263 ± 0.0001	1.0262 ± 0.0001	1.0262 ± 0.0001
DOX (1.5%)	0.0030	0.0031 ± 0.0001	0.0031 ± 0.0001	0.0033 ± 0.0002
2PP *(two photon polymerization)*				
DMPA (2%)	0.0020	0.0021 ± 0.0001	0.0023 ± 0.0001	0.0026 ± 0.0004

Formulations: Photo-cured DOX Gelatin_Crosslinker weight (PHDOXG_0.01; PHDOXG_0.05; PHDOXG_0.1);
Source: Author (2023).

3.1.15 GNPs Redispersion

Nanoparticles were transferred to the aqueous phase according to the methodology proposed by Peres et al. (2018) and Steinmacher et al. (2017) with some modifications. The redispersion was carried out by adding 0.5 mL of purified GNPs dispersions into 1.5 mL of an aqueous SDS solution (0.3 wt.%). Samples were then stirred overnight at 100 rpm and at room temperature to completely remove cyclohexane excess by evaporation. Subsequently, the particle size and PDI were immediately measured via DLS by transferring 0.25 µL of redispersed GNPs to a glass cuvette containing 1.5 mL of distilled water using a Nanosizer (Malvern Instruments GmbH, U.K) and the measurements were conducted at 25 ºC.

3.1.16 Zeta potential (ζ)

Colloidal stability was indirectly evaluated by measuring the superficial charge density of GNPs according to the methodology proposed by Baseer et al. (2019); Cordeiro et al. (2021) with some modifications. For that, the zeta potential was determined by

electrophoretic light scattering (ELS) with a Zetasizer (Malvern Instruments GmbH, U.K). The pH-dependence of GNPs stability was evaluated by performing studies at different pH (5.0, 6.5 and 7.4) using distilled water or PBS solutions as solvent. To evaluate the charge behavior at low pH values, a preliminary study was also conducted at the same conditions with PBS at pH 3.0. Subsequently the GNPs redispersion, 25 µL of redispersed GNPs were resuspended in 1.5 mL of distilled water or PBS solutions in an Eppendorf tube. The resulting samples were used for zeta potential measurements at 37 °C, after two minutes of sample-equipment equilibration, at a scattering angle of 173º using the following parameters for the system, water refractive index (R.I. = 1.333); water dielectric constant (k = 74.83); water viscosity (μ = 0.6965 cP) and gelatin coefficient attenuator (α = 0.010). All experiments were carried out in duplicate and the mean values and standard deviations were calculated from each measurement in triplicate.

Morphology and particle size

3.1.17 Particle size (D_p) and polydispersity index (PDI)

The intensity average nanoparticles diameter (D_p) and the polydispersity index (PDI) were determined by dynamic light scattering (DLS). To access the droplet and nanoparticle size, an aliquot of 0.25 µL of inverse miniemulsion or latex was transferred to a glass cuvette containing 1.5 mL of cyclohexane, in the beginning (droplet) and at the end of polymerization reactions (particle) and readings were recorded at 25 ºC in triplicate at an angle of 173º using a Nanosizer (Malvern Instruments GmbH, U.K). The size of redispersed nanoparticles in distilled water was measured at the same conditions used to cyclohexane, however, the solvent parameters as refractive index and viscosity were changed suitably in equipment software for both solvents. Refractive index and viscosity of cyclohexane (R.I. = 1.423 and μ = 0.8920 cP) and water (R.I. = 1.330 and μ = 0.8872 cP) both at 25 ºC, were used in the measurements, respectively. The refractive index of gelatin applied (R.I. = 1.59) is based on the polystyrene protein standard.

3.1.18 Microscopy analyses

Morphology and particle size of the redispersed DOX-unloaded GNPs were evaluated by Transmission Electron Microscopy (TEM) at 100 kV as proposed by Cordeiro et al. (2021). Then, 5 µL of dispersion (0.1% solids content) was dripped on a

carbon-coated copper grid (300 mesh) and dried for 48 h at room temperature. Subsequently, samples were stained with 2% of uranyl acetate for 10 min in a dark room environment and the uranyl acetate excess was removed with a filter paper and grid were again submitted to dry for more 48 h at room temperature in a dark environment. Finally, TEM images were accessed by an electronic microscope (TEM, JEOL JEM-1011, Peabody, USA) and image captures were made in a representative sample content.

In addition, in order to evaluate the morphology and the effective drug encapsulation (incorporation or accumulation of the hydrophilic drug) after five days of GNPs redispersion in water, the doxorubicin fluorescence at 480 nm in the inner core was measured and used as the encapsulation indicative of the drug model, for that fluorescence microscopy measurements were carried out with objective lenses at 20 and 40X of magnification using an optical microscope (Olympus, BX41) equipped with a fluorescent lamp and using the suitable filters for this evaluation. Then, the images were captured by Q-capture Pro 5.1 Q-imaging® software. To the same objective, the confocal laser scanning microscopy (CLSM) was also carried out in photopolymerized DOX-GNPs after five days of GNPs redispersion in water with excitation and emission wavelengths at 470 and 585 nm (FAN et al., 2018; KAUFFMAN et al., 2016; LIU et al., 2013), respectively, using a confocal microscope (Leica Microsystems, TCS SP5/DMI 6000, Illinois, USA) equipped with a fluorescent lamp using the suitable filter for evaluation and images were captured by LAS AF Lite software. In the optical and confocal cases, analysis was carried out after five days of aqueous redispersion to promote the swelling of GNPs (size increase) allowing their identification.

3.1.19 Encapsulation efficiency (EE)

For the encapsulation efficiency (EE, %) estimation, the methodology proposed by Cordeiro et al. (2020), Huang et al. (2020) and Peres et al. (2018) was used with some modifications. The blank was prepared by centrifuging the GNPs dispersed in cyclohexane (without DOX) twice for 30 min at 3,500 rpm (Mini Spin Plus, Eppendorf, Hamburg, Germany) to purify the inverse miniemulsion and separate the solid phase from the liquid phase. The clear supernatant solution was removed, and absorbance was determined at room temperature in a 96-well microplate reader (Biotek® – EPOCHH-SN, Agilent Technologies, Santa Clara, USA) at 480 nm. For all experiments containing

DOX-loaded GNPs, the procedure as kept the same. Subsequently, the absorbance was compared to a prepared DOX calibration curve, Figure (24) and applied to Equation (30).

$$EE\ (\%) = \left(\frac{w_c - w_f}{w_f}\right) \times 100 \quad (30)$$

In which w_c ($\mu_g \cdot mL^{-1}$) is the total doxorubicin concentration at the beginning of the process and w_f ($\mu_g \cdot mL^{-1}$) is the concentration of supernatant (nonencapsulated) doxorubicin.

3.1.20 DOX calibration curve

The mean absorbance of the model drug (DOX) at different concentrations was plotted to form a calibration curve. The DOX calibration curve (Figure 24, y = 0.002·X– 0.0011 and R^2 = 0.9978) in the dilutions range of (0.5 to 55 µg·mL^{-1}) was prepared in the dark with distilled water, in duplicate. Samples were read at 480 nm as proposed by Peres et al. (2018) using a 96-well microplate reader (Biotek® – EPOCHH-SN, Agilent Technologies, Santa Clara, USA). This curve was used as reference to encapsulation efficiency studies.

Figure 24 – Doxorubicin calibration curve.

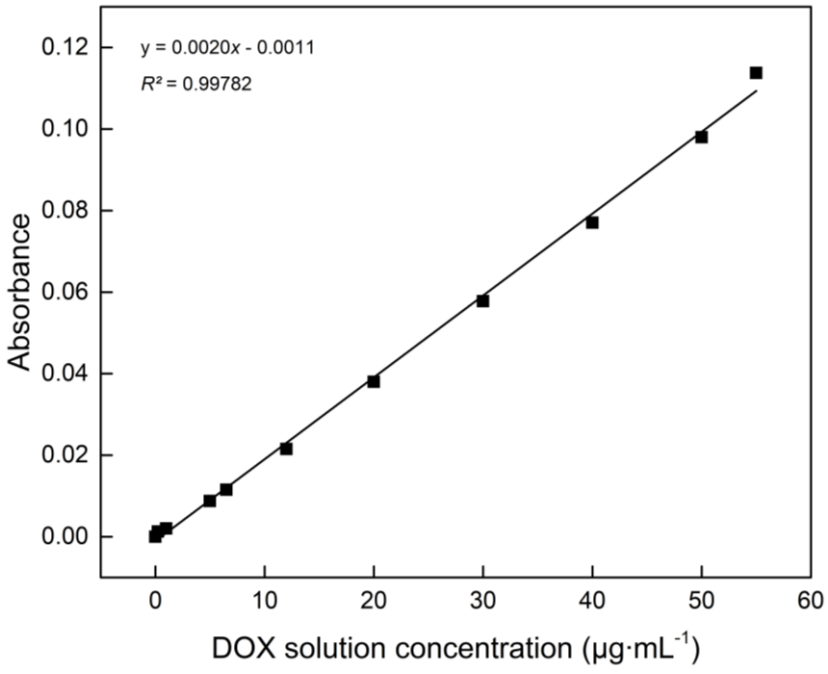

Source: Author (2023).

3.1.21 Statistical Analysis

The results were treated with Microsoft Excel (Office, 2019), Origin 9.1 and STATISTICA 7.0. The Shapiro-Wilk test was applied to verify the data normality and they were submitted to ANOVA (variance analysis) at significance level of 95% with (*p-value* ≤ 0.05) to evaluate the significantly statistics differences between the means and to the Tukey test to evaluate the mainly differences. Conversely, data that did not present normality were submitted to Kruskal-Wallis ANOVA test and median test. Afterwards, were submitted to multiple comparisons of mean ranks with (*p-value* ≤ 0.05 or *p-value* ≤ 0.10).

4 RESULTS AND DISCUSSION

4.1 GELATIN AND HYDROGELS CHARACTERIZATION

4.1.1 Gelatin Molecular weight (M_w) evaluation

Molecular weight averages and molecular weight distribution of neat, freeze-dried gelatin were assessed by two different techniques gel permeation chromatography (GPC) and light scattering (LS). Number and weight average molecular weights (M_n and M_w) and dispersity (Đ) determined by GPC are presented in Table 8.

Table 8 – Average molecular weights (M_n and M_w) and dispersity (Đ) of gelatin determined by GPC.

Sample	Peak	M_n (g·mol^{-1})	M_w (g·mol^{-1})	Đ
Gelatin	1	471,278	539,127	1.144
	2	28,303	271,203	2.516

Source: Author (2023).

The estimated gelatin molecular weight (M_w) and polydispersity (Đ) are in accordance with values reported in literature for porcine type A gelatin. The results found for the first peak showed a narrow and monodisperse distribution while the second peak presents a broad and polydisperse distribution (MALVERN, 2017[b]). Generally, the molecular weight distribution of gelatins is bimodal and the first elution peak is related to the portions of γ-chain (higher M_w) and the second to the portions of β-chain (lower M_w), as found here and in the works carried out by Haema et al. (2014), Meyer & Morgenstern (2003) and Peng, Martineau & Shek (2008).

Haema et al. (2014) reported values of M_n = 83,000 kDa, M_w = 157,000 kDa and Đ = 1.8 for porcine type A gelatin (Sigma Aldrich) using the GPC/SEC technique and calibration with polyethylene oxide (PEO) standard as in the present study.

Meyer & Morgenstern (2003) evaluated samples of type B gelatin and acid soluble collagen (ACS) via SEC-MALS (*size exclusion chromatography coupled to a multi-angle light scattering*) and detected that around 8% of the fractions of gelatin presented M_w > 300 kg·mol^{-1}. The authors also reported that larger gelatin molecules in the sample may be due to the incomplete disintegration of collagen fibrils that may be covalently crosslinked with molecules derived from collagen itself and which were not

cleaved during hydrolysis to produce gelatin. As mentioned by these authors, even with a very broad molecular weight distribution, the higher molecular weight components (M_w > 500 kg·mol^{-1}) were not separated and were eluted in the void volume, and parts of lower molecular components were also not separated by the column and the scattering intensity of small gelatin molecules (M_w < 20 kg·mol^{-1}) was too low to calculate with sufficient accuracy.

As reported by Herrick, Marziarz & Liu (2018) the SEC technique is suitable for analyzing polypeptides and low molecular weight gelatin molecules when low molecular weight standards are used, however, in the region of ultra-high molecular weight (≈ 10^6 Da), SEC has a poor resolution because of the total size limit of packed columns being commonly coupled to other detection systems e.g., FFF (*Field Flow Fractionation*) and AFIFFF-MALS (*Asymmetrical Flow Field Flow Fractionation coupled to an Ultraviolet and Multi Angle Light Scattering*). Commonly, the reported values for molecular weight distribution of type A and B gelatins from SEC are in the order of 10 and 400 kDa, but values above (≈ 10^6 Da) are also reported and commonly referred to as "microgels".

In addition, the weight average molecular weight was also estimated by static light scattering (SLS), in triplicate, via linear adjustment (y = 3.69523·X + 0.0018 and R^2 = 0.9895) to the Rayleigh Equation, Equation (19). Molecular weight was found to be in the range of 543,478 ± 5,810 kDa and the 2^{nd} virial's coefficient equal to 0.0018 ± 1.72·10^{-4} mL·mol·min^{-1}, as presented in Figure 41, Appendix A.

The second virial coefficient (A_2), a temperature-dependent parameter, determines the solution nonideality, which is close to an ideal solution in a wide range of concentrations when A_2 = 0. This occurs when the entropy of mixing compensates repulsive polymer–solvent interactions or attractive polymer–polymer interactions. In this context, the second virial coefficient represents deviations from ideality caused by interactions between two molecules (TERAOKA, 2002; pg. 79). Herein, the value of the second virial coefficient found at 50 ºC, suggests a proximity to an ideal solution and a suitable polymer-solvent (gelatin-water) interaction for being nearly to zero.

Molecular weight results from both techniques presented a fair agreement with each other. Moreover, SLS is considered an absolute method and has shown to be a reliable and useful tool for characterizing the molecular weight of proteins. On the other hand, the M_n and, consequently, the PDI cannot be estimated by SLS as they can be by GPC, which in turn has the limitation of being a relative method based on calibration standard.

However, as mentioned by Duthen et al. (2018), these approaches may have some limitations in detection and could over or underestimate the real molecular weight of complex aqueous polymers, to render more accurate estimations SLS (or MALS) detector is commonly coupled to a GPC equipment or using other techniques such as the AsFIFFF-UV/MALS (*Asymmetrical Flow Field Flow Fractionation coupled to an Ultraviolet and Multi Angle Light Scattering*), which proved to be more sensitive approaches in the detection of gelatins molecular weights, presenting values over $1 \cdot 10^7$ $g \cdot mol^{-1}$.

4.1.2 Synthesis of covalently crosslinked gelatin hydrogels in solution

The synthesis of the PBAEs gelatin-based hydrogels was carried out by a one-pot aza-Michael addition reaction of the free primary amino groups (± 0.305 mmol of lysine$\cdot g_{gelatin}^{-1}$) and, subsequently, the secondary amines from gelatin chain and the secondary amines (N–H) formed after the addition to acrylate groups of 1,4-butanediol diacrylate (crosslinker). According to Billiet et al. (2013), in addition to lysine, other free amino groups from gelatin as hydroxylysine and ornithine can also covalently react with carbonyls to form amides or unsaturated bonds to form crosslinked networks. The crosslinking reaction takes place quickly (± 2 h), being possible to visualize the gel formation inside the reactor. However, it was decided to continue for a period of 24 h to ensure that reaction was complete. This statement corroborates the results reported by Billiet et al. (2013) and Nichol et al. (201) during the synthesis of acrylated and methacrylated gelatin hydrogels, with a maximum reaction time of 1 h under conditions like those used in this work.

In addition, and considering the studies conducted by Shooshtari & Van de Mark (2001[a,b]) and Mallik & Das (1960) on 1,4-addition reactions mechanisms for primary and secondary amines with acrylic and diacrylic esters, it was proposed a concerted mechanism as described by Shooshtari & Van de Mark (2001[a]) and shown in the scheme of Figures 25 and 26. After nucleophilic attack by amines, the first step consists of a proton transfer (a), and followed by formation of a stable intermediate compound (b), forming the covalently crosslinked gelatin hydrogel (Figure 26). However, even the concerted mechanism being widely accepted, as reported, and proposed by Mallik & Das (1960) and Bernasconi (1989), concomitantly ionic mechanisms and formation of intermediate zwitterionic compounds throughout the reaction may also occur.

Figure 25 – Concerted mechanism for the synthesis of covalently crosslinked gelatin hydrogels.

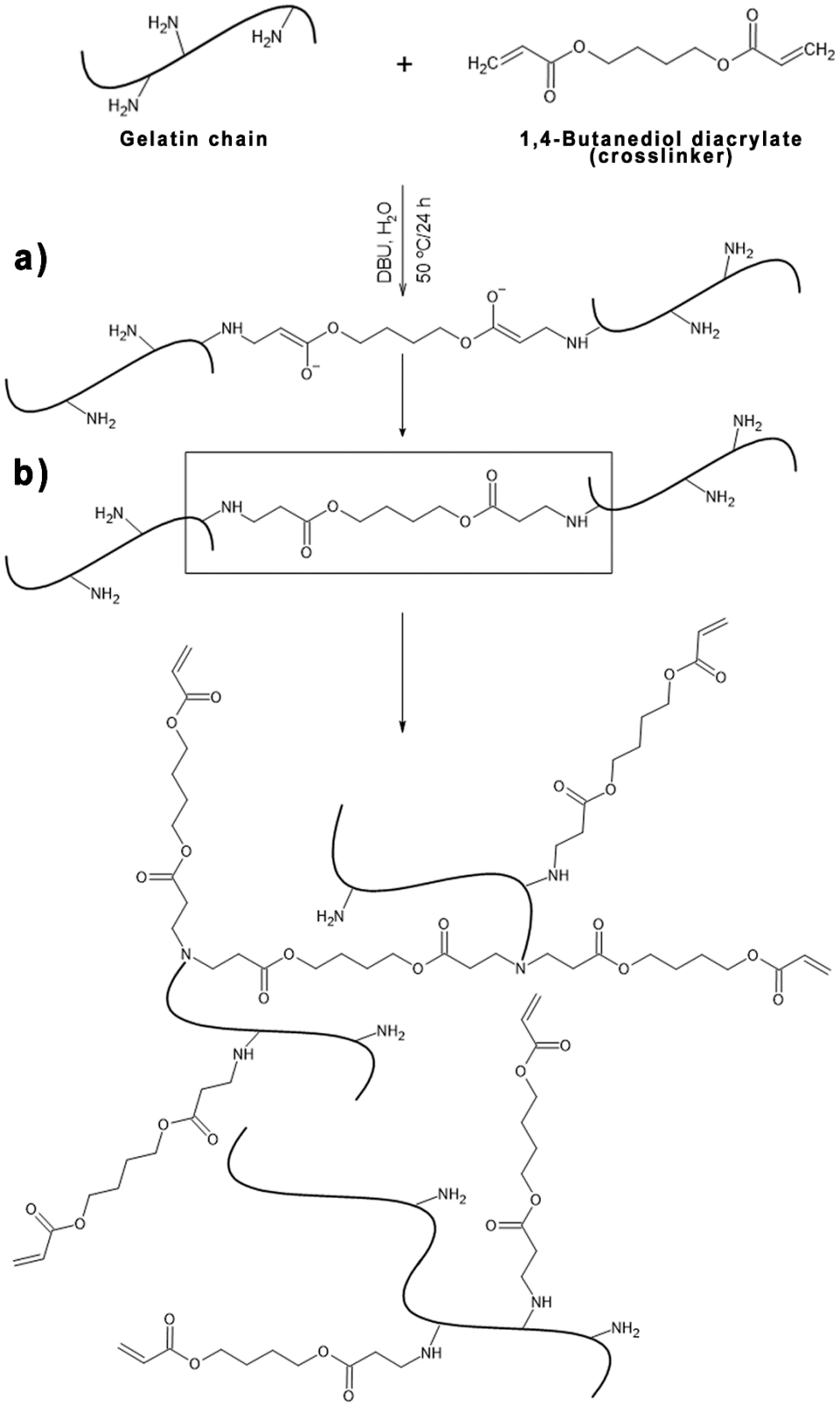

Drawn in ChemSketch and Photoshop CS6 (2023);
Source: Author (2023).

Figure 26 – Representation of the covalently crosslinked gelatin hydrogel.

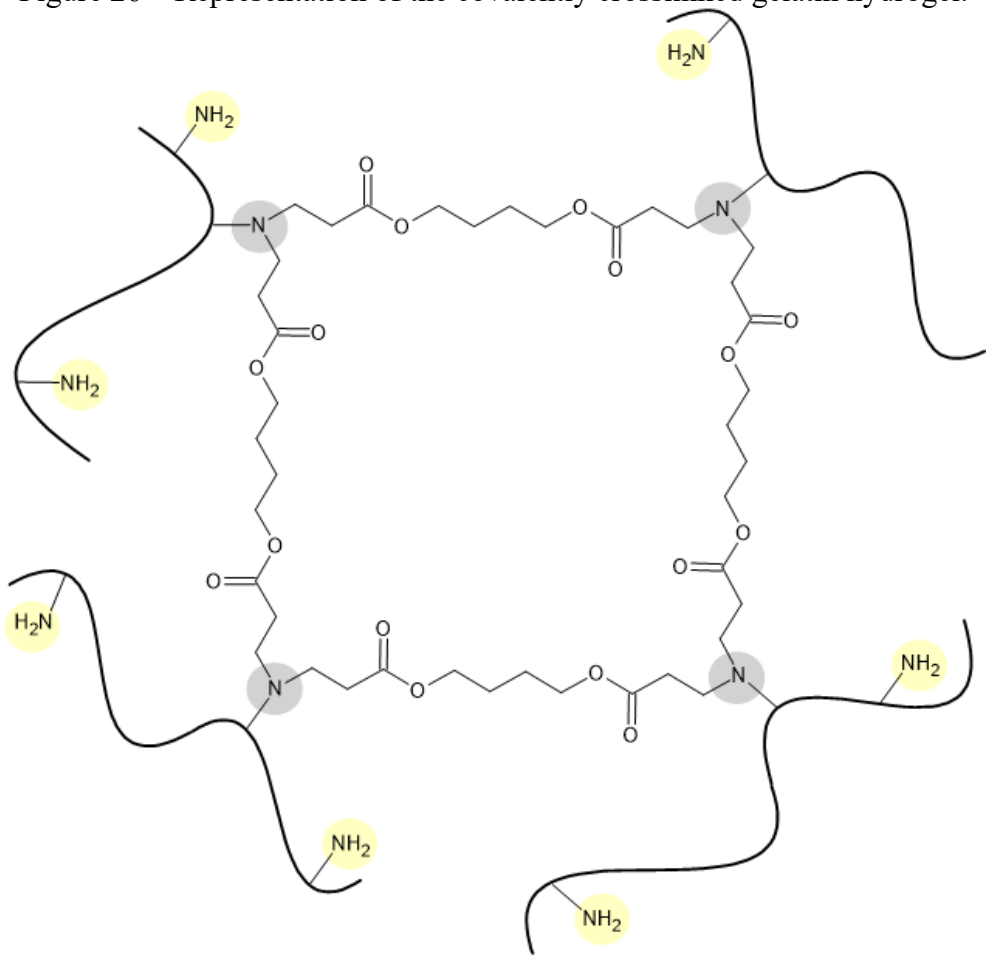

Legend: (●) – Primary amino group and (●) – Tertiary amino group (formed)
Drawn in ChemSketch and Photoshop CS6 (2023);
Source: Author (2023).

A similar approach was performed by Arslan (2020) during the covalently crosslinked gelatin hydrogels preparation for the use in biomedical applications. The author used an acrylated β-cyclodextrin as crosslinker agent to successfully crosslink gelatin using DBU as catalyst through of aza-Michael addition reaction for diclofenac sodium salt encapsulation.

Furthermore, it is worth mentioning that, in this work, we proved another important evidence reported in literature concerned to the reactivity of vinylic compounds. Initially, an attempt was made to crosslinking gelatin with ethylene glycol dimethacrylate (EGDMA) under the same reaction conditions as the hydrogels crosslinked with 1,4-BDDA were (20% w/v to solvent and equal concentration of mmol DBU to mmol EGDMA). The main difference between these crosslinkers is the presence of methyl group in the EGDMA acrylic groups that makes it more hindered and more hydrophobic than 1,4-BDDA.

In addition to aza-Michael reaction (a), other attempts with different mechanisms were carried out (all these formulations are presented in Table 22, Appendix A) to promote gelatin crosslinking with EGDMA, such as:

a) aza-Michael addition in solution at 50 ºC for 24 h;

b) aza-Michael addition in solution at 50 ºC for 24 h, followed by free radical polymerization using potassium persulfate (KPS) as thermal initiator (2% $w_{initiator}/w_{monomer}$) at 70 ºC for 24 h;

c) aza-Michael addition in solution at 50 °C for 24 h, followed by free radical photopolymerization with IG2959 (2% $w_{initiator}/w_{monomer}$) as photoinitiator under inert environment (N_2 purge) at 40 ºC for 4 h;

d) aza-Michael addition in solution at 50 ºC for 24 h in solution, followed by free radical photopolymerization with IG2959 (2% $w_{initiator}/w_{monomer}$) in the presence of a hydroxyethylmethacrylate (HEMA) monomer at 40 ºC for 4 h under inert environment (N_2 purge).

In Table 9 the reaction conditions are summarized as well as the solubility of synthesized hydrogels in hot water at 50 ºC to evaluate the crosslinking efficiency.

Table 9 – Solubility of hydrogels synthesized using EGDMA as crosslinker.

Sample	**Reaction conditions**	**Solubility in hot water (50 ºC)**
a) G_EGDMA	Solution polymerization (50 ºC, 24 h)	Totally soluble
b) G_EGDMA_KPS	Solution polymerization (50 ºC, 24 h) followed by free radical polymerization (70 ºC, 4 h)	Totally soluble
c) G_EGDMA_IG2959	Solution polymerization (24 h, 50 ºC) followed by free radical photopolymerization (40 ºC, 4 h)	Totally soluble
d) G_EGDMA_IG2959_ HEMA	Solution polymerization (24 h, 50 ºC) followed by free radical photopolymerization (40 ºC, 4 h) with co-monomer (HEMA)	Partially soluble

Source: Author (2023).

Nonetheless, it was found in all cases, that crosslinking did not occur because the final polymers obtained were totally soluble in hot water, except for the formulation (d). However, on contrary to 1,4-BDDA purifications, in all EGDMA tests, solutions were purified in cool ethanol or acetone to remove the reagents excess since solid hydrogels were not formed as evidenced in 1,4-BDDA formulations. As found in the works carried out by Mallik & Das (1960) and González et al. (2015), the presence of the methyl group at the α position of the double bond in the alkyl methacrylates causes a steric hindrance to nucleophilic attack by amine groups and, consequently, the reduction of electrophilic character in the addition type reactions. Then, due to this hindrance, the EGDMA is less reactive (poor Michael acceptor) than 1,4-BDDA in the aza-Michael addition reactions affinity order which reduces the possibility of binding and, consequently, the expected crosslinking. For these reasons and from the above tests carried out, the 1,4-butanediol diacrylate was chosen as crosslinker agent for all experiments performed and the following characterizations made corresponds to hydrogels prepared only via aza-Michael addition approach using this crosslinker.

4.1.3 Density and volume by helium pycnometry

The measured gelatin density is in accordance with literature values reported by Gilchrist et al. (2019), Vigata et al. (2021), Osetrov, Uspenskaya & Sitnikova (2021) and Xing et al. (2014) with $\rho_{gelatin}$ = 1.345 g·cm^{-3}. For crosslinked hydrogels, the true density varied from 1.29 up to 1.55 g·cm^{-3} and presented normal distribution by Shapiro-Wilk test. Statistically, the density and the swelling ratio shown differences between the means at significance level of 95% (*p-value* ≤ 0.05) by ANOVA and all samples differ from each other by Tukey's test as shown in Table 10.

Table 10 – Physical parameters and swelling ratio values.

Sample	(ρ) – True density (g·cm^{-3})	SR – Swelling Ratio (%)
Gelatin	1.34 ± 0.0057^{a}	-
G_0.15	1.55 ± 0.0049^{b}	961.67 ± 32.83^{a}
G_0.30	1.29 ± 0.0031^{c}	1547.20 ± 64.42^{b}
G_0.45	1.39 ± 0.0048^{d}	2563.50 ± 60.71^{c}

Results are shown as mean (n = 10) for density and (n = 6) for swelling followed by ± standard deviation (SD);
Different letters in the same column indicate statistically significant differences between the means by Tukey's test at significance level of 95% (*p-value* ≤ 0.05);
Source: Author (2023).

The lowest density was found for formulation G_0.30 (1:1) and the highest for G_0.15 (1:0.5) and G_0.45 (1:1.5) showed an intermediate value. The density values found are accordingly to those reported by Ofner & Bubnis (1996) for crosslinked gelatin hydrogels using glutaraldehyde (GTA), with values varying from 1.29 to 1.39 g·cm^{-3}. Additionally, other measured parameters such as volume and specific volume were presented in Table 23, Appendix A.

4.1.4 Swelling ratio (SR)

The hydrogels total water absorption in percentage (%) was accessed by measuring the total weight of a soaked hydrogel after 72 h of swelling in water at 37 ºC, Figure 27. In addition, the swelling kinetics were not carried out to avoid weight losses during weighing and to keep all polymers intact until the equilibrium was achieved.

Figure 27 – Swelling ratio (%) of gelatin hydrogels at 37 ºC.

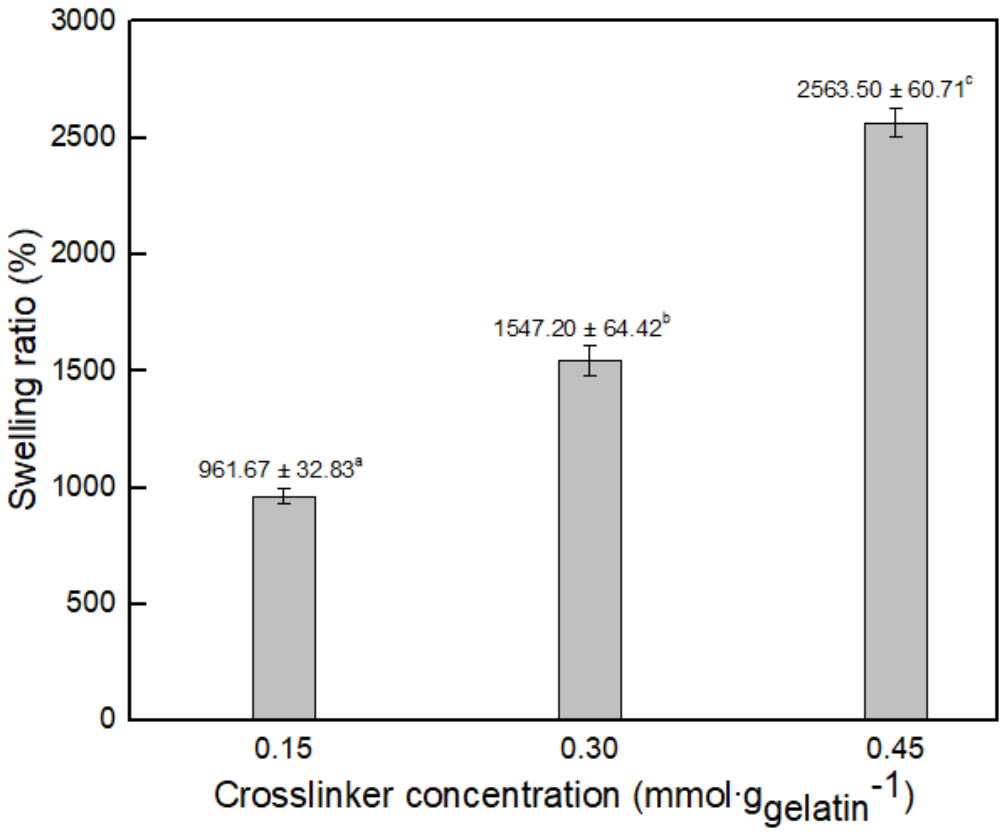

Results are shown as mean (n = 6) followed by ± standard deviation (SD);
Different letters at bars indicate statistically significant differences between the means by Tukey's test at significance level of 95% (p-*value* ≤ 0.05);
Source: Author (2023).

Moreover, the highest swelling ratio (%), Figure 27, was found for the highest crosslinker concentration (G_0.45 – 25.64 ± 0.60 $g_{water} \cdot g_{hydrogel}^{-1}$) and decreases in decreasing crosslinker concentration order (G_0.30 – 15.47 ± 0.64 $g_{water} \cdot g_{hydrogel}^{-1}$ < G_0.15 – 9.61 ± 0.32 $g_{water} \cdot g_{hydrogel}^{-1}$). In addition, the means presented statistical differences at significance level of 95% by ANOVA analysis and all the samples differ to each other by presenting significantly statistically differences by the Tukey's test (*p-value* ≤ 0.05). The statistical differences point the significant effect of varying crosslinker concentration on the hydrogels swelling. On the other hand, the presence of a greater amount of crosslinker (*SAP – superabsorbent polymer*) in the more substituted hydrogels can also provide to polymer a greater absorbent capacity due to inherent characteristics of these compounds, such as high-water absorption capacity (WAC), high water retention even under pressure, ionic sensitivity, flexibility, among others, as previously mentioned (see Item 2.2 – Literature review).

Additionally, the swelling ratio (SR) increased with the modification degree (DM) increased. In this sense, the insertion of acrylate moieties from the incomplete crosslinking can keep the hydrophilic nature of gelatin suggesting a less crosslinked networks which allows the absorption of a great amount of water, as later confirmed by the crosslinking density values (q).

For hydrogels, the swelling behavior is an important parameter to evaluate as it influences solute diffusion, surface properties and mobility, mechanical properties, and by being intrinsically related to their structural properties, solvent affinity, crosslinking density, pore size and hydrophilicity, which can affect their entirely applications (NICHOL et al., 2010; YOON et al., 2016). Based on that, using the crosslinking strategy via aza-Michael addition reaction, the hydrophilicity of gelatin can be preserved, which allows high swelling ratio values to be achieved, as found here. Even though some works in the literature are capable of crosslinking gelatin using the "acrylation" (derivatization) approach followed by a free radical polymerization, usually, one of the most appealing characteristics of gelatin is lost, which is the fact that is a highly hydrophilic polymer.

In addition, the notable ability of gelatin of enhancing the swelling ratio of hydrogels can be found in the work carried out by Treesuppharat et al. (2017), in which, crosslinked gelatin-bacterial cellulose hydrogels showed great swelling ratios between 400 to 600% of water uptake, even using the high reactive and hydrophobic, GTA as crosslinker. A similar study to that elaborated here was made by Arslan (2020), the author reported swelling ratio values between 340 up to 940% for gelatin-based hydrogels

crosslinked with β-cyclodextrin via Michael addition. In another work conducted by Yoon and colleagues (2016), when preparing methacrylated fish-skin gelatin hydrogels, the authors verified a maximum swelling value of approximately 40 with methacrylation degree of 26.4 ± 7.5%. On the other hand, when comparing fish and porcine skin gelatins at polymer concentration of 5% w/v and with high methacrylation degree (91.4 ± 3.1%), swelling ratios of 19.8 ± 0.8 and 11.2 ± 1.1 were obtained, respectively. In contrast to Yoon et al. (2016), herein, at polymer concentration of 20% w/w and DM of 26% (medium substitution) it was obtained a swelling ratio of 15.5 ± 0.64 $g_{water} \cdot g_{hydrogel}^{-1}$. However, the DM is much lower than those reported by authors, mainly due to the more hydrophobic characteristic of their hydrogels. In the work of Nichol et al. (2010), during swelling studies of methacrylated hydrogels, the authors reported that at polymer concentrations of 10 and 15% w/v and low methacrylation degree (19.7 ± 0.7%), the higher swelling ratio found was approximately close to 20. However, similar values were obtained when using 5% w/v of polymer concentration but with medium methacrylation degree (53.8 ± 0.5%).

It is important to mention that in all cited works, the post photo-crosslinking of the acrylated or methacrylated hydrogels led to the loss of inherent hydrophilic nature of gelatin mainly due to the conversion of the polar groups involved in the reactions, into apolar groups, which turn them more hydrophobic and less propense to absorb water, and because they were also photo-crosslinked after synthesis which probably contributed for the lower swelling since hydrogels were more covalently linked. According to Udayakumar et al. (2021), the solubility, reactivity, absorption, and biodegradability of natural polymers such as gelatin are determined by the number of polar groups present in the polymer backbone. In addition, as reported by Khan & Ranjha (2014), due to the presence of hydrophilic groups in the polymeric chain, high swellings can be achieved since they can also interact with water forming hydrogens bonds or ionic interactions.

Furthermore, after swelling, all hydrogels displayed a transparent color as found by Arslan (2020). In addition, as also mentioned by Nichol et al. (2010), swelling can significantly impact the overall shape of patterned hydrogels as can be observed in this work, Figure 28.

Figure 28 – Swelled crosslinked hydrogels (37 ºC for 72 h).

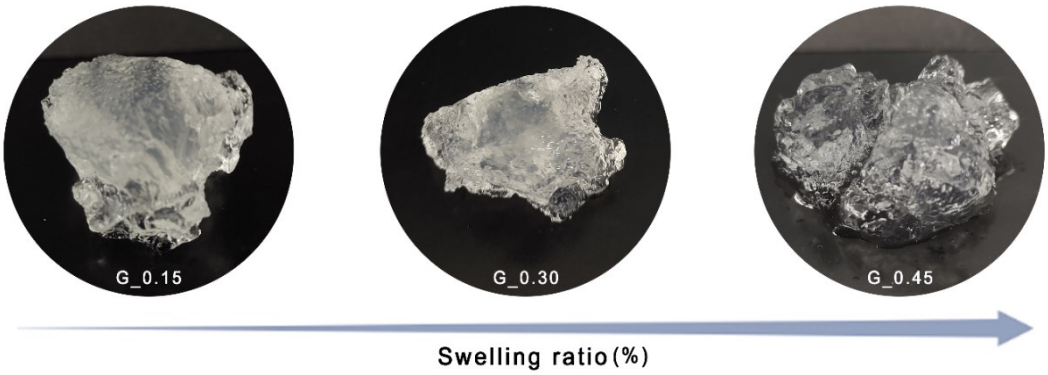

Source: Author (2023).

4.1.5 Insoluble fraction (%)

The gel-fraction of a hydrogel can be used as qualitative indication for crosslinking efficiency (BILLIET et al., 2013; CAO et al., 2020). It can be found in literature several reports which have been estimated the sol-gel fraction of hydrogels using different type of approaches. To quote, the most used techniques are the Soxhlet extraction (Bukhari et al. 2015), syringe test – filtration using GPC filter (Tolentino, 2022) or drying after swelling (Billiet et al. 2013 and Cao et al. 2020) which validate to each other being commonly applied to characterize those fractions.

In this work, it is worth mentioning that for our experiments we have also tried to determine the insoluble fraction using such cited approaches. A Soxhlet extraction was carried out for 6 to 8 h using a thimble made of paper filter and cellulose acetate membrane, but due to losses that occurred during the process, the method failed to render reproducibility. For the syringe test, attempts using distilled water, DMSO and acetic acid as solvents were carried out, but the obstruction and clogging of the GPC filter also difficulted the correct estimation.

Furthermore, from our observations, we considered that true soluble fraction was removed during hydrogel purification directly after synthesis, since water in excess was added to solution to remove non-reacted reactants that were still present. In order not to underestimate or super-estimate results, the total soluble and gel fractions of the synthesized hydrogels were determined after the swelling experiments followed by drying in an oven. For that, the remaining fraction was named “insoluble fraction” instead of “gel-fraction”.

Then, from these observations, there are presented in Figure 29 the insoluble fractions (%) obtained after drying swollen samples at 37 ºC for 72 h.

Figure 29 – Insoluble fraction (%) of gelatin hydrogels at 37 ºC.

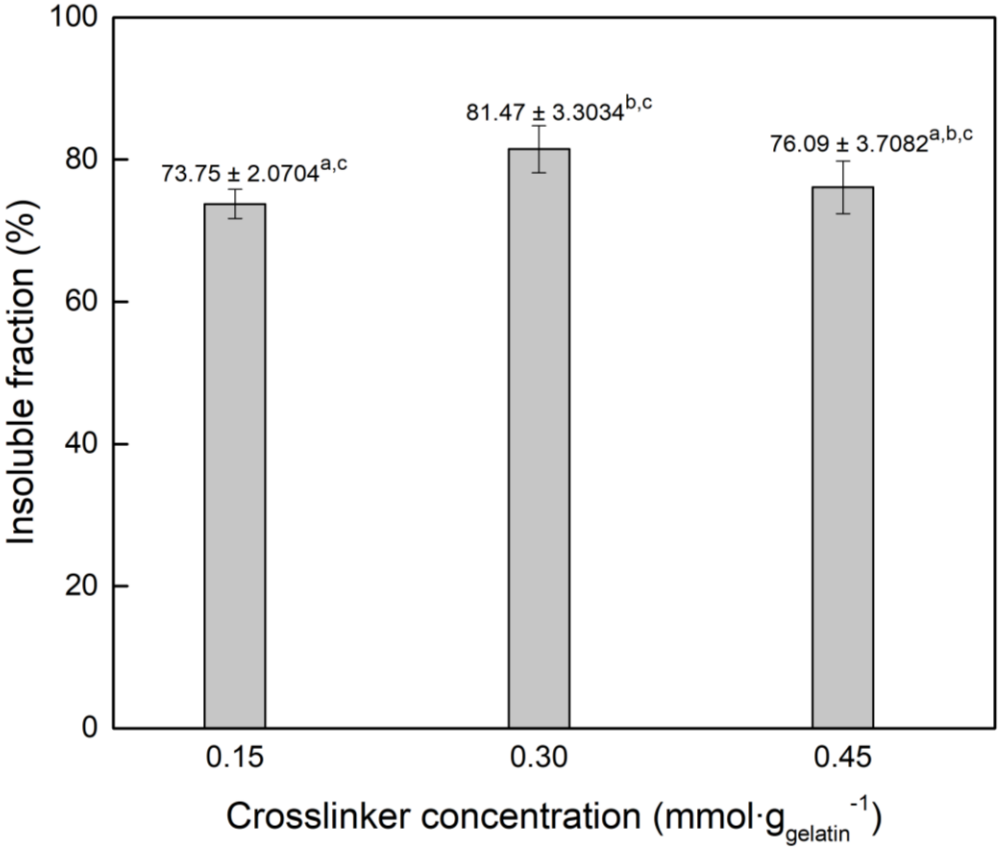

Results are shown as mean (n = 6) followed by ± standard deviation (SD);
Different letters at bars indicate significantly statistical differences between the means by Tukey's test at significance level of 95% (*p-value* ≤ 0.05);
Source: Author (2023).

Overall, the use of 20% w/w of gelatin for synthesis provided hydrogels with insoluble fractions (≥ 73%) after drying and only G_0.15 and G_0.30 formulation showed statistically significant differences between the means by Tukey's test (~8% of difference in the insoluble fraction). In addition, a slight increase in the insoluble fraction was observed with increase of crosslinker concentration, however, the residual photoreactive acrylic groups from the asymmetric aza-Michael additions of the symmetric crosslinker are rendered useful to further increase the insoluble fraction through photopolymerization, for example.

These results were in accordance with those reported by Billiet et al. (2013) during gelatin acrylamide and methacrylamide hydrogels synthesized via chemical derivatization followed by a photo-crosslinking approach, the obtained gel-fraction

values varied from 79.25 up to 96.92% and were assessed after swelling ratio experiments (as in the present study), varying the polymer concentration from 5 up to 20%. In other study conducted by Bukhari et al. (2015), gelatin/acrylic acid hydrogels were prepared via free radical polymerization using ammonium persulfate as thermal initiator and ethylene glycol dimethacrylate (EGDMA) as crosslinker, these hydrogels showed an increase in gel-fractions between 84.4 up to 95.2% measured after Soxhlet extraction and drying by increasing the reactants concentration.

According to Van Den Bulcke et al. (2000), the insertion of acrylic moieties in the gelatin chain can preserve its inherent water-soluble characteristic. In addition, as mentioned by Honarkar & Barikani (2009) and Ono et al. (2000), the observed polymeric losses can be associated with remained polar functional groups, such as amines and carboxylic acids, and with a loosely crosslinked network that can fall apart leading to solubilization after swelling.

An indirect measurement of crosslinking is based on the difference between the initial and final weight of hydrogels, after purification and freeze-drying processes and before swelling experiments, since crosslinked hydrogels synthesized are insoluble in any solvent, the hot water purification process (50 °C) would only remove reactants excess. However, losses of polymeric mass during the hydrogel removal and purification processes were evidenced, which could lead to underestimated results. Although, weight yields after purification, freeze-drying and before insoluble fraction determination were greater than 20% for all formulations.

4.1.6 Amines consumption assessment by TNBS essay

The total ε-amino groups content (mmol of lysine·$g_{gelatin}^{-1}$), the modification extent (X_m, mmol of lysine·$g_{gelatin}^{-1}$) and the modification degree (DM, %) results were presented in Table 11. Herein, the values obtained for the free primary amines content was (0.305 ± 0.0065 mmol of lysine·$g_{gelatin}^{-1}$) for the type A porcine skin gelatin and were in accordance with values reported in the literature by Zatorski et al. (2020), Kuijpers et al. (2000) and Sisso, Boit & Deforest (2020).

Additionally, for all hydrogel's formulations, the number of mmol of lysine·$g_{gelatin}^{-1}$ decreased with increase of crosslinker concentration and presented significantly statistically differences between the means by Tukey's test. The values of modification degree (%) varied between 26.4 ± 2.1% for the hydrogels prepared with

lower (G_0.15), 53.2 ± 2.5% with medium (G_0.30), and 62.9 ± 3.6% with higher (G_0.45) crosslinker concentration.

Table 11 – Amine's consumption evaluation from TNBS essay.

Sample	**ε-amino groups** mmol of lysine·$g_{gelatin}^{-1}$	**Modification extent (X_m)** mmol of lysine·$g_{gelatin}^{-1}$	**Modification degree (DM)** (%)
Neat gelatin (n = 4)	0.305 ± 0.0065[a]	-	-
G_0.15 (n = 3)	0.228 ± 0.0090[b]	0.0777 ± 0.0090	26.4 ± 2.1[a]
G_0.30 (n = 3)	0.144 ± 0.0100[c]	0.1610 ± 0.0100	53.2 ± 2.5[b]
G_0.45 (n = 3)	0.114 ± 0.0141[d]	0.1919 ± 0.0141	62.9 ± 3.6[c]

Results are shown as mean (n = 4 or n = 3) followed by ± standard deviation (SD);
Different letters at the same column indicate significantly statistical differences between the means by Tukey's test at significance level of 95% (p-$value \leq 0.05$);
Source: Author (2023).

The modification extent (X_m) and the modification degree (DM) increased with increase of crosslinker concentration and from ANOVA also presented significant statistically differences at significance level of 95% (p-$value \leq 0.05$) with all formulations differing to each other by the Tukey's test. These results indicate the significative effect of crosslinker molar ratio variation on the consume of free primary amino groups (ε-NH_2). However, a slight difference ($\approx$ 10%) in the DM between formulations (G_0.30) and (G_0.45) was verified with increasing of crosslinker concentration in 1.5 times (0.30 up to 0.45 mmol).

As mentioned by Liu et al. (2019) and proved by Shooshtari & Van de Mark (2001), the structure of poly(β-amino esters) (PBAEs) depends mainly on the reaction sites (N) occupied in the acrylates (N_A) and amines (N_B) used in the polymerization.

Herein, it was verified that the excess addition of crosslinker (G_0.45 and G_0.30) in relation to the ε-NH_2 of gelatin allowed the synthesis of a more substituted hydrogels in relation to the formulation (G_0.15) prepared with lower crosslinker concentration. Considering only the ε-NH_2 consumption as an indicator of substitution and crosslinking, the increase in crosslinker concentration led to a greater consumption of these groups as indicated by X_m, presenting the highest DM found. It can be associated with the more crosslinker reaction sites free (acrylates) and available to react than the total ε-NH_2 content present ($N_B >>> N_A$), making it difficult, for the amine's interaction with the same crosslinker molecule as would promote the network closing and the crosslinking increasing. However, these results are very interesting from the point of view

of biomedical applications as it allows post-modifications by the presence of pendant photo-crosslinkable acrylate moieties in the polymeric chain, as can be found in the works mentioned below.

Even though the following studies have used different approaches to "acrylate" or "methacrylate" gelatin, close modification/substitution degrees to those found here were reported. The results found by Nichol and co-workers (2010) during the synthesis of methacrylated gelatin hydrogels for creating cell-laden microtissues and microfluidic devices reported methacrylation degrees of 19.7 ± 0.7% (for low methacrylation), 53.8 ± 0.5 % (for medium methacrylation) and 81.4% ± 0.4% (for high methacrylation) measured by ^{1}H-NMR technique. In another study, during the synthesis of acrylated and methacrylated gelatin hydrogels for cell-laden constructions, Billiet et al. (2013) reported substitution degrees of 66 ± 1.0% for methacrylated gelatin and 66 ± 2.8% for acrylated gelatin, also measured by ^{1}H-NMR, varying gelatin concentration in the range of 5 up to 20%. In the work conducted by Yoon et al. (2016), were determined the methacrylation degree of methacrylated gelatin hydrogels for tissue engineering applications through TNBS essay (as in the present study), obtaining values of 26.4 ± 7.5% (for low methacrylation), 55.9 ± 5.3 % (for medium methacrylation) and 91.4% ± 3.1% (for high methacrylation) using 10% of gelatin from fish source.

In addition, although the crosslinker excess in the reaction medium provided a greater DM, it is a consensus that the number of reaction sites of a primary amine is (N_B = 2) and it can react with two reaction sites of acrylates (N_A = 2). However, the reaction with secondary amines, such as those from histidine, can also occurs even if it is present at lower concentrations or possessing lower reactivity than primary ones, leading to consume the excess of added crosslinker and helping to promote an increase in the DM or participating of the crosslinking mechanism. Nonetheless, as mentioned by Meyer and Morgenstern (2003), gelatin has an unequal distribution of amino acids along polypeptide chain and by that, it is not known for sure (quantitatively) the initial concentration of secondary amines that are available to react and how many secondary amines actually formed reacted to form tertiary amines or to crosslink network, since from the TNBS test, it is possible to quantify only the number of primary amines present and consumed. Besides all these observations, such hypotheses were not evaluated, quantified, and considered here. In addition, as mentioned by González et al. (2015), the significantly lower reactivity of the secondary amines formed, and the complex and highly branched

structure of gelatin can lead to topological restrictions and also reduce the reactivity of the original secondary amines of polymer.

Thus, based on these results and in addition to variation of crosslinker concentration, it is possible to infer that the different DM (%) obtained for the gelatin hydrogels may also be associated with the different concentrations of both secondary amines (original and formed) present in the gelatin chain and to the accessibility of the N–H bonds that are effectively found available to react. These results suggest that even though the modification degree and the modification extent had been determined only based on free primary amine's content, those values as well as the crosslinking density can be higher if secondary amines were correctly accounted.

4.1.7 FTIR analysis

From ATR spectra, Figure 30, it was possible to identify some characteristic peaks of freeze-dried neat gelatin and in the freeze-dried chemically crosslinked hydrogels synthesized.

According to several reports, usually, four spectral regions can be identified in gelatin spectra, such as peaks at 2300-3600 cm^{-1} (Amide-A), 1644-1656 cm^{-1} (Amide I), 1335-1560 cm^{-1} (Amide II), and 670-1240 cm^{-1} (Amide III) (AKBARZADEGAN et al., 2021; WANG et al., 2017). The broad peaks observed at 3280, 3286, 3293 and 3295 cm^{-1} are attributed to N–H stretch groups (YAO et al., 2019; BUKHARI et al., 2015). The vibration peaks at 2919, 2930, 2931, 2395 cm^{-1} and at 2850, 2859 and 2873 cm^{-1} are assigned to aliphatic C–H stretches (GRANDE-TOVAR; VALEJO; ZULUAGA, 2018; KULKARNI et al., 2021; WAN ISHAK et al., 2018). The peaks assigned at 1633 and 1641 cm^{-1} are related to (C=O) located in the same region of C–N and N–H bending of amide I (KULKARNI et al., 2021; RATHER et al., 2022; WANG et al., 2017). The peaks at 1525, 1538, 1544 cm^{-1} are attributed to N–H bending and C–H stretching vibration of amide II (BILLIET et al., 2013; FAN et al., 2005; GENG et al., 2021 and WANG et al., 2017). As mentioned by Wang et al. (2017), after the grafting reaction, the formation of secondary amines results in the shifting of C–N stretching vibration peak to higher wave numbers, as observed herein.

For amide III, the peaks at 1234, 1238 and 1239 cm^{-1} are attributed to N–H bending and C–N stretching, while the peaks at 1446, 1442 and 1450 cm^{-1} are associated to aliphatic C–H bending, respectively (BUKHARI et al., 2015; FAN et al., 2005;

ROKHADE et al., 2006; WAN ISHAK et al., 2018). The symmetric and asymmetric bending vibrations of methyl groups were assigned at peaks 1386 (neat gelatin) up to 1388, 1392 and 1398 cm^{-1} (DAS et al., 2017). In addition, the range between 1398 – 1450 cm^{-1} could also be related to the deformation of hydroxyl (–OH) groups from the carboxylic acid moieties as informed by Grande-Tovar; Valejo & Zuluaga, (2018). According to Pradini et al. (2018) and Rather et al. (2022) these vibration peaks are the most useful and beneficial tool for analysis of protein secondary structures in the IR spectral region.

Figure 30 – FTIR of freeze-dried polymers.

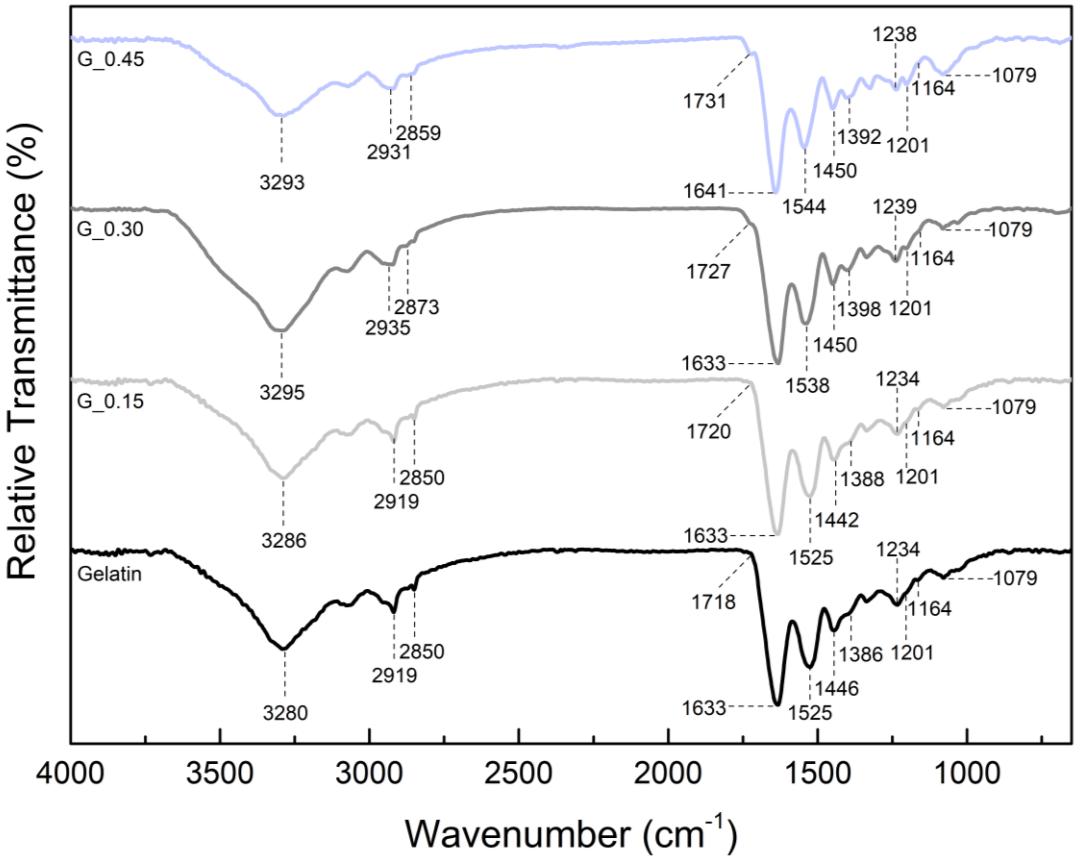

Source: Author (2023).

In all hydrogel's formulations it is possible to verify the miscibility and the presence of the non-reacted 1,4-BDDA around 1730 cm^{-1}. The peaks assigned at 1720 (weak), 1727, and 1731 cm^{-1} are associated to (C=O) stretch of α, β-unsaturated esters and were not verified in the spectrum of the freeze-dried neat gelatin (1718 cm^{-1}).

The peaks assigned between 1000 – 1100 cm^{-1} are attributed to C–O and C–O–O stretching vibrations in carbohydrate residue of collagen and represents amide I in proteoglycan carbohydrate residues as well as the carboxylic acids of the amino acids'

groups and of the crosslinker coupled (AKBARZADEGAN et al., 2021; GARCIA-VAQUERO & MIRZAPOUR-KOUHDASHT, 2023). The C–O ester stretches with bands of moderate intensity at peaks 1079 cm^{-1} could be overlapped typical stretching vibration of the C–N bond from amino groups (at 1164 cm^{-1}) which did not react with the 1,4-butanediol diacrylate (GRANDE-TOVAR; VALEJO; ZULUAGA, 2018; TREESUPPHARAT et al., 2017). Furthermore, the peaks at 1164 cm^{-1} were attributed to the primary amino groups ($–NH_2$) of gelatin, which suffered a progressive slight reduction with the increase of the DM, suggesting the effective grafting and/or formation of crosslinked network between gelatin and 1,4-butanediol diacrylate as also proposed by Grande-Tovar; Valejo & Zuluaga, (2018).

Additionally, another points interesting to note is the fact of these peaks' occurrence are more pronounced in decreasing order from the higher crosslinker concentrations to the lower ones (G_0.45 > G_0.30 > G_0.15), suggesting that the 1,4-butanediol diacrylate coupling being accordingly with TNBS essay which proved that G_0.45 sample is the most substituted hydrogel (with pendant acrylate moieties).

4.1.8 X-ray diffraction

To evaluate the intrinsic nature of freeze-dried neat gelatin and in the freeze-dried chemically crosslinked hydrogels, the XRD analyses were carried out and patterns are shown in Figure 31.

Two characteristic diffraction peaks at 2Θ = 8º and ≈ 17 – 20º may be found in the neat gelatin diffractogram, respectively. As reported by Radev et al. (2009) these peaks reveal that the gelatin structure is essentially amorphous. Nevertheless, according to Kulkarni et al. (2021) the peak at 2Θ = 8º is associated to the double helix diameter and the intensity to the triple helix segments of gelatin. However, in the study conducted by Al Islam et al. (2016) the authors found this peak sharper at 2Θ = 7.7º. The peak at 8º was found only in the neat gelatin sample, suggesting the modification of gelatin structure in all hydrogel's formulations synthesized, as expected.

A broader peak at 2Θ = 20.2º was evidenced in gelatin and G_0.30 samples and this peak is correlated to the semi-crystalline nature of gelatin as mentioned by Al Islam et al. (2016), Sherafatkhah Azari et al. (2021), Swaroop et al. (2019) and Yao et al. (2019). Nonetheless, a downward shift in this peak at 17.2º (gelatin), 16.65º (G_0.15) and 16.3º

(G_0.45) was evidenced and are also associated to this semi-crystalline structure and has more pronounced sharp in G_0.45 and G_0.15 formulations.

These findings are in accordance to results reported by Kulkarni et al. (2021) in which this peak was more pronounced at 18º in gelatin-chitosan blends and Yao et al. (2019) found this peak at 21.7º in gelatin-cellulose microgels. In addition, in all hydrogel's formulations this peak presented a lower intensity when compared to neat gelatin. Moreover, samples G_0.15 and G_0.45 presented a couple of small peaks at 13.9º (G_0.15), 13.45º (G_0.45) and almost imperceptible at 13.45º (G_0.30) and represent the semi-crystalline part of hydrogels while de broad peaks the amorphous moiety.

Figure 31 – Diffractogram of freeze-dried polymers.

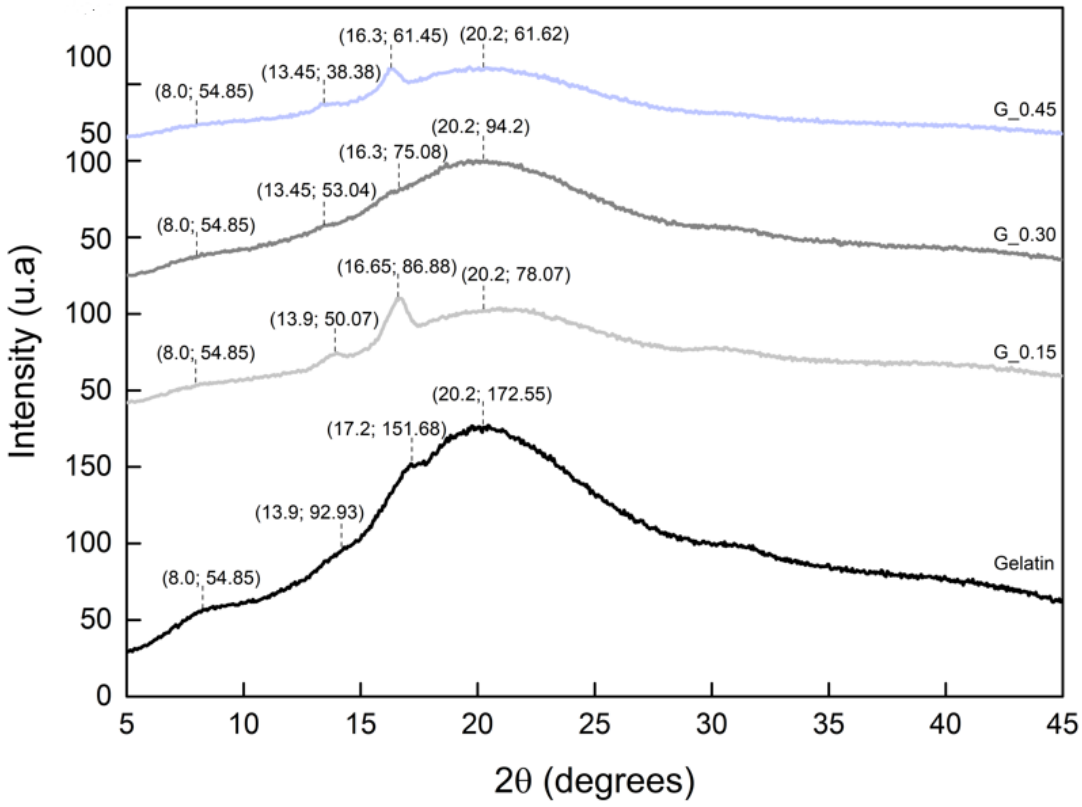

Source: Author (2023).

Additionally, another interesting point to note is that in all hydrogel patterns there was an intensity decrease after incorporating of 1,4-BDDA which may suggest the establishment of intermolecular interactions such as crosslinking causing a destruction in the regularity of neat gelatin pattern as mentioned and evidenced in the works carried out by Kulkarni et al. (2021), Swaroop et al. (2019) and Sherafatkhah Azari et al. (2021).

4.2 THERMAL PROPERTIES

To evaluate thermal properties of freeze-dried gelatin and of the covalently crosslinked hydrogels, thermogravimetric analysis was carried out and the thermograms (TGA) are illustrated in Figure 32, DTG (Figure 33) and DSC (Figures 34 and 35). Additionally, all samples were kept in an oven at 40 ºC before analysis to avoid moisture absorption.

4.2.1 Thermogravimetric analysis (TGA)

For all samples analyzed, the first degradation process peak occurs from 40 ºC until approximately 125 ºC with a maximum around of 90.2 ºC (Figure 32) and it might be associated with evaporation of physically adsorbed water molecules (moisture) (KUMAR et al., 2020; ROY & RHIM, 2021). The weight losses due to water evaporation is about of 3% to 4.5%. These water molecules are in bonded state and not in its free form and the results obtained were in accordance with those reported by Kulkarni et al. (2021), Salles, Lombello and d'Ávila (2015) and Roy & Rhim (2022).

Figure 32 – Thermograms of freeze-dried polymers.

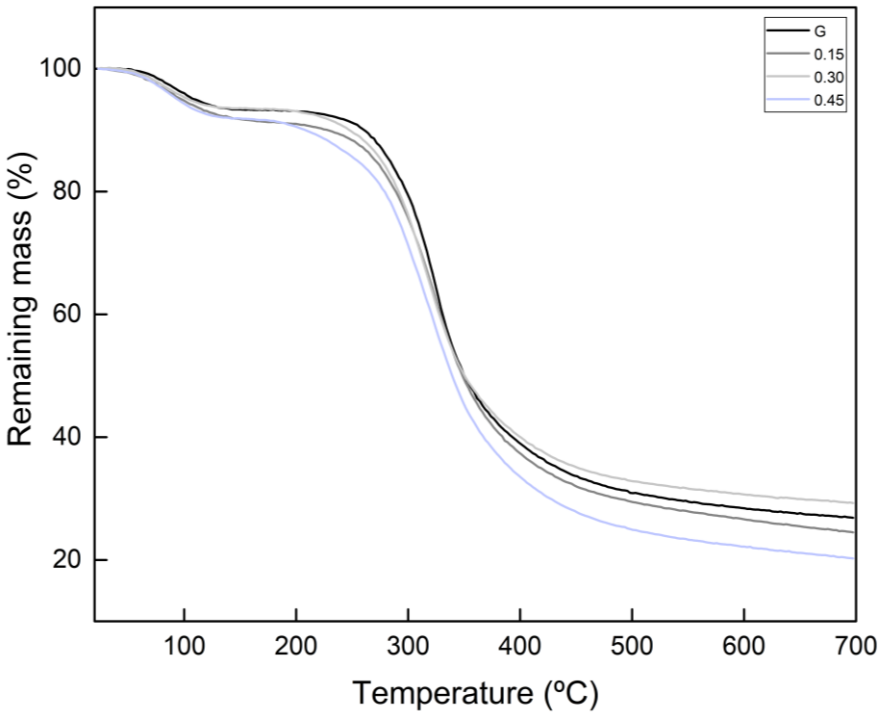

Source: Author (2023).

Overall, for all samples evaluated, degradation starts at a temperature of approximately 200 ºC with weight loss of approximately 64.8 to 72% occurring in the range of 150 to 450 ºC in which the highest change occurs at around 300 ºC which is associated to gelatin thermal decomposition (ROY & RHIM, 2021). In this process, samples undergo endothermic reactions of hydrolysis and oxidation (MATTOS, 2011; pg. 101; SALLES, LOMBELLO AND D'ÁVILA, 2015).

Nevertheless, the thermal decomposition pattern of the hydrogels denotes that the crosslinker (1,4-BDDA) addition slightly affect the thermal stability of neat gelatin, as those reported by Roy & Rhim (2021). Similar behavior was found in the study conducted by Kumar et al. (2020) when ZnO nanoparticles were incorporated into chitosan-gelatin films. Nonetheless, the authors found more thermal stability during ZnO addition by the increasing in compactness of these films. In addition, the incorporation of 1,4-butanediol diacrylate into gelatin may cause plasticization of the sample, leading to a reduction in the thermal and mechanical properties, this effect will be more deeply discussed in the following DSC analysis.

According to Mattos, (2011, pg. 101), in the final step above 420 to 700°C, exothermic reactions occur at the end of pyrolysis derived collagen. Therefore, a mass loss of 70.7% up to 79.8% leaving approximately 20.2 to 29.2% ashes were formed by carbon residues (Table 12).

Table 12 – Remaining fraction (%) and ash content by TGA evaluation.

Sample	W_0 **(mg)**	**Remained fraction (%)**	
		T_{max} **(~300 ºC)**	**Ash (700 ºC)**
Gelatin	10.55 ± 0.071	63.03 ± 0.097	26.88 ± 0.142
G_0.15	10.20 ± 0.018	64.27 ± 0.018	24.5 ± 0.289
G_0.30	11.70 ± 1.556	72.47 ± 1.537	29.26 ± 0.368
G_0.45	10.15 ± 0.071	70.35 ± 0.084	20.25 ± 0.018

Results are shown as mean (n = 2) followed by ± standard deviation (SD);
Source: Author (2023).

The residual ash content (%) at 700 ºC and the remaining weight fraction (%) at maximum decomposition temperature (from ≈ 300ºC up to 327 ºC) of neat gelatin and chemically crosslinked hydrogels were presented in Table 12, and it was not significantly affected by substitution or crosslinking, with differences of approximately 9%. Similar

results were found by Roy & Rhim (2022) when evaluated thermal stability of genipin crosslinked gelatin-chitosan films.

From DTG (Figure 33) evaluation, is possible to verify the same trend, in which the more pronounced peaks were found at 301.7 ºC (G_0.45), 306.7 ºC (G_0.30), 321.7 ºC (G_0.15) and 326.7 ºC for neat gelatin. As mentioned by Roy & Rhim (2021) these degradation peaks are related to the thermal polymer decomposition. The decomposition temperatures did not change too much with crosslinking, around 20 ºC between the neat gelatin and hydrogels, but increased from the hydrogels prepared with lower to higher crosslinker concentration (G_0.45 > G_0.30 > G_0.15), indicating that substitution and/or crosslinking impacts their thermal behavior.

Figure 33 – DTG curves of the neat gelatin and of the gelatin hydrogels.

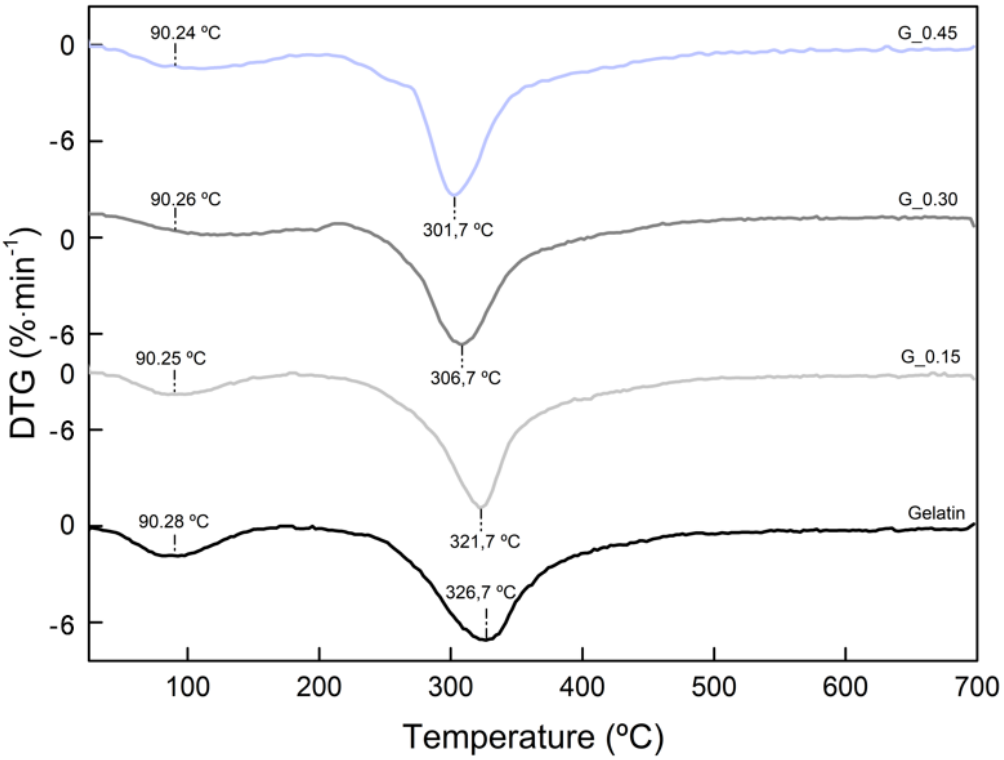

Source: Author (2023).

In addition, it is possible to verify that around 200 ºC the gelatin denaturation process begins. This behavior was also evidenced in the DSC curves presented in Figure 35 by the slight displacement observed in the curves at this temperature, another phenomenon was also identified at 300 ºC related to the polymer decomposition.

4.2.2 Differential Scanning Calorimetry (DSC)

DSC curves from STA equipment were obtained during TGA analysis and are shown in Figure 34, and it was possible to identify in all samples an event close to 185 – 220 ºC, which can be associated to denaturation/melting of polymers being more pronounced in the neat gelatin. However, another thermal transition with broader endothermic peak occurs around 280 – 340 ºC and is associated with polymeric decomposition as mentioned by Kulkarni et al. (2021). Furthermore, in all cases the thermal history of polymers was not removed, since TGA considers the weight loss during analysis.

Figure 34 – DSC curves of polymers assessed at the first heating cycle.

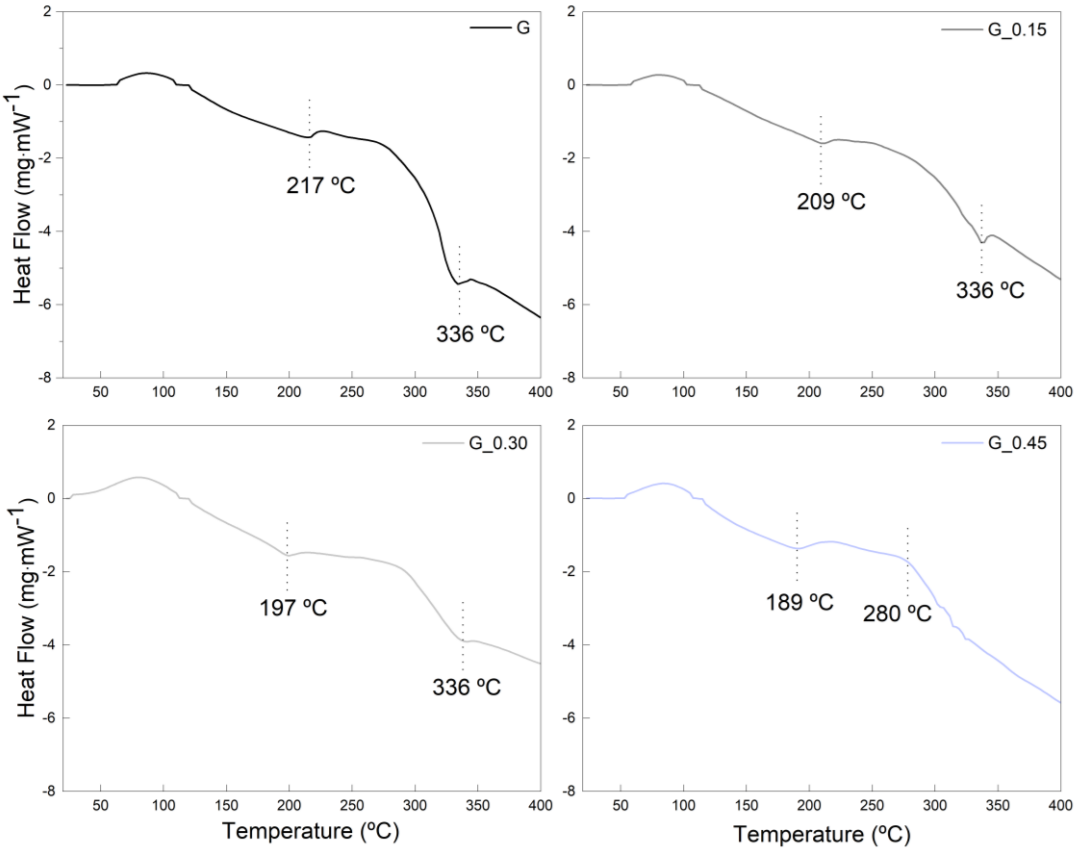

Source: Author (2023).

A true T_g is usually difficult to be estimated and several values are reported in the literature. As reported by Marshall & Petri (1980), Mateev et al. (1997) and Rosellini et al. (2020), the disagreement between the preparation methods, calibration, type of technique and control of the moisture content in these polymers are crucial factors for an adequate determination of this parameter and inconsistency of values are commonly

found. In addition to previously cited variables, these variations are mainly because of gelatin possess gel behavior with temperature, is a complex, amorphous and highly heterogeneous biopolymer obtained from different sources and methods being commonly recommended the combination of other techniques for a more accurate determination, such as rheometry or DMA, for example.

Based on that, in Figure 35 are shown DSC curves obtained from the second approach (erasing the first thermal cycle of samples and using a specific calorimeter equipment, Jade DSC), and a broad endothermic peak between 50 and 120 ºC was noticed for all formulations. These peaks were attributed to the removal of free and adsorbed water on the surface of the hydrogels (approximately 4.5%) and to the gelatin helix-coil transition.

Figure 35 – DSC curves of polymers.

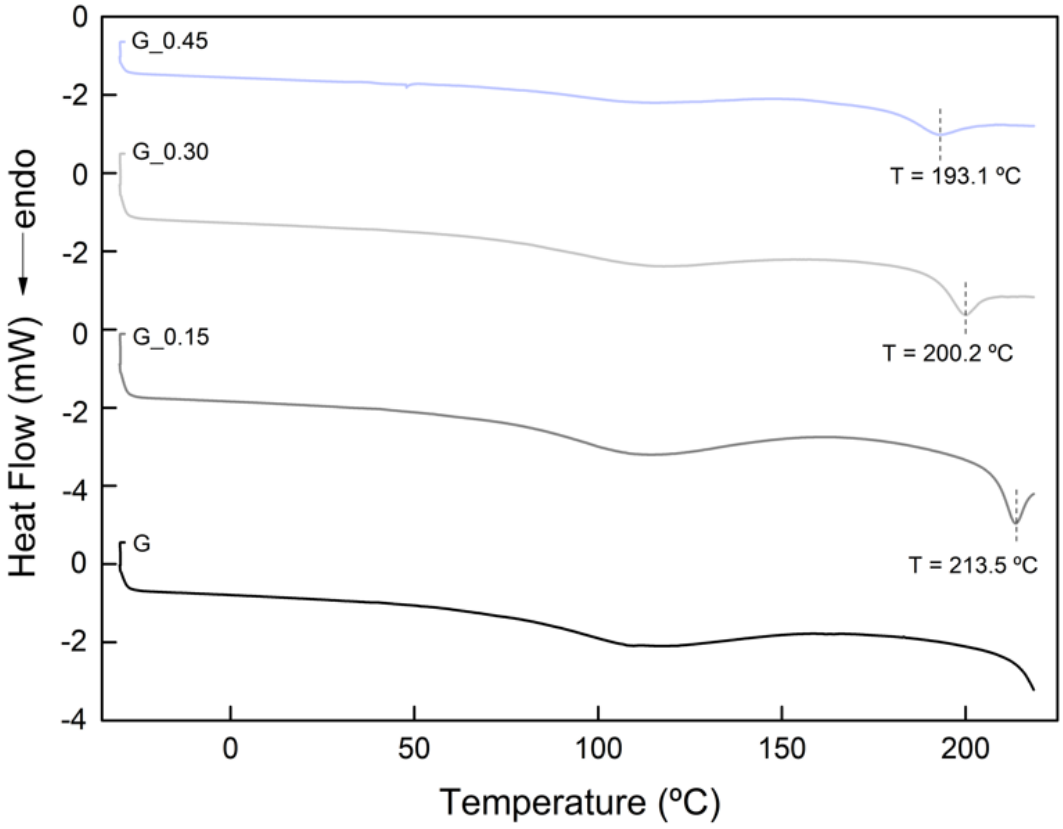

Source: Author (2023).

An approximate T_g value of around 200 ºC is reported in the literature for pure freeze-dried gelatin obtained from porcine skin, as proposed in the work of Marshall & Petri (1980). In addition, the T_g displacement may overlap the melting temperature of polymer, which is in the range between 220 and 230 ºC. Herein, the temperatures

observed for these events between 190 to 215 ºC were lower for the hydrogels in descending order of crosslinker concentration (G_0.45 (193 ºC) > G_0.30 (200.2 ºC) > G_0.15 (213.5 ºC)) when compared to neat gelatin (≥ 220 ºC) and are associated to denaturing or unfolding or melting temperature (T_m) of gelatin. Nevertheless, the higher T_g value was evidenced for the neat gelatin and the broadness of the first peak may be considered as the overlapping of T_g of the gelatin amino acid composition as reported by Al Islam et al. (2016).

The same DSC curve pattern for gelatin was published by Rosellini et al. (2020), with an estimated T_g value between 220 and 250 ºC. In the work of Mateev et al. (1997), a mathematical model was developed to estimate the T_g of proteins based on the T_g of individual amino acids. The T_g values estimated by the model and those measured by DSC, DMA and viscoelastic analyzes showed excellent agreement for the instrumental determination of the T_g of proteins such as collagen (188 ºC), gelatin (200 ºC) and elastin (256 ºC), and values experimental temperatures of 192 and 217 and 252 ºC, respectively.

As stated by Dzeikala et al. (2023), the limited changes of the positions of mers and segments of polymer chain may increase the T_g and the heat capacity in the macromolecules due to the formation of new connections which is mediated by crosslinking. Furthermore, as it is a fibrous protein, the plasticizing effect of water and alcohols in the gelatin is reported in several studies in the literature. As reported by Marshall & Petri (1980), when using hermetically sealed pans, the plasticizing effect of water can be avoided, and it is possible to observe the glass transition temperature followed by the melting of the polymer. However, here, the verified reduction of T_g and T_m of the hydrogels when compared to neat gelatin was attributed to plasticizing effect of the diol (1,4-butanediol diacrylate) which was inserted in the polymeric structure through Michael addition. In this sense, as mentioned by Vanin et al. (2005), the plasticizing effect is characterized by a decrease in the Van der Walls forces, which reduces interchain interactions increasing the flexibility of polymer chains. This effect is plasticizer concentration-dependent and can causes interferences in the workability and final characteristics of products, mainly in the mechanical strength and thermal properties, as supported by Suderman, Isa and Sarbon (2018) and Vanin et al. (2005) for gelatin-based films.

In addition, similar thermal behavior was observed for the two approaches used and the thermal stability found here is feasible for the type of application chosen. In

addition, as mentioned by Slaughter et al. (2009) hydrogels are typically soft and elastic due to their thermodynamic compatibility with water being generally used above their T_g in many biomedical applications.

It is worth to mention that some preliminary studies to evaluate the thermal behavior of neat gelatin were conducted to estimate a true T_g. For that, it was varied the temperature range from -30 ºC up to 250 ºC and heat rate of 10 or 20 ºC·min^{-1}. The DSC curves obtained are shown in the Figure 42, Appendix A, and it is possible to identify that T_g is located between 200 and 250 ºC (see item d), and in some cases, it overlaps the first broader peak of gelatin which is considered as the melting temperature (T_m) of polymer as suggest by Marshall & Petri (1980) and Rosellini et al. (2020).

4.3 FLORY-REHNER THEORY OF POLYMER SWELLING

For the hydrogels network structure evaluation, the density and the specific volume of the pure polymer was used ($\rho_{gelatin}$ = 1.34 g·cm^{-3} and $\bar{v}_{gelatin}$ = 0.7486 cm^3·g^{-1}) and the molecular weight of the repeat unit (M_r) from the molecular weight of the amino acid chain equal to 91.19 g·mol^{-1} as suggested by Vigata et al. (2021) and Gilchrist et al. (2019) was used in all calculations.

4.3.1 Network structure evaluation from Flory-Rehner theory

Flory-Rehner's equations were used to evaluate the influence of crosslinking on water mass gain (water absorption) and on network structure (mesh size) from experimental data on the swelling of hydrogels in distilled water at 37 ºC for 72 h. The parameters values were calculated and are shown in Table 13.

From the results obtained, it was noted that with the increase in the crosslinker concentration there was an increase in the values of the molecular weight between crosslinks ($\overline{M_C}$), the unperturbed end-to-end distance $(r_0{}^2)^{1/2}$, the elongation factor (α) and the mesh size of the network (ξ) as also found for the (Q_v) values.

As mentioned by Nistane et al. (2002) lower χ implies higher polymer-solvent interaction, indicating higher solubility. In this study, the χ values were in the range of approximately 0.50 up to 0.52 for all formulations evaluated, indicating that polymer–polymer and solvent-solvent contacts are preferred instead of polymer–solvent contacts.

These values agree with those reported by several authors as can be found in Vigata et al. (2021); Osetrov, Uspenskaya and Sitnikova (2021); Ma et al. (2013); Mudassir & Ranjha (2008); Xue, Champ and Huglin (2001); Sen, Yakar & Güven, (1998) and Ofner & Bubnis (1996) with χ values varying from 0.44 to 0.70 for gelatin-based polymers.

Table 13 – Flory-Rehner parameters determined from swelling experiments.

Parameters	**Sample**		
	G_0.15	G_0.30	G_0.45
Q_v	12.51 ± 0.4385	20.33 ± 0.8606	33.91 ± 0.8110
$\upsilon_{2,s}$	0.0800 ± 0.023[a]	0.0493 ± 0.0021[b]	0.0295 ± 0.0007[c]
χ	0.526 ± 0,0021[a]	0.516 ± 0,0007[b]	0.510 ± 0,0002[c]
M_n		471,278[1]	
M_r		91.19	
$\overline{M_C}$	186,711.88 ± 26,276.72[a]	225,587.19 ± 12,290.74[b]	234,085.29 ± 1,694.04[b,c]
q	$1.37{\cdot}10^{-3} \pm 7.15{\cdot}10^{-7}$[a]	$2.80{\cdot}10^{-4} \pm 2.25{\cdot}10^{-7}$[b]	$7.22{\cdot}10^{-6} \pm 2.72{\cdot}10^{-8}$[b,c]
G	0.280 ± 0.002[a]	$0.055 \pm 4.81{\cdot}10^{-4}$[a,b]	$0.007 \pm 3.31{\cdot}10^{-5}$[b,c]
$(r_0{}^2)^{1/2}$	325.57 ± 10.13[a]	346.79 ± 9.53[b]	353.36 ± 1.28[b,c]
α	2.321 ± 0.0027[a]	2.729 ± 0.0039[b]	3.237 ± 0.0026[c]
ξ	731.58 ± 61.04[a]	946.65 ± 39.25[a,b]	1143.69 ± 13.24[b,c]

Results are shown as mean (n = 6) followed by ± standard deviation (SD);
Different letters at the same line indicate statistically significant differences between the means by Tukey's or Kruskal-Wallis's tests at significance level of 95% (*p-value* ≤ 0.05);
[1]Estimated by GPC;
Parameters: Q_v – equilibrium volumetric swelling (dimensionless); q – crosslinking density (mol·g^{-1})×10^{-3}; G – shear modulus (kPa); $\upsilon_{2,s}$– volume fraction (dimensionless); χ – Flory-Huggins (polymer-solvent interact) parameter (dimensionless);
M_n – average number molecular weight before crosslink (g·mol^{-1}); M_r – molecular weight of the repeated unit (g·mol^{-1}); $\overline{M_C}$ – molecular weight between crosslinks (g·mol^{-1}); $(r_0{}^2)^{1/2}$ – root-mean-square end-to-end distance of the polymer chains between crosslinks (unperturbed distance) (Å); α – elongation of the polymer chain in any direction (dimensionless); ξ – network mesh size (Å);
Source: Author (2023).

The χ values slightly decreased with the increase of DM, suggesting a higher interaction between hydrogel-solvent, possibly because the hydrogels prepared with higher crosslinker concentrations (G_0.30 and G_0.45) allow a higher interaction with water (more opened chain) than the hydrogels prepared with lower crosslinker concentration (G_0.15) by being more covalently bonded (crosslinked). In addition, high q values provide more hardened hydrogels, while low q values provide more malleable/looser and with more entanglements, which favors it to expand more. However, when (q) is too little, they are very fragile and much looser and starts to fall apart when swell too much. In this study, the capacity of hydrogels to absorb and interact with water

was also confirmed by the decrease of q, $\overline{M_C}$ and mesh sizes values with increase of DM, indicating more opened networks/weakly crosslinked.

The Flory's characteristic ratio (C_n) for large chains, such as in gelatins, has its value tending to infinite (C_∞) and was estimated from Equation (17) as proposed by Ma et al. (2013). The calculated C_∞ value is equal to 7.8193 and was used for the mesh size estimation and agrees to reported values for polypeptides, including modified gelatins with C_∞ = 8.26 by Ma et al. (2013), C_n = 8.8785 by Vigata et al. (2021) and Gilchrist et al. (2019).

As reported by Van Den Bulcke et al. (2000), the incorporation of vinyl side groups along the gelatin chains clearly interferes with the helix formation. Then, the experimentally measured elongation factor (α) showed a slight increase varying from 2.32 ± 0.002 up to 3.24 ± 0.002 for the experimental conditions used. It is reported in the literature, an approximated value equal to 2.0 for the conformation of gelatin in solution, under different conditions, as reported by Billiet et al. (2013), Mwangi & Ofner, (2004) and Von Hippel, (1965).

From statistic evaluation, the data (Q_v, $v_{2,s}$, χ, $\overline{M_C}$, $(r_0^2)^{1/2}$, α, q and G), presented normal distribution by Shapiro-Wilk test and statistically significant differences at significance level of 95% (*p-value* ≤ 0.05) by ANOVA analysis, with exception for G (with *p-value* ≤ 0.1). The Tukey's test indicates the parameters SR, $v_{2,s}$, χ, and α, presented statistically significant differences among all samples. Nonetheless, for the molecular weight between crosslinks ($\overline{M_C}$), crosslinking density (q), and for the unperturbed end-to-end chain distance $(r_0^2)^{1/2}$ only sample G_0.15 ($\overline{M_C}$ = 186,711.88 ± 26,276.72 g·mol^{-1}; q = 1.37·10^{-3} ± 7.15·10^{-7} mmol·g^{-1}, and $(r_0^2)^{1/2}$ = 325.57 ± 10.13) differs from the others samples (G_0.30 and G_0.45) at the statistical significance level (*p-value* ≤ 0.05). In addition, only the mesh size (ξ) did not present a normal distribution, and a non-parametric statistical analysis was performed comparing multiple independent samples (by groups). By using the Kruskal-Wallis's variance test, it was observed statistically significant differences at a significance level of 95% (*p-value* ≤ 0.05) and based on multiple comparisons of mean ranks, the means of these samples were analyzed. It was showed by the median test, statistically significant differences at a significance level of 95% (*p-value* ≤ 0.05) and by the multiple comparison test only G_0.15 and G_0.45 differ from each other at statistical significance level (*p-value* ≤ 0.05). Similarly, for the G values, through ANOVA it was not observed significantly statistically

differences at a significance level of 95% (*p-value* was > 0.05), but at significance level of 90% (*p-value* ≤ 0.1), significantly statistically differences between the means were observed for hydrogels prepared with lower (G_0.15) to the higher crosslinker concentration (G_0.45) formulations.

The mesh size is not only a measure of the distance between crosslinks, according to Slaughter et al. (2009) and Nicodemus & Bryant (2008), it is considered a critical parameter as it influences the permeability and diffusion of drugs and other molecules in biodegradable hydrogels, among other valuable parameters. In addition, according to Lin & Matters (2006) for biomedical applications, typical mesh size values between 5 to 100 nm are reported for swollen hydrogels. However, their mesh size is usually higher than the size of drugs and small molecules, that can avoid the possibility of retards the drug diffusion when at in swollen state. In contrast, the sustained release of macromolecules, such as oligonucleotides and proteins, can be achieved from swollen hydrogels due to the significant hydrodynamic radii of these molecules. In this work, values between 73 to 114 nm were obtained for the mesh size and finding in the range cited by Lin & Matters (2006) for the most biomedical applications. Also, the values obtained are accordingly with those reported by Vigata et al. (2021) for gelatin methacryloyl hydrogels (GelMa) with values between 4 to 61.6 nm, varying the GelMa concentration from 5 to 15% and the ionic strength from 15 to 300 mM during swelling. Other work conducted by Gilchrist and co-workers (2019) were reported mesh size values for methacrylamide gelatin hydrogels (GelMa) between 32 to 72 nm, and the value increased with the reduction of GelMa concentration. In addition, as mentioned by Ma et al. (2013) even though the Flory-Rehner theory represents a rather ideal picture of crosslinked polymers, the determined experimentally mesh size values are more influenced by entanglements, loops, or dangling chains.

Further, as pointed out by Lee, Bouhadir and Mooney (2004), the mechanical properties of the gel are strongly correlated to the swelling ratio with effect on the q. However, it was observed the same characteristic as one cited by Vigata et al. (2021), in which, higher mesh sizes correlate with lower mechanical stiffness due to the higher swelling ratio of these samples. Nonetheless, from our results, it was verified that the crosslinking density (q) and the shear modulus (G) decreased with increasing of crosslinker concentration, suggesting that the softer hydrogel is the less crosslinked, as expected. Additionally, these “lower” mechanical resistance achieved can also be attributed to the plasticizer effect of the crosslinker employed, as previously discussed.

Nonetheless, Gilchrist and colleagues (2019) reported values of G_{low} = 0.51 ± 0.03 kPa; G_{med} = 1.74 ± 0.22 kPa and G_{high} = 4.80 ± 0.3 kPa for methacrylamide gelatin hydrogels at fixed conditions (degree of functionalization of 85%, 0.1% of photoinitiator concentration, and with 4%, 5% and 7.5% of GelMA). However, these hydrogels were prepared via radical photopolymerization, and above results were obtained using the stress-relaxation indentation tests, different to the approaches used here, and in which values were calculated theoretically.

Evaluating the crosslinking density (q), it was found that the q value for the formulation prepared with higher crosslinker concentration (G_0.45) was approximately 190 times lower than those found for G_0.15 and 38.8 times lower when compared to G_0.30, as evidenced by the high DM found for these samples ($DM \approx$ 53 and 63%), respectively, and as previously discussed for TNBS results. In addition, the values decreased from $1.37 \cdot 10^{-3} \pm 7.15 \cdot 10^{-7}$ mmol·g^{-1} to $7.22 \cdot 10^{-6} \pm 2.72 \cdot 10^{-8}$ mmol·g^{-1} by increasing crosslinker concentration from 0.15 to 0.45 mmol. In the work carried out by Billiet and colleagues (2013), authors concluded that the synthesized acrylamide-gelatin hydrogels provided a tighter network with lower mesh sizes (11.4 to 25 nm) than methacrylamide ones (13.9 to 35.7 nm). Conversely, crosslinking density showed to be higher in the acrylamide hydrogels (1.35 up to $3.39 \cdot 10^{-4}$ mol·cm^{-3}) than methacrylamide ones (0.88 up to $2.44 \cdot 10^{-4}$ mol·cm^{-3}) varying GelMa concentration in the range of 5 to 15%. The values reported by Billiet et al. (2013) agreed to those found in this work, even at different reaction conditions/approaches used.

The use of crosslinker in excess can promotes significantly differences in several parameters and properties of the hydrogels. Herein, it was verified that the hydrogels synthesized with excess of crosslinker provided polymers with thermal and mechanical properties reduced with the increase of DM probably due to the plasticizing effect of the crosslinker and also due to the preservation of the hydrophilic characteristic of gelatin even after modification/crosslinking.

On the other hand, it was observed an increase of the mesh size, molecular weight between crosslinks and the swelling ratio with DM increases. Additionally, the observed increased also indicates less crosslinked hydrogels, corroborating with results obtained in the swelling experiments, in which, the lower “acrylated” hydrogels has the lower swelling ratios by being more crosslinked, and as confirmed by the calculated q values (Table 13).

It was schematized in Figure 36, the Flory-Rehner's parameters obtained for the synthesized hydrogels.

Figure 36 – Network mesh size from Flory-Rehner equations.

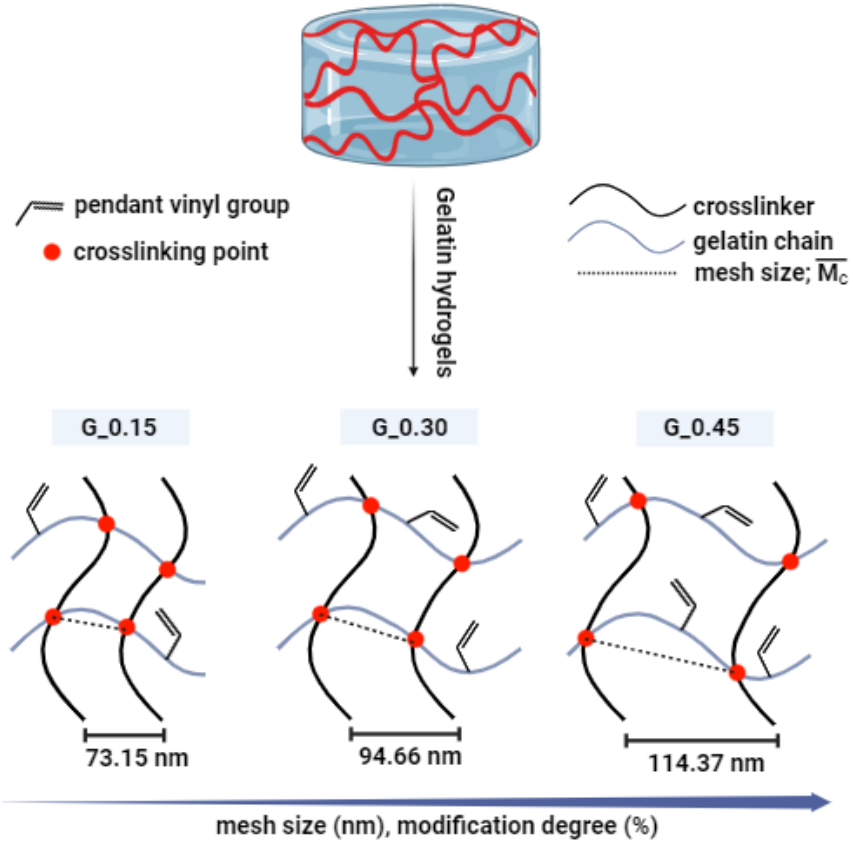

Drawn in biorender.com and Photoshop CS6 (2023);
Source: Author (2023).

Briefly, although these hydrogels were not submitted to a dual crosslinking such as, a post- free radical photopolymerization and/or photo-crosslinking reaction, after crosslinking through aza-Michael addition as typically reported in literature, all those results obtained from Flory-Rehner theory confirming that incorporation of different molar concentrations of 1,4-butanediol diacrylate has a statistically significant effect on several parameters of the synthesized hydrogels.

As stated by Peppas et al. (2006), even there some mathematical models for describing the phenomenon, the theoretical treatment of swelling of ionic hydrogels is much more complex. By that, the ionic contribution (ΔG_{ion}) was not considered in the equating due to the difficulty in estimate the actual moiety of ionic groups formed during hydrogels "acrylation" and/or crosslinking which truly contributed to enhanced swelling found, in addition to the presence of others hydrophilic and protonable groups capable of

interacting with water, and by the fact that reaction was not carried out using ionic solvents, such as PBS or salt solutions.

Moreover, for the freeze-dried hydrogels, visually, they displayed white color and rigid structure for hydrogels prepared with the lowest (G_0.15) and intermediate (G_0.30) crosslinker concentrations to hydrogels prepared with higher crosslinker concentration (G_0.45), as shown in the Figure 37.

Figure 37 – Freeze-dried gelatin hydrogels.

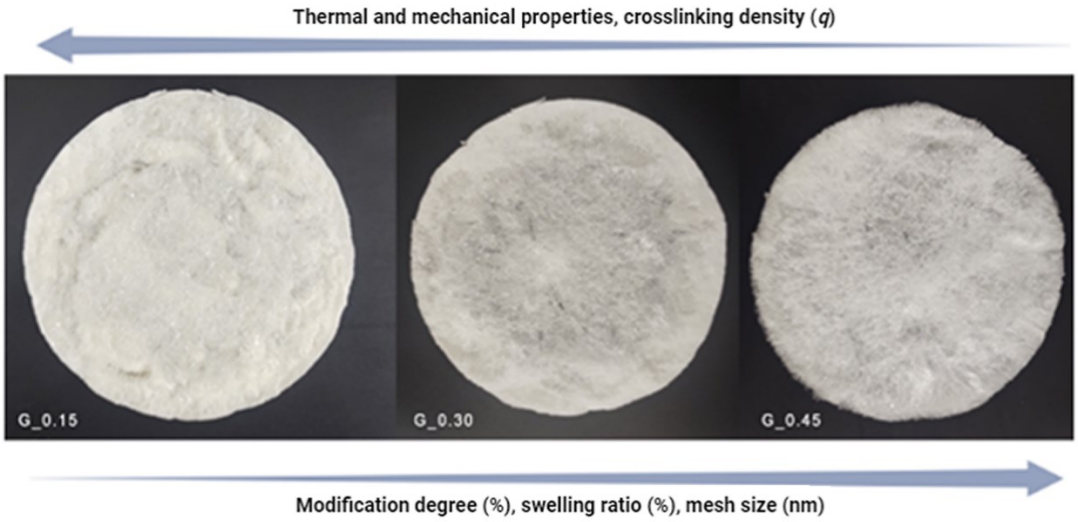

Source: Author (2023).

In addition, physically, after the freeze-drying process, the G_0.45 formulation was the softest hydrogel synthesized, as also indicated by calculated G values, with porous and foam-like appearance as reported by Yoon et al. (2016) and Nichol et al. (2010) during the gelatin-methacryloyl (GelMA) hydrogels synthesis. Furthermore, the softer structures were obtained in descending order of DM (G_0.45 < G_0.30 < G_0.15) and are accordingly to the G values calculated.

Additionally, the elongation factor (α) also increased with increasing of crosslinker concentration. Conversely, it was verified that less substituted polymer (G_0.15) possess a more rigid structure visually and sensorially with lower elongation factor (α = 2.32 ± 0.002) and higher shear modulus (G = 0.280 ± 0.002 kPa). The bigger elongation factors (α) in solution are attributed to less crosslinked networks and to the stretch of gelatin chains mainly due to the plasticizing effect of this compound, as verified from the previously discussed thermal results.

4.4 GELATIN NANOPARTICLES SYNTHESIS

4.4.1 GNPs crosslinking

The total concentration of ε-amino groups (mmol of lysine·$g_{gelatin}^{-1}$), the modification extent (X_m, mmol of lysine·$g_{gelatin}^{-1}$) and the modification degree (DM, %) ± standard deviation of the synthesized GNPs is shown in Table 14.

Table 14 – Crosslinking evaluation of the GNPs from TNBS essay.

Sample	ε-amino groups mmol of lysine·$g_{gelatin}^{-1}$	Modification extent (X_m) mmol of lysine·$g_{gelatin}^{-1}$	Modification degree (DM) (%)
G_0.01	0.166 ± 0.021	0.139 ± 0.021	45.60 ± 6.95
PHG_0.01	0.131 ± 0.017	0.174 ± 0.017	56.96 ± 5.63
DOXG_0.01	0.121 ± 0.004	0.185 ± 0.004	60.51 ± 1.39
PHDOXG_0.01	0.166 ± 0.002	0.140 ± 0.002	45.78 ± 0.62
G_0.05	0.145 ± 0.006	0.160 ± 0.006	52.40 ± 1.85
PHG_0.05	0.123 ± 0.003	0.183 ± 0.003	59.84 ± 0.91
DOXG_0.05	0.131 ± 0.009	0.175 ± 0.006	57.20 ± 2.83
PHDOXG_0.05	0.126 ± 0.001	0.179 ± 0.001	58.73 ± 0.12
G_0.1	0.139 ± 0.004	0.166 ± 0.004	54.51 ± 1.30
PHG_0.1	0.090 ± 0.013	0.215 ± 0.013	70.39 ± 4.12
DOXG_0.1	0.112 ± 0.002	0.194 ± 0.002	63.46 ± 0.66
PHDOXG_0.1	0.119 ± 0.004	0.186 ± 0.004	60.92 ± 1.41

Results are shown as mean (n = 2) followed by ± standard deviation (SD);
Source: Author (2023).

From the data obtained by the TNBS essay and considering the total free primary amine (ϵ-NH_2) content equal to 0.305 ± 0.0065 mmol of lysine·$g_{gelatin}^{-1}$, the concentration of ϵ-NH_2 groups lost (X_m) after the synthesis of GNPs varied between the lower value of 0.139 ± 0.021 mmol of lysine·$g_{gelatin}^{-1}$ (G_0.01) to the higher value of 0.215 ± 0.013 mmol of lysine·$g_{gelatin}^{-1}$ (PHG_0.1).

On the one hand, the DM varied between 45.6 ± 6.95% for the lowest DM to 70.39 ± 4.12% for the highest DM with crosslinker concentration ranging from 0.01 up to 0.1 g and different methodologies of prepare. Additionally, for the GNPs synthesized with the same crosslinker concentration and different techniques of prepare the DM increased maximum 14.9% using 0.01 g, 7.4% with 0.05 g and 15.9% with 0.1 g of crosslinker, not taken in account the standard deviations of the formulations. It was possible to observe

that by increasing the crosslinker concentration and keeping the same methodology of prepare (e.g., G_0.01 to G_0.05 to G_0.1) there was a slightly increase in the DM of the GNPs (except to PHG_0.1). The highest DM was evidenced for the sample PHG_0.1 (70.39 ± 4.12%) which was also synthesized with the higher crosslinker concentration (0.1 g). However, considering the calculated standard deviation of ± 4.12%, this value is according with those found for other samples using the same crosslinker concentration.

Furthermore, the formulations prepared with the higher crosslinker concentration (0.1 g) showed the highest consumption of ϵ-NH_2 (X_m) and, consequently, the higher DM (%), as also found for crosslinking reactions. In this sense, it can be inferred that photopolymerization is able to create more linear chains between the crosslinks, increasing the entanglement, which can also allow for greater swelling. These results found for "acylated"/crosslinked GNPs showed a fair agreement with those obtained for hydrogels synthesized in solution with DM varying between 26 up to 63%. Then, the maximum DM differences, considering the higher DM value of GNPs (70.4%) and of crosslinked hydrogels (63%) were approximately 7.5%. Moreover, in addition to crosslinker excess, the high DM found (45 up to 70%) for GNPS can also be associated to the large surface area of the nanoparticles that allows the binding of crosslinker molecules in various parts of the particle surface at interface.

On the other hand, the DM of the formulations containing DOX varied between from 45.7 to 60.5% using 0.01 g of crosslinker, from 57.2 to 58.7% using 0.05 g of crosslinker, and from 60.9 to 63.4% using 0.1 g of crosslinker. However, it is necessary to investigate more deeply if DOX causes an interference in the measurement of DM due to its fluorescent characteristic and photooxidative behavior or if participates of the reaction, since it has amino groups in its structure.

Additionally, as reported by Halbardier et al. (2022) during 3D printed shape memory polymers (SMP) synthesis, the aza-Michael addition reaction and radical photopolymerization can be adjusted to occurs concomitantly. Herein, the observed increase in the consume of free primary amino groups for some photopolymerized formulations may be attributed to conditions used in the photopolymerization which can trigger the aza-Michael reaction to occur at the same time, albeit slowly, since the reaction was not completely quenched. Furthermore, the use of a free radical photopolymerization and/or photo-crosslinking techniques can help to increase the reactivity of acrylic groups, and, consequently, the chance of react with the remained unreacted free amines of gelatin,

crosslinking itself (via homopolymerization) or creating linear chains between the previously formed crosslinks.

4.4.2 Particle size and PDI

The intensity average particle diameter of droplets and nanoparticles, as well as the polydispersion index (PDI) of the synthesized GNPs are shown in Table 15.

Table 15 – Particle size and polydispersity index (PDI) of the synthesized GNPs.

Sample	Droplet size (nm)	PDI	Nanoparticle size (nm)	PDI
G_0.01	201 ± 5	0.12 ± 0.03	191 ± 1	0.09 ± 0.01
G_0.05	207 ± 3	0.14 ± 0.01	187 ± 1	0.10 ± 0.03
G_0.1	212 ± 3	0.15 ± 0.03	203 ± 4	0.12 ± 0.06
PHG_0.01	210 ± 5	0.21 ± 0.06	199 ± 10	0.13 ± 0.01
PHG_0.05	209 ± 8	0.13 ± 0.02	201 ± 2	0.10 ± 0.03
PHG_0.1	208 ± 4	0.15 ± 0.03	186 ± 4	0.10 ± 0.03
DOXG_0.01	207 ± 8	0.13 ± 0.04	192 ± 7	0.13 ± 0.02
DOXG_0.05	208 ± 1	0.14 ± 0.01	201 ± 7	0.17 ± 0.10
DOXG_0.1	210 ± 6	0.14 ± 0.02	199 ± 7	0.10 ± 0.02
PHDOXG_0.01	206 ± 5	0.15 ± 0.03	192 ± 3	0.12 ± 0.02
PHDOXG_0.05	210 ± 2	0.16 ± 0.07	194 ± 4	0.10 ± 0.04
PHDOXG_0.1	197 ± 5	0.14 ± 0.02	191 ± 1	0.08 ± 0.01

Results are shown as mean (n = 2) followed by ± standard deviation (SD);
The GNPs were dispersed in cyclohexane at 20 ºC;
Source: Author (2023).

For all formulations, droplet diameters varied between 197 and 212 nm and nanoparticles (dispersed in cyclohexane) between 186 and 203 nm. In addition, the polydispersity index was ≤ 0.2, indicating good colloidal dispersion of the particles, in the range over which the distribution algorithms operate best (BASEER et al., 2019; SHAWN, 2018). Such values are within the expected range for nanoparticles intended for biomedical applications as mentioned by Cordeiro et al. (2020) and Hueppe, Wurm and Landfester, (2022) a size close to 200 nm is considered ideal as it favors GNPs longtime circulation in the bloodstream leading to a preferential pathway through highly vascularized tissues, and in drug delivery systems for tumor therapy favoring their retention inside the tumor cells. The particle size and PDI values are also in agreement with those reported by Ethirajan et al. (2008) for crosslinked gelatin nanoparticles via

interfacial polymerization with glutaraldehyde in inverse miniemulsion. Similar results were found by Baseer et al. (2019) during gelatin nanoparticles synthesis by nanoprecipitation and Peres et al. (2018) during N-acryloyl-L-glutamic acid (L-AGA) e poly(L-AGA-co-BIS) nanogels synthesis in inverse miniemulsion.

It is shown in Table 16, the mean diameter and polydispersity index (PDI) of the GNPs after redispersion in an aqueous phase containing SDS (0.3 wt.%).

Table 16 – Particle size and PDI of the redispersed GNPs.

Sample	Redispersed GNP size (nm)	Size peaks (nm)	Intensity (%)	PDI
G_0.01	186 ± 5	144 ± 58 509 ± 160 5409 ± 303	68 30 2	0.44 ± 0.03
G_0.05	156 ± 1	179 ± 78 4619 ± 820	96 4	0.27 ± 0.02
G_0.1	213 ± 6	386 ± 159 129 ± 38 5412 ± 300	59 39 2	0.40 ± 0.03
PHG_0.01	164 ± 6	205 ± 108 5381 ± 322	98 2	0.35 ± 0.02
PHG_0.05	171 ± 8	223 ± 164 5424 ± 291	98 2	0.44 ± 0.12
PHG_0.1	145 ± 6	176 ± 98 4719 ± 770	98 2	0.26 ± 0.03
DOXG_0.01	-	-	-	-
DOXG_0.05	195 ± 2	234 ± 155 4936 ± 653	94 6	0.39 ± 0.05
DOXG_0.1	-	-	-	-
PHDOXG_0.01	204 ± 12	148 ± 65 520 ± 186 5279 ± 421	65 32 3	0.51 ± 0.05
PHDOXG_0.05	-	-	-	-
PHDOXG_0.1	-	-	-	-

Results are shown as mean (n = 2) followed by ± standard deviation (SD);
The GNPs were redispersed in aqueous SDS (0.3 wt.%) solution at 20 ºC and followed by resuspending in distilled water for size determination;
Formulations with (-) did not attend quality report criteria from equipment;
Source: Author (2023).

For the redispersed GNPs, the quality report criteria were not attended for all redispersed samples due to the presence of large or sedimenting particles, fluorescence, absorbance (colored samples) as informed by equipment reading. In addition, the results provided by the report explain the fact that in these cases, all formulations contained doxorubicin (fluorophore), and the samples that attended quality criteria presented broad multimodal distributions.

These difficulties in particle diameter size measurement for redispersed GNPs may be associated with the proximity between the refractive index of the continuous phase (1.33 for water) and that of the dispersed phase (1.45 for gelatin and 1.456 for crosslinker), preventing a more accurate size measurement. Furthermore, the use of a DLS-MALS may be more effective in measuring the diameter of redispersed GNPs, as verified in Peres et al. (2018) work.

The mean diameters varied between 145 ± 6 and 213 ± 6 nm, but in some formulations, the presence of particles larger than 5.42 μm was also observed, suggesting aggregation between smaller swollen GNPs. In addition, particle aggregates with sizes larger than 10 μm may not be identified by the DLS due to the detection limitation of the equipment. Another fact concerns to swelling ratio of the GNPs, since they are hydrophilic nanoparticles, this causes the swelling to favor the observed increase in size after redispersion step. Due to this, the PDI also showed high values (> 0.5) indicating some particle agglomeration, evidenced by the size increase. This also includes the fact that gelatin nanoparticles have a sticky appearance (gelatinous) and are more easily agglomerated.

As observed previously, for crosslinking in solution, it was found that swelling ratio varied between 962 and 2563% which can directly affect the particle size by favors a higher swelling. However, for GNPs synthesis, in all formulations synthesized, the crosslinker was used in excess, and not know exactly how many it influences in the real particle swelling value. Nevertheless, an approach was made to estimate the particle size from the GNPs diameter when dispersed in cyclohexane. For that, it was considered the lower and the higher particle size value of the formulations dispersed in cyclohexane and was assumed that de swollen nanoparticles density is equal to water density, and the approximately swelled particle size was determined according to Equation 31.

$$D_{p,swollen} = D_{p,original} \times \left[\left(\frac{SR}{100}\right) \times \left(\frac{\rho_{gelatin}}{\rho_{water}}\right)\right]^{1/3} \quad (31)$$

In which, $D_{p,swollen}$ and $D_{p,original}$ are the particle diameters in nm; SR is the swelling ratio, dimensionless; $\rho_{gelatin}$ and ρ_{water} are polymer density and solvent density in g·cm^{-3}.

The estimated particle size values of redispersed GNPs by means of Equation 31 are presented in Table 17.

Table 17 – Estimated redispersed GNPs particle size.

Sample	$D_{p,swelled}$ **(nm)**	
	For SR = 1000%	For SR = 2500%
For $D_{p,cyclohexane}$ = 186 nm	442	600
For $D_{p,cyclohexane}$ = 203 nm	482	654

Source: Author (2023).

The estimated mean diameters for the swollen particles varied between 442 up to 654 nm (Table 17) with swelling varying between 1000 and 2500% and are accordingly with those predicted by DLS.

4.4.3 Colloidal stability

The effect of pH on the zeta potential of GNPs redispersed in water and PBS solutions was further monitored in different experimental conditions. In the present work, a preliminary study using PBS solution at pH 3.0 and 37 ºC was conducted by measuring zeta potential of the resuspending GNPs and evaluating the pH effect on the particle size as shown in Table 18.

Table 18 – Preliminary zeta potential study.

Sample	**Zeta potential (mV)**	**Particle size (nm)**	**PDI**
G_0.1 (pH 3.0)	+7.6 ± 3.2	742 ± 13.6	0.92 ± 0.065
G_0.1 (pH 6.5)	-76.1 ± 9	441.8 ± 20.4	0.59 ± 0.037

Results are shown as mean (n = 3) followed by ± standard deviation (SD);
Gelatin_Crosslinker concentration (G_0.1).
Source: Author (2023).

Initially, it was expected a cationic behavior of the GNPs with the reduction of pH below isoelectric point of gelatin (IP: 6 – 9). However, in the study conducted by

Ahsan & Rao (2017) it is possible to verify that the change of isoelectric point of type A gelatins occurred around pH 7.0 and positive zeta potentials were found at pH below 6.5 reaching a maximum at pH 3.0 (value in which all groups are protonated). As mentioned by authors, a decrease of pH below 4.0 leads to the protonation of the acid amino acids (acid aspartic and glutamic, respectively) which have pK_a equal to 3.9 and 4.3 and is expected that at pH below 3.5 all the side chains are fully protonated, and a further decrease may have no effect on the ionization state of protein. The authors also mention that the increase of Cl^- ions from the HCl using to decrease pH may lead to ion par formation and to the Debye-Hückel shielding effect which contribute for decreasing of zeta potential of protein.

In this work, it was verified that at pH 3.0, particles presented positive zeta potential values as also evidenced by Ahsan & Rao (2017). In addition, the pH effect on particle size indicated a considerable size increase with pH decrease. This fact can be explained by the complete protonation of amino groups present that favors a higher swelling of the GNPs, leading to an increase in the particle size due to GNPs destabilization, as observed. However, at pH above 3.0, the cationic behavior was not evidenced as expected, and it was associated to the Debye-Hückel screening effect by the excess of Cl^-ions from HCl solution used to decrease pH of PBS solutions, to the high IP of gelatin itself, and also to the remaining SDS excess of the redispersed-GNPs solution which was not completely removed before resuspending.

The surfactant (SDS) used has an ionic characteristic and can contribute to neutralize the formed cationic charges from protonable groups. In addition, due to its ionic character and as it is in excess can also contribute for the negative zeta potentials found. The main challenges for SDS excess removal concerns to the total gelatin weight content (20% w/w) used for synthesis which difficult the separation process via filtration/centrifugation using amicon (100 kDa) or filtration using GPC filter (0.22 μm) as well as the high gelatin molecular weight (> 500 kDa) used and by its sticky appearance which also difficult the SDS excess removal by centrifugation or dialysis using cellulose acetate membrane (pore size not specified) in order to avoid particle agglomeration, drug diffusion (if loaded) and morphological/structural changes before zeta potential readings and further characterizations. Nonetheless, to overcome these challenges, some reports recommending the use of specifics filtration membranes (dialysis) or tangential flow filtration (TFF) for this purpose (BASEER et al., 2019).

It is shown in Table 19, the values obtained for the zeta potential (ξ) ± SD of the redispersed GNPs for all the synthesized formulations. Essays at different pH were conducted and the zeta potential of the GNPs presented negative values for all formulations, being the higher value found, in modulus, equal to 74 mV.

Table 19 – Zeta potential of the redispersed GNPs at 37 ºC.

Sample	**ξ (mV) ± SD**		
	PBS, pH = 5.0	Distilled water, pH = 6.5	PBS, pH = 7.4
G_0.01	-6.2 ± 1	-59.2 ± 0.9	-10.6 ± 1
G_0.05	-8 ± 0.8	-61.7 ± 1.8	-11.2 ± 1.6
G_0.1	-10.9 ± 0.8	-74.4 ± 0.6	-15.7 ± 1.2
PHG_0.01	-24 ± 0.8	-42.8 ± 0.6	-28.6 ± 1.5
PHG_0.05	-26.2 ± 1	-49.4 ± 1.1	-32.3 ± 1.3
PHG_0.1	-33.5 ± 0.4	-61.8 ± 0.5	-36.2 ± 0.4
DOXG_0.01	-2 ± 0.2	-56.4 ± 1.5	-18 ± 1.3
DOXG_0.05	-3.4 ± 0.1	-60.9 ± 1.8	-23 ± 0.6
DOXG_0.1	-6.1 ± 0.5	-71 ± 0.1	-28 ± 1.1
PHDOXG_0.01	-34.7 ± 1.4	-44.5 ± 1.9	-25.7 ± 1.1
PHDOXG_0.05	-39.3 ± 0.9	-50.3 ± 1.3	-27.7 ± 1.1
PHDOXG_0.1	-45.1 ± 1.2	-59.9 ± 0.3	-31.8 ± 0.7

Results are shown as mean (n = 2) followed by ± standard deviation (SD);
Source: Author (2023).

The zeta potential of GNPs suspension is expected to be zero at the isoelectric pH of type A gelatin (pH 6 – 9), however, the smallest modulus found in this range was -10.56 mV for the pure GNPs. As mentioned by Hoeller, Sperger and Valenta (2009), Honary & Zahir (2013[a,b]), absolute zeta potential values of 30 mV indicate adequate stability, above 60 mV stability is excellent, short-term potential close to 20 mV and fast aggregation in the range of -5 mV to 5 mV.

In general, with some exceptions, the values obtained for zeta potential indicated a good colloidal stability of the GNPs dispersion, without aggregates formation at different pH. Among the formulations, the lower potential variation (± 21.8 mV) occurred at pH 7.4, followed by pH 6.5 (± 31.5 mV) and pH 5.0 (± 39.0 mV). It is reported that high charge densities on the surface of particles in buffer solutions promote greater stability by increasing repulsive forces between particles.

However, the values obtained at pH 5.0 and 7.4 may also be associated to the Debye-Hückel screening effect and to the previous steric stability provided by the

redispersion of GNPs in aqueous solution with surfactant (SDS 0.3% wt.) since no changes in charges from (-) to (+) were verified with pH variation, as previously mentioned, and as also verified by the use of Tween 80 in the Hoeller, Sperger and Valenta (2009) work. Moreover, for the pure GNPs was verified a short-term stability with values between -6.1 up to -15.7 mV.

Nevertheless, it was found that at pH 5.0, the highest values obtained for the zeta potential were for non-photopolymerized GNPs indicating a tendency towards phase reversion due to the destabilization in an acid medium and suggesting a possible agglomeration between particles with potential ranging from -2.01 to -10.8 mV. These results may suggest that photopolymerization provided greater stability to redispersed GNPs even in face of pH variations. Except for water pH, in the other cases, the photo-GNPs showed a higher zeta potential in modulus than the non-photopolymerized ones. On the other hand, at pH 6.5, all formulations indicated excellent colloidal stability with values between -42.8 to -74.3 mV.

The values obtained for the zeta potential at pH 7.4 agree with those reported in the work by Ofokansi et al. (2010) in which the zeta potential of pure gelatin nanoparticles was approximately -23 mV at pH 7.0, verifying that fluorescein isothiocyanate dextran (FITC-D) encapsulation did not alter the surface charge density. In the work conducted by Cordeiro et al. (2021) similar behavior to those reported in this study was observed when also encapsulating hydrophilic drugs (4-nitrochalcone and diethyldithiocarbamate) in BN (beeswax nanoparticles) via double emulsion with zeta potential ranging from -34 to -50 mV.

In the study conducted by Baseer et al. (2019), the zeta potential of GNPs was expected to be zero at isoelectric point of type B gelatin (pH 4 – 5). However, authors observed a shift in the IP of GNPs suspension towards (pH 6 – 7). As supported by the authors, it was attributed to the crosslinker and the crosslinking mechanism itself, since gelatin has twice as many arginine (5%) amino acid residues than L-lysine (2.7%) and considering that all lysine (pK_a = 10.5) groups were involved in the crosslinking mechanism, the free residues of arginine (pK_a = 12.5) leads to the evidenced IP increase at higher pH values.

The results found here were consistent and followed the same trend to those findings reported by Baseer and co-workers (2019) and Vigata et al. (2021). In addition to the possibility of occurrence of all cited mechanisms contributions, such as the Debye-Hückel screening effect, the presence of aqueous SDS (ionic surfactant in excess), and

the IP increase (free arginine residues), is believed that polyanionic characteristic of 1,4-butanediol diacrylate (pK_a = 6.5) also contributed to obtaining negative zeta potentials, in addition to the fact that GNPs are highly substituted ($DM \geq 45\%$) which can also contribute to a shift of the IP, as observed. However, at preliminary study when pH becomes sufficient lower (pH 3.0) to protonate all groups, the cationic behavior was verified.

4.4.4 Encapsulation Efficiency studies

The encapsulation efficiency values (%) as well as the amount of encapsulated drug ($\mu g_{DOX} \cdot g_{polymer}^{-1}$) in GNPs dispersed in cyclohexane and in GNPs redispersed in aqueous medium (water with SDS 0.3 wt.%) are presented in Table 20.

Table 20 – Encapsulation efficiency and drug loading of DOX-loaded GNPs.

Sample	EE_C (%)	$Loading_C$ $\mu g_{DOX} \cdot g_{polymer}^{-1}$	EE_W (%)	$Loading_W$ $\mu g_{DOX} \cdot g_{polymer}^{-1}$
DOXG_0.01	94.7 ± 0.23	29.8 ± 0.74	27.2 ± 0.05	8.6 ± 0.18
DOXG_0.05	94.6 ± 0.60	30.3 ± 2.86	27.8 ± 0.67	8.6 ± 0.60
DOXG_0.1	94.7 ± 0.22	28.9 ± 0.60	29.6 ± 1.86	9.0 ± 0.78
PHDOXG_0.01	95.9 ± 0.33	29.2 ± 0.78	29.2 ± 1.30	8.9 ± 0.60
PHDOXG_0.05	95.6 ± 0.33	29.1 ± 0.78	32.4 ± 1.10	9.9 ± 0.57
PHDOXG_0.1	96.2 ± 0.36	31.3 ± 2.16	34.5 ± 0.03	11.2 ± 0.74

Results are shown as mean (n = 2) followed by ± standard deviation (SD);
GNPs dispersed in cyclohexane at 20 ºC (EE_C and $Loading_C$) and GNPs redispersed in distilled water at 20 ºC (EE_W and $Loading_W$);
Source: Author (2023).

The maximum doxorubicin loading efficiency attained for the GNPs dispersed in cyclohexane was 96.2% at 1.5% (w/w) of drug content. On the other hand, when redispersed the maximum encapsulation efficiency was approximately 35%. In the work by Peres et al. (2018) the authors encapsulated doxorubicin in nanoparticles of *N*-acryloyl-L-glutamic acid (L-AGA) and poly(L-AGA-co-BIS) via inverse miniemulsion polymerization, achieving encapsulation efficiencies greater than 83% and drug loading higher than 41 $g_{DOX} \cdot g_{polymer}^{-1}$ when water-redispersed. Furthermore, as mentioned by the authors, this is since possible hydrogen bonds between doxorubicin and the polymer prevent the diffusion of DOX into the aqueous medium even under conditions of temperature and pH.

It was verified that photopolymerized samples showed slightly higher encapsulation and drug loading after redispersion than non-photopolymerized DOX-loaded GNPs. This fact may be associated with the reactions of the unreacted acrylate groups of the crosslinker with the remaining free amino groups and to the homopolymerization of crosslinker, providing a greater retention of the drug within GNPs when water-redispersed by the formation of a more condensed hydrophobic surface.

The high release of DOX in aqueous medium (Table 20) may be due to the process of redispersion of nanoparticles in aqueous SDS 0.3 wt.% solution, due to the GNPs swelling and the affinity of the drug with water. In addition to magnetic stirring (100 rpm) during redispersion (48 h), during the purification process to subsequently reading the supernatant and determine the encapsulation efficiency, the sample is centrifuged twice for 30 min at 3,500 rpm, these processes can accelerate the rate diffusion of drug to water leading to a greater amount released, as verified in this study.

Furthermore, as verified in the synthesis of hydrogels in solution, the more substituted hydrogels (higher acrylate ratio to amine ratio) showed higher swelling ratios, in the case of GNPs, the fact that they are highly substituted, "acrylated" ($DM_{\min} \geq 45\%$) can also leads to higher swelling ratios, and consequently, to a greater drug release due to drug-affinity with water. In addition, a maximum increase of 7.32% in the encapsulation efficiency of photopolymerized particles in relation to non-photopolymerized particles was verified.

4.4.5 Morphology and particle size assessment by TEM

The particle diameter and morphology evaluation of crosslinked GNPs were assessed by TEM and micrographs were obtained in octuplicates from each analyzed sample, subsequently, the best images were chosen to represent the total sample distribution, as shown in Figure 38.

According to TEM images is possible to conclude that water redispersed GNPs possess a roughly spherical morphology with varied particle diameters, and it is also verified from the results obtained by optical and confocal laser scanning microscopy (CLSM) which supports this information. Some authors as Baseer et al. (2019), Ethirajan et al. (2008) found the same morphology to GNPs assessed by TEM even using different preparation methodologies.

Figure 38 – Unloaded crosslinked GNPs with different crosslinker concentrations.

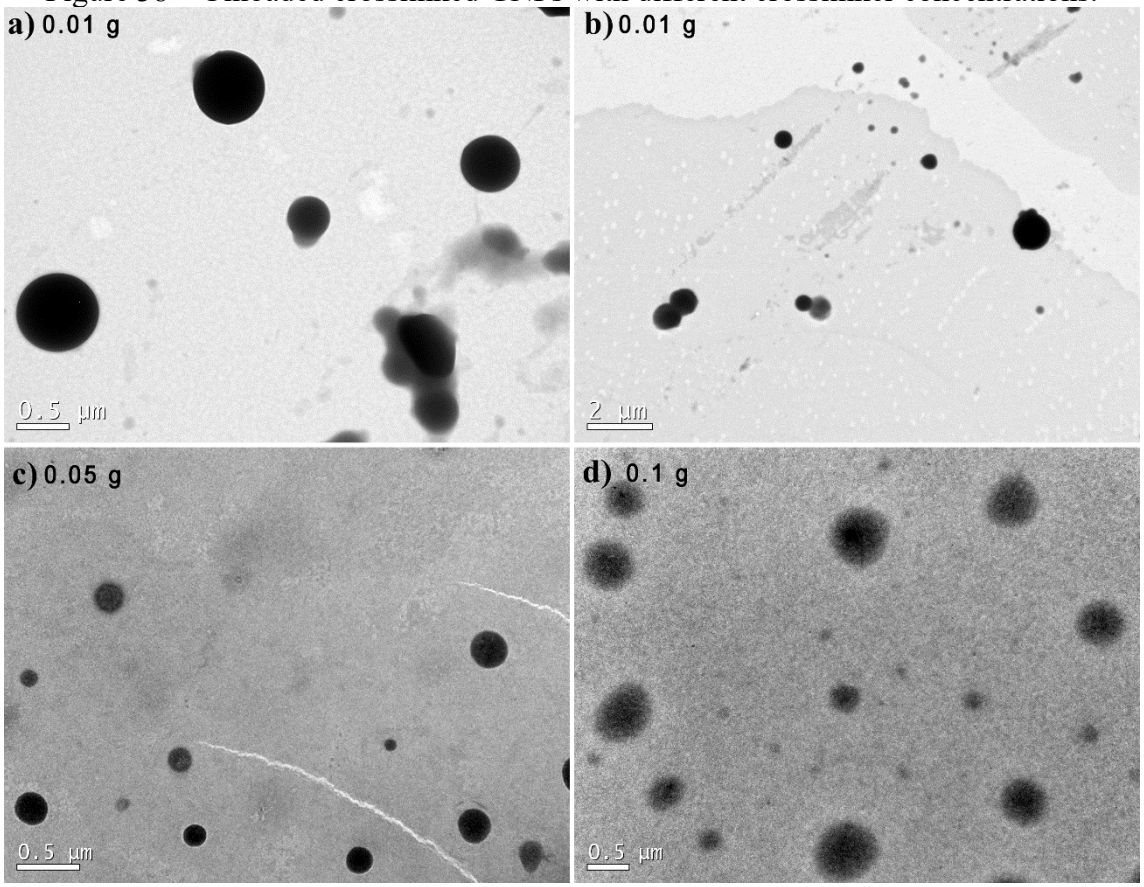

Figures a) scaling at 0.5 µm and b) scaling at 2 µm are the inverse miniemulsion formulation using 0.01 g of crosslinker (samples sputter coated with carbon). Figures c) and d) both scaling at 0.50 µm are the formulations using 0.05 and 0.1 g of crosslinker, respectively, (samples were stained with uranyl acetate (2%));
Source: Author (2023).

In addition, negative staining with uranyl acetate (Figure 38: c and d) causes no differences in the observation of particle contours comparing with carbon coated samples (Figure 38: a and b). However, some flattening was evidenced in certain particles, and may be correlated to sample preparation that can modify the original GNPs shape. Furthermore, the heat generated by light beam from microscope can also deform and affect the size of particles and such factors can impact the diameter as mentioned by Cordeiro et al. (2020) when evaluating lipid nanoparticles.

From the ImageJ software, the average particle diameter of the GNPs (Figure 38, d) was estimated to be equal to D_p = 499.29 ± 178.5 nm, as shown in Figure 43 – Appendix A, and the total number of particles counted was in around 120 nanoparticles. As illustrated, particles were well dispersed indicating no particle aggregation and good dilution range to reading (0.1% solid concentration). The estimated value by TEM is in accordance with the previously estimated particle size in the swollen state with

$D_{p,swollen\,(186\,nm)}$ = 442 nm for SR of 1000% and 600 nm for SR of 2500%, and $D_{p,swollen\,(203\,nm)}$ = 482 nm for SR of 1000% and 654 nm for SR of 2500%. However, for TEM, particles were in the dry state and can be deformed forming discs.

The values found from transmission electron microscopy (TEM) agree with those predicted by means of DLS in which the redispersed particles had shown varied particle size and PDI. In general, it cannot be stated that particle size obtained by TEM were significantly higher or lower than those analyzed by DLS (Table 16) but the data presented a fair agreement with each other. It can be attributed to the presence of smaller particles observed in the micrographs which were also difficult to count, leading to an under or super estimated mean size value. Another plausible explanation concerns the sample drying on the grid before analysis, in which portions of water also can evaporate causing changes in the particle size and contributing to their loss of perfectly spherical morphology. As mentioned by FAN et al. (2018), these differences are related to particles are in dry state when determined by TEM, while by DLS measurement are performed in the hydrated state. Another important point to be highlighted is the variance in particle size by the two techniques employed, TEM and DLS, making it possible to verify nanoparticles of different sizes that may be correlated to sample preparation, different swelling ratio during redispersion and specificity of the applied technique.

However, DLS has restrictions for redispersed nanoparticles, being commonly used the multi angle light scattering (MALS), as previously mentioned. Furthermore, the average particle diameter measured by DLS is based on the average of the diameters of all intensities and does not represent actual particle size.

4.5 FLUORESCENCE STUDIES

4.5.1 Optical microscopy

From the micrographs obtained by optical microscopy, Figure 39, the black border well-defined around GNPs-surface can suggests a thick layer formation at GNPs surface that can be related to the interfacial polymerization occurred between the liquid-liquid interface.

It is shown in Figure 39 – c) and d), optical microscopy in a 40X magnification lens. The fluorescence analysis was carried out immediately after redispersion (48 h), the DOX loading was assessed in the optical microscope, making it possible to verify the

success in encapsulating the drug within the redispersed GNPs, as shown in Figure 39, a) – white filter and b) – red filter.

Figure 39 – Optical fluorescence images of the redispersed DOXG_0.1 at 40X.

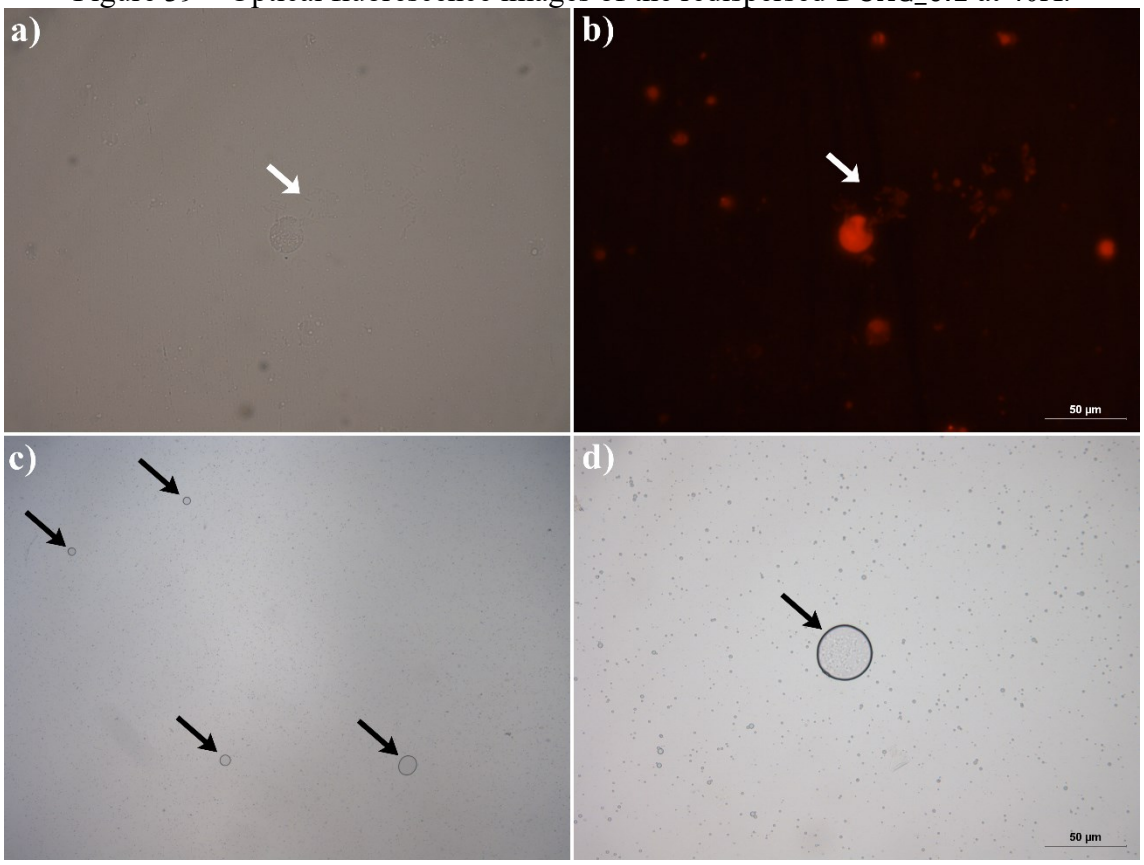

All samples scaling of 50 µm for the formulations of GNPs prepared using 0.01 g of crosslinker; a) white and b) red filter; c) and d) white filter of different part of the same sample.
Source: Author (2023).

Even though the GNPs were previously redispersed in aqueous SDS 0.3 wt.% solution to increase their size by swelling and to be identified under the microscopy, particles smaller than approximately 1.7 µm were not accounted due to lenses range restriction of microscope which could overestimate the real mean particle size. However, after analysis, the average particle diameter size (± 120 particles) estimated by the ImageJ software was in the range of D_p = 2.08 ± 0.374 µm excluding the central particle (D_p = 33.3 µm) from the calculation (Figure 44 – Appendix A).

4.5.2 Encapsulation assessment by confocal laser scanning microscopy (CLSM)

From the CLSM (Figure 40), it was possible to observe the DOX fluorescence (at 585 nm), as intended. In addition, for this analyze, it was selected the formulation that encapsulated the highest drug content (11.2 $\mu g_{DOX}.g_{polymer}^{-1}$).

Figure 40 – CLSM image of GNPs DOX-loaded swelled for 5 days.

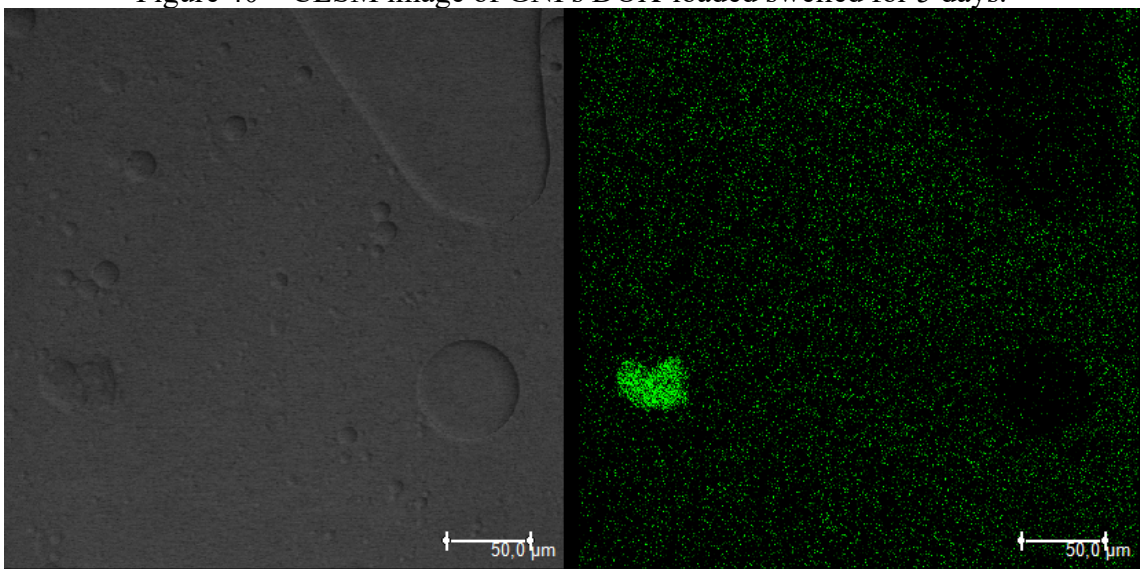

Sample scaling of 50 µm for photopolymerized redispersed GNPs formulations prepared using 0.1 g of crosslinker (PHGDOX_0.1) assessed using green filter;
Source: Author (2023).

In addition to DOX's affinity for water and as reported by Bayram et al. (2022), that DOX release is accelerated under acidic conditions, such as those used in these experiments, from zeta potential studies, it was found that at pH (5.0), the GNPs were anionic and stable, which would lead us to believe that the fluorescence observed comes from the drug encapsulation (as observed in the optical microscopy) by the fact that cationic GNPs destabilization begins to occur in acidic pH and it would be expected that freer DOX would be observed.

Besides, despite of the long swelling time before analysis (five days), which aimed to promote an increase in particle size due to the magnification restriction of the microscope lenses, from the fluorescence of DOX, it was possible to verify its presence in the samples, but it was not possible to state with absolute certainty whether the observed fluorescence comes from encapsulated or free DOX, being recommended cellular internalization studies for better visualization and interpretation of results, as carried out in the studies conducted by Potineni et al. (2003), Ma et al. (2013) and Yoon et al. (2016).

Nonetheless, it was also expected that DOX release would be influenced by GNPs redispersion that involves magnetic stirring, leading to a greater drug rate diffusion. Furthermore, some spaces with sizes ranging between 5.6 and 87.5 μm were identified as shown in Figure 40, and it is also not known for sure whether these measurements correspond to the agglomeration of smaller swollen particles or if they could be related to presence of bubbles arising from sample preparation.

5 FINAL CONSIDERATIONS

5.1 CONCLUSION

The use of the aza-Michael addition reaction proved to be a viable tool for preparing crosslinked PBAEs gelatin-based hydrogels allowing to obtain biomaterials with adjustable formulations and properties based on varying crosslinker concentration. In addition, novel GNPs crosslinked with 1,4-butanediol diacrylate were successfully synthesized via inverse miniemulsion technique from the interfacial polymerization which also allows the post modification via free radical photopolymerization reaction to serve as carriers of the hydrophilic drug doxorubicin.

From Flory-Rehner theory, a satisfactory adjustment to hydrogels swelling data was verified and changes in the chemical structure were identified from FTIR and XRD analyses, indicating the insertion of acrylate moieties in the gelatin chain and/or the crosslinking occurrence. The swelling ratio, the network mesh size as well as the mechanical and thermal properties can be tunable by varying the crosslinker molar ratio. However, despite of plasticizer effect of the crosslinker on gelatin, all formulations seem to be thermally suitable for the intended biomedical application.

Additionally, the synthesis of stable and polydisperse nanoparticles with sizes of approximately 200 nm were obtained when dispersed in the original organic continuous medium (cyclohexane). However, the water-redispersed GNPs showed a considerable increase in particle size and higher PDI values. Further, a fair agreement was also obtained by TEM analysis with an average diameter size measured of approximately 500 nm. Nonetheless, the cationic behavior was evidenced at lower pH values (≤ 3.0) when all groups are expected to be protonated. Through microscopy analyses, the redispersed GNPs presented almost perfectly spherical morphology. It was also found a moderated drug loading from encapsulation efficiency studies after nanoparticles redispersion. Optical microscopy clearly showed the drug encapsulation within GNPs through DOX fluorescence.

The gelatin-based nanoparticles synthesized here are an innovative and technological alternative for the encapsulation of hydrophilic cargo and have potential to

be applied in several biomedical applications including, drug delivery systems for cancer treatments.

5.2 SUGGESTIONS FOR FUTURE WORK

As suggestion for future work, the studies related to biodegradability and cytotoxicity of the synthesized hydrogels and nanogels as well as the adjustment of inverse miniemulsion formulation and the use of other approaches to purify the redispersed GNPs DOX-loaded may be a more effective alternative to increase drug encapsulation efficiency. Additionally, the conduction of studies in relation to drug release kinetics, the photooxidative effects of the drug and ionic contributions in the hydrogels swelling from the modified Flory-Rehner's equations are also recommended.

REFERENCES

AHSAN, S. M.; RAO, C. M. The role of surface charge in the desolvation process of gelatin: implications in nanoparticle synthesis and modulation of drug release. **International journal of nanomedicine**, p. 795-808, 2017.

AJEKWENE, K. K. Properties and applications of acrylates. **Acrylate polymers for advanced applications**, p. 35-46, 2020.

AKBARZADEGAN, R.; AHARI, H.; SHARIFAN, A.; ANVAR, A. A. Overview of the studies on authentication of gelatin using Fourier Transform Infrared spectroscopy coupled with chemometrics. **Human, Health and Halal Metrics**, v. 1, n. 2, p. 86-93, 2021.

AL ISLAM, M. A.; RAHMAN, A. F. M. M.; IFTEKHAR, S.; SALEM, K. S.; SULTANA, N.; BARI, M. L. Morphology, thermal stability, electrical, and mechanical properties of graphene incorporated poly (vinyl alcohol)-gelatin nanocomposites. **Int. J. Compos. Mater**, v. 6, n. 6, p. 172-182, 2016.

ALIPAL, J.; PU'AD, N. M.; LEE, T. C.; NAYAN, N. H. M.; SAHARI, N.; BASRI, H.; ABDULLAH, H. Z. A review of gelatin: Properties, sources, process, applications, and commercialisation. **Materials Today: Proceedings**, v. 42, p. 240-250, 2021.

ANDRADE, K. S. **Extração e microencapsulamento de extratos de interesse biológico provenientes de pimenta-do-reino (Piper nigrum L.) e de pimenta rosa (Schinus terebinthifolius R.).** Tese de Doutorado em Engenharia de Alimentos. 164 pg. Florianópolis, Santa Catarina, Brazil, 2015.

APRIYANTO, A.; COMPART, J.; FETTKE, J. A review of starch, a unique biopolymer–Structure, metabolism and in planta modifications. **Plant Science**, p. 111223, 2022.

ARAMWIT, P.; JAICHAWA, N.; RATANAVARAPORN, J.; SRICHANA, T. A. comparative study of type A and type B gelatin nanoparticles as the controlled release carriers for different model compounds. **Materials Express**, v. 5, n. 3, p. 241-248, 2015.

ARANAZ, I.; ALCÁNTARA, A. R.; CIVERA, M. C.; ARIAS, C.; ELORZA, B.; HERAS CABALLERO, A.; ACOSTA, N. An overview of its properties and applications. **Polymers**, v. 13, n. 19, p. 3256, 2021.

ARAKAWA, C. K.; DEFOREST, C. A. Polymer design and development. In: Biology and engineering of stem cell niches. **Academic Press**, 2017. p. 295-314.

ARRIBAS, P.; GARCÍA-PAYO, M. C.; KHAYET, M.; GIL, L. Improved antifouling performance of polyester thin film nanofiber composite membranes prepared by interfacial polymerization. **Journal of Membrane Science**, v. 598, p. 117774, 2020.

ARSLAN, M. In situ Crosslinking System of Gelatin with Acrylated β-cyclodextrin Towards the Fabrication of Hydrogels for Sustained Drug Release. **Journal of the Turkish Chemical Society Section A: Chemistry**, v. 7, n. 2, p. 597-608, 2020.

ASUA, J. M. Miniemulsion polymerization. **Progress in polymer science**, v. 27, n. 7, p. 1283-1346, 2002.

AWE, O. W.; ZHAO, Y.; NZIHOU, A.; MINH, D. P.; LYCZKO, N. A review of biogas utilisation, purification and upgrading technologies. **Waste and Biomass Valorization**, v. 8, p. 267-283, 2017.

BAEKELAND, L. H. Method of making insoluble products of phenol and formaldehyde. U.S. Patent n. 942,699, 7 dez. 1909. Available on: <https://patents.google.com/patent/US942699A/en>. Accessed in: 12, May, 2023.

BANNUNAH, A. M.; VLLASALIU, D.; LORD, J.; STOLNIK, S. Mechanisms of nanoparticle internalization and transport across an intestinal epithelial cell model: effect of size and surface charge. **Molecular pharmaceutics**, v. 11, n. 12, p. 4363-4373, 2014.

BARANWAL, J.; BARSE, B.; FAIS, A.; DELOGU, G. L.; KUMAR, A. Biopolymer: A sustainable material for food and medical applications. **Polymers**, v. 14, n. 5, p. 983, 2022.

BAKHTIAR, C.; HARDY, D. T. **Lectures on Organic Chemistry**. World Scientific Publishing Company, 1997.

BARCELOS, L. M.; BORGES, M. G.; SOARES, C. J.; MENEZES, M. S.; HUYNH, V.; LOGAN, M. G.; PFEIFER, C. S. Effect of the photoinitiator system on the polymerization of secondary methacrylamides of systematically varied structure for dental adhesive applications. **Dental Materials**, v. 36, n. 3, p. 468-477, 2020.

BAROLI, B. Photopolymerization of biomaterials: issues and potentialities in drug delivery, tissue engineering, and cell encapsulation applications. **Journal of Chemical Technology & Biotechnology: International Research in Process, Environmental & Clean Technology**, v. 81, n. 4, p. 491-499, 2006.

BASSAM, N.; LAURE, C.; JEAN-FRANÇOIS, B.; YANN, R.; ZEPHIRIN, M. Aza-Michael versus aminolysis reactions of glycerol carbonate acrylate. **Green Chemistry**, v. 15, n. 7, p. 1900-1909, 2013.

BASEER, A.; KOENNEKE, A.; ZAPP, J.; KHAN, S. A.; SCHNEIDER, M. Design and Characterization of Surface-Crosslinked Gelatin Nanoparticles for the Delivery of Hydrophilic Macromolecular Drugs. **Macromolecular Chemistry and Physics**, v. 220, n. 18, p. 1900260, 2019.

BAUER, F.; DECKER, U.; NAUMOV, S.; RIEDEL, C. Photoinitiator-free UV curing and matting of acrylate-based nanocomposite coatings: Part 3. **Progress in Organic Coatings**, v. 77, n. 6, p. 1085-1094, 2014.

BAYDIN, T.; AARSTAD, O. A.; DILLE, M. J.; HATTREM, M. N.; DRAGET, K. I. Long-term storage stability of type A and type B gelatin gels: The effect of Bloom strength and co-solutes. **Food Hydrocolloids**, v. 127, p. 107535, 2022.

BAYRAM, N. N.; ULU, G. T.; TOPUZOĞULLARI, M.; BARAN, Y.; DINÇER İŞOĞLU, S. HER2-Targeted, Degradable Core Cross-Linked Micelles for Specific and Dual pH-Sensitive DOX Release. **Macromolecular Bioscience**, v. 22, n. 1, p. 2100375, 2022.

BEHERA, S.; MAHANWAR, P. A. Superabsorbent polymers in agriculture and other applications: A review. **Polymer-Plastics Technology and Materials**, v. 59, n. 4, p. 341-356, 2020.

BERG, J. M.; TYMOCZKO, J. L. **Stryer biochemie**. Heidelberg: Springer Spektrum, 2018.

BERGMANN, E. D.; GINSBURG, D.; PAPPO, R. The Michael Reaction in Org. React. Vol. 10. 1959.

BERNASCONI, C. F. Nucleophilic addition to olefins. Kinetics and mechanism. **Tetrahedron**, v. 45, n. 13, p. 4017-4090, 1989.

BERNE, D.; CAILLOL, S.; LADMIRAL, V.; LECLERC, E. Synthesis of polyester thermosets via internally catalyzed Michael-addition of methylene compounds on a 2-(trifluoromethyl) acrylate-derived building block. **European Polymer Journal**, v. 175, p. 111362, 2022.

BESSE, V.; DERBANNE, M. A.; PHAM, T. N.; COOK, W. D.; LE PLUART, L. Photopolymerization study and adhesive properties of self-etch adhesives containing bis (acyl) phosphine oxide initiator. **Dental Materials**, v. 32, n. 4, p. 561-569, 2016.

BHATTACHARJEE, S. Understanding the burst release phenomenon: Toward designing effective nanoparticulate drug-delivery systems. **Therapeutic Delivery**, v. 12, n. 1, p. 21-36, 2021.

BI, D.; YANG, X.; YAO, L.; HU, Z.; LI, H.; XU, X.; LU, J. Potential food and nutraceutical applications of alginate: A review. **Marine Drugs**, v. 20, n. 9, p. 564, 2022.

BILLIET, T.; GASSE, B. V.; GEVAERT, E.; CORNELISSEN, M.; MARTINS, J. C.; DUBRUEL, P. Quantitative Contrasts in the Photopolymerization of Acrylamide and Methacrylamide-Functionalized Gelatin Hydrogel Building Blocks. **Macromolecular bioscience**, v. 13, n. 11, p. 1531-1545, 2013.

BOSSION, A.; JONES, G. O.; TATON, D.; MECERREYES, D.; HEDRICK, J. L.; ONG, Z. Y.; SARDON, H. Non-isocyanate polyurethane soft nanoparticles obtained by surfactant-assisted interfacial polymerization. **Langmuir**, v. 33, n. 8, p. 1959-1968, 2017.

BOZEC, L.; ODLYHA, M. Thermal denaturation studies of collagen by microthermal analysis and atomic force microscopy. **Biophysical journal**, v. 101, n. 1, p. 228-236, 2011.

BRASKEM. **Technical Bulletin, n.1 – PVC,** (2002). Available in:https://www.braskem.com.br/Portal/Principal/Arquivos/html/boletm_tecnico/Plasticantes.pdf. Accessed in 9th, Oct. 2023.

BRODSKY, B.; RAMSHAW, J. A. The collagen triple-helix structure. **Matrix biology**, v. 15, n. 8-9, p. 545-554, 1997.

BRUCK, S. D. Extension of the Flory-Rehner theory of swelling to an anisotropic polymer system. Journal of Research of the National Bureau of Standards. Section A, **Physics and Chemistry**, v. 65, n. 6, p. 485, 1961.

BRUICE, P. Y. **Organic chemistry, 8th edition**. University of California, Santa Barbara. Published by Pearson, 2017.

BU, L. L.; WANG, H. Q.; PAN, Y.; CHEN, L.; WU, H.; WU, X.; SUN, Z. J. Gelatinase-sensitive nanoparticles loaded with photosensitizer and STAT3 inhibitor for cancer photothermal therapy and immunotherapy. **Journal of Nanobiotechnology**, v. 19, p. 1-13, 2021.

BUKHARI, S. M. H.; KHAN, S.; REHANULLAH, M.; RANJHA, N. M. Synthesis and characterization of chemically crosslinked acrylic acid/gelatin hydrogels: effect of pH and composition on swelling and drug release. **International Journal of Polymer Science**, v. 2015, 2015.

BUPPHATHONG, S.; QUIROZ, C.; HUANG, W.; CHUNG, P. F.; TAO, H. Y.; LIN, C. H. Gelatin methacrylate hydrogel for tissue engineering applications—a review on material modifications. **Pharmaceuticals**, v. 15, n. 2, p. 171, 2022.

CAM, M. E.; YILDIZ, S.; ALENEZI, H.; CESUR, S.; OZCAN, G. S.; ERDEMIR, G.; EDIRISINGHE, M. Evaluation of burst release and sustained release of pioglitazone-loaded fibrous mats on diabetic wound healing: an in vitro and in vivo comparison study. **Journal of the Royal Society Interface**, v. 17, n. 162, p. 20190712, 2020.

CAMPIGLIO, C. E.; PONZINI, S.; DE STEFANO, P.; ORTOLEVA, G.; VIGNATI, L.; DRAGHI, L. Crosslinking optimization for electrospun gelatin: Challenge of preserving fiber topography. **Polymers**, v. 12, n. 11, p. 2472, 2020.

CANAL, T.; PEPPAS, N. A. Correlation between mesh size and equilibrium degree of swelling of polymeric networks. **Journal of biomedical materials research**, v. 23, n. 10, p. 1183-1193, 1989.

CAO, Y.; LEE, B. H.; IRVINE, S. A.; WONG, Y. S.; BIANCO PELED, H.; VENKATRAMAN, S. Inclusion of crosslinked elastin in gelatin/PEG hydrogels favourably influences fibroblast phenotype. **Polymers**, v. 12, n. 3, p. 670, 2020.

CAO, Y.; UHRICH, K. E. Biodegradable and biocompatible polymers for electronic applications: A review. **Journal of Bioactive and Compatible Polymers**, v. 34, n. 1, p. 3-15, 2019.

CAPEK, I. On inverse miniemulsion polymerization of conventional water-soluble monomers. **Advances in colloid and interface science**, v. 156, n. 1-2, p. 35-61, 2010.

CARVALHO, C.; SANTOS, R. X.; CARDOSO, S.; CORREIA, S.; OLIVEIRA, P. J.; SANTOS, M. S.; MOREIRA, P. I. Doxorubicin: the good, the bad and the ugly effect. **Current medicinal chemistry**, v. 16, n. 25, p. 3267-3285, 2009.

CASTEGNA, A.; DRAKE, J.; POCERNICH, C.; BUTTERFIELD, D. A. Protein carbonyl levels—an assessment of protein oxidation. **Methods in biological oxidative stress**, p. 161-168, 2003.

CAVALLO, A.; MADAGHIELE, M.; MASULLO, U.; LIONETTO, M. G.; SANNINO, A. Photo-crosslinked poly (ethylene glycol) diacrylate (PEGDA) hydrogels from low molecular weight prepolymer: swelling and permeation studies. **Journal of Applied Polymer Science**, v. 134, n. 2, 2017.

CAYOT, P.; TAINTURIER, G. The quantification of protein amino groups by the trinitrobenzenesulfonic acid method: a reexamination. **Analytical biochemistry**, v. 249, n. 2, p. 184-200, 1997.

CHALMIN, P. The history of plastics: from the Capitol to the Tarpeian Rock. **Field actions science reports**. **The Journal of Field Actions**, n. Special Issue 19, p. 6-11, 2019. Available in:< https://journals.openedition.org/factsreports/5071#quotation>. Accessed in: 11th Feb. 2023.

CHAWLA, R.; RANI, V.; MISHRA, M. Nanoparticulate Carriers—Versatile Delivery Systems. **Nanopharmaceutical Advanced Delivery Systems**, p. 31-54, 2021.

CHECK, C.; CHARTOFF, R.; CHANG, S. Inkjet printing of 3D nano-composites formed by photopolymerization of an acrylate monomer. **Reactive and Functional Polymers**, v. 97, p. 116-122, 2015.

CHEN, W. Q.; MA, J. A. 4.01 Stabilized Nucleophiles with Electron Deficient Alkenes, Alkynes, Allenes. **Comprehensive Organic Synthesis II**, 1–85, 2014.

CHEN, J.; WU, J.; RAFFA, P.; PICCHIONI, F.; KONING, C. E. Superabsorbent Polymers: From long-established, microplastics generating systems, to sustainable, biodegradable and future proof alternatives. **Progress in Polymer Science**, v. 125, p. 101475, 2022.

CHENG, J.; SHI, W.; ZHANG, L.; ZHANG, R. A novel polyester composite nanofiltration membrane formed by interfacial polymerization of pentaerythritol (PE) and trimesoyl chloride (TMC). **Applied Surface Science**, v. 416, p. 152-159, 2017.
CHEMSPIDER. Search and share chemistry. 1,4-Butanediol diacrylate – Chemical structure, 2023. Available on: <http://www.chemspider.com/Chemical-Structure.63781.html>. Accessed in: 12th, March, 2023.

CHENG, J.; SHI, W.; ZHANG, L.; ZHANG, R. A novel polyester composite nanofiltration membrane formed by interfacial polymerization of pentaerythritol (PE) and trimesoyl chloride (TMC). **Applied Surface Science**, v. 416, p. 152-159, 2017.

CHIONG, J. A.; TRAN, H.; LIN, Y.; ZHENG, Y.; BAO, Z. Integrating emerging polymer chemistries for the advancement of recyclable, biodegradable, and biocompatible electronics. **Advanced Science**, v. 8, n. 14, p. 2101233, 2021.

CHO, J. S.; KWON, A.; CHO, C. G. Microencapsulation of octadecane as a phase-change material by interfacial polymerization in an emulsion system. **Colloid and polymer science**, v. 280, p. 260-266, 2002.

CHOI, H.; PARK, J.; LEE, J. Sustainable Bio-Based Superabsorbent Polymer: Poly (itaconic acid) with Superior Swelling Properties. **ACS Applied Polymer Materials**, v. 4, n. 6, p. 4098-4108, 2022.

CLAAßEN, C.; CLAAßEN, M. H.; TRUFFAULT, V.; SEWALD, L.; TOVAR, G. E.; BORCHERS, K.; SOUTHAN, A. Quantification of substitution of gelatin methacryloyl: best practice and current pitfalls. **Biomacromolecules**, v. 19, n. 1, p. 42-52, 2018.

CLEGG, K. M.; LEE, Y. K.; MCGILLIGAN, J. F. Trinitrobenzenesulphonic acid and ninhydrin reagents for the assessment of protein degradation in cheese samples. **International Journal of Food Science & Technology**, v. 17, n. 4, p. 517-520, 1982.

COESTER, C. J.; LANGER, K.; VON BRIESEN, H.; KREUTER, J. Gelatin nanoparticles by two step desolvation a new preparation method, surface modifications and cell uptake. **Journal of microencapsulation**, v. 17, n. 2, p. 187-193, 2000.

CORDEIRO, A. P.; FEUSER, P. E.; FIGUEIREDO, P. G.; DA CUNHA, E. S.; MARTINEZ, G. R.; MACHADO-DE-AVILA, R. A.; SAYER, C. In vitro synergic activity of diethyldithiocarbamate and 4-nitrochalcone loaded in beeswax nanoparticles against melanoma (B16F10) cells. **Materials Science and Engineering: C**, v. 120, p. 111651, 2021.

CORNILLE, A.; ECOCHARD, Y.; BLAIN, M.; BOUTEVIN, B.; CAILLOL, S. Synthesis of hybrid polyhydroxyurethanes by Michael addition. **European Polymer Journal**, v. 96, p. 370-382, 2017.

CROSSEN, S. L.; GOSWAMI, T. Nanoparticulate carriers for drug delivery. **Journal of Pharmaceutical and Biopharmaceutical Research**, v. 4, n. 1, p. 237, 2022.
DALPOZZO, R.; BARTOLI, G.; BENCIVENNI, G. Asymmetric organocatalytic reactions of α, β-unsaturated cyclic ketones. **Symmetry**, v. 3, n. 1, p. 84-125, 2011.

DANG, X.; LI, Y.; YANG, M. Biodegradable waterborne polyurethane grafted with gelatin hydrolysate via solvent-free copolymerization for potential porous scaffold material. **Journal of the Mechanical Behavior of Biomedical Materials**, v. 92, p. 79-89, 2019.

DANIELSEN, S. P.; BEECH, H. K.; WANG, S.; EL-ZAATARI, B. M.; WANG, X.; SAPIR, L.; RUBINSTEIN, M. Molecular characterization of polymer networks. **Chemical reviews**, v. 121, n. 8, p. 5042-5092, 2021.

DAS, A.; BANIK, B. K. **Microwaves in chemistry applications: fundamentals, methods and future trends**. Elsevier, 2021.

DE, R.; MAHATA, M. K.; KIM, K. T. Structure-Based Varieties of Polymeric Nanocarriers and Influences of Their Physicochemical Properties on Drug Delivery Profiles. **Advanced Science**, v. 9, n. 10, p. 2105373, 2022.

DEFRATES, K.; MARKIEWICZ, T.; GALLO, P.; RACK, A.; WEYHMILLER, A.; JARMUSIK, B.; HU, X. Protein polymer-based nanoparticles: Fabrication and medical applications. **International journal of molecular sciences**, v. 19, n. 6, p. 1717, 2018.

DESHMUKH, K.; AHAMED, M. B.; DESHMUKH, R. R.; PASHA, S. K.; BHAGAT, P. R.; CHIDAMBARAM, K. Biopolymer composites with high dielectric performance: interface engineering. In: **Biopolymer composites in electronics**. Elsevier, 2017. p. 27-128.

DESSAUER, R. **Photochemistry, history and commercial applications of hexaarylbiimidazoles: all about HABIs**. Elsevier, 2006.

DEVALAPALLY, H.; SHENOY, D.; LITTLE, S.; LANGER, R.; AMIJI, M. Poly (ethylene oxide)-modified poly (beta-amino ester) nanoparticles as a pH-sensitive system for tumor-targeted delivery of hydrophobic drugs: part 3. Therapeutic efficacy and safety studies in ovarian cancer xenograft model. **Cancer chemotherapy and pharmacology**, v. 59, p. 477-484, 2007.

DHAND, A. P.; GALARRAGA, J. H.; BURDICK, J. A. Enhancing biopolymer hydrogel functionality through interpenetrating networks. **Trends in biotechnology**, v. 39, n. 5, p. 519-538, 2021.

DICKINSON, E. Biopolymer-based particles as stabilizing agents for emulsions and foams. **Food Hydrocolloids**, v. 68, p. 219-231, 2017.

DONG, Z.; YUAN, Q.; HUANG, K.; XU, W.; LIU, G.; GU, Z. Gelatin methacryloyl (GelMA)-based biomaterials for bone regeneration. **RSC advances**, v. 9, n. 31, p. 17737-17744, 2019.

DOU, Z.; TANG, H.; CHEN, K.; LI, D.; YING, Q.; MU, Z.; WANG, H. Highly elastic and self-healing nanostructured gelatin/clay colloidal gels with osteogenic capacity for minimally invasive and customized bone regeneration. **Biofabrication**, v. 15, n. 2, p. 025001, 2023.

DUTHEN, S.; ROCHAT, C.; KLEIBER, D.; VIOLLEAU, F.; DAYDÉ, J.; RAYNAUD, C.; LEVASSEUR-GARCIA, C. Physicochemical characterization and study of molar mass of industrial gelatins by AsFlFFF-UV/MALS and chemometric approach. **Plos one**, v. 13, n. 10, p. e0203595, 2018.

ECHAVE, M. C.; SÁNCHEZ, P.; PEDRAZ, J. L.; ORIVE, G. Progress of gelatin-based 3D approaches for bone regeneration. **Journal of Drug Delivery Science and Technology**, v. 42, p. 63-74, 2017.

EDWARDS, F. C.; DI, Y.; DYE, J. F. In vitro assessment of the cytotoxicity and inflammatory potential of glutaraldehyde as a crosslinking agent for protein scaffolds.

In: **Tissue Engineering**. 140 HUGUENOT STREET, 3RD FL, NEW ROCHELLE, NY 10801 USA: MARY ANN LIEBERT INC, 2007. p. 1711-1712.

EFTHIMIADOU, E. K.; THEODOSIOU, M.; TONIOLO, G.; ABU-THABIT, N. Y. Stimuli-responsive biopolymer nanocarriers for drug delivery applications. **Stimuli Responsive Polymeric Nanocarriers for Drug Delivery Applications**, Volume 1, p. 405-432, 2018.

EHRMANN, A. Non-toxic crosslinking of electrospun gelatin nanofibers for tissue engineering and biomedicine—A review. **Polymers**, v. 13, n. 12, p. 1973, 2021.

EL-AASSER, M. S.; SUDOL, E. D. Miniemulsions: overview of research and applications. **JCT Res**, v. 1, n. 1, p. 21-31, 2004.

EL-MELIGY, M. A.; VALACHOVÁ, K.; JURÁNEK, I.; TAMER, T. M.; ŠOLTÉS, L. Preparation and Physicochemical Characterization of Gelatin–Aldehyde Derivatives. **Molecules**, v. 27, n. 20, p. 7003, 2022.

ELTOUKHY, A. A.; SIEGWART, D. J.; ALABI, C. A.; RAJAN, J. S., LANGER, R.; ANDERSON, D. G. Effect of molecular weight of amine end-modified poly (β-amino ester) s on gene delivery efficiency and toxicity. **Biomaterials**, v. 33, n. 13, p. 3594-3603, 2012.

EREN, T. N.; KARIKSIZ, N.; DEMIRCI, G.; TUNCEL, D.; OKTE, N.; ACAR, H. Y.; AVCI, D. Irgacure 2959-functionalized poly (ethyleneimine) s as improved photoinitiators: enhanced water solubility, migration stability and visible-light operation. **Polymer Chemistry**, v. 12, n. 18, p. 2772-2785, 2021.

ETHIRAJAN, A.; SCHOELLER, K.; MUSYANOVYCH, A.; ZIENER, U.; LANDFESTER, K. Synthesis and optimization of gelatin nanoparticles using the miniemulsion process. **Biomacromolecules**, v. 9, n. 9, p. 2383-2389, 2008.

FADDA, G. C.; LAIREZ, D.; ARRIO, B.; CARTON, J. P.; LARRETA-GARDE, V. Enzyme-catalyzed gel proteolysis: an anomalous diffusion-controlled mechanism. **Biophysical journal**, v. 85, n. 5, p. 2808-2817, 2003.

FALCA, G.; MUSTEATA, V. E.; CHISCA, S.; HEDHILI, M. N.; ONG, C.; NUNES, S. P. Naturally extracted hydrophobic solvent and self-assembly in interfacial polymerization. **ACS Applied Materials & Interfaces**, v. 13, n. 37, p. 44824-44832, 2021.

FAN, L.; DU, Y.; HUANG, R.; WANG, Q.; WANG, X.; ZHANG, L. Preparation and characterization of alginate/gelatin blend fibers. **Journal of Applied Polymer Science**, v. 96, n. 5, p. 1625-1629, 2005.

FAN, D.; YU, J.; YAN, R.; XU, X; WANG, Y.; XIE, X.; HUANG, H. Preparation and evaluation of doxorubicin-loaded micelles based on glycyrrhetinic acid modified gelatin conjugates for targeting hepatocellular carcinoma. **Journal of Nanomaterials**, v. 2018, 2018.

FARRIS, S.; SONG, J.; HUANG, Q. Alternative reaction mechanism for the crosslinking of gelatin with glutaraldehyde. **Journal of agricultural and food chemistry**, v. 58, n. 2, p. 998-1003, 2010.

FAROOQ, U.; TEUWEN, J.; DRANSFELD, C. Toughening of epoxy systems with interpenetrating polymer network (IPN): A review. **Polymers**, v. 12, n. 9, p. 1908, 2020.

FDA. United States Food and Drug Administration. GRAS Substances (SCOGS) Database. Link available: < http://wayback.archive-it.org/7993/20171031062708/https://www.fda.gov/Food/IngredientsPackagingLabeling/GRAS/SCOGS/ucm261307.htm>. Acessed in 23th nov., 2022.

FIELDS, R. [38] The rapid determination of amino groups with TNBS. In: **Methods in enzymology**. Academic Press, 1972. p. 464-468.

FISHER, J. P.; DEAN, D.; ENGEL, P. S.; MIKOS, A. G. Photoinitiated polymerization of biomaterials. **Annual review of materials research**, v. 31, n. 1, p. 171-181, 2001.

FLARIS, V.; SINGH, G. Recent developments in biopolymers. **Journal of Vinyl and Additive Technology**, v. 15, n. 1, p. 1-11, 2009.

FLORY, P. J.; KRIGBAUM, W. R. Thermodynamics of high polymer solutions. **Annual review of physical chemistry**, v. 2, n. 1, p. 383-402, 1951.

FLORY, P. J.; REHNER JR, J. Statistical mechanics of cross-linked polymer networks II. Swelling. **The journal of chemical physics**, v. 11, n. 11, p. 521-526, 1943.

FREDHEIM, G. E.; BRAATEN, S. M.; CHRISTENSEN, B. E. Molecular weight determination of lignosulfonates by size-exclusion chromatography and multi-angle laser light scattering. **Journal of Chromatography A**, v. 942, n. 1-2, p. 191-199, 2002.

FREELAND, B.; MCCARTHY, E.; BALAKRISHNAN, R.; FAHY, S.; BOLAND, A.; ROCHFORT, K. D.; GAUGHRAN, J. A Review of Polylactic Acid as a Replacement Material for Single-Use Laboratory Components. **Materials**, v. 15, n. 9, p. 2989, 2022.

FROIDEVAUX, V.; NEGRELL, C.; CAILLOL, S.; PASCAULT, J. P.; BOUTEVIN, B. Biobased amines: from synthesis to polymers; present and future. **Chemical Reviews**, v. 116, n. 22, p. 14181-14224, 2016.

FUKUNAKA, Y.; IWANAGA, K.; MORIMOTO, K.; KAKEMI, M.; TABATA, Y. Controlled release of plasmid DNA from cationized gelatin hydrogels based on hydrogel degradation. **Journal of controlled release**, v. 80, n. 1-3, p. 333-343, 2002.

GARCIA-VAQUERO, M.; MIRZAPOUR-KOUHDASHT, A. A review on proteomic and genomic biomarkers for gelatin source authentication: Challenges and future outlook. **Heliyon**, 2023.

GARRISON, M. D.; STORCH, P. J.; ECK, W. S.; ADAMS, V. H.; FEDICK, P. W.; HARVEY, B. G. BPA-free high-performance sustainable polycarbonates derived from non-estrogenic bio-based phenols. **Green Chemistry**, v. 23, n. 20, p. 8016-8029, 2021.

GELITA. **Technical information: typical amino acid composition of GELITA Collagen Peptides (Hydrolysate)**. Available on: < https://www.gelita.com/sites/default/files/documents/2019-11/15035%20Peptides%20Technik-Broschuere%202019%20%2816p%29%20eng%20A4%20RZ02%20%28WEB%29.pdf >. Accessed in 12th, Dec. 2022.

GENEST, A.; PORTINHA, D.; FLEURY, E.; GANACHAUD, F. The aza-Michael reaction as an alternative strategy to generate advanced silicon-based (macro) molecules and materials. **Progress in Polymer Science**, v. 72, p. 61-110, 2017.

GEORGE, A.; SANJAY, M. R.; SRISUK, R.; PARAMESWARANPILLAI, J.; SIENGCHIN, S. A comprehensive review on chemical properties and applications of biopolymers and their composites. **International journal of biological macromolecules**, v. 154, p. 329-338, 2020.

GEWIRTZ, D. A. A critical evaluation of the mechanisms of action proposed for the antitumor effects of the anthracycline antibiotics adriamycin and daunorubicin. **Biochemical pharmacology**, v. 57, n. 7, p. 727-741, 1999.

GHANI, N. A. Effect of pH on functional, rheological and structural properties of eel (Monopterus sp.) skin gelatin compared to bovine gelatin. **International Food Research Journal**, 2016.

GHARIEH, A.; KHOEE, S.; MAHDAVIAN, A. R. Emulsion and miniemulsion techniques in preparation of polymer nanoparticles with versatile characteristics. **Advances in colloid and interface science**, v. 269, p. 152-186, 2019.

GHAVAMINEJAD, A.; ASHAMMAKHI, N.; WU, X. Y.; KHADEMHOSSEINI, A. Crosslinking strategies for 3D bioprinting of polymeric hydrogels. **Small**, v. 16, n. 35, p. 2002931, 2020.

GHAZINEZHAD, M.; BOZORGIAN, A.; GHOLAMI DASTNAEI, P. A Review of Frontal Polymerization in the Chemical Industry. **International Journal of New Chemistry**, v. 9, n. 4, p. 623-646, 2022.

GHORANI, B.; EMADZADEH, B.; REZAEINIA, H.; RUSSELL, S. J. Improvements in gelatin cold water solubility after electrospinning and associated physicochemical, functional and rheological properties. **Food Hydrocolloids**, v. 104, p. 105740, 2020.

GILCHRIST, A. E.; LEE, S.; HU, Y.; HARLEY, B. A. Soluble Signals and Remodeling in a Synthetic Gelatin-Based Hematopoietic Stem Cell Niche. **Advanced healthcare materials**, v. 8, n. 20, p. 1900751, 2019.

GOBI, R.; RAVICHANDIRAN, P.; BABU, R. S.; YOO, D. J. Biopolymer and synthetic polymer-based nanocomposites in wound dressing applications: a review. **Polymers**, v. 13, n. 12, p. 1962, 2021.

GOHIL, J. M.; RAY, P. A review on semi-aromatic polyamide TFC membranes prepared by interfacial polymerization: Potential for water treatment and desalination. **Separation and Purification Technology**, v. 181, p. 159-182, 2017.

GOLUBEVAS, R.; STANKEVICIUTE, Z.; ZARKOV, A.; GOLUBEVAS, R., HANSSON, L.; RAUDONIS, R.; GARSKAITE, E. Acrylate–gelatin–carbonated hydroxyapatite (cHAP) composites for dental bone-tissue applications. **Materials Advances**, v. 1, n. 6, p. 1675-1684, 2020.

GONZÁLEZ, G.; FERNÁNDEZ-FRANCOS, X.; SERRA, À.; SANGERMANO, M. RAMIS, X. Environmentally-friendly processing of thermosets by two-stage sequential aza-Michael addition and free-radical polymerization of amine–acrylate mixtures. **Polymer Chemistry**, v. 6, n. 39, p. 6987-6997, 2015.

GOPI, S.; AMALRAJ, A.; SUKUMARAN, N. P.; HAPONIUK, J. T.; THOMAS, S. Biopolymers and their composites for drug delivery: a brief review. In: **Macromolecular Symposia**. 2018. p. 1800114.

GOOCH, J. W. (Ed.). **Encyclopedic dictionary of polymers**. Springer Science & Business Media, 2010.

GRANDE-TOVAR, C. D.; VALLEJO, W.; ZULUAGA, F. Equilibrium and kinetic study of lead and copper ion adsorption on chitosan-grafted-polyacrylic acid synthesized by surface initiated atomic transfer polymerization. **Molecules**, v. 23, n. 9, p. 2218, 2018.

GRECO, G.; ULFO, L.; TURRINI, E.; MARCONI, A.; COSTANTINI, P. E.; MARFORIO, T. D.; CALVARESI, M. Light-Enhanced Cytotoxicity of Doxorubicin by Photoactivation. **Cells**, v. 12, n. 3, p. 392, 2023.

GREEN, W. A. **Industrial photoinitiators: a technical guide**. CRC Press, 2010.

GRIGALE-SOROCINA, Z.; KALNINS, M.; SIMANOVSKA, J.; VINDEDZE, E.; BIRKS, I.; BRAZDAUSKA, E. Effect of additives on UV-activated urethane acrylate polymerization composite coatings. **Materials Science**, v. 22, n. 1, p. 54-59, 2016.

GROVER, C. N.; GWYNNE, J. H.; PUGH, N.; HAMAIA, S.; FARNDALE, R. W.; BEST, S. M.; CAMERON, R. E. Crosslinking and composition influence the surface properties, mechanical stiffness and cell reactivity of collagen-based films. **Acta biomaterialia**, v. 8, n. 8, p. 3080-3090, 2012.

GUO, Y.; TEO, V. L.; TING, S. R.; ZETTERLUND, P. B. Miniemulsion polymerization based on in situ surfactant formation without high-energy homogenization: effects of organic acid and counter ion. **Polymer journal**, v. 44, n. 5, p. 375-381, 2012.

GÜLSU, A.; KILLI, B.; ALPER, M. Paclitaxel delivery by cationic gelatin nanoparticles. **ChemistrySelect**, v. 7, n. 1, p. e202103495, 2022.

GZIUT, K.; KOWALCZYK, A.; SCHMIDT, B.; IDZIK, T. J.; SOŚNICKI, J. G. Influence of Methacrylate and Vinyl Monomers on Radical Bulk Photopolymerization

Process and Properties of Epoxy-Acrylate Structural Adhesives. **Polymers**, v. 15, n. 4, p. 926, 2023.

HABANJAR, O.; DIAB-ASSAF, M.; CALDEFIE-CHEZET, F.; DELORT, L. 3D cell culture systems: tumor application, advantages, and disadvantages. **International journal of molecular sciences**, v. 22, n. 22, p. 12200, 2021.

HAEMA, K.; OYAMA, T. G.; KIMURA, A.; TAGUCHI, M. Radiation stability and modification of gelatin for biological and medical applications. **Radiation Physics and Chemistry**, v. 103, p. 126-130, 2014.

HALBARDIER, L.; GOLDBACH, E.; CROUTXÉ-BARGHORN, C.; SCHULLER, A. S.; ALLONAS, X. Combined aza-Michael and radical photopolymerization reactions for enhanced mechanical properties of 3D printed shape memory polymers. **RSC advances**, v. 12, n. 47, p. 30381-30385, 2022.

HALIMA, N. B. Poly (vinyl alcohol): review of its promising applications and insights into biodegradation. **RSC advances**, v. 6, n. 46, p. 39823-39832, 2016.

HAMMARLING, K.; SANDBERG, M.; ENGHOLM, M.; ANDERSSON, H.; NILSSON, H. E. Synthesis, Curing Behavior and Swell Tests of pH-Responsive Coatings from Acryl-Terminated Oligo (β-Amino Esters). **Chemosensors**, v. 6, n. 1, p. 10, 2018.

HARDING, S. E.; JUMEL, K. Light scattering. **Current protocols in protein science**, v. 11, n. 1, p. 7.8. 1-7.8. 14, 1998.

HE, F.; SHOOSHTARI, K.; COLLIER, H. Experimental investigation into one-step and two-step polymerization via Michael addition from primary amine. In: ABSTRACTS OF PAPERS OF THE AMERICAN CHEMICAL SOCIETY. 1155 16TH ST, NW, WASHINGTON, DC 20036 USA: AMER CHEMICAL SOC, 2001. p. U261-U261.

HE, F.; SHOOSHTARI, K.; COLLIER, H. Synthesis and characterization of series monomers and polymers of 2, 2'-biimidazole. In: ABSTRACTS OF PAPERS OF THE AMERICAN CHEMICAL SOCIETY. 1155 16TH ST, NW, WASHINGTON, DC 20036 USA: AMER CHEMICAL SOC, 2001. p. U264-U264.

HERNÁNDEZ-BARAJAS, J.; HUNKELER, D. J. Inverse-emulsion copolymerization of acrylamide and quaternary ammonium cationic monomers with block copolymeric surfactants: copolymer composition control using batch and semi-batch techniques. **Polymer**, v. 38, n. 2, p. 449-458, 1997.

HERRICK, D. Z.; MAZIARZ, E. P.; LIU, X. M. Analysis of gelatin using various separation and detection technologies. **J Anal Pharm Res**, v. 7, n. 6, p. 669-672, 2018.

HOELLER, S.; SPERGER, A.; VALENTA, C. Lecithin based nanoemulsions: a comparative study of the influence of non-ionic surfactants and the cationic phytosphingosine on physicochemical behaviour and skin permeation. **International journal of pharmaceutics**, v. 370, n. 1-2, p. 181-186, 2009.

HONARKAR, H.; BARIKANI, M. Applications of biopolymers I: chitosan. **Monatshefte für Chemie-Chemical Monthly**, v. 140, p. 1403-1420, 2009.

HONARY, S.; ZAHIR, F. Effect of zeta potential on the properties of nano-drug delivery systems-a review (Part 1). **Tropical journal of pharmaceutical research**, v. 12, n. 2, p. 255-264, 2013a.

HONARY, S.; ZAHIR, F. Effect of zeta potential on the properties of nano-drug delivery systems-a review (Part 2). **Tropical journal of pharmaceutical research**, v. 12, n. 2, p. 265-273, 2013b.

HORI, K.; SOTOZONO, C.; HAMURO, J.; YAMASAKI, K.; KIMURA, Y.; OZEKI, M.; KINOSHITA, S. Controlled-release of epidermal growth factor from cationized gelatin hydrogel enhances corneal epithelial wound healing. **Journal of controlled release**, v. 118, n. 2, p. 169-176, 2007.

HUANG, X.; BRAZEL, C. S. On the importance and mechanisms of burst release in matrix-controlled drug delivery systems. **Journal of controlled release**, v. 73, n. 2-3, p. 121-136, 2001.

HUANG, C. H.; CHUANG, T. J.; KE, C. J.; YAO, C. H. Doxorubicin–Gelatin/Fe3O4–Alginate dual-layer magnetic nanoparticles as targeted anticancer drug delivery vehicles. **Polymers**, v. 12, n. 8, p. 1747, 2020.

HUE, C. T.; HANG, N. T. M.; KARAPUN, M. Y.; RAZUMOVSKAYA, R. G. PHYSICOCHEMICAL CHARACTERISTICS OF GELATIN EXTRACTED FROM THE SCALES OF SEABREAM SPARUS LATUS HOUTTUYN (USING RAW MATERIAL FROM VIETNAM). **Vestnik of Astrakhan State Technical University. General Series**, v. 63, n. 1, 2017.

HUEPPE, N.; WURM, F. R.; LANDFESTER, K. Nanocarriers with Multiple Cargo Load—A Comprehensive Preparation Guideline Using Orthogonal Strategies. **Macromolecular rapid communications**, p. 2200611, 2022.

HUI, C.; QINGYU, C.; JING, W.; XIAOHONG, X.; HONGBO, L.; ZHANJUN, L. Interfacial enhancement of carbon fiber/nylon 12 composites by grafting nylon 6 to the surface of carbon fiber. **Applied Surface Science**, v. 441, p. 538-545, 2018.

HMDB. Human Metabolome Database. **1,4-Butanediol diacrylate information**. Available on: <https://hmdb.ca/metabolites/HMDB0244202#spectra>. Assessed in: 03rd, Jun. 2023.

HUNKELER, D.; HAMIELEC, A. E. Mechanism, kinetics and modelling of inverse-microsuspension polymerization: 2. Copolymerization of acrylamide with quaternary ammonium cationic monomers. **Polymer**, v. 32, n. 14, p. 2626-2640, 1991.

HUNKELER, D.; HAMIELEC, A. E.; BAADE, W. Mechanism, kinetics and modelling of the inverse-microsuspension homopolymerization of acrylamide. **Polymer**, v. 30, n. 1, p. 127-142, 1989.

HWANG, S. R.; PARK, M. S. Property analysis of photo-polymerization-type 3d-printed structures based on multi-composite materials. **Applied Sciences**, v. 11, n. 18, p. 8545, 2021.

IDREES, H.; ZAIDI, S. Z. J.; SABIR, A.; KHAN, R. U.; ZHANG, X.; HASSAN, S. U. A review of biodegradable natural polymer-based nanoparticles for drug delivery applications. **Nanomaterials**, v. 10, n. 10, p. 1970, 2020.

IMANZADEH, G.; AHMADI, F.; ZAMANLOO, M.; MANSOORI, Y. Tetrabutylammonium bromide media aza-Michael addition of 1, 2, 3, 6-tetrahydrophthalimide to symmetrical fumaric esters and acrylic esters under solvent-free conditions. **Molecules**, v. 15, n. 10, p. 7353-7362, 2010.

IQBAL, S.; ZHAO, Z. Poly (β amino esters) copolymers: Novel potential vectors for delivery of genes and related therapeutics. **International Journal of Pharmaceutics**, p. 121289, 2021.

IYER, A. K.; SINGH, A.; GANTA, S.; AMIJI, M. M. Role of integrated cancer nanomedicine in overcoming drug resistance. **Advanced drug delivery reviews**, v. 65, n. 13-14, p. 1784-1802, 2013.

J MEHTA, M.; BHARMORIA, P.; BHAYANI, K.; KUMAR, A. Gelatin solubility and processing in ionic liquids: An approach towards waste to utilization. **ChemistrySelect**, v. 2, n. 31, p. 9895-9900, 2017.

JACOB, J.; HAPONIUK, J. T.; THOMAS, S.; GOPI, S. Biopolymer based nanomaterials in drug delivery systems: A review. **Materials today chemistry**, v. 9, p. 43-55, 2018.

JADACH, B.; ŚWIETLIK, W.; FROELICH, A. Sodium alginate as a pharmaceutical excipient: novel applications of a well-known polymer. **Journal of Pharmaceutical Sciences**, 2022.

JADOUN, S.; ANNA DILFI, K. F. Silver nanoparticles with natural polymers. **Polymer Nanocomposites Based on Silver Nanoparticles: Synthesis, Characterization and Applications**, p. 139-157, 2021.

JAISWAL, S.; DUTTA, S. B.; NAYAK, D.; GUPTA, S. Effect of doxorubicin on the near-infrared optical properties of indocyanine green. **ACS omega**, v. 6, n. 50, p. 34842-34849, 2021.

JI, F.; ZHOU, W.; ZHANG, Z.; ZHANG, B. Effects of Relative Molecular Weight Distribution and Isoelectric Point on the Swelling Behavior of Gelatin Films. **Frontiers in Chemistry**, v. 10, 2022.

JOHLIN, J. M. The isoelectric point of gelatin and its relation to the minimum physical properties of gelatin. **Journal of Biological Chemistry**, v. 86, n. 1, p. 231-243, 1930.

JOHNSON-ARBOR, K.; DUBEY, R. Doxorubicin. In: **StatPearls [Internet]**. StatPearls Publishing, 2022.

JOSEPH, T. M.; KAR MAHAPATRA, D.; ESMAEILI, A.; PISZCZYK, Ł.; HASANIN, M. S.; KATTALI, M.; THOMAS, S. Nanoparticles: Taking a unique position in medicine. **Nanomaterials**, v. 13, n. 3, p. 574, 2023.

KALE, R. N.; BAJAJ, A. N. Ultraviolet spectrophotometric method for determination of gelatin crosslinking in the presence of amino groups. **Journal of Young Pharmacists**, v. 2, n. 1, p. 90-94, 2010.

KARIMI, E.; IRANSHAHI, M.; ALMASI-RAD, A.; KARIMI, E. Synthesis of Melphalan and Parthenolide hybride and Investigation of Their Cytotoxicity Activity Against Breast Cancer. **Jundishapur Scientific Medical Journal**, v. 19, n. 1, p. 11-25, 2020.

KAUFFMAN, M. K.; KAUFFMAN, M. E.; ZHU, H.; JIA, Z.; LI, Y. R. Fluorescence-based assays for measuring doxorubicin in biological systems. **Reactive oxygen species (Apex, NC)**, v. 2, n. 6, p. 432, 2016.

KHAN, S. A. **Gelatin nanoparticles as potential nanocarriers for macromolecular drugs**. 2014. Gelatin Nanoparticles as Potential Nanocarriers for Macromolecular Drugs. Doctoral dissertation, 115 pg. Philipps-Universität Marburg, 2014. https://doi.org/10.17192/z2014.0380.

KHAN, S.; RANJHA, N. M. Effect of degree of crosslinking on swelling and on drug release of low viscous chitosan/poly (vinyl alcohol) hydrogels. **Polymer bulletin**, v. 71, p. 2133-2158, 2014.

KHRAMTSOV, P.; BURDINA, O.; LAZAREV, S.; NOVOKSHONOVA, A.; BOCHKOVA, M.; TIMGANOVA, V.; RAYEV, M. Modified desolvation method enables simple one-step synthesis of gelatin nanoparticles from different gelatin types with any bloom values. **Pharmaceutics**, v. 13, n. 10, p. 1537, 2021.

KLIER, J.; FUCHS, S.; MAY, A.; SCHILLINGER, U.; PLANK, C.; WINTER, G.; COESTER, C. A nebulized gelatin nanoparticle-based CpG formulation is effective in immunotherapy of allergic horses. **Pharmaceutical research**, v. 29, n. 6, p. 1650-1657, 2012.

KONGTON, P.; RATANAVARAPORN, J.; KITSONGSERMTHON, J.; DAMRONGSAKKUL, S. Physical characteristics and curcumin entrapment efficiency of gelatin/Thai silk fibroin microspheres. In: 2016 9th **Biomedical Engineering International Conference (BMEiCON)**. IEEE, 2016. p. 1-5.

KOU, S. G.; PETERS, L.; MUCALO, M. Chitosan: A review of molecular structure, bioactivities and interactions with the human body and micro-organisms. **Carbohydrate Polymers**, p. 119132, 2022.

KUIJPERS, A. J.; ENGBERS, G. H.; KRIJGSVELD, J.; ZAAT, S. A.; DANKERT, J.; FEIJEN, J. Crosslinking and characterisation of gelatin matrices for biomedical applications. **Journal of Biomaterials Science**, **Polymer Edition**, v. 11, n. 3, p. 225-243, 2000.

KULKARNI, A. S.; SAJJAN, A. M.; KHAN, T. Y.; BADRUDDIN, I. A.; KAMANGAR, S.; BANAPURMATH, N. R.; SHARANAPPA, A. Development and Characterization of Biocompatible Membranes from Natural Chitosan and Gelatin for Pervaporative Separation of Water–Isopropanol Mixture. **Polymers**, v. 13, n. 17, p. 2868, 2021.

KUMAR, S.; MUDAI, A.; ROY, B.; BASUMATARY, I. B.; MUKHERJEE, A.; DUTTA, J. Biodegradable hybrid nanocomposite of chitosan/gelatin and green synthesized zinc oxide nanoparticles for food packaging. **Foods**, v. 9, n. 9, p. 1143, 2020.

KUZNETSOVA, Y. L.; SUSTAEVA, K. S.; VAVILOVA, A. S.; MARKIN, A. V.; LYAKAEV, D. V.; MITIN, A. V.; SEMENYCHEVA, L. L. Tributylborane in the synthesis of graft-copolymers of gelatin and acrylamide. **Journal of Organometallic Chemistry**, v. 924, p. 121431, 2020.

KYRIACOS, D. Polycarbonates. In: **Brydson's Plastics Materials**. Butterworth-Heinemann, 2017. p. 457-485.

LAI, H.; LIU, X.; QU, M. Nanoplastics and Human Health: Hazard Identification and Biointerface. **Nanomaterials**, v. 12, n. 8, p. 1298, 2022.

LANDFESTER, K. Synthesis of colloidal particles in miniemulsions. **Annu. Rev. Mater. Res**., v. 36, p. 231-279, 2006.

LANG, M.; HIRNER, S.; WIESBROCK, F.; FUCHS, P. A review on modeling cure kinetics and mechanisms of photopolymerization. **Polymers**, v. 14, n. 10, p. 2074, 2022.

LANGLEY, S. M.; ROONEY, S. J.; DALRYMPLE-HAY, M. J.; SPENCER, J. M.; LEWIS, M. E.; PAGANO, D.; BONSER, R. S. Replacement of the proximal aorta and aortic valve using a composite bileaflet prosthesis and gelatin-impregnated polyester graft (Carbo-Seal): early results in 143 patients. **The Journal of Thoracic and Cardiovascular Surgery**, v. 118, n. 6, p. 1014-1020, 1999.

LARSON, C. E.; GREENBERG, D. M. A paradoxical solubility phenomenon with gelatin. **Journal of the American Chemical Society**, v. 55, n. 7, p. 2798-2799, 1933.

LAUTENBACH, V.; HOSSEINPOUR, S.; PEUKERT, W. Isoelectric point of proteins at hydrophobic interfaces. **Frontiers in Chemistry**, v. 9, p. 712978, 2021.

LAWRENCE, S. A. **Amines: synthesis, properties and applications**. Cambridge University Press, 2004.

LEE, B. H.; LUM, N.; SEOW, L. Y.; LIM, P. Q.; TAN, L. P. Synthesis and characterization of types A and B gelatin methacryloyl for bioink applications. **Materials**, v. 9, n. 10, p. 797, 2016.

LEE, B. H.; SHIRAHAMA, H.; CHO, N. J.; TAN, L. P. Efficient and controllable synthesis of highly substituted gelatin methacrylamide for mechanically stiff hydrogels. **RSC advances**, v. 5, n. 128, p. 106094-106097, 2015.

LEE, K. Y.; BOUHADIR, K. H.; MOONEY, D. J. Controlled degradation of hydrogels using multi-functional crosslinking molecules. **Biomaterials**, v. 25, n. 13, p. 2461-2466, 2004.

LELKES, P. I.; MARCINKIEWICZ, C.; LAZAROVICI, P.; BAHARLOU, S. M.; GERSTENHABER, J. A. **Soy-Derived Bioactive Peptides for Use in Compositions and Methods for Wound Healing, Tissue Engineering, and Regenerative Medicine**. U.S. Patent Application n. 17/392,024, 7 jul. 2022.

LI, P.; DOU, X.; FENG, C.; SCHÖNHERR, H. Enhanced cell adhesion on a bio-inspired hierarchically structured polyester modified with gelatin-methacrylate. **Biomaterials science**, v. 6, n. 4, p. 785-792, 2018.

LI, D. Q.; LI, J.; DONG, H. L.; LI, X.; ZHANG, J. Q.; RAMASWAMY, S.; XU, F. Pectin in biomedical and drug delivery applications: A review. **International Journal of Biological Macromolecules**, v. 185, p. 49-65, 2021a.

LI, F.; LI, J.; WEN, X.; ZHOU, S.; TONG, X.; SU, P.; SHI, D. Anti-tumor activity of paclitaxel-loaded chitosan nanoparticles: An in vitro study. **Materials Science and Engineering**: C, v. 29, n. 8, p. 2392-2397, 2009.

LI, X.; SU, Y.; HAN, X.; YAN, Q.; SUN, Q. Effects of biopolymer ratio and pH value on the complex formation between whey protein isolates and soluble Auricularia auricular polysaccharides. **Food Science of Animal Products**, 2023.

LI, Y. Y., WANG, B., MA, M. G., & WANG, B. Review of recent development on preparation, properties, and applications of cellulose-based functional materials. **International Journal of Polymer Science**, v. 2018, 2018.

LIM, D. S.; CHUNG, J. K.; YUN, J. S.; PARK, M. S. Fabrication of 3D Printed Ceramic Part Using Photo-Polymerization Process. **Polymers**, v. 15, n. 7, p. 1601, 2023.

LIM, K. S.; GALARRAGA, J. H.; CUI, X.; LINDBERG, G. C.; BURDICK, J. A.; WOODFIELD, T. B. Fundamentals and applications of photo-crosslinking in bioprinting. **Chemical reviews**, v. 120, n. 19, p. 10662-10694, 2020.

LIMOUZIN, C.; CAVIGGIA, A.; GANACHAUD, F.; HÉMERY, P. Anionic polymerization of n-butyl cyanoacrylate in emulsion and miniemulsion. **Macromolecules**, v. 36, n. 3, p. 667-674, 2003.

LIN, C.; METTERS, A. T. Hydrogels in controlled release formulations: network design and mathematical modeling. **Advanced drug delivery reviews**, v. 58, n. 12-13, p. 1379-1408, 2006.

LIN, J.; PAN, D.; SUN, Y.; OU, C.; WANG, Y.; CAO, J. The modification of gelatin films: Based on various cross-linking mechanism of glutaraldehyde at acidic and alkaline conditions. **Food Science & Nutrition**, v. 7, n. 12, p. 4140-4146, 2019.

LIN, S.; GU, L. Influence of crosslink density and stiffness on mechanical properties of type I collagen gel. **Materials**, v. 8, n. 2, p. 551-560, 2015.

LIU, Y., LI, Y., KESKIN, D., & SHI, L. Poly (β-Amino Esters): synthesis, formulations, and their biomedical applications. **Advanced healthcare materials**, v. 8, n. 2, p. 1801359, 2019.

LIU, D.; YU, B.; JIANG, X.; YIN, J. Responsive hybrid microcapsules by the one-step interfacial thiol–ene photopolymerization. **Langmuir**, v. 29, n. 17, p. 5307-5314, 2013.

LIU, Y.; WENG, R.; WANG, W.; WEI, X.; LI, J.; CHEN, X.; LI, Y. Tunable physical and mechanical properties of gelatin hydrogel after transglutaminase crosslinking on two gelatin types. **International journal of biological macromolecules**, v. 162, p. 405-413, 2020.

LIZYMOL, P. P.; KRISHNAN, V. K. A comparison of efficiency of two photoinitiators for polymerization of light-cure dental composite resins. **Journal of applied polymer science**, v. 107, n. 5, p. 3337-3342, 2008.

LLORENTE, O.; AGIRRE, A.; CALVO, I.; OLASO, M.; TOMOVSKA, R.; SARDON, H. Exploring the advantages of oxygen-tolerant thiol-ene polymerization over conventional acrylate free radical photopolymerization processes for pressure-sensitive adhesives. **Polymer Journal**, v. 53, n. 11, p. 1195-1204, 2021.

LÓPEZ, A. S.; RAMOS, M. P.; HERRERO, R.; VILARIÑO, J. M. L. Synthesis of magnetic green nanoparticle–Molecular imprinted polymers with emerging contaminants templates. **Journal of Environmental Chemical Engineering**, v. 8, n. 4, p. 103889, 2020.

LYNN, D. M.; AMIJI, M. M.; LANGER, R. pH-responsive polymer microspheres: Rapid release of encapsulated material within the range of intracellular pH. **Angewandte Chemie**, v. 113, n. 9, p. 1757-1760, 2001.

LYNN, D. M.; LANGER, R. Degradable poly (β-amino esters): synthesis, characterization, and self-assembly with plasmid DNA. **Journal of the American Chemical Society**, v. 122, n. 44, p. 10761-10768, 2000.

MA, S.; NATOLI, M.; LIU, X.; NEUBAUER, M. P.; WATT, F. M.; FERY, A.; HUCK, W. T. Monodisperse collagen–gelatin beads as potential platforms for 3D cell culturing. **Journal of Materials Chemistry B**, v. 1, n. 38, p. 5128-5136, 2013.

MACHADO, T. O.; BECKERS, S. J.; FISCHER, J.; MÜLLER, B.; SAYER, C.; DE ARAÚJO, P. H.; WURM, F. R. Bio-based lignin nanocarriers loaded with fungicides as a versatile platform for drug delivery in plants. **Biomacromolecules**, v. 21, n. 7, p. 2755-2763, 2020.

MADKHALI, O.; MEKHAIL, G.; WETTIG, S. D. Modified gelatin nanoparticles for gene delivery. **International journal of pharmaceutics**, v. 554, p. 224-234, 2019.

MAITRA, J.; SHUKLA, V. K. Crosslinking in hydrogels-a review. **Am. J. Polym. Sci**, v. 4, n. 2, p. 25-31, 2014.

MALLIK, K. L.; DAS, M. N. Studies on kinetics of addition of secondary amines to acrylic esters. **Zeitschrift für Physikalische Chemie**, v. 25, n. 3_4, p. 205-216, 1960.

MALKAR, R. S.; JADHAV, A. L.; YADAV, G. D. Innovative catalysis in Michael addition reactions for CX bond formation. **Molecular Catalysis**, v. 485, p. 110814, 2020.

MALVERN INSTRUMENTS. Static Light Scattering Technologies for GPC – SEC explained. 2015a. Available on: https://www.chem.uci.edu/~dmitryf/manuals/Fundamentals/SLS%20Technologies%20GPC-SEC%20Explained.pdf. Accessed: in 10, Oct. 2022.

MALVERN INSTRUMENTS. Guide to molecular weight – with the Zetasizer. 2017b. Available on: https://www.materials-talks.com/guide-to-molecular-weight-with-the-zetasizer/. Accessed: in 12, Oct. 2022.

MANZANARES-GUEVARA, L. A.; LICEA-CLAVERIE, A.; OROZ-PARRA, I.; LICEA-NAVARRO, A. F. On the cytotoxicity of a cationic tertiary amine PEGylated nanogel as nanocarrier for anticancer therapies. **MRS Communications**, v. 8, n. 3, p. 1204-1210, 2018.

MARIOD, A. A.; FADUL, H. Gelatin, source, extraction and industrial applications. **Acta Scientiarum Polonorum Technologia Alimentaria**, v. 12, n. 2, p. 135-147, 2013.

MASSUGA, F.; LARSON, M. A.; KUASOSKI, M.; OLIVEIRA, S. L. D. Plastic Waste and Sustainability: Reflections and Impacts of the Covid-19 Pandemic in the Socio-Cultural and Environmental Context. **Revista de Gestão Social e Ambiental**, v. 16, p. e02860-e02860, 2022.

MASULLO, F., BELDENGRÜN, Y.; MIRAS, J.; MACKIE, A. D.; ESQUENA, J.; AVALOS, J. B. Phase behavior of gelatin/maltodextrin aqueous mixtures studied from a combined experimental and theoretical approach. **Fluid Phase Equilibria**, v. 524, p. 112675, 2020.

MATHER, B. D.; VISWANATHAN, K.; MILLER, K. M.; LONG, T. E. Michael addition reactions in macromolecular design for emerging technologies. **Progress in Polymer Science**, v. 31, n. 5, p. 487-531, 2006.

MATYJASZEWSKI, K.; DAVIS, T. P. **Handbook of radical polymerization**. Wiley-Interscience: Hoboken, NJ, USA, 2002; ISBN 9780471461579.

MEISLICH, H.; NECHAMKIN, H.; SHAREFKIN, J.; HADEMENOS. **Schaum's Outline of Organic Chemistry**. McGraw-Hill Education, 2013.

MEYER, M.; MORGENSTERN, B. Characterization of gelatine and acid soluble collagen by size exclusion chromatography coupled with multi angle light scattering (SEC-MALS). **Biomacromolecules**, v. 4, n. 6, p. 1727-1732, 2003.

MICHAEL, A. Ueber die Addition von Natriumacetessig-und Natriummalonsäureäthern zu den Aethern ungesättigter Säuren. **Journal für Praktische Chemie**, v. 35, n. 1, p. 349-356, 1887.

MIYAWAKI, O.; OMOTE, C.; MATSUHIRA, K. Thermodynamic analysis of sol–gel transition of gelatin in terms of water activity in various solutions. **Biopolymers**, v. 103, n. 12, p. 685-691, 2015.

MOCHIZUKI, M. Synthesis, properties and structure of polylactic acid fibres. In: **Handbook of textile fibre structure**. Woodhead Publishing, 2009. p. 257-275.

MOHANTY, B.; ASWAL, V. K.; KOHLBRECHER, J.; BOHIDAR, H. B. Synthesis of gelatin nanoparticles via simple coacervation. **Journal of Surface Science and Technology**, v. 21, n. 3/4, p. 149, 2005.

MOLLAH, M. Z. I.; ZAHID, H. M.; MAHAL, Z.; FARUQUE, M. R. I.; KHANDAKER, M. U. The Usages and Potential Uses of Alginate for Healthcare Applications. **Frontiers in molecular biosciences**, p. 918, 2021.

MORÁN, M. C.; ROSELL, N.; RUANO, G.; BUSQUETS, M. A.; VINARDELL, M. P. Gelatin-based nanoparticles as DNA delivery systems: Synthesis, physicochemical and biocompatible characterization. **Colloids and Surfaces B: Biointerfaces**, v. 134, p. 156-168, 2015.

MUCCI, V.; VALLO, C. Efficiency of 2,2-dimethoxy-2-phenylacetophenone for the photopolymerization of methacrylate monomers in thick sections. **Journal of Applied Polymer Science**, v. 123, n. 1, p. 418-425, 2012.

MUDASSIR, J.; RANJHA, N. M. Dynamic and equilibrium swelling studies: crosslinked pH sensitive methyl methacrylate-co-itaconic acid (MMA-co-IA) hydrogels. **Journal of Polymer Research**, v. 15, p. 195-203, 2008.

MUIR, V. G.; BURDICK, J. A. Chemically modified biopolymers for the formation of biomedical hydrogels. **Chemical reviews**, v. 121, n. 18, p. 10908-10949, 2020.

MULYANI, S.; SETYABUDI, F. M. S.; PRANOTO, Y.; SANTOSO, U. Physicochemical properties of gelatin extracted from buffalo hide pretreated with different acids. **Korean Journal for Food Science of Animal Resources**, v. 37, n. 5, p. 708, 2017.

MWANGI, J. W.; OFNER III, C. M. Crosslinked gelatin matrices: release of a random coil macromolecular solute. **International journal of pharmaceutics**, v. 278, n. 2, p. 319-327, 2004.

MYUNG, D.; WATERS, D.; WISEMAN, M.; DUHAMEL, P. E.; NOOLANDI, J.; TA, C. N.; FRANK, C. W. Progress in the development of interpenetrating polymer network hydrogels. **Polymers for advanced technologies**, v. 19, n. 6, p. 647-657, 2008.

NAGALAKSHMAIAH, M.; AFRIN, S.; MALLADI, R. P.; ELKOUN, S.; ROBERT, M.; ANSARI, M. A.; KARIM, Z. Biocomposites: Present trends and challenges for the future. **Green composites for automotive applications**, p. 197-215, 2019.

NATH, J.; AHMED, A.; SAIKIA, P.; CHOWDHURY, A.; DOLUI, S. K. Acrylic acid grafted gelatin/LDH based biocompatible hydrogel with pH-controllable release of vitamin B12. **Applied Clay Science**, v. 190, p. 105569, 2020.

NICHOL, J. W.; KOSHY, S. T.; BAE, H.; HWANG, C. M.; YAMANLAR, S.; KHADEMHOSSEINI, A. Cell-laden microengineered gelatin methacrylate hydrogels. **Biomaterials**, v. 31, n. 21, p. 5536-5544, 2010.

NICODEMUS, G. D.; BRYANT, S. J. Cell encapsulation in biodegradable hydrogels for tissue engineering applications. Tissue Engineering Part B: **Reviews**, v. 14, n. 2, p. 149-165, 2008.

NISTANE, J.; CHEN, L.; LEE, Y.; LIVELY, R.; RAMPRASAD, R. Estimation of the Flory-Huggins interaction parameter of polymer-solvent mixtures using machine learning. **MRS Communications**, v. 12, n. 6, p. 1096-1102, 2022.

NITSUWAT, S.; ZHANG, P.; NG, K.; FANG, Z. Fish gelatin as an alternative to mammalian gelatin for food industry: A meta-analysis. **LWT**, v. 141, p. 110899, 2021.

NOOR, N. Q. I. M.; RAZALI, R. S.; ISMAIL, N. K.; RAMLI, R. A.; RAZALI, U. H. M.; BAHAUDDIN, A. R.; SHAARANI, S. M. Application of green technology in gelatin extraction: A review. **Processes**, v. 9, n. 12, p. 2227, 2021.

NOWAK, D.; ORTYL J.; KAMIŃSKA-BOREK I.; KUKUŁA K.; TOPA M.; POPIELARZ R. **Polym. Test**, v. 64, p. 313-320, 2017.

OBIREDDY, S. R.; CHINTHA, M.; KASHAYI, C. R.; VENKATA, K. R. K. S.; SUBBARAO, S. M. C. Gelatin-coated dual cross-linked sodium alginate/magnetite nanoparticle microbeads for controlled release of doxorubicin. **ChemistrySelect**, v. 5, n. 33, p. 10276-10284, 2020.

OFNER, III, C. M.; BUBNIS, W. A. Chemical and swelling evaluations of amino group crosslinking in gelatin and modified gelatin matrices. **Pharmaceutical research**, v. 13, p. 1821-1827, 1996.

OFOKANSI, K.; WINTER, G.; FRICKER, G.; COESTER, C. Matrix-loaded biodegradable gelatin nanoparticles as new approach to improve drug loading and delivery. **European Journal of Pharmaceutics and Biopharmaceutics**, v. 76, n. 1, p. 1-9, 2010.

OKAMOTO, M.; JOHN, B. Synthetic biopolymer nanocomposites for tissue engineering scaffolds. **Progress in Polymer Science**, v. 38, n. 10-11, p. 1487-1503, 2013.

OMPRAKASH RATHI, J.; SUBRAY SHANKARLING, G. Recent advances in the protection of amine functionality: a review. **ChemistrySelect**, v. 5, n. 23, p. 6861-6893, 2020.

ONO, K.; SAITO, Y.; YURA, H.; ISHIKAWA, K.; KURITA, A.; AKAIKE, T.; ISHIHARA, M. Photocrosslinkable chitosan as a biological adhesive. **Journal of**

Biomedical Materials Research: An Official Journal of The Society for Biomaterials and The Japanese Society for Biomaterials, v. 49, n. 2, p. 289-295, 2000.

OSETROV, K.; USPENSKAYA, M.; SITNIKOVA, V. The influence of oxidant on gelatin–tannin hydrogel properties and structure for potential biomedical application. **Polymers**, v. 14, n. 1, p. 150, 2021.

OSORIO, F. A.; BILBAO, E.; BUSTOS, R.; ALVAREZ, F. Effects of concentration, bloom degree, and pH on gelatin melting and gelling temperatures using small amplitude oscillatory rheology. **International Journal of Food Properties**, v. 10, n. 4, p. 841-851, 2007.

OUELLETTE, R. J.; RAWN, J. D. Principles of organic chemistry. Amines and amides. Academic Press**, Organic Chemistry Study Guide**, 2015, p. 465-494.

OVSIANIKOV, A.; CHICHKOV, B. N. Three-dimensional microfabrication by two-photon polymerization technique. **Computer-aided tissue engineering**, p. 311-325, 2012.

PAPPAS, S. P.; ASMUS, R. A. Photoinitiated polymerization of methyl methacrylate with benzoin methyl ether. III. Independent photogeneration of the ether radical. **Journal of Polymer Science: Polymer Chemistry Edition**, v. 20, n. 9, p. 2643-2653, 1982.

PARHI, R. Crosslinked hydrogel for pharmaceutical applications: a review. **Advanced pharmaceutical bulletin,** v. 7, n. 4, p. 515-530, 2017.

PARK, S. B.; LIH, E.; PARK, K. S.; JOUNG, Y. K.; HAN, D. K. Biopolymer-based functional composites for medical applications. **Progress in Polymer Science**, v. 68, p. 77-105, 2017.

PECIAK, K.; LAURINE, E.; TOMMASI, R.; CHOI, J. W.; BROCCHINI, S. Site-selective protein conjugation at histidine. **Chemical science**, v. 10, n. 2, p. 427-439, 2019.

PENG, H. T.; MARTINEAU, L.; SHEK, P. N. Hydrogel-elastomer composite biomaterials: 3. Effects of gelatin molecular weight and type on the preparation and physical properties of interpenetrating polymer networks. **Journal of Materials Science: Materials in Medicine**, v. 19, p. 997-1007, 2008.

PEPPAS, N. A.; HILT, J. Z.; KHADEMHOSSEINI, A.; LANGER, R. Hydrogels in biology and medicine: from molecular principles to bionanotechnology. **Advanced materials**, v. 18, n. 11, p. 1345-1360, 2006.

PEPPAS, N. A.; MERRILL, E. W. Crosslinked poly (vinyl alcohol) hydrogels as swollen elastic networks. **Journal of Applied Polymer Science**, v. 21, n. 7, p. 1763-1770, 1977.

PERES, L. B.; DOS ANJOS, R. S.; TAPPERTZHOFEN, L. C.; FEUSER, P. E.; DE ARAÚJO, P. H.; LANDFESTER, K.; MUÑOZ-ESPÍ, R. pH-responsive physically and chemically crosslinked glutamic-acid-based hydrogels and nanogels. **European Polymer Journal**, v. 101, p. 341-349, 2018.

PERRETT, D.; NAYUNI, N. K. Efficacy of current and novel cleaning technologies (ProReveal) for assessing protein contamination on surgical instruments. **Decontamination in hospitals and healthcare**, p. 598-619, 2014.

PEYRTON, J.; AVÉROUS, L. Aza-michael reaction as a greener, safer, and more sustainable approach to biobased polyurethane thermosets. **ACS Sustainable Chemistry & Engineering**, v. 9, n. 13, p. 4872-4884, 2021.

PLUCINSKI, A.; LYU, Z.; SCHMIDT, B. V. Polysaccharide nanoparticles: From fabrication to applications. **Journal of Materials Chemistry B**, v. 9, n. 35, p. 7030-7062, 2021.

POTINENI, A.; LYNN, D. M.; LANGER, R.; AMIJI, M. M. Poly (ethylene oxide)-modified poly (β-amino ester) nanoparticles as a pH-sensitive biodegradable system for paclitaxel delivery. **Journal of Controlled Release**, v. 86, n. 2-3, p. 223-234, 2003.

PRADINI, D.; JUWONO, H.; MADURANI, K. A.; KURNIAWAN, F. A preliminary study of identification halal gelatin using quartz crystal microbalance (QCM) sensor. **Malaysian Journal of Fundamental and Applied Sciences**, v. 14, n. 3, p. 325-330, 2018.

PUBCHEM. Compound – 1,4-Butanediol diacrylate, 2023. Available on: <https://pubchem.ncbi.nlm.nih.gov/compound/1_4-Butanediol-diacrylate>. Accessed in: 13th, March, 2023.

PUSKÁS, I.; SZEMJONOV, A.; FENYVESI, É.; MALANGA, M.; SZENTE, L. Aspects of determining the molecular weight of cyclodextrin polymers and oligomers by static light scattering. **Carbohydrate polymers**, v. 94, n. 1, p. 124-128, 2013.

QIN, H.; CHEN, X.; LUO, D.; WANG, B.; TAN, Q.; LIANG, H.; HUANG, J. Synthesis of Thermo-, Oxidation-, pH-, and CO2-Responsive Polymers via the Combination of Aza-Michael and Thiol-Michael Reactions in One Pot. **Macromolecular Rapid Communications**, v. 40, n. 21, p. 1900342, 2019.

RAAIJMAKERS, M. JT.; BENES, N. E. Current trends in interfacial polymerization chemistry. **Progress in polymer science**, v. 63, p. 86-142, 2016.

RADEV, L.; FERNANDES, M.; SALVADO, I.; KOVACHEVA, D. Organic/Inorganic bioactive materials Part III: in vitro bioactivity of gelatin/silicocarnotite hybrids. **Open Chemistry**, v. 7, n. 4, p. 721-730, 2009.

RADMANESH, F.; TENA, A.; SUDHÖLTER, E. J.; HEMPENIUS, M. A.; BENES, N. E. Nonaqueous Interfacial Polymerization-Derived Polyphosphazene Films for Sieving or Blocking Hydrogen Gas. **ACS Applied Polymer Materials**, v. 5, n. 3, p. 1955-1964, 2023.

RAHIMI, A.; GARCÍA, J. M. Chemical recycling of waste plastics for new materials production. **Nature Reviews Chemistry**, v. 1, n. 6, p. 0046, 2017.

RATHER, J. A.; MAJID, S. D.; DAR, A. H.; AMIN, T.; MAKROO, H. A.; MIR, S. A.; DAR, B. N. Extraction of Gelatin From Poultry Byproduct: Influence of Drying Method on Structural, Thermal, Functional, and Rheological Characteristics of the Dried Gelatin Powder. **Frontiers in Nutrition**, v. 9, 2022.

RAWAT, S.; MAITI, A. Facile preparation of iron oxyhydroxide–biopolymer (Chitosan/Alginate) beads and their comparative insights into arsenic removal. **Separation and Purification Technology**, v. 272, p. 118983, 2021.

REZAEI, A.; FATHI, M.; JAFARI, S. M. Nanoencapsulation of hydrophobic and low-soluble food bioactive compounds within different nanocarriers. **Food hydrocolloids**, v. 88, p. 146-162, 2019.

RISTROPH, K. D.; PRUD'HOMME, R. K. Hydrophobic ion pairing: encapsulating small molecules, peptides, and proteins into nanocarriers. **Nanoscale advances**, v. 1, n. 11, p. 4207-4237, 2019.

RIVERA-RAMÍREZ, J. D.; ESCALANTE, J.; LÓPEZ-MUNGUÍA, A.; MARTY, A.; CASTILLO, E. Thermodynamically controlled chemoselectivity in lipase-catalyzed aza-Michael additions. **Journal of Molecular Catalysis B: Enzymatic**, v. 112, p. 76-82, 2015.

ROKHADE, A. P.; AGNIHOTRI, S. A.; PATIL, S. A.; MALLIKARJUNA, N. N.; KULKARNI, P. V.; AMINABHAVI, T. M. Semi-interpenetrating polymer network microspheres of gelatin and sodium carboxymethyl cellulose for controlled release of ketorolac tromethamine. **Carbohydrate polymers**, v. 65, n. 3, p. 243-252, 2006.

ROMAN-BENN, A.; CONTADOR, C. A.; LI, M. W.; LAM, H. M.; AH-HEN, K.; ULLOA, P. E.; RAVANAL, M. C. Pectin: An overview of sources, extraction and applications in food products and health. **Food Chemistry Advances**, p. 100192, 2023.

ROSELLINI, E.; MADEDDU, D.; BARBANI, N.; FRATI, C.; GRAIANI, G.; FALCO, A.; CASCONE, M. G. Development of biomimetic alginate/gelatin/elastin sponges with recognition properties toward bioactive peptides for cardiac tissue engineering. **Biomimetics**, v. 5, n. 4, p. 67, 2020.

ROY, S.; RHIM, J. W. Fabrication of bioactive binary composite film based on gelatin/chitosan incorporated with cinnamon essential oil and rutin. **Colloids and Surfaces B: Biointerfaces**, v. 204, p. 111830, 2021.

ROY, S.; RHIM, J. W. Genipin-Crosslinked Gelatin/Chitosan-Based Functional Films Incorporated with Rosemary Essential Oil and Quercetin. **Materials**, v. 15, n. 11, p. 3769, 2022.

RUHEMANN, S. CXXXII. – Cyclic di-and tri-ketones**. Journal of the Chemical Society**, Transactions, v. 97, p. 1438-1449, 1910.

SALDIVAR-GUERRA, E.; VIVALDO-LIMA, E. **Handbook of polymer synthesis, characterization, and processing**. John Wiley & Sons, 2013.

SALMINEN, H.; SACHS, M.; SCHMITT, C.; WEISS, J. Complex Coacervation and Precipitation Between Soluble Pea Proteins and Apple Pectin. **Food Biophysics**, v. 17, n. 3, p. 460-471, 2022.

SAMIR, A.; ASHOUR, F. H.; HAKIM, A. A.; BASSYOUNI, M. Recent advances in biodegradable polymers for sustainable applications. **npj Materials Degradation**, v. 6, n. 1, p. 1-28, 2022.

SANWLANI, S.; KUMAR, P.; BOHIDAR, H. B. Hydration of gelatin molecules in glycerol–water solvent and phase diagram of gelatin organogels. **The Journal of Physical Chemistry B**, v. 115, n. 22, p. 7332-7340, 2011.

SAPKOTA, A.; ARYAL, S. Ninhydrin Test- Definition, Principle, Procedure, Result, Uses. **Microbe Notes**, May 19, 2022. Accessed in: Sep. 12, 2022. Available on: https://microbenotes.com/ninhydrin-test/.

SARFRAZ, M.; SHI, W.; GAO, Y.; CLAS, S. D.; ROA, W.; BOU-CHACRA, N.; LÖBENBERG, R. Immune response to antituberculosis drug-loaded gelatin and polyisobutyl-cyanoacrylate nanoparticles in macrophages. **Therapeutic Delivery**, v. 7, n. 4, p. 213-228, 2016.

SCHROEDER, W.; ARENAS, G.; VALLO, C. Monomer conversion in a light-cured dental resin containing 1-phenyl-1, 2-propanedione photosensitizer. **Polymer international**, v. 56, n. 9, p. 1099-1105, 2007.

SCHWALM, R. Photoinitiators and photopolymerization. **Encyclopedia of Materials: Science and Technology**, p. 6946-6951, 2001.

SEAH, M. Q.; LAU, W. J.; GOH, P. S.; TSENG, H. H.; WAHAB, R. A.; ISMAIL, A. F. Progress of interfacial polymerization techniques for polyamide thin film (nano) composite membrane fabrication: a comprehensive review. **Polymers**, v. 12, n. 12, p. 2817, 2020.

SEMAN, M. A.; KHAYET, M.; HILAL, N. Nanofiltration thin-film composite polyester polyethersulfone-based membranes prepared by interfacial polymerization. **Journal of membrane science**, v. 348, n. 1-2, p. 109-116, 2010.

SEN, M.; YAKAR, A.; GÜVEN, O. Determination of average molecular weight between cross-links (Mc) from swelling behaviours of diprotic acid-containing hydrogels. **Polymer**, v. 40, n. 11, p. 2969-2974, 1999.

SETTERSTROM, J. A.; TICE, T. R.; MYERS, W. E. Development of encapsulated antibiotics for topical administration to wounds. **Recent advances in drug delivery systems**, p. 185-198, 1984.

SHADI, L.; KARIMI, M.; ENTEZAMI, A. A. Preparation of electroactive nanofibers of star-shaped polycaprolactone/polyaniline blends. **Colloid and polymer science**, v. 293, p. 481-491, 2015.

SHARMA, K.; KUMAR, K.; MISHRA, N. Nanoparticulate carrier system: a novel treatment approach for hyperlipidemia. **Drug delivery**, v. 23, n. 3, p. 684-699, 2016.

SHARMA, A. K.; KAITH, B. S.; ARORA, S. Synthesis of gelatin and green tea based stretchable self-healing material of biomedical importance. **Reactive and Functional Polymers**, v. 172, p. 105188, 2022.

SHEEHAN, J. D.; EBIKADE, E.; VLACHOS, D. G.; LOBO, R. F. Lignin-Based Water-Soluble Polymers Exhibiting Biodegradability and Activity as Flocculating Agents. **ACS Sustainable Chemistry & Engineering**, v. 10, n. 34, p. 11117-11129, 2022.

SHEN, Q. Advances in unusual interfacial polymerization techniques. **Polymer**, p. 125788, 2023.

SHENOY, D.; LITTLE, S.; LANGER, R.; AMIJI, M. Poly (ethylene oxide)-modified poly (β-amino ester) nanoparticles as a pH-sensitive system for tumor-targeted delivery of hydrophobic drugs. 1. In vitro evaluations. **Molecular pharmaceutics**, v. 2, n. 5, p. 357-366, 2005a.

SHENOY, D.; LITTLE, S.; LANGER, R.; AMIJI, M. Poly (ethylene oxide)-modified poly (β-amino ester) nanoparticles as a pH-sensitive system for tumor-targeted delivery of hydrophobic drugs: part 2. In vivo distribution and tumor localization studies. **Pharmaceutical research**, v. 22, p. 2107-2114, 2005b.

SHENOY, R.; BOWMAN, C. N. A Comprehensive Kinetic Model of Free-Radical-Mediated Interfacial Polymerization. **Macromolecular Theory and Simulations**, v. 22, n. 2, p. 115-126, 2013.

SHERAFATKHAH AZARI, S.; ALIZADEH, A.; ROUFEGARINEJAD, L.; ASEFI, N.; HAMISHEHKAR, H. Preparation and characterization of gelatin/β-glucan nanocomposite film incorporated with ZnO nanoparticles as an active food packaging system. **Journal of Polymers and the Environment**, v. 29, p. 1143-1152, 2021.

SHINODA, T.; SATAKE, K. The spectrophotometric determination as trinitrophenyl derivatives of amino acids and peptides resolved on paper by electrophoresis and chromatography. **The Journal of Biochemistry**, v. 50, n. 4, p. 293-298, 1961.

SHOOSHTARI, K. A. "Michael addition of amines to α-ß unsaturated esters" (2000). Doctoral Dissertations. 55. University of Missouri - Rolla. 188 pages. https://scholarsmine.mst.edu/doctoral_dissertations/55.

SHOOSHTARI, K. A.; VAN DE MARK, M. R. Factors affecting amine-acrylic Michael addition as reactive diluents and polymer synthesis. **POLYMER PREPRINTS-AMERICA**, v. 42, n. 1, p. 458-459, 2001a.

SHOOSHTARI, K. A.; VAN DE MARK, M. R. Michael addition of amines to acrylates: Macrocycle formation. In: **ABSTRACTS OF PAPERS OF THE AMERICAN CHEMICAL SOCIETY**. 1155 16TH ST, NW, WASHINGTON, DC 20036 USA: AMER CHEMICAL SOC, 2001b. p. U302-U302.

SHOOSHTARI, K. A.; VAN-DE-MARK, M. R. Mechanistic investigation of poly acrylates and poly methacrylates pyrolysis. 1996.

SIGMA ALDRICH. Product, 1,4-Butanediol diacrylate, 2023a. Available on: <https://www.sigmaaldrich.com/BR/pt/product/aldrich/411744>. Accessed in: 10th, March, 2023.

SIGMA ALDRICH. SDS, 1,4-Butanediol diacrylate, 2023b. Available on: <https://www.sigmaaldrich.com/BR/pt/sds/aldrich/411744>. Accessed in: 10th, March, 2023.

SIGMA ALDRICH. Technical documents – IR Spectrum Table, 2023. Available on: < https://www.sigmaaldrich.com/BR/pt/technical-documents/technical-article/analytical-chemistry/photometry-and-reflectometry/ir-spectrum-table>. Accessed in: 08th, April, 2023.

SINGH, A. V. Biopolymers in drug delivery: a review. **Pharmacologyonline**, v. 1, p. 666-674, 2011.

SINGH, R.; SHITIZ, K.; SINGH, A. Chitin and chitosan: biopolymers for wound management. **International wound journal**, v. 14, n. 6, p. 1276-1289, 2017.

SISSO, A. M.; BOIT, M. O.; DEFOREST, C. A. Self-healing injectable gelatin hydrogels for localized therapeutic cell delivery. **Journal of Biomedical Materials Research Part A**, v. 108, n. 5, p. 1112-1121, 2020.

SKOPINSKA-WISNIEWSKA, J.; TUSZYNSKA, M.; OLEWNIK-KRUSZKOWSKA, E. Comparative study of gelatin hydrogels modified by various cross-linking agents. **Materials**, v. 14, n. 2, p. 396, 2021.

SLAUGHTER, B. V.; KHURSHID, S. S.; FISHER, O. Z.; KHADEMHOSSEINI, A.; PEPPAS, N. A. Hydrogels in regenerative medicine. **Advanced materials**, v. 21, n. 32-33, p. 3307-3329, 2009.

SONG, Y.; FAN, J. B. WANG, S. Recent progress in interfacial polymerization. **Materials Chemistry Frontiers**, v. 1, n. 6, p. 1028-1040, 2017.

SPONCHIONI, M.; PALMIERO, U. C.; MOSCATELLI, D. Thermo-responsive polymers: Applications of smart materials in drug delivery and tissue engineering. **Materials Science and Engineering: C**, v. 102, p. 589-605, 2019.

STEINMACHER, F. R. Encapsulação simultânea de compostos hidrofílicos e hidrofóbicos em Micropartículas Multicompartimentadas pela PLLA e Amido Reticulado. Tese de doutorado, 170 pg. Doutorado em Engenharia Química, Florianópolis, Brazil, 2014.

STEINMACHER, F. R.; BAIER, G.; MUSYANOVYCH, A.; LANDFESTER, K.; ARAÚJO, P. H.; SAYER, C. Design of crosslinked starch nanocapsules for enzyme-triggered release of hydrophilic compounds. **Processes**, v. 5, n. 2, p. 25, 2017.

STRASSBURG, S.; MAYER, K.; SCHEIBEL, T. Functionalization of biopolymer fibers with magnetic nanoparticles. **Physical Sciences Reviews**, v. 7, n. 10, p. 1091-1117, 2022.

SU, K.; WANG, C. Recent advances in the use of gelatin in biomedical research. **Biotechnology letters**, v. 37, p. 2139-2145, 2015.

SU, J. F.; WANG, L. X.; REN, L. Synthesis of polyurethane microPCMs containing n-octadecane by interfacial polycondensation: Influence of styrene-maleic anhydride as a surfactant. **Colloids and Surfaces A: Physicochemical and Engineering Aspects**, v. 299, n. 1-3, p. 268-275, 2007.

SUDERMAN, N.; ISA, M. I. N.; SARBON, N. M. The effect of plasticizers on the functional properties of biodegradable gelatin-based film: A review. **Food bioscience**, v. 24, p. 111-119, 2018.

SUHAIL, M.; KHAN, A.; ROSENHOLM, J. M.; MINHAS, M. U.; WU, P. C. Fabrication and characterization of diclofenac sodium loaded hydrogels of sodium alginate as sustained release carrier. **Gels**, v. 7, n. 1, p. 10, 2021.

SUHAIMA, N. R.; SUYATMA, N. E.; HUNAEFI, D.; JAYANEGARA, A. Comparison of fish and mammalian gelatin film properties: A meta-analysis. **AIMS Agriculture and Food**, v. 7, n. 3, p. 461-480, 2022.

SULTANA, S.; ALI, M. E.; AHAMAD, M. N. U. Gelatine, collagen, and single cell proteins as a natural and newly emerging food ingredients. In: **Preparation and processing of religious and cultural foods**. Woodhead Publishing, 2018. p. 215-239.

SWAROOP, K.; GAANA, M. J.; SHRUTHI, S. S.; SHRINIDHI, SHRIKANT, L. P.; VINAYAK, A. K.; SOMASHEKARAPPA, H. M. Studies on swelling behaviour of radiolytically synthesised PVA/gelatin hydrogels. In: **AIP Conference Proceedings**. AIP Publishing LLC, 2019. p. 030050.

THANAVEL, R.; SEONG SOO, A. A. Biocompatible and biodegradable polymers for biomedical application. 2013.

TEMESGEN, S.; RENNERT, M.; TESFAYE, T.; NASE, M. Review on spinning of biopolymer fibers from starch. **Polymers**, v. 13, n. 7, p. 1121, 2021.

TERAOKA, I. **Polymer Solutions: An Introduction to Physical Properties.** 2002.

TIAN, J.; YANG, G.; HUANG, H.; LIU, M.; LIU, L.; ZHANG, X.; WEI, Y. Recent progress and development for the fabrication of antibacterial materials through mussel-inspired chemistry. **Journal of Environmental Chemical Engineering**, v. 8, n. 6, p. 104383, 2020.

TIWARI, A. **Practical Biochemistry: A Student Companion**. LAP Lambert Academic Publishing, 2015.

TOLENTINO, I. L. S. **Fotopolimerização tiol-eno do mirceno em massa, solução e miniemulsão**. Dissertação de Mestrado em Engenharia Química, 73 pg. Florianópolis, Brazil, 2022.

TOMAL, W.; ORTYL, J. Water-soluble photoinitiators in biomedical applications. **Polymers**, v. 12, n. 5, p. 1073, 2020.

TOMPA, H. Polymer Solutions. **Academic Press**; New York, NY, USA: 1956.

TREESUPPHARAT, W.; ROJANAPANTHU, P.; SIANGSANOH, C.; MANUSPIYA, H.; UMMARTYOTIN, S. Synthesis and characterization of bacterial cellulose and gelatin-based hydrogel composites for drug-delivery systems. **Biotechnology reports**, v. 15, p. 84-91, 2017.

TRUONG-LE, V. L.; WALSH, S. M.; SCHWEIBERT, E.; MAO, H. Q.; GUGGINO, W. B.; AUGUST, J. T.; LEONG, K. W. Gene transfer by DNA–gelatin nanospheres. **Archives of Biochemistry and Biophysics**, v. 361, n. 1, p. 47-56, 1999.

TSENG, C. L.; CHEN, K. H.; SU, W. Y.; LEE, Y. H.; WU, C. C.; LIN, F. H. Cationic gelatin nanoparticles for drug delivery to the ocular surface: in vitro and in vivo evaluation. **Journal of Nanomaterials**, v. 2013, p. 7-7, 2013.

TU, Z. C.; HUANG, T.; WANG, H.; SHA, X. M.; SHI, Y.; HUANG, X. Q.; LI, D. J. Physico-chemical properties of gelatin from bighead carp (Hypophthalmichthys nobilis) scales by ultrasound-assisted extraction. **Journal of food science and technology**, v. 52, p. 2166-2174, 2015.

UDAYAKUMAR, G. P.; MUTHUSAMY, S.; SELVAGANESH, B.; SIVARAJASEKAR, N.; RAMBABU, K.; BANAT, F.; SHOW, P. L. Biopolymers and composites: Properties, characterization and their applications in food, medical and pharmaceutical industries. **Journal of Environmental Chemical Engineering**, v. 9, n. 4, p. 105322, 2021.

UGELSTAD, J.; EL-AASSER, M. S.; VANDERHOFF, J. W. Emulsion polymerization: Initiation of polymerization in monomer droplets. **Journal of Polymer Science: Polymer Letters Edition**, v. 11, n. 8, p. 503-513, 1973.

UNCC, UNITED NATIONS CLIMATE CHANGE. **27th Global Climate Change Conference**. Available on: https://unfccc.int/cop27. Accessed in: 10, March, 2023.

USGS – United States Geological Survey. U.S. Department of the Interior – Science for a changing world. **Water density**. (2018). Available in: https://www.usgs.gov/special-topics/water-science-school/science/water-density#:~:text=The%20density%20of%20water%20is,is%20an%20important%20water%20measurement. Accessed in: 08th Nov. 2022.

VALARINI JUNIOR, O.; CARDOSO, F. A. R.; DE SOUZA, G. B. M.; MACHADO GIUFRIDA, W.; CARDOZO-FILHO, L. Single step encapsulation process of ivermectin in biocompatible polymer using a supercritical antisolvent system process. **Asia-Pacific Journal of Chemical Engineering**, v. 16, n. 5, p. e2672, 2021.

VAN DEN BULCKE, A. I.; BOGDANOV, B.; DE ROOZE, N.; SCHACHT, E. H.; CORNELISSEN, M.; BERGHMANS, H. Structural and rheological properties of methacrylamide modified gelatin hydrogels. **Biomacromolecules**, v. 1, n. 1, p. 31-38, 2000.

VAN HOORICK, J.; GRUBER, P.; MARKOVIC, M.; TROMAYER, M.; VAN ERPS, J.; THIENPONT, H.; VAN VLIERBERGHE, S. Cross-linkable gelatins with superior mechanical properties through carboxylic acid modification: increasing the two-photon polymerization potential. **Biomacromolecules**, v. 18, n. 10, p. 3260-3272, 2017.

VANDEWALLE, S.; VAN DE WALLE, M.; CHATTOPADHYAY, S.; DU PREZ, F. E. Polycaprolactone-b-poly (N-isopropylacrylamide) nanoparticles: Synthesis and temperature induced coacervation behavior. **European Polymer Journal**, v. 98, p. 468-474, 2018.

VANDERHOOFT, J. L.; ALCOUTLABI, M.; MAGDA, J. J.; PRESTWICH, G. D. Rheological properties of cross-linked hyaluronan–gelatin hydrogels for tissue engineering. **Macromolecular bioscience**, v. 9, n. 1, p. 20-28, 2009.

VANIN, F. M.; SOBRAL, P. J. D. A.; MENEGALLI, F. C.; CARVALHO, R. A.; HABITANTE, A. M. Q. B. Effects of plasticizers and their concentrations on thermal and functional properties of gelatin-based films. **Food Hydrocolloids**, v. 19, n. 5, p. 899-907, 2005.

VELASCO-RODRIGUEZ, B.; DIAZ-VIDAL, T.; ROSALES-RIVERA, L. C.; GARCÍA-GONZÁLEZ, C. A.; ALVAREZ-LORENZO, C.; AL-MODLEJ, A.; TABOADA, P. Hybrid methacrylated gelatin and hyaluronic acid hydrogel scaffolds. Preparation and systematic characterization for prospective tissue engineering applications. **International journal of molecular sciences**, v. 22, n. 13, p. 6758, 2021.

VENKATACHALAM, D.; KALIAPPA, S. Superabsorbent polymers: A state-of-art review on their classification, synthesis, physicochemical properties, and applications. **Reviews in Chemical Engineering**, v. 39, n. 1, p. 127-171, 2023.

VENKATESAN, J.; KIM, S. K.; ANIL, S. **Polysaccharide Nanoparticles: Preparation and Biomedical Applications**. Elsevier, 2022.

VIGATA, M.; MEINERT, C.; BOCK, N.; DARGAVILLE, B. L.; HUTMACHER, D. W. Deciphering the molecular mechanism of water interaction with gelatin methacryloyl hydrogels: Role of ionic strength, ph, drug loading and hydrogel network characteristics. **Biomedicines**, v. 9, n. 5, p. 574, 2021.

VIJAYAKUMAR, V.; SAMAL, S. K.; MOHANTY, S.; NAYAK, S. K. Recent advancements in biopolymer and metal nanoparticle-based materials in diabetic wound healing management. **International Journal of Biological Macromolecules**, v. 122, p. 137-148, 2019.

VIKULINA, A. S.; CAMPBELL, J. Biopolymer-Based Multilayer Capsules and Beads Made via Templating: Advantages, Hurdles and Perspectives. **Nanomaterials**, v. 11, n. 10, p. 2502, 2021.

VINOGRADOV, M. G.; TUROVA, O. V.; ZLOTIN, S. G. Recent advances in the asymmetric synthesis of pharmacology-relevant nitrogen heterocycles via stereoselective aza-Michael reactions. **Organic & Biomolecular Chemistry**, v. 17, n. 15, p. 3670-3708, 2019.

VON HIPPEL, P. H. The Macromolecular Chemistry of Gelatin. **Journal of the American Chemical Society**, v. 87, n. 8, p. 1824-1824, 1965.

XING, Q.; YATES, K.; VOGT, C.; QIAN, Z.; FROST, M. C.; ZHAO, F. Increasing mechanical strength of gelatin hydrogels by divalent metal ion removal. **Scientific reports**, v. 4, n. 1, p. 1-10, 2014.

XU, K.; CANTU, D. A.; FU, Y.; KIM, J.; ZHENG, X.; HEMATTI, P.; KAO, W. J. Thiol-ene Michael-type formation of gelatin/poly (ethylene glycol) biomatrices for three-dimensional mesenchymal stromal/stem cell administration to cutaneous wounds. **Acta biomaterialia**, v. 9, n. 11, p. 8802-8814, 2013.

WAGNER, A.; MÜHLBERGER, M.; PAULIK, C. Photoinitiator-free photopolymerization of acrylate-bismaleimide mixtures and their application for inkjet printing. **Journal of Applied Polymer Science**, v. 136, n. 29, p. 47789, 2019.

WAN ISHAK, W. H.; AHMAD, I.; RAMLI, S.; MOHD AMIN, M. C. I. Gamma irradiation-assisted synthesis of cellulose nanocrystal-reinforced gelatin hydrogels. **Nanomaterials**, v. 8, n. 10, p. 749, 2018.

WANG, T.; ZHU, X. K.; XUE, X. T.; WU, D. Y. Hydrogel sheets of chitosan, honey and gelatin as burn wound dressings. **Carbohydrate polymers**, v. 88, n. 1, p. 75-83, 2012.

WANG, C.; CHATANI, S.; PODGÓRSKI, M.; BOWMAN, C. N. Thiol-Michael addition miniemulsion polymerizations: functional nanoparticles and reactive latex films. **Polymer Chemistry**, v. 6, n. 20, p. 3758-3763, 2015.

WANG, C.; MENG, R.; WANG, R.; SHEN, Z. Synthesis and mechanism study of gelatin grafted acetone formaldehyde sulphonates as oil-well cement dispersant. **Rsc Advances**, v. 7, n. 50, p. 31779-31788, 2017.

WANG, Z.; MA, W.; HU, D.; WU, L. Synthesis and characterization of microencapsulated methyl laurate with polyurethane shell materials via interfacial polymerization in Pickering emulsions. **Colloids and Surfaces A: Physicochemical and Engineering Aspects**, v. 600, p. 124958, 2020.

WANG, L.; CHANG, M. W.; AHMAD, Z.; ZHENG, H.; LI, J. S. Mass and controlled fabrication of aligned PVP fibers for matrix type antibiotic drug delivery systems. **Chemical Engineering Journal**, v. 307, p. 661-669, 2017.

WANG, Y.; WANG, Q.; XIA, Q. C.; YANG, W. J.; WANG, X. X.; SUN, S. P.; XING, W. Nanocapsule controlled interfacial polymerization finely tunes membrane surface charge for precise molecular sieving. **Chemical Engineering Journal**, v. 409, p. 128198, 2021.

WANG, Y.; ZHU, T.; KUANG, H.; SUN, X.; ZHU, J.; SHI, Y.; HONG, T. Preparation and evaluation of poly (ester-urethane) urea/gelatin nanofibers based on different crosslinking strategies for potential applications in vascular tissue engineering. **RSC advances**, v. 8, n. 63, p. 35917-35927, 2018.

WEISSMUELLER, N. T.; LU, H. D.; HURLEY, A.; PRUD'HOMME, R. K. Nanocarriers from GRAS zein proteins to encapsulate hydrophobic actives. **Biomacromolecules**, v. 17, n. 11, p. 3828-3837, 2016.

WEI, W.; ZHU, M.; WU, S.; SHEN, X.; LI, S. Stimuli-responsive biopolymers: An inspiration for synthetic smart materials and their applications in self-controlled catalysis. **Journal of Inorganic and Organometallic Polymers and Materials**, v. 30, p. 69-87, 2020.

WILLIAMS, J. K.; YOO, J. J.; ATALA, A. Regenerative medicine approaches for tissue engineered heart valves. **principles of regenerative medicine**, p. 1041-1058, 2019.

WITTING, M.; OBST, K.; FRIESS, W.; HEDTRICH, S. Recent advances in topical delivery of proteins and peptides mediated by soft matter nanocarriers. **Biotechnology Advances**, v. 33, n. 6, p. 1355-1369, 2015.

WONG, C.; SHITAL, P.; CHEN, R.; OWIDA, A.; MORSI, Y. Biomimetic electrospun gelatin–chitosan polyurethane for heart valve leaflets. **Journal of Mechanics in Medicine and Biology**, v. 10, n. 04, p. 563-576, 2010.

WORCH, J. C.; STUBBS, C. J.; PRICE, M. J.; DOVE, A. P. Click nucleophilic conjugate additions to activated alkynes: exploring thiol-yne, amino-yne, and hydroxyl-yne reactions from (bio) organic to polymer chemistry. **Chemical Reviews**, v. 121, n. 12, p. 6744-6776, 2021.

WU, D.; SCOTT, C.; HO, C. C.; CO, C. C. Aqueous-core capsules via interfacial free radical alternating copolymerization. **Macromolecules**, v. 39, n. 17, p. 5848-5853, 2006.

XIANG, L.; LIU, X.; ZHANG, H.; ZHAO, N.; ZHANG, K. Thermoresponsive self-healable and recyclable polymer networks based on a dynamic quinone methide–thiol chemistry. **Polymer Chemistry**, v. 11, n. 38, p. 6157-6162, 2020.

XIAO, S.; ZHAO, T.; WANG, J.; WANG, C.; DU, J.; YING, L.; XU, K. Gelatin methacrylate (GelMA)-based hydrogels for cell transplantation: an effective strategy for tissue engineering. **Stem cell reviews and reports**, v. 15, p. 664-679, 2019.

XIE, H.; YANG, K. K.; WANG, Y. Z. Photo-crosslinking: a powerful and versatile strategy to develop shape-memory polymers. **Progress in Polymer Science**, v. 95, p. 32-64, 2019.

XU, F.; WU, Q.; CHEN, X.; LIN, X.; WU, Q. A Single lipase-catalysed one-pot protocol combining aminolysis resolution and aza-michael addition: an easy and efficient way to synthesise β-amino acid esters. **European Journal of Organic Chemistry**, v. 2015, n. 24, p. 5393-5401, 2015.

XUE, W.; CHAMP, S.; HUGLIN, M. B. Network and swelling parameters of chemically crosslinked thermoreversible hydrogels. **Polymer**, v. 42, n. 8, p. 3665-3669, 2001.

YAASHIKAA, P. R.; KUMAR, P. S.; KARISHMA, S. Review on biopolymers and composites–evolving material as adsorbents in removal of environmental pollutants. **Environmental Research**, v. 212, p. 113114, 2022.

YANG, G.; XIAO, Z.; REN, X.; LONG, H.; QIAN, H.; MA, K.; GUO, Y. Enzymatically crosslinked gelatin hydrogel promotes the proliferation of adipose tissue-derived stromal cells. **PeerJ**, v. 4, p. e2497, 2016.

YANG, S.; ZHEN, H.; SU, B. Polyimide thin film composite (TFC) membranes via interfacial polymerization on hydrolyzed polyacrylonitrile support for solvent resistant nanofiltration. **RSC advances**, v. 7, n. 68, p. 42800-42810, 2017.

YAO, Y.; WANG, H.; WANG, R.; CHAI, Y.; JI, W. Fabrication and performance characterization of the membrane from self-dispersed gelatin-coupled cellulose microgels. **Cellulose**, v. 26, p. 3255-3269, 2019.

YASMIN, R.; SHAH, M.; KHAN, S. A.; ALI, R. Gelatin nanoparticles: a potential candidate for medical applications. **Nanotechnology Reviews**, v. 6, n. 2, p. 191-207, 2017.

YE, E.; CHEE, P. L.; PRASAD, A.; FANG, X.; OWH, C.; YEO, V. J. J.; LOH, X. J. Supramolecular soft biomaterials for biomedical applications. **In-Situ Gelling Polymers: For Biomedical Applications**, p. 107-125, 2015.

YE, Q.; WANG, Y.; WILLIAMS, K.; SPENCER, P. Characterization of photopolymerization of dentin adhesives as a function of light source and irradiance. **Journal of Biomedical Materials Research Part B: Applied Biomaterials: An Official Journal of The Society for Biomaterials, The Japanese Society for Biomaterials, and The Australian Society for Biomaterials and the Korean Society for Biomaterials**, v. 80, n. 2, p. 440-446, 2007.

YOON, H. J.; SHIN, S. R.; CHA, J. M.; LEE, S. H.; KIM, J. H.; DO, J. T.; BAE, H. Cold water fish gelatin methacryloyl hydrogel for tissue engineering application. **PloS one**, v. 11, n. 10, p. e0163902, 2016.

YUNG, C. W.; WU, L. Q.; TULLMAN, J. A.; PAYNE, G. F.; BENTLEY, W. E.; BARBARI, T. A. Transglutaminase crosslinked gelatin as a tissue engineering scaffold. **Journal of Biomedical Materials Research Part A: An Official Journal of The Society for Biomaterials, The Japanese Society for Biomaterials, and The Australian Society for Biomaterials and the Korean Society for Biomaterials**, v. 83, n. 4, p. 1039-1046, 2007.

ZACHARIÁŠOVÁ, B.; HABEROVÁ, K.; ORAVEC, M.; JANČOVIČOVÁ, V. Plasma treatment of gelatin photography. **Acta Chimica Slovaca**, v. 12, n. 1, p. 27-33, 2019.

ZATORSKI, J. M.; MONTALBINE, A. N.; ORTIZ-CÁRDENAS, J. E.; POMPANO, R. R. Quantification of fractional and absolute functionalization of gelatin hydrogels by

optimized ninhydrin assay and 1 H NMR. **Analytical and bioanalytical chemistry**, v. 412, p. 6211-6220, 2020.

ZHAI, X.; MA, Y.; HOU, C.; GAO, F.; ZHANG, Y.; RUAN, C.; LIU, W. 3D-printed high strength bioactive supramolecular polymer/clay nanocomposite hydrogel scaffold for bone regeneration. **ACS Biomaterials Science & Engineering**, v. 3, n. 6, p. 1109-1118, 2017.

ZHAN, J.; MORSI, Y.; EI-HAMSHARY, H.; AL-DEYAB, S. S.; MO, X. In vitro evaluation of electrospun gelatin–glutaraldehyde nanofibers. **Frontiers of Materials Science**, v. 10, p. 90-100, 2016.

ZHANG, F.; FAN, J. B.; WANG, S. Interfacial polymerization: from chemistry to functional materials. **Angewandte Chemie International Edition**, v. 59, n. 49, p. 21840-21856, 2020.

ZHANG, Y.; NAEBE, M. Lignin: A review on structure, properties, and applications as a light-colored UV absorber. **ACS Sustainable Chemistry & Engineering**, v. 9, n. 4, p. 1427-1442, 2021.

ZHANG, Z.; LIN, J.; LIU, Z.; TIAN, G.; LI, X. M.; JING, Y.; LI, X. D. Photo-Crosslinking To Delineate Epigenetic Interactome. **Journal of the American Chemical Society**, v. 144, n. 46, p. 20979-20997, 2022.

ZHANG, Y.; SU, Y.; PENG, J.; ZHAO, X.; LIU, J.; ZHAO, J.; JIANG, Z. Composite nanofiltration membranes prepared by interfacial polymerization with natural material tannic acid and trimesoyl chloride. **Journal of Membrane Science**, v. 429, p. 235-242, 2013.

ZHAO, L.; ZHANG, B. Doxorubicin induces cardiotoxicity through upregulation of death receptors mediated apoptosis in cardiomyocytes. **Scientific reports**, v. 7, n. 1, p. 44735, 2017.

ZHU, M.; CAO, Z.; ZHOU, H.; XIE, Y.; LI, G.; WANG, N.; QU, X. Preparation of environmentally friendly acrylic pressure-sensitive adhesives by bulk photopolymerization and their performance. **RSC advances**, v. 10, n. 17, p. 10277-10284, 2020.

ZHUANG, C.; TAO, F.; CUI, Y. Anti-degradation gelatin films crosslinked by active ester based on cellulose. **RSC Advances**, v. 5, n. 64, p. 52183-52193, 2015.

ZOHOURIAN, M. M.; KABIRI, K. Superabsorbent polymer materials: a review. 2008.
ZWIOREK, K.; BOURQUIN, C.; BATTIANY, J.; WINTER, G.; ENDRES, S.; HARTMANN, G.; COESTER, C. Delivery by cationic gelatin nanoparticles strongly increases the immunostimulatory effects of CpG oligonucleotides. **Pharmaceutical research,** v. 25, p. 551-562, 2008.

APPENDIX A

Table 21 – Physico-chemical composition and microbiological quality of type A gelatin from porcine skin (Gelnex).

Physico-chemical Tests	Unity	Min.	Max.	Test Results	Method
Bloom (6,67%. 10ºC)	grams	270.0	290	277.0	GMIA/GME[1]
Viscosity (6,67%, 60ºC)	mPs	36.0	50.0	46	GMIA/GME
Moisture	%	-	12.0	10.5	GMIA/GME
Ashes	%	-	1.0	≤ 1.0	GMIA/GME
pH (1%)	n/a	4.7	6.5	5.55	GMIA
Sulfur dioxide (SO_2)	ppm	-	10.0	≤ 10.0	GME
Hydrogen peroxide (H_2O_2)	ppm	-	10.0	≤ 10.0	GME
Arsenic (As)	ppm	-	0.8	≤ 0.8	A.O.A.C[2]
Copper (Cu)	ppm	-	30.0	≤ 30.0	A.O.A.C
Chromium (Cr)	ppm	-	5.0	≤ 5.0	A.O.A.C
Lead (Pb)	ppm	-	1.5	≤ 1.5	A.O.A.C
Cadmium (Cd)	ppm	-	0.5	≤ 0.5	A.O.A.C
Mercury (Hg)	ppm	-	0.15	≤ 0.15	A.O.A.C
Zinc (Zn)	ppm	-	50.0	≤ 50.0	A.O.A.C
Pentachlorophenol (C_6HCl_5O)	ppm	-	0.30	≤ 0.3	A.O.A.C
Nitrogen (N)	%	15.0	-	≥ 15.0	Kjeldahl

Microbiological Tests	Unity	Specified limit	Test Results	Method
Total Bacteria Count (TBC)	UFC/g	< 1000	< 1000	USP[3]
E. coli	/10 g	Negative	Negative	USP
Salmonella ssp.	/25 g	Absent	Absent	A.O.A.C

[1]GMIA/GME – Gelatin Manufacturers Institute of America and Gelatin Manufacturers of Europe
[2]A.O.A.C – Association of Official Agricultural Chemists
[3]USP – United States Pharmacopeia.

Table 22 – Formulations for prepare gelatin hydrogels using EGDMA as crosslinker and different methodologies of synthesis.

Sample a)	**$Weight_{theoretical}$ (g)**	**$Weight_{real}$ (g)**
		1.0017
Gelatin	1.0	1.0151
		1.0008
	0.01	
	or	0.0108
EGDMA	0.05	0.0522
	or	0.1023
	0.1	
		0.0553
DBU	0.05	0.0512
		0.0501
		5.0023
Water	5.0	5.0008
		5.0107
Sample b)	**$Weight_{theoretical}$ (g)**	**$Weight_{real}$ (g)**
Gelatin	1.0	1.0102
EGDMA	0.05	0.0522
DBU	0.05	0.0541
Water	5.0	5.0018
KPS (2 wt.%)	0.02	0.0211
Sample c)	**$Weight_{theoretical}$ (g)**	**$Weight_{real}$ (g)**
Gelatin	1.0	1.0027
EGDMA	0.05	0.0558
DBU	0.05	0.0511
Water	5.0	5.0118
IG2959 (2 wt.%)	0.02	0.0208
Sample d)	**$Weight_{theoretical}$ (g)**	**$Weight_{real}$ (g)**
Gelatin	1.0	1.0019
EGDMA	0.05	0.0502
DBU	0.05	0.0510
Water	5.0	5.0615
IG2959 (2 wt.%)	0.02	0.0241
HEMA (2 wt.%)	0.02	0.0203

EGDMA – ethylene glycol dimethacrylate; DBU – 1,8-Diazabicyclo(5.4.0)undec-7-ene; KPS – potassium persulfate; HEMA – 2-hydroxyethyl methacrylate; IG2959 – Irgacure 2959 (photoinitiator);
Source: Author (2023).

Table 23 - Estimated physical parameters by helium picnometry.

Sample	(ρ) – True density ($g \cdot cm^{-3}$)	(V) – Volume (cm^3)	($\bar{v}$) – Specific Volume ($cm^3 \cdot g^{-1}$)
Gelatin	1.34 ± 0.0057^a	0.9010 ± 0.0038^a	0.7486 ± 0.0057^a
G_0.15	1.55 ± 0.0049^b	0.6350 ± 0.0020^b	0.6448 ± 0.0049^b
G_0.30	1.29 ± 0.0031^c	0.8133 ± 0.0020^c	0.7735 ± 0.0031^c
G_0.45	1.39 ± 0.0048^d	0.7269 ± 0.0025^d	0.7190 ± 0.0048^d

Results are shown as mean (n = 10) followed by ± standard deviation (SD);
Different letters in the same column indicate statistically significant differences between the means by Tukey's test at significance level of 95% (*p-value* ≤ 0.05);
Source: Author (2023).

Figure 41 – Gelatin M_w and 2^{nd} virial coefficient results from Debye plot.

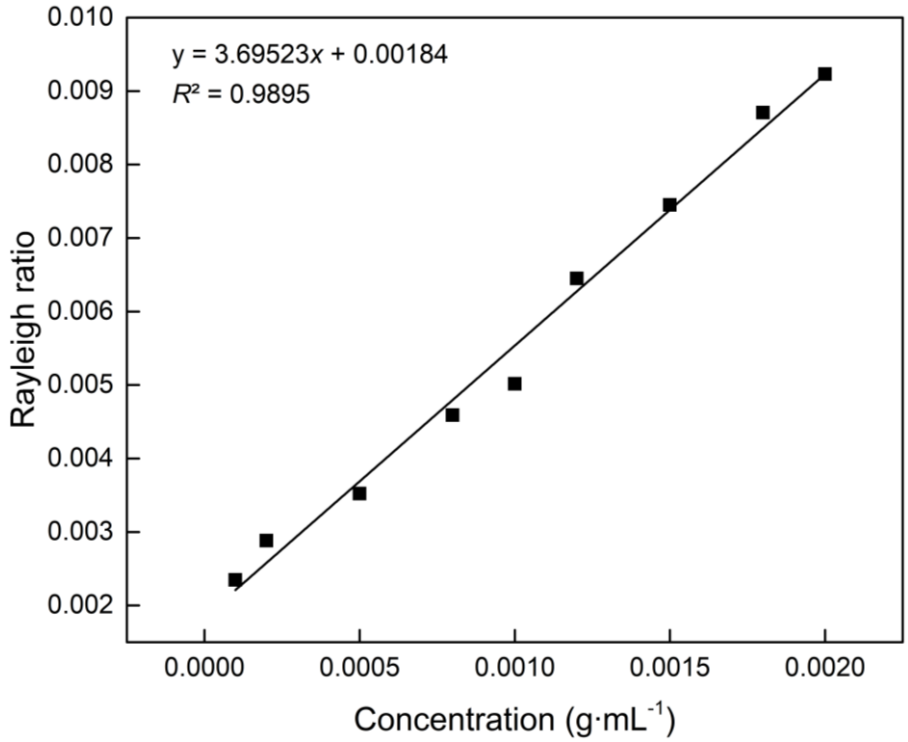

Source: Author (2023).

Figure 42 – DSC curves of neat gelatin at different heating conditions.

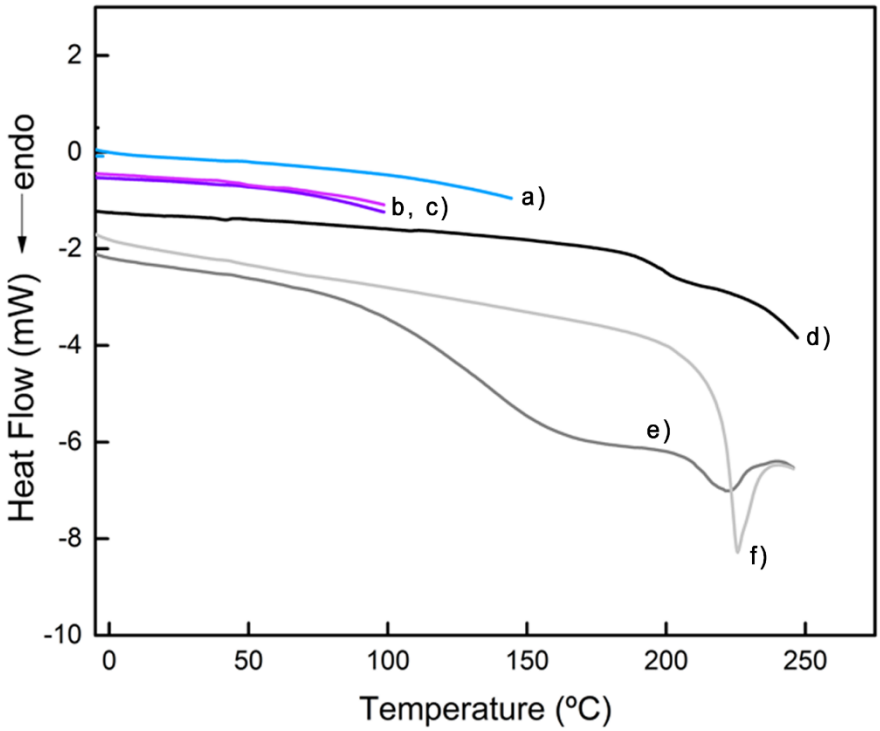

a) Second run, until 150 ºC, and at 10 ºC·min^{-1}; b and c) Second run of two independent samples, until 100 ºC and at 10 ºC·min^{-1}; d) second run, until 250 ºC and at 10 ºC·min^{-1}; e and f) First and second run of the same sample, respectively, until 250 ºC and at 20 ºC·min^{-1}
Source: Author (2023).

Figure 43 – Estimated particle diameter of the pure G_0.1 formulation.

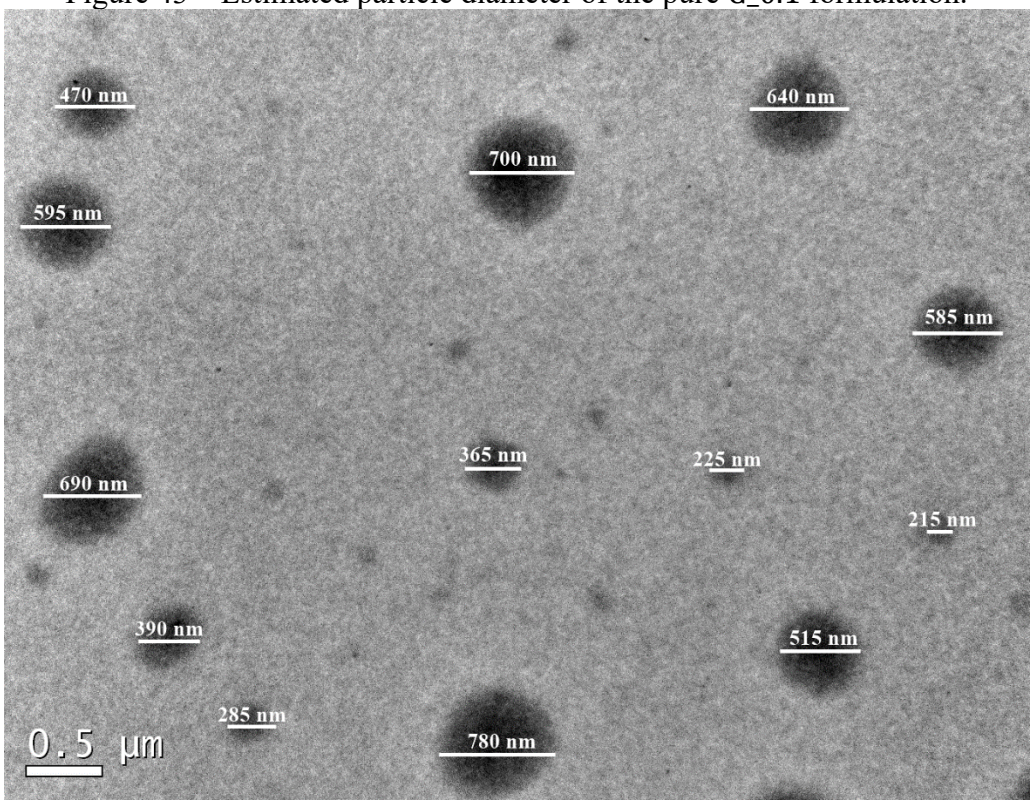

Scaling of 500 nm for the inverse miniemulsion using 0.1 g of crosslinker;
Source: Author (2023).

Figure 44 – Optical microscopy image of redispersed DOXG_0.01 formulation.

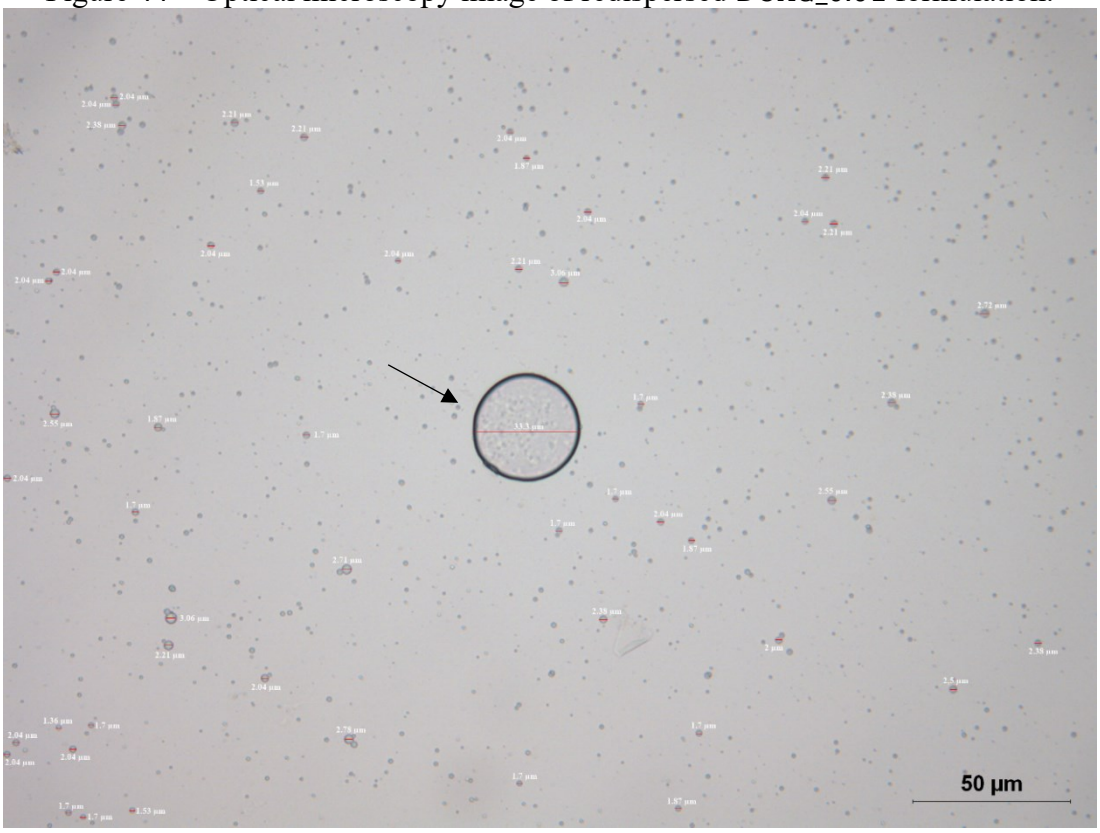

Scaling of 50 µm for the inverse miniemulsion using 0.01 g of crosslinker;
Source: Author (2023).